Sediment Pathways on Ebb-Tidal Deltas
New Tools and Techniques for Analysis

Pearson, S.G.

DOI
10.4233/uuid:c2fe811c-dc2e-4e1f-bb0c-dc43f11cd1eb

Publication date
2022

Document Version
Final published version

Citation (APA)
Pearson, S. G. (2022). *Sediment Pathways on Ebb-Tidal Deltas: New Tools and Techniques for Analysis*. [Dissertation (TU Delft), Delft University of Technology]. https://doi.org/10.4233/uuid:c2fe811c-dc2e-4e1f-bb0c-dc43f11cd1eb

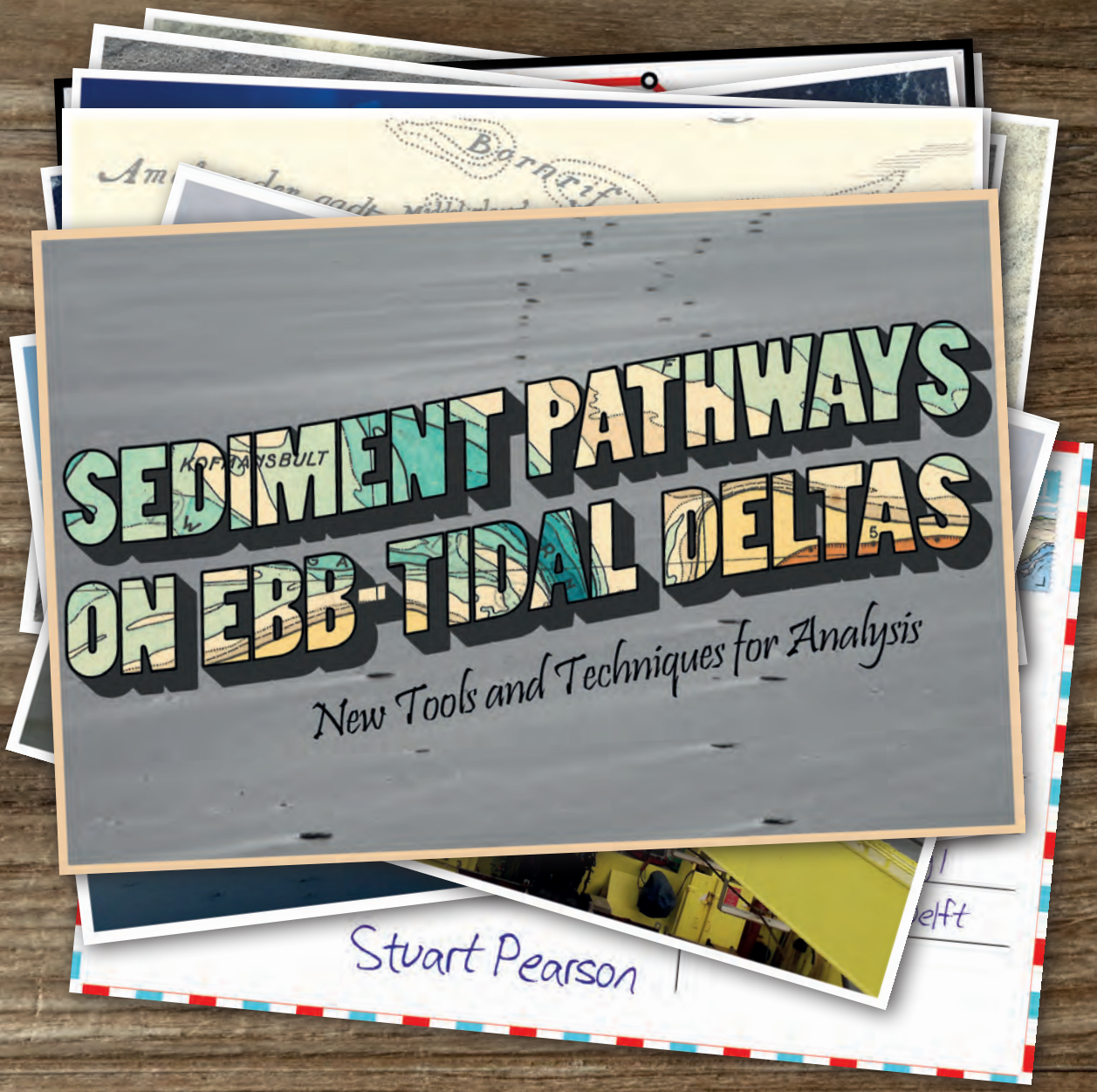
SEDIMENT PATHWAYS
ON EBB-TIDAL DELTAS
New Tools and Techniques for Analysis
Stuart Pearson

Sediment Pathways on Ebb-Tidal Deltas

New Tools and Techniques for Analysis

SEDIMENT PATHWAYS ON EBB-TIDAL DELTAS

NEW TOOLS AND TECHNIQUES FOR ANALYSIS

Proefschrift

ter verkrijging van de graad van doctor
aan de Technische Universiteit Delft,
op gezag van de Rector Magnificus Prof.dr.ir. T.H.J.J. van der Hagen,
voorzitter van het College voor Promoties,
in het openbaar te verdedigen op dinsdag 8 maart 2022 om 15:00 uur

door

Stuart Grant PEARSON

Civiel ingenieur, Technische Universiteit Delft, Nederland,
Master of Science in Coastal & Marine Engineering and Management,
Technische Universiteit Delft, Nederland,
Norwegian University of Science & Technology, Noorwegen,
& University of Southampton, Verenigd Koninkrijk;
geboren te Richmond, BC, Canada.

Dit proefschrift is goedgekeurd door de promotoren.

Samenstelling promotiecommissie:

Rector Magnificus,	voorzitter
Prof.dr.ir. Z.B. Wang	Technische Universiteit Delft, promotor
Dr.ir. B.C. van Prooijen	Technische Universiteit Delft, promotor
Onafhankelijke leden:	
Prof.dr. C. Winter	Christian-Albrechts Universität zu Kiel, DE
Prof.dr. D.M. FitzGerald	Boston University, USA
Prof.dr. K.M. Wijnberg	Universiteit Twente, NL
Prof.dr.ir. J.A. Roelvink	IHE Delft/Technische Universiteit Delft, NL
Prof.dr.ir. A.J.H.M. Reniers	Technische Universiteit Delft, reservelid
Overige leden:	
Dr.ir. E.P.L. Elias	Deltares, NL

This work is part of the research programme 'Collaboration Program Water' with project number 14489 (SEAWAD), which is (partly) financed by NWO Domain Applied and Engineering Sciences.

Keywords:	sediment transport pathway, ebb-tidal delta, connectivity, Ameland
Printed by:	Ridderprint, www.ridderprint.nl
Cover by:	Stuart G. Pearson.
Front & Back:	Postcards from Ameland, representing different facets of this project.

ISBN 978-94-6384-300-3

An electronic version of this dissertation is available at
http://repository.tudelft.nl/.

At night one can hear the sound of the ocean as it nudges the land. Almost as if it is insistently pushing the land further back. The sound is not of storm but rather one of patient persistence and it is not at all audible in the summer months. Yet it is now as rhythmical as the pulsing of the blood in its governance by the moon.

Alistair MacLeod, “No Great Mischief"

I love creeks and the music they make.
And rills, in glades and meadows, before
they have a chance to become creeks.
I may even love them best of all
for their secrecy. I almost forgot
to say something about the source!
Can anything be more wonderful than a spring?
But the big streams have my heart too.
And the places streams flow into rivers.
The open mouths of rivers where they join the sea.
The places where water comes together
with other water. Those places stand out
in my mind like holy places.
But these coastal rivers!
Just looking at it makes my blood run
and my skin tingle. I could sit
and watch these rivers for hours.
Not one of them like any other.
I'll take all the time I please this afternoon
before leaving my place alongside this river.
It pleases me, loving rivers.
Loving them all the way back to their source.
Loving everything that increases me

Raymond Carver, "Where Water Comes Together with Other Water"

CONTENTS

SUMMARY

IN AN ERA of rising seas and other challenges posed by climate change, coastal regions like the Netherlands are facing ever graver threats. Strategic sand nourishments could mitigate the threat of coastal erosion and sea level rise on barrier island coasts while limiting ecological impacts. However, insufficient knowledge of sediment transport pathways at tidal inlets and ebb-tidal deltas prevents an informed response in these areas.

The main goal of this project was to describe and quantify the pathways that sediment takes on an ebb-tidal delta. To reach this goal, we focused our analyses on Ameland ebb-tidal delta in the Netherlands. Before we could begin to tackle this challenge, we needed to develop new tools and techniques for analyzing a combination of field measurements and numerical models. These include a method for analyzing the stratigraphy and mapping the morphodynamic evolution of ebb-tidal deltas, a new metric for characterizing suspended sediment composition, and innovative use of sediment tracers. We also established a quantitative approach for looking at and thinking about sediment pathways via the sediment connectivity framework, and developed a Lagrangian model to visualize and predict these pathways efficiently.

Using these tools, we quantified the small-scale details of physical processes moving grains of sand around on the ebb-tidal delta ($\mathcal{O}(1-100\mu m)$), then zoomed out to reveal the transport patterns and pathways emerging at a larger scale ($\mathcal{O}(1-10km)$). Advancing our understanding of ebb-tidal delta morphodynamics in the past and present strengthens our basis for predicting its behaviour in the future.

By analyzing historical bathymetry (Chapter 3), we show that Ameland ebb-tidal delta is a highly dynamic system characterized by shoal and channel migration in a clockwise direction around the inlet, at a rate of approximately 14^o/decade. These shoals in the active part of the ETD are continuously reworked on timescales of less than 10 years. Sediment in Ameland ebb-tidal delta is predominantly well-sorted, fine sand, with muddier material found in the distal regions offshore. There is a clear clockwise fining trend and reduction in grain size variation, behaviour consistent with the clockwise migration of sediment around the delta.

Next, we looked at variations in suspended sediment transport on the ebb-tidal delta as a function of grain size ($\mathcal{O}(1-100\mu m)$) and under the influence of different hydrodynamic forcings (Chapters 4 & 5). The sediment on the seabed of Ameland ebb-tidal delta is mainly sand, but our field measurements reveal the overwhelming presence of muddy sediment travelling in suspension. Sand tends to be locally resuspended at ebb and flood, while mud is transported back and forth from the Wadden Sea, dominating suspension at slack tide. During storms, sand is easily resuspended by waves, and mud can remain in suspension for days afterwards.

We then took a contrasting perspective on sediment transport by carrying out a Lagrangian tracer study (Chapter 6). Using fluorescent and magnetic sand particles, we highlighted the nature of grain size-selective sediment transport and demonstrated the viability of sediment tracing as a tool for monitoring nourishment dispersal.

To manage information about sediment pathways at different space and time scales, we developed the sediment connectivity framework (Chapter 7). Using graph theory, we decompose complex systems of coastal sediment pathways into networks of nodes and links. We demonstrate that system connectivity is a clear function of grain size and time, with networks of smaller sediment particles growing more widely and rapidly. This approach also enables us to identify the main bypassing routes across the inlet. Most crucially, connectivity provides a means of quantifying and understanding the large-scale sediment transport patterns that emerge upward from small-scale processes, rather than aggregating these processes from the top down.

Lastly, we introduced a Lagrangian sediment transport model, SedTRAILS, in order to visualize and predict sediment pathways (Chapter 8). Used in conjunction with connectivity, it forms a powerful tool for examining emergent sediment transport patterns. A key advantage of SedTRAILS is that it visualizes complex model outputs in an intuitive way, yielding more value from those models and enhancing communication with stakeholders and non-scientific audiences.

The techniques developed here are useful in a wider range of coastal settings beyond Ameland, and are already being applied in practice. We foresee that the main impacts of this project will be to improve nourishment strategies, numerical modelling, and field data analysis. This dissertation also points forward to numerous opportunities for further investigation, including the continued development of the connectivity framework and SedTRAILS. By managing our coastal sediment more effectively, we will set the stage for a more sustainable future, in spite of the challenges that lie ahead.

SAMENVATTING

IN EEN TIJDPERK waarin de zeespiegel stijgt en klimaatverandering ook andere uitdagingen met zich meebrengt, worden kustregio's zoals Nederland geconfronteerd met steeds grotere dreigingen. Strategische geplaatste zandsuppleties kunnen de dreigende kusterosie en zeespiegelstijging langs de kusten van Waddeneilanden verminderen en tegelijkertijd de ecologische effecten beperken. Onvoldoende kennis van de sedimenttransportpaden in de zeegaten en buitendelta's verhindert echter een onderbouwd ingrijpen in deze gebieden.

Het belangrijkste doel van dit proefschrift was het beschrijven en kwantificeren van de paden die sediment in een buitendelta aflegt. Om dit doel te bereiken, hebben we onze analyses gericht op de buitendelta van Ameland in Nederland. Voordat we deze uitdaging konden aangaan, moesten we nieuwe hulpmiddelen en technieken ontwikkelen voor het analyseren van een combinatie van veldmetingen en numerieke modellen. Deze omvatten een methode voor het analyseren van de stratigrafie en het in kaart brengen van de morfologische ontwikkeling van buitendelta's, een nieuw maatstelsel voor het karakteriseren van de samenstelling van gesuspendeerd sediment en innovatief gebruik van sedimenttracers. We hebben ook een kwantitatieve methode ontwikkeld om sedimenttransportpaden te beschouwen en te evalueren middels het sedimentconnectiviteitsraamwerk, en een Lagrangiaans model ontwikkeld om deze routes efficiënt te visualiseren en te voorspellen.

Met behulp van deze methoden hebben we de kleinschalige details gekwantificeerd van de fysische processen die zandkorrels in de buitendelta doen verplaatsen ($\mathcal{O}(1-100\mu m)$), en zoomden vervolgens uit om de transportpatronen en -paden te onthullen die die op grotere schaal aanwezig zijn ($\mathcal{O}(1-10km)$). Het verbeteren van ons begrip van de morfodynamica van buitendelta's in het verleden en heden versterkt onze voorspelkracht van het gedrag van deze gebieden in de toekomst.

Door historische bodemliggingen te analyseren (Hoofdstuk 3), laten we zien dat de buitendelta van Ameland een zeer dynamisch systeem is dat wordt gekenmerkt door een migratie van platen en geulen met de klok mee rond het zeegat, met een rotatiesnelheid van ongeveer 14^o /decennium. Deze platen in het actieve deel van de buitendelta worden continu herwerkt op een tijdschaal van minder dan 10 jaar. Sediment in de buitendelta van Ameland is over het algemeen goed gesorteerd fijn zand, en materiaal met meer slib aanwezig in gebieden verder van de kust. Met de klok mee wordt het sediment fijner en neemt de variatie in korrelgrootte af, gedrag dat consistent is met de migratie van sediment met de klok mee rond de buitendelta.

Vervolgens hebben we gekeken naar variaties in zwevend sedimenttransport op de buitendelta als functie van de korrelgrootte ($\mathcal{O}(1-100\mu m)$) en onder invloed van verschillende hydrodynamische krachten (Hoofdstukken 4 & 5). Het sediment op de zeebodem van de buitendelta van Ameland bestaat voornamelijk uit zand, maar onze veldmetingen laten de overweldigende aanwezigheid van slib in suspensie zien. Zand wordt bij eb en vloed meestal plaatselijk opnieuw gesuspendeerd, terwijl slib vanuit de Waddenzee heen en weer wordt getransporteerd en bij laagwater de suspensie domineert. Tijdens stormen wordt

zand gemakkelijk weer in suspensie gebracht door golven, en slib kan daarna nog dagenlang in suspensie blijven.

Vervolgens hebben we een ander perspectief op het sedimenttransport beschouwd door het uitvoeren van een Lagrangiaanse tracerstudie (Hoofdstuk 6). Met behulp van fluorescerende en magnetische zanddeeltjes hebben we de aard van korrelgrootte-selectief sedimenttransport uitgelicht en de haalbaarheid aangetoond van sedimenttracering als een hulpmiddel voor het monitoren van de verspreiding van suppleties.

Om met informatie over sedimentroutes op verschillende ruimte- en tijdschalen te kunnen omgaan, hebben we het sedimentconnectiviteitsraamwerk ontwikkeld (Hoofdstuk 7). Met behulp van de grafentheorie ontleden we complexe sedimentpaden in kustsystemen in netwerken van knooppunten en verbindingen. We demonstreren dat systeemconnectiviteit een duidelijke functie is van de korrelgrootte en tijd, waarbij netwerken van kleinere sedimentdeeltjes breder en sneller groeien. Deze aanpak stelt ons ook in staat om de belangrijkste paden te identificeren waarover het sediment het zeegat passeert. Het meest cruciale is dat connectiviteit een manier biedt om de grootschalige sedimenttransportpatronen – voortkomend uit kleinschalige processen – te kwantificeren en te begrijpen, in plaats van deze processen van bovenaf te aggregeren.

Ten slotte hebben we een Lagrangiaans sedimenttransportmodel, SedTRAILS, geïntroduceerd om sedimentroutes te visualiseren en te voorspellen (Hoofdstuk 8). Uit de beweging van individuele deeltjes ontstaat gaandeweg patronen. Als dit model gebruikt wordt in combinatie met het connectiviteitsprincipe, vormt het een krachtig hulpmiddel voor het onderzoeken van deze sedimenttransportpatronen. Een belangrijk voordeel van SedTRAILS is dat het complexe modelresultaten op een intuïtieve manier visualiseert, meer waarde uit de modellen haalt en de communicatie met belanghebbenden en niet- wetenschappelijke doelgroepen verbetert.

De hier ontwikkelde technieken zijn ook buiten Ameland bruikbaar in een breed scala van kustgebieden en worden nu al in de praktijk toegepast. We voorzien dat dit project met name de verbetering van suppletiestrategieën, numerieke modellering en analyse van veldgegevens mogelijk maakt. Dit proefschrift wijst ook op een tal van mogelijkheden voor verder onderzoek, inclusief het door ontwikkelen van het connectiviteitsraamwerk en SedTRAILS. Door ons kustsediment effectiever te beheren, maken we de weg vrij voor een duurzamere toekomst, ondanks de uitdagingen die voor ons liggen.

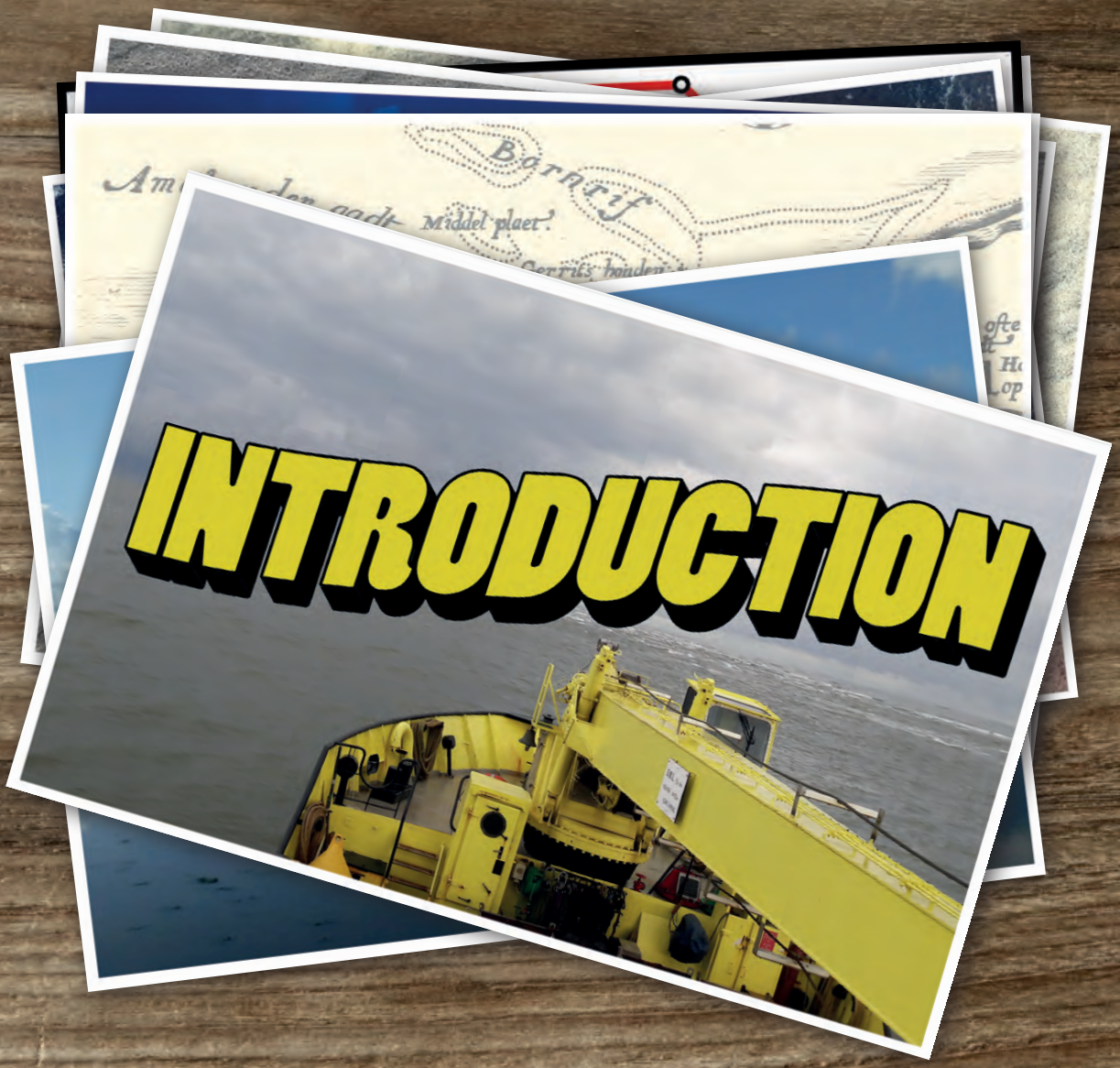
INTRODUCTION

Dear Reader,

The Netherlands has beautiful beaches and dunes, which actually protect the country from flooding. To keep everyone safe, they place lots of sand along the coast to build these natural defenses. However, the coast of the Wadden Islands is a lot more complicated, and we need to figure out how sand moves around there if we are going to protect it. Where does all the sand go? We don't even have the right tools to answer this question yet, so we will need to try some new approaches. Wish us luck!

Stuart

Delft University of Technology
Stevinweg 1
2628 CN Delft

1

INTRODUCTION

KEY POINTS:

- **Motivation**:
  - Strategic sand nourishments could mitigate the threat of coastal erosion and sea level rise on barrier island coasts while limiting ecological impacts.
  - Insufficient knowledge of sediment transport pathways at tidal inlets and ebb-tidal deltas prevents an informed response.
- **Main Research Goal:**
  - Describe and quantify the pathways that sediment takes on an ebb-tidal delta, using the example of Ameland Inlet in the Netherlands.
- **Approach**:
  - Use field measurements and numerical models to enhance our understanding of physical processes in tidal inlet and ebb-tidal delta systems.
  - Create practical tools and frameworks for addressing coastal sediment management concerns in these environments.

1

1.1. DUTCH COASTAL VULNERABILITY

To live in the Netherlands is to face an existential threat from the sea. For centuries, the Dutch have fought floods and other marine calamities by learning from past disasters and engineering their landscape in response. This has included widespread diking and land reclamation, the construction of coastal dams and barriers, and the fundamental reshaping of their coastal system. Although these solutions have enabled Dutch society to flourish until now, will they still suffice in the future?

How can we keep Dutch feet dry in the face of climate change, sea level rise, and ground subsidence? Our current safety from coastal flooding has its foundation in broad, sandy beaches and massive dunes that form a protective buffer against waves and storm surges (Figure 1.1). Without regularly topping up the supply of sand stored along the coast, waves would gnaw at the foot of the dunes until there was nothing left of the protective buffer. The waves and tides effectively drive a gigantic conveyor belt that perpetually carts sand away from the beaches and dunes and down the coast.

If not maintained, the long-term safety of the Netherlands could be in jeopardy. The Dutch flooding problem is thus not just a case of having "too much water", but also one of having too little sand (*Van Der Molen and Van Dijck*, 2000; *Mulder et al.*, 2011). This need for constant replenishment will be exacerbated by rising sea levels, since the coastline will retreat and the demand for sand will be amplified (*Haasnoot et al.*, 2020). Climate change will present the Dutch with new challenges in the next century and beyond (*Katsman et al.*, 2011).

Figure 1.1: Tiny grains of sand from Ameland ebb-tidal delta, 10 million of them in just a handful. It is these grains that form the Netherlands' main defense against coastal flooding (see also Appendix D). As they are jostled by waves and whisked away by tides, patterns emerge from these sand grains that shape our coasts over hundreds of kilometers and across generations.

1.2. COASTAL SAND NOURISHMENTS

Over the past four decades, the established practice of building "hard" structures like dikes and dams shifted towards using "soft" solutions that directly addressed the need to maintain sufficient sand on the coast. In 1990, the Dutch government drew a literal line in the sand, and established the *Basiskustlijn*, which represents the low-water mark along its entire coast circa that time. If the mean coastline position at a given point threatens to retreat landward past the Basiskustlijn, it must be supplemented with additional sand, a policy known as "Dynamic Preservation" (*Hillen and Roelse*, 1995; *Koster and Hillen*, 1995). The current policy takes a holistic view of the coastal system, considering how the Netherlands' total sediment balance shifts with sediment exchange between the coastal foundation, offshore, dunes, and estuaries, plus across the Belgian and German borders (*Lodder and Slinger*, 2021).

Operationally, the sediment supply of the Dutch coast is continually replenished by dredging sand from the North Sea and spreading it (or "nourishing") along the coast, whether on beaches or slightly deeper on the shoreface (*Huisman et al.*, 2019). In this way, they "hold the line" and add sand to specific locations to maintain flood protection standards there. Each year since 2000, $12 \times 10^6 m^3$ of sand has been added to the coastal foundation (*Kustfundament*, the zone between the -20 m depth contour and the landward side of the dunes, Figure 1.2a) (*van der Spek and Lodder*, 2015). Nourishment is widely practiced on long, straight beaches like those of the Holland coast, both here in the Netherlands and around the world (*Hanson et al.*, 2002; *Cooke et al.*, 2012; *Hanley et al.*, 2014; *Ludka et al.*, 2018; *Liu et al.*, 2019; *de Schipper et al.*, 2021).

As the Dutch nourishment program matured, there was growing recognition of the environmental impact that frequent nourishments can have along the coast. Every time a section of coast is nourished, seabed habitats are buried by the added sand, and the changed topography and sand grain characteristics of the nourished beach may also disrupt coastal ecosystems (*Speybroeck et al.*, 2006). Recognition of these impacts coincided with a shift to a new paradigm of "Building with Nature", instead of fighting against it (*Mulder et al.*, 2011; *Temmerman et al.*, 2013; *van Slobbe et al.*, 2013). A single large nourishment on the coast with a lifespan of several decades is expected to be more efficient, economical, and less disruptive to coastal ecosystems in the long run than placing smaller beach or shoreface nourishments every few years (*Stive et al.*, 2013; *Brière et al.*, 2018). The waves and tides then redistribute the sand over a larger area and contribute to coastal protection.

In a first pilot study of this new philosophy, the Sand Engine or Zandmotor was constructed on the coast of South Holland in 2011 (*Stive et al.*, 2013; *de Schipper et al.*, 2016; *Luijendijk et al.*, 2017). The fate of a nourishment like the Sand Engine is well-explained by basic theories of coastal sediment transport. Straight, alongshore uniform coastlines (like in Holland) can be conceptualized as one-dimensional systems, with wave-driven alongshore currents moving sand up or down the coast like conveyor belts. In the absence of structural erosion or accretion on a given coast, beach nourishments on a straight coastline like the Sand Engine will gradually diffuse away from their initial location until the coastline flattens out to its original condition. The ecological impact of the Sand Engine is complex, but it was actually found to have increased local biodiversity via the creation of new habitats on an otherwise straight coastline (*Herman et al.*, 2021). Based on similar principles, other meganourishments ($> 5 \times 10^6 m^3$ of sand) have since been constructed, such as at the Hondsbossche Zeewering in North Holland (*Kroon et al.*, 2017; *Wittebrood et al.*, 2018).

1

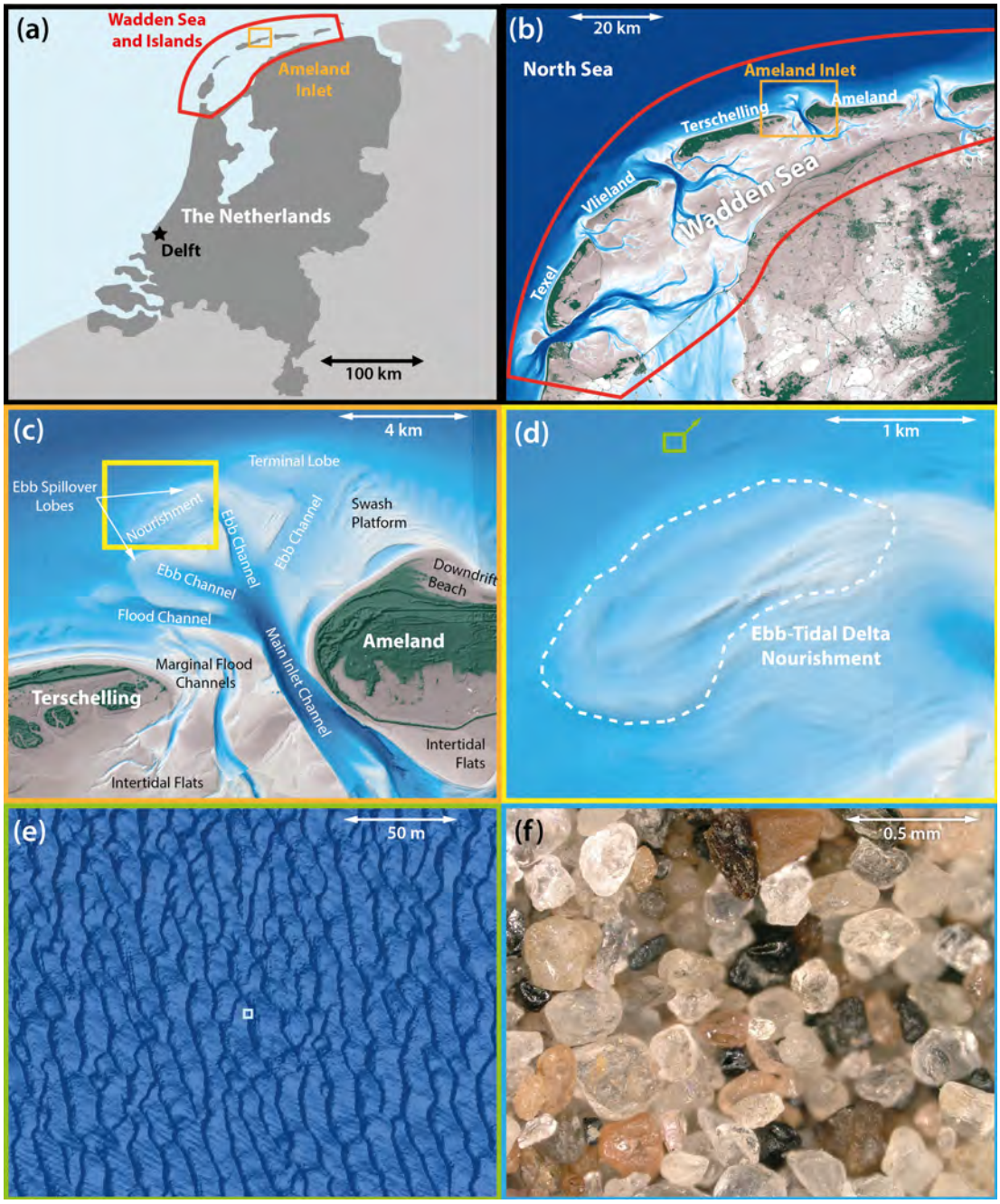

Figure 1.2: Overview of the study site at different spatial scales. (a) Overview map of the Netherlands indicating the location of the Wadden Sea and main study site at Ameland Inlet ($\mathcal{O}(100-1000km)$). (b) The Dutch Wadden Sea ($\mathcal{O}(10-100km)$). (c) Ameland inlet and ebb-tidal delta circa 2021 ($\mathcal{O}(1-10km)$). (d) Nourishment on Ameland ebb-tidal delta ($\mathcal{O}(100-1000m)$). (e) Bedforms on the seabed located just offshore of the ebb-tidal delta ($\mathcal{O}(0.01-100m)$). (f) Individual grains of sand on the ebb-tidal delta ($\mathcal{O}(0.01-1mm)$).

1.3. THE CHALLENGES OF NOURISHING NEAR TIDAL INLETS

The relatively straight coasts of Holland make up only part of the Dutch coastline. The northern coast consists of a series of barrier islands punctuated by tidal inlets which connect the North Sea to the Wadden Sea (Figure 1.2b). The straight "conveyor belts" of alongshore currents that move sediment along the island beaches are interrupted by tidal inlets, 2 to 10 km-wide gaps through which the Wadden Sea empties and refills twice daily. Tidal inlets exert a strong influence on the sediment balance and consequent erosion or accretion of their adjacent coastlines (*Ranasinghe et al.*, 2013; *Bamunawala et al.*, 2021). The Wadden Sea acts as a sediment sink in the Dutch coastal system, leading to a demand for sediment from the North Sea coasts around the Wadden Sea (*Wang et al.*, 2018). These parts of the coast may thus require more frequent and intense nourishment programs to stabilize them (*Elias and van der Spek*, 2017).

The viability of sand nourishments in these environments is determined in part by complex management requirements. Coastal managers are concerned with not only maintaining the volume of sand in beaches and dunes along the primary defenses of the islands, but also with the prospect of ensuring that the intertidal shoals and flats of the Wadden Sea keep pace with sea level rise and subsidence (*Fokker et al.*, 2018; *Vermeersen et al.*, 2018). If sediment supply to these intertidal areas is insufficient to build them up, then there is the risk that they will "drown", altering valuable habitat and exacerbating the flood risk to the mainland. The Wadden Sea is the most extensive contiguous intertidal area in the world, and was designated a UNESCO World Heritage Site due to its unique ecosystem and role as key stopover for migratory birds (*Reise et al.*, 2010). However, the capacity of the tidal inlets and availability of sediment to feed the Wadden Sea is still poorly quantified (*Elias et al.*, 2012a; *Wang et al.*, 2018; *Lodder et al.*, 2019; *Becherer et al.*, 2018).

The value of the Wadden Sea extends beyond its rich ecosystem and role in flood protection, and potential solutions must satisfy a diverse array of stakeholders (*Kabat et al.*, 2012; *Giebels et al.*, 2013; *Baptist et al.*, 2017). Tourism and fishing industries are also important to the local economy (*Imeson and Van Den Bergh*, 2006; *Sijtsma et al.*, 2012; *Floor et al.*, 2016). It is thus imperative that coastal protection measures do not come at the cost of irreparable environmental damage or disruption to important local industries. This balancing act is made even more difficult by the technical challenges and uncertainties associated with executing successful nourishments in and around tidal inlets.

Competition and collaboration between waves and tides on the convoluted coast of the Wadden Islands move sand in seemingly chaotic patterns and constantly reshape the landscape. We have an especially poor understanding of the pathways that sediment takes as it moves between the islands across vast underwater sand deposits ("ebb-tidal deltas", or ETDs), although this knowledge is essential for effective nourishments. Much of the sediment feeding the Wadden Sea is supplied by the ebb-tidal deltas, which are limited in size and shrinking quickly (*Elias et al.*, 2012a). These massive piles of sand also act as natural breakwaters, shielding the Wadden Sea and parts of the adjacent coasts from wave action (*FitzGerald*, 1988). In order to maintain the local sediment budget and preserve these natural defence systems, it is thus necessary to consider nourishing ebb-tidal deltas. The complexity of this environment and our limited experience with nourishing in such locations means that existing techniques may not work well there. While the total amount of sand contained in these ebb-tidal deltas is generally correlated to the volume of water transported through the inlet on every tidal cycle (or "tidal prism") (*O'Brien*, 1966), their precise

shape and volume fluctuates continuously. Mapping the behaviour of tidal inlets to enable better prediction of their morphodynamics is thus a key research priority for the coming years (*Power et al.*, 2021).

The transport pathways connecting one island to the next form a knot of shifting conveyor belts[1], in a process cumulatively known as sediment bypassing (*Bruun and Gerritsen*, 1959; *FitzGerald*, 1983; *Elias et al.*, 2019). The chief morphological consequence of this bypassing process is the migration of shoals and channels across the ebb-tidal delta, which can directly influence the erosion or accretion of adjacent shorelines (*FitzGerald et al.*, 1984; *Kana et al.*, 1999a; *Garel et al.*, 2014a) and pose challenges for navigability (*Cleary*, 2002). The direction of migration is controlled by the channels and subsequent redistribution/reworking of sand by waves and currents. Inlet channels tend to be tidally forced into alignment with the direction of the incoming tidal propagation (towards the updrift coast of the Dutch Wadden inlets). Wave-driven sediment transport tends to distort the channels in a downdrift direction (counter to the preferred tidal alignment in the Dutch Wadden inlets) (*Sha*, 1989a). If this distortion becomes so great that the channel is no longer an efficient conduit for flow, it may then switch back to a more efficient alignment, and begin anew in processes known as "ebb-tidal-delta breaching" or "outer channel shifting"(*FitzGerald et al.*, 2000). This switch may occur gradually or rapidly, often during spring tides or storms when discharge is highest (*FitzGerald*, 1988). As it tends to repeat in similar patterns, sediment bypassing is often described as a cyclical process (*Oertel*, 1977; *Israel and Dunsbergen*, 1999; *Gaudiano and Kana*, 2001; *Cheung et al.*, 2007; *Ridderinkhof et al.*, 2016; *Lenstra et al.*, 2019a), although the exact nature of this cyclicity is disputed (*Elias et al.*, 2019).[2]

Sediment that does not bypass the inlet may instead become entrained within the ebb-tidal delta or recirculate there (*Herrling and Winter*, 2018; *Son et al.*, 2011). The tidal inlet can also be a net sink of sediment, with sand being imported into the basin on the incoming tide and then being deposited there. This import (or alternatively, export) of sediment is highly dependent on the morphology and hydrodynamics (i.e., tidal asymmetry and other residual currents) of the basin in question (*Stive and Wang*, 2003; *Wang et al.*, 2020). In many inlets, humans interfere with the bypassing process, blocking sediment pathways with jetties or dredging to maintain navigation channels (*Beck*, 2019).

The picture is further complicated when variations in sediment grain size are considered. Stronger forces are generally needed to transport larger particles, meaning that on the Dutch coast, coarse sand ($0.25 - 1.0 mm$) is only moved by strong tidal currents and large waves during storms. Finer sand ($0.063 - 0.250 mm$) is mobilized much more readily, while the finest silt and clay ("mud") particles ($< 0.063 mm$) are so easily transported that they can remain in suspension for days at a time (unless consolidated). The aforementioned bypassing processes and indeed sediment transport pathways in general are strongly grain size-dependent. Grain size is thus a key parameter in determining the fate and persistence of a nourishment (*Dean*, 2002; *Hanson et al.*, 2002), as well as its ecological impact (*Bishop et al.*, 2006; *Peterson et al.*, 2014). Ultimately, particle size also determines depositional behaviour and will influence the ability for the Wadden Sea to keep up with sea level rise (*Lodder et al.*, 2019; *Colina Alonso et al.*, 2021), so it is essential to be able to predict grain size-dependent pathways.

Forecasting the fate of a nourishment on an ebb-tidal delta is thus not a trivial task:

[1] Alternatively, consider the moving staircases of Hogwarts (*Rowling*, 1997).

[2] *"Questions of cyclicity produce much warmth and much paper."* – Derek V. Ager

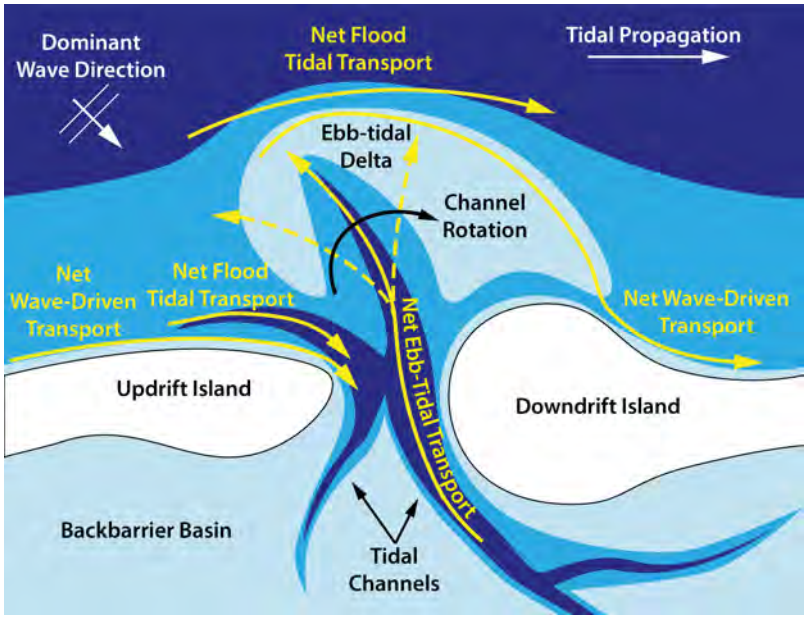

Figure 1.3: Conceptual diagram illustrating dominant net transport pathways and channel rotation for an idealized, mixed-energy tidal inlet similar to Ameland Inlet (the Netherlands) (*Elias et al.*, 2019) and typical of the Wadden Sea (e.g., *Sha* (1989a)). Yellow arrows indicate sediment pathways, and darker blue colours correspond to deeper areas.

there are innumerable pathways that its sediment can take, and its dispersal is steered by complex physical processes that are difficult to measure and model. In contrast to the relatively simple sediment transport conveyor belts of a straight coastline, the pathways on an ebb-tidal delta become a tangled pile of spaghetti. Attempts to numerically simulate the evolution of ETDs have resulted in mixed successes (*Wang et al.*, 2016; *Bak*, 2017; *Lenstra et al.*, 2019a; *Bertin et al.*, 2020) but lack predictive skill at the 5 to 20-year timescales crucial for planning engineering works (*Elias*, 2018). Part of this relates to shortcomings in our process-based models, for which we need to collect more field measurements to make improvements. Previous research on ebb-tidal deltas has also tended to focus more on their potential as a *source* for nourishment sand rather than as a *destination* for it (*Kana et al.*, 2014; *Elko et al.*, 2020; *Beck*, 2019). As such, we do not have good answers to even basic questions like, "what kind of sediment is moving around?", "where on an ETD should we nourish?", and "where does all the sediment go?".

If we do not have answers to these questions before nourishing, we run the risks of unwanted impacts to the Wadden Sea (will nourished sand reach the basin and disrupt vulnerable habitats there?), of triggering large morphological changes (e.g., channel shifting or shoal migration in such a way that negatively affects the adjacent coastlines), of disrupting navigation, or of an inefficient, expensive design.

We consider Ameland Inlet as a "living laboratory" (*Wallinga et al.*, 2021) for deepening our knowledge of ebb-tidal delta dynamics and for developing tools and techniques to determine the fate of nourished sediment. The challenges facing Ameland are not unique to the Dutch Wadden Sea, and are relevant for other barrier coast and inlet systems around the

world, including the German and Danish Wadden Sea (*Sha*, 1989a; *FitzGerald et al.*, 1984; *Benninghoff and Winter*, 2019), France (*Robin et al.*, 2009), Spain (*Morales et al.*, 2001), Portugal (*Garel et al.*, 2014b), Italy (*Fontolan et al.*, 2007), Brazil (*Ambrosio et al.*, 2020), the US West (*Beck and Arnold*, 2019), East (*Kana et al.*, 1999a), and Gulf coasts (*Powell et al.*, 2006), China (*Zhang et al.*, 2020a), Japan (*Okabe and Kato*, 2018), New Zealand (*Hicks and Hume*, 1996), to provide just a few examples. As such, the lessons learned in Ameland can be applied far and wide.

1.4. SHIFTING SCALES FROM SAND GRAINS TO EBB-TIDAL DELTAS

A conceptual challenge facing coastal managers is the matter of how sediment dynamics vary at different spatial and temporal scales (Figure 1.4), and how those dynamics cascade up or down the scales. The physical processes shaping our coasts span from micron-sized clay particles buffeted around by turbulent fluctuations that last mere fractions of a second, to the migration and flexing of whole continents via plate tectonics, imperceptible within our lifetimes.[3] The 'scale cascade' concept (Figure 1.4) is widely used in coastal science (*De Vriend*, 1991; *Cowell et al.*, 2003; *Vitousek et al.*, 2017a), and boils down to this: large landscapes take a long time to change, whereas smaller features in those landscapes evolve much more quickly. Larger scales provide boundary conditions for smaller ones, and in turn, patterns emerge from disorder at small scales to shape the larger ones. Fortunately, this scale cascade constrains our analysis, as it means that we are typically not concerned with significant changes to large landscapes over short periods or to small features like bedforms over long periods (*Kleinhans et al.*, 2005).

At the scale of the entire Dutch coastal system (Figure 1.2a,b, $\mathcal{O}(100-1000km)$), the underlying geological setting and longer-term processes like sea level rise matter most. The location of individual islands and inlets in the Wadden Sea change on scales of decades to centuries, while the position of channels and shoals within those inlets may vary on a scale of months to years(Figure 1.2c,d, $\mathcal{O}(100m-10km)$). Bedforms like dunes and megaripples are smaller still, and vary accordingly on even briefer timescales (Figure 1.2e, $\mathcal{O}(0.01-100m)$). At the smallest scale, sand grains may move around in a matter of seconds (Figure 1.2f, $\mathcal{O}(0.01-1mm)$).

The general demand for sediment is determined at the largest scales (is there enough sand within the entire Dutch coastal system?), but the details of where it is placed depend on meeting coastal protection goals at a much smaller scale. However, it is still possible to meet both large and small-scale needs by nourishing carefully (*Elias*, 2021).

Human interventions like dredging or nourishments can shape coastal systems at multiple spatial and temporal scales, such that small changes may lead to widespread irreversible consequences (*Wang et al.*, 2015). A sustainable sediment management plan must therefore be carefully placed in context with the cascade of physical processes acting at all scales.

In addition to these conceptual gaps, we also lack the tools and techniques necessary to analyze and predict sediment transport pathways. We need ways to make sense of large bathymetric datasets, to characterize suspended sediment in mixed sand-mud environments, to monitor the dispersal of sand grains, to simulate sediment pathways, and a conceptual framework to manage all this information. This dissertation thus focuses on meeting the need for these new approaches.

[3] *"...dinosaurs riding stone galleons westward*
an inch a year for centuries
lived and died like sailors" – *Al Purdy* (1996)

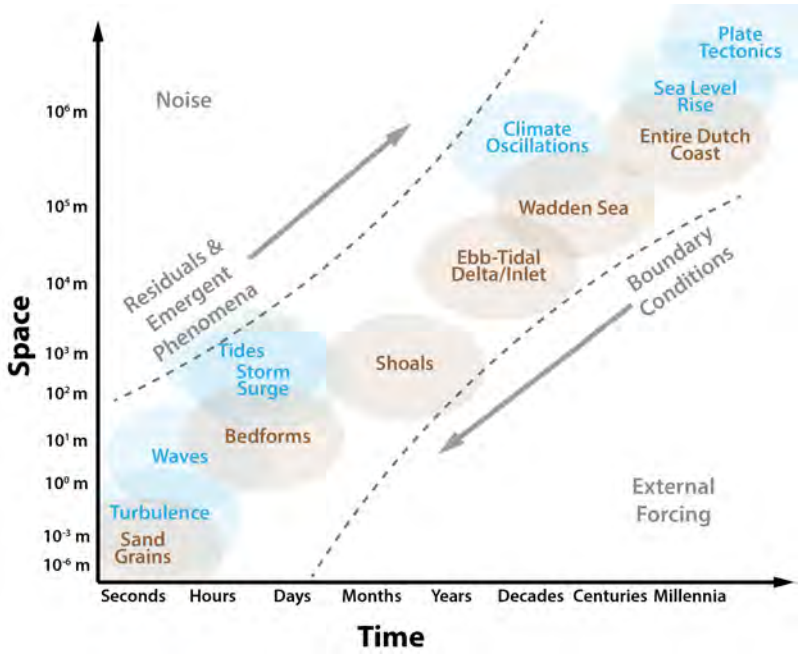

Figure 1.4: Overview of the scale cascade for the Dutch coastal system, adapted from *De Vriend* (1991); *Cowell et al.* (2003); *Vitousek et al.* (2017a). **Physical processes driving the system are labelled in blue** and **morphological features in brown**, although it should be noted that when and where a given phenomenon starts and ends is seldom clear-cut, and may span several orders of magnitude. Residual and emergent phenomena at smaller scales propagate upward to affect features at larger scales, while larger-scale phenomena serve as boundary conditions for smaller scales.

MAIN MOTIVATION FOR RESEARCH:

- Barrier coast systems like the Dutch Wadden Islands and Sea are vulnerable to coastal erosion and sea level rise
- To avert these threats while limiting ecological impacts may require strategic nourishments in a complex, dynamic environment (i.e., at tidal inlets and ebb-tidal deltas)
- There is insufficient knowledge of sediment transport pathways at these locations and across different space/time scales, making it a challenge to predict the fate of nourishments there
- In addition to this knowledge gap, we also lack the tools and approaches necessary to analyze and predict sediment pathways

1

1.5. RESEARCH APPROACH

To address these concerns, the Kustgenese 2.0 (*Coastal Genesis 2.0)* and SEAWAD projects (of which this dissertation is a part) were initiated (*Rijkswaterstaat*, 2020). An extensive field measurement campaign at Ameland Inlet was conducted in Fall 2017 (*Van Prooijen et al.*, 2020), and four PhD research projects at three Dutch universities were initiated, in partnership with the Dutch Ministry of Infrastructure (*Rijkswaterstaat*) and numerous other public and private institutions. These projects are focused on intra-wave sediment transport and wave transformation (*de Wit et al.*, 2019, 2020), bedform dynamics (*Brakenhoff et al.*, 2019a,b, 2020a), benthic ecology (*Holzhauer et al.*, 2020, 2021), and sediment transport pathways on Ameland ebb-tidal delta (this dissertation). Furthermore, a pilot ebb-tidal delta nourishment was constructed in 2018 and intensively monitored. The outcome of these projects will be used to inform Dutch coastal management policies and plans in the years to come.

The main goal of this dissertation is to identify and understand the pathways that sediment takes on an ebb-tidal delta, using the example of Ameland Inlet in the Netherlands. Resolving these matters requires the synthesis of multiple lines of evidence, by interpreting and combining field measurements with numerical simulations. Here we focus on the development of new tools and techniques for analyzing and interpreting sediment pathways on ebb-tidal deltas at varying space and time scales. The following tasks were carried out in response to these goals:

1. **Describe the historical morphological evolution of Ameland ebb-tidal delta.**
   Chapter 2 provides key background information on the project's main study site, Ameland inlet and ebb-tidal delta. In particular, we focus on historical bathymetry to understand how this area has evolved in the past on decadal timescales and spatial scales of $\mathcal{O}(100m - 10km)$. This gives us an understanding of what led to the present conditions and how the delta might behave in the future, using an unprecedentedly long and high-resolution historical dataset (from 1500 to the present). **Chapter 3** builds on that work, presenting a new approach to analyzing high-resolution bathymetric data which allows us to construct stratigraphic models and map the dynamics of ebb deltas in a more convenient coordinate system.
2. **Characterize hydrodynamics and suspended sediment on Ameland ebb-tidal delta.**
   In **Chapters 4** and **5**, we delve into the physical processes responsible for shaping the ebb-tidal delta by analyzing in situ (Eulerian) field measurements. To do so, we examine $\mathcal{O}(1 - 100\mu m)$-scale variations in particle size on the seabed and at a fixed point in the water column for several weeks (**Chapter 4**). This approach does not yield enough information to fully diagnose suspended sediment composition, so we then propose a novel indicator of relative optical and acoustic backscatter to measure mixed sediment in suspension (**Chapter 5**).
3. **Quantify sediment dispersal on the ebb-tidal delta using sediment tracers.**
   In contrast to **Chapters 4** and **5**, we next analyze Lagrangian measurements of tracer sediment (i.e., tracking the fate of individual sand grains as they move along the seabed). Via this approach we describe the spreading and sorting behaviour of sand on the ebb-tidal delta in **Chapter 6** from individual grains up to the scale of a nourishment ($\mathcal{O}(100m - 1km)$).

4. **Define conceptual framework for systematically quantifying sediment transport pathways in coastal environments.**
   Using existing approaches to systematically analyze sediment pathways is challenging, so in **Chapter 7** we present the graph theory-based conceptual framework of coastal sediment connectivity. By schematizing coastal systems as a series of connected networks, we visualize complex transport patterns and provide new quantitative metrics for analysis. Furthermore, it allows us to transcend the different scales, using detailed process-based models ($\mathcal{O}(100\mu m)$) to compute sediment pathways across the entire ETD ($\mathcal{O}(1-10km)$) and quantify the patterns that emerge. At this scale, we can better inform coastal management and policy.
5. **Develop Lagrangian sediment transport model and visualization tool to predict sediment transport pathways.**
   To move from a descriptive to predictive analysis of sediment pathways, we develop and test a numerical sediment tracer model in **Chapter 8**. This approach greatly expands the visualization and analysis potential for existing coastal sediment transport models, particularly when used in conjunction with connectivity.

The dissertation concludes with a synthesis of the key findings, research impacts, and future outlook in **Chapter 9**.


Amelander gadt
Middel plaet
Coggedieps rif
of gronden
Greetings from beautiful
AMELAND
Inlet & Ebb-Tidal Delta!

Dear Reader,

In order to figure out how the coast will evolve in the future, we need to learn more about what it did in the past and what it is doing today. We started by looking at lots of old maps. We then went with a huge team to Ameland to take measurements of the waves, tides, sand, mud, and more. Let's see what we can do with all this information!

Stuart

Delft University of
Technology
Stevinweg 1
2628 CN Delft

2

AMELAND INLET & EBB-TIDAL DELTA

KEY POINTS:

- Ameland Inlet connects the Dutch Wadden Sea with the North Sea, and features a large deposit of sand at its seaward side, the ebb-tidal delta
- Over 400 years of bathymetric surveys paint a rich portrait of the ebb-tidal delta's morphological evolution
- The inlet is a mesotidal, mixed-energy system ($\Delta\eta_{tidal} \approx 2.5m$, $H_s \approx 1.4m$) heavily influenced by the wind
- The ebb-tidal delta consists mainly of well-sorted fine sand
- To quantify all of this, a field measurement campaign was undertaken at the site in 2017 as part of the Kustgenese 2.0/SEAWAD project.

Parts of this chapter have been published in the following articles and reports, to which the author made substantial contributions:

Elias, E.P.L., van der Spek, A.J.F., **Pearson, S.G.**, & Cleveringa, J. (2019). *Understanding sediment bypassing processes through analysis of high-frequency observations of Ameland Inlet, the Netherlands.* Marine Geology. [Link]

Elias, E.P.L, **Pearson, S.G.**., van der Spek, A., & Pluis, S. (*In press*). *Understanding meso-scale processes at a mixed-energy tidal inlet: Ameland Inlet, the Netherlands — implications for coastal maintenance.* Ocean & Coastal Management.

Pearson, S.G., Tonnon, P.K. (2018). *Kustgenese 2.0; overview of available sediment data at Ameland inlet, The Netherlands*: Deltares report 1220339-007-ZKS-0003.

van Prooijen, B.C., Tissier, M.F.S., de Wit, F.P., **Pearson, S.G.**, et al. (2020). *Measurements of Hydrodynamics, Sediment, Morphology and Benthos on Ameland Ebb-Tidal Delta and Lower Shoreface.* Earth System Science Data. [Link]

2

IN order to address the general problem of describing and quantifying the pathways that sediment takes on an ebb-tidal delta, this dissertation considers the example of Ameland Inlet in the Netherlands. In this chapter, we examine how the shape of the ebb-tidal delta and the size of the sand grains within it vary in space and time. We begin by considering the field measurements carried out as part of the SEAWAD and Kustgenese 2.0 projects, in order to set the stage for the rest of the dissertation. We examine historical maps and grain size data to understand how Ameland Inlet and ebb-tidal delta have evolved in the past and what they look like today. This is followed by an introduction to the hydrodynamic forcing that shapes the delta: waves, tides, wind-induced flows, and freshwater input. Lastly, we consider the contributions of other studies within SEAWAD and Kustgenese 2.0, to put them in context with this dissertation. The challenges faced in predicting the future evolution of ebb-tidal deltas are formidable, but the wealth of data available from Ameland provides us with a solid foundation on which to build future developments.

2.1. INTRODUCTION

The entire Dutch coast has been heavily modified over the last 1000 years, and these works intensified during the 20th century, dramatically altering the landscape. Most of the estuaries in the south and north parts of the country have been utterly transformed via damming or dredging as part of flood defense or navigation works. By contrast, Ameland Inlet has been relatively untouched in recent decades, with only minor shore protection works along its east side. Flanked by the barrier islands of Ameland and Terschelling, Ameland Inlet was selected for further study since it was thought to exhibit more natural dynamics than the other inlets. Furthermore, extensive field measurements of waves (*Zijderveld and Peters*, 2009; *van Dongeren et al.*, 2011) and bathymetry (*Elias et al.*, 2019) provided a solid basis for further analysis.

The raw brutality of waves and currents colliding on ever-shifting shoals have left tidal inlets with a well-deserved reputation for being difficult and expensive places to collect field measurements (*Van Prooijen et al.*, 2020). Unfortunately, it is this brutality that we are most interested in quantifying, and yet these observations are few and far between (e.g., *Elias et al.* (2012b); *Salles et al.* (2015); *Bertin et al.* (2020)). High-quality measurements of hydrodynamics and suspended sediment are essential for calibrating and validating numerical models. Even though remote sensing brings many promising opportunities for frequent, long-term spatial measurements of ebb-tidal delta dynamics (e.g., *Pianca et al.* (2014); *Ridderinkhof et al.* (2016); *Ford and Dickson* (2018); *Zhang et al.* (2020a)), crucial aspects of hydrodynamics, sediment transport, and subtidal morphological change are not yet adequately captured. There is thus a need for detailed *in situ* measurements of the physical processes acting in these environments.

To respond to this need, the Dutch government (*Rijkswaterstaat*) initiated the Kustgenese 2.0 research program in collaboration with Deltares. Part of this program was an extensive field campaign at Ameland Inlet in the Netherlands in Fall 2017 (Figure 2.1). This campaign was carried out in close collaboration with the universities of Delft, Utrecht and Twente, via the SEAWAD project. Hydrodynamics, bathymetry, salinity, sediment composition, and benthic species distribution were measured at various locations on the ebb-tidal delta, in the inlet gorge and in the basin.[1]

[1]The Kustgenese 2.0/SEAWAD datasets obtained in 2017 and 2018 are accessible via https://doi.org/10.4121/collection:seawad. The repositories include the raw and processed data as well as relevant metadata and processing scripts.

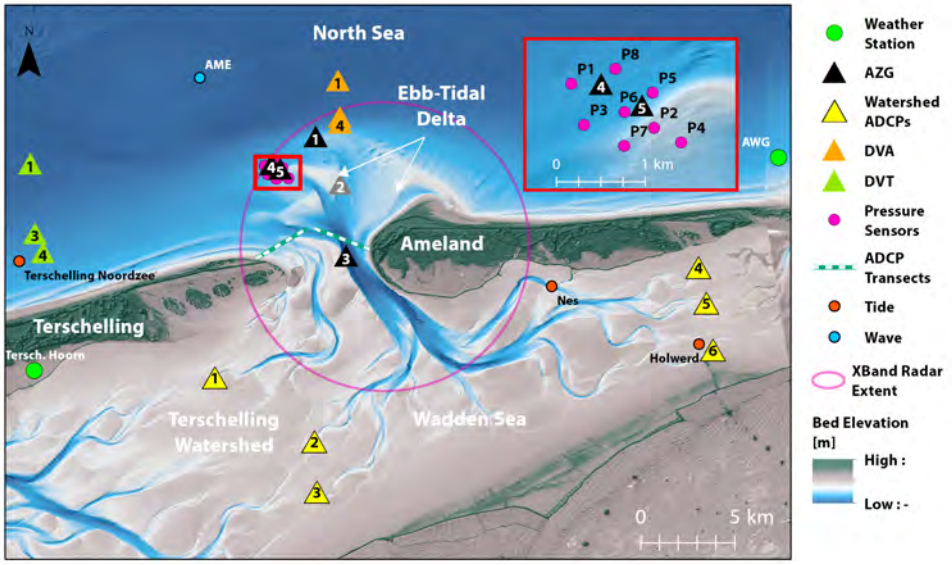

Figure 2.1: Locations of hydrodynamic, sediment, and atmospheric measurements carried out during the Kustgenese field campaigns in 2017-2018 (AZG = *Amelander Zeegat*, DVA = *Diepe Vooroever Ameland*, DVT = *Diepe Vooroever Terschelling*). Modified from *Van Prooijen et al.* (2020).

The *Amelander Zeegat* (AZG) campaign spanned August until October 2017, and featured four measurement frames across Ameland Inlet and ebb-tidal delta. These frames featured a host of instruments measuring hydrodynamics and water quality, some of which are analyzed in later chapters of this dissertation (Chapters 4, 5, & 6). In addition, pressure sensors were deployed to measure wave transformation at the seaward edge of the delta. To monitor exchange with adjacent regions of the Wadden Sea, water level and current velocity measurements were taken along the Terschelling and Ameland tidal divides (watersheds). In addition to these stationary (Eulerian) measurements, Lagrangian measurements of tidal currents and sediment were made via drifters and tracers (Chapter 6), respectively. Discharge measurements were taken at transects across the inlet, and the site was continuously monitored via an X-Band radar station located in the lighthouse at the western tip of Ameland (*Gawehn et al.*, 2020). Together, these measurements provide a detailed glimpse at the dynamics of Ameland ebb-tidal delta.

2.2. MORPHOLOGICAL EVOLUTION

Bathymetric surveys of Ameland date back to over 400 years, beginning with crude navigational charts made in the 1500s (Figure 2.2). These charts indicate morphological features that persist to the present day, including the main Borndiep channel and Bornrif swash platform and shoal complex. The configuration of channels and shoals reveal many changes during this period, but because of the limited accuracy of these maps and the long intervals between surveys, it is difficult to assemble a continuous narrative of morphodynamic change from them.

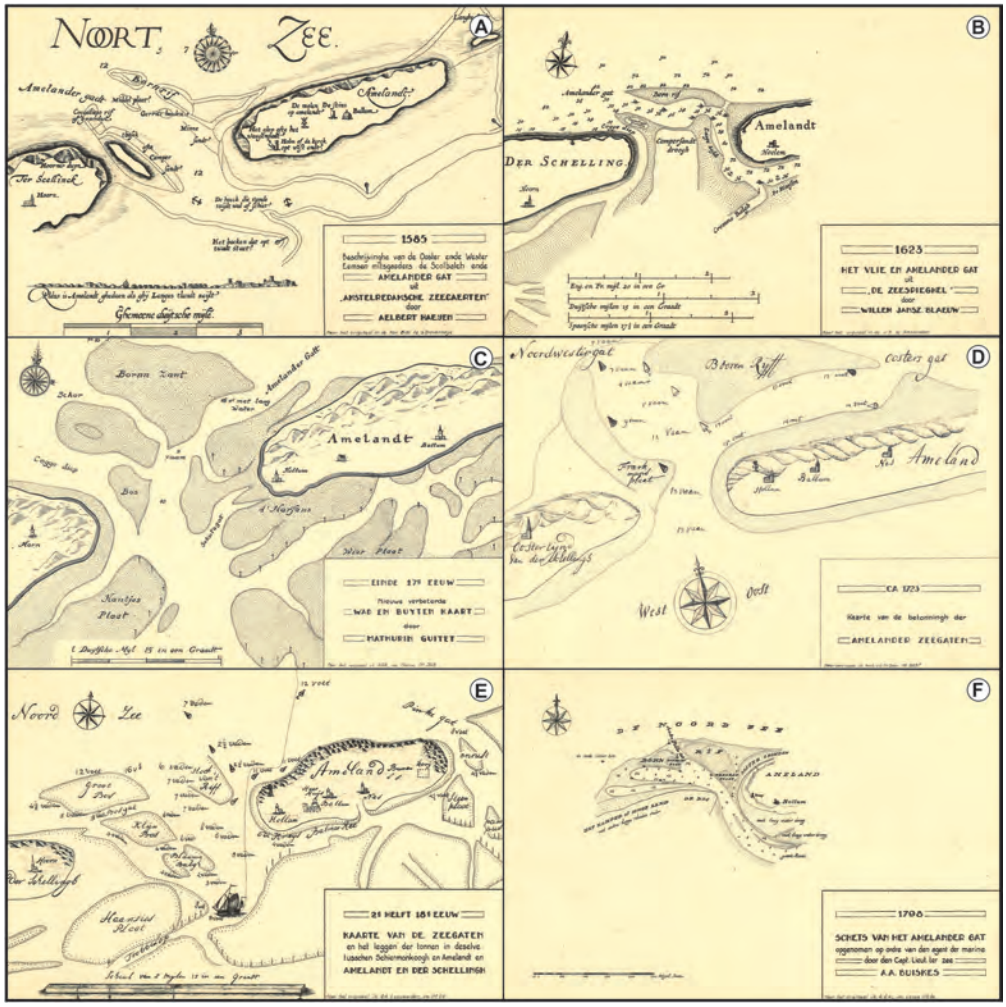

Figure 2.2: Compilation of bathymetric charts of Ameland Inlet for the years (a) 1585, (b) 1623, (c) end of the 17th century, (d) 1723, (e) second half of the 18th century, and (f) 1798. Source: *Elias et al.* (2019).

The quality of mapping improved in the 1800s and early 1900s, when the inlet was surveyed by the Hydrographic Service of the Royal Netherlands Navy (Figure 2.3). In more recent years (Figures 2.4, 2.5, & 2.6), the inlet has been regularly surveyed as part of Rijkswaterstaat's *Vaklodingen* monitoring program.

A geomorphic transition in morphodynamics occurred around 1926, as the main ebb-channel migrated from an updrift to a downdrift position in the inlet gorge. The change in channel position and stability fundamentally changed the ebb-tidal delta dynamics and sediment bypassing behaviour. The sediment bypassing process changed from outer channel shifting to main ebb-channel switching, as the Westgat took prominence over the Akkepollegat.

The large influence of the ebb-tidal delta dynamics on the shoreline response of the updrift and downdrift sides of the inlet is clearly identified. Growth and decay (net erosion) of the island tip of the updrift island (Terschelling) occurs, while sequences of sediment bypassing result in shoal attachment to the downdrift coastline of Ameland.

No clear evidence exists that a long-term morphodynamic cycle occurs on the scale of Ameland Inlet. Instead, morphodynamic changes start with the accumulation of sediment in various places until tipping points are reached. The mechanisms pushing the ebb-tidal delta towards these tipping points are repetitive. These accumulations tend to repeat in similar areas but are never exactly the same, so we never get a true cycle.

Shoal instabilities are initially small morphodynamic changes and would not be considered to affect the ebb-tidal delta and inlet dynamics as a whole, but as shown in Figures 2.5 and 2.6, they can trigger a new sediment bypassing cycle and result in complete relocation of ebb-tidal delta scale channels and shoals. Such subtle dynamics are difficult to capture in the existing conceptual models and empirical relationships. These differences are however essential for understanding tidal inlet and channel morphodynamics and hence coastal management.

The morphodynamic behaviour of Ameland Inlet is described extensively by *Elias et al.* (2019) and *Elias et al.* (2022), and is interpreted in greater depth in Chapter 3 of this dissertation.

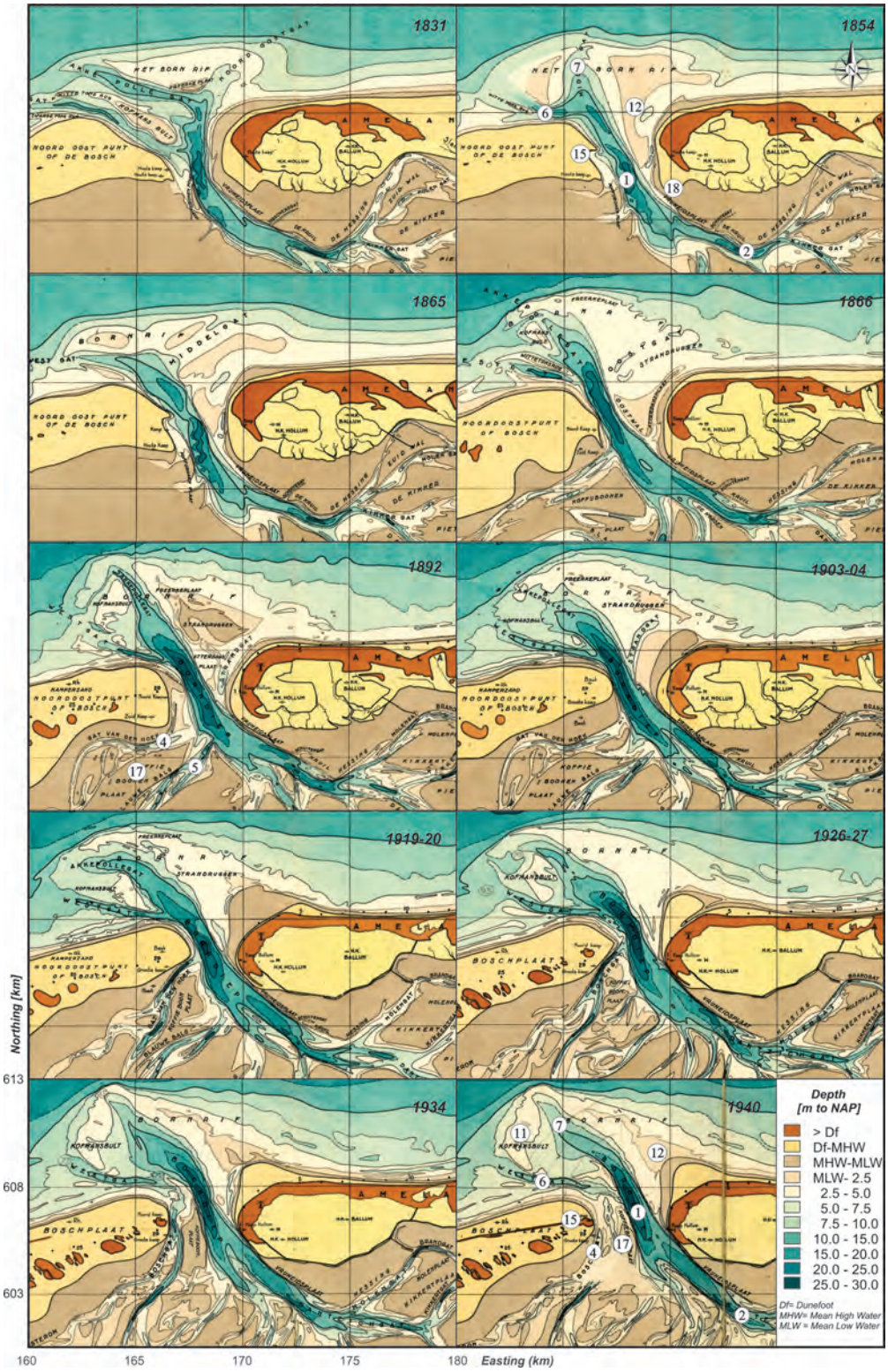

Figure 2.3: Bathymetric charts of Ameland Inlet for the period 1831-1940. See *Beckering Vinckers* (1943) for a detailed description of the charts. Source: *Elias et al.* (2019).

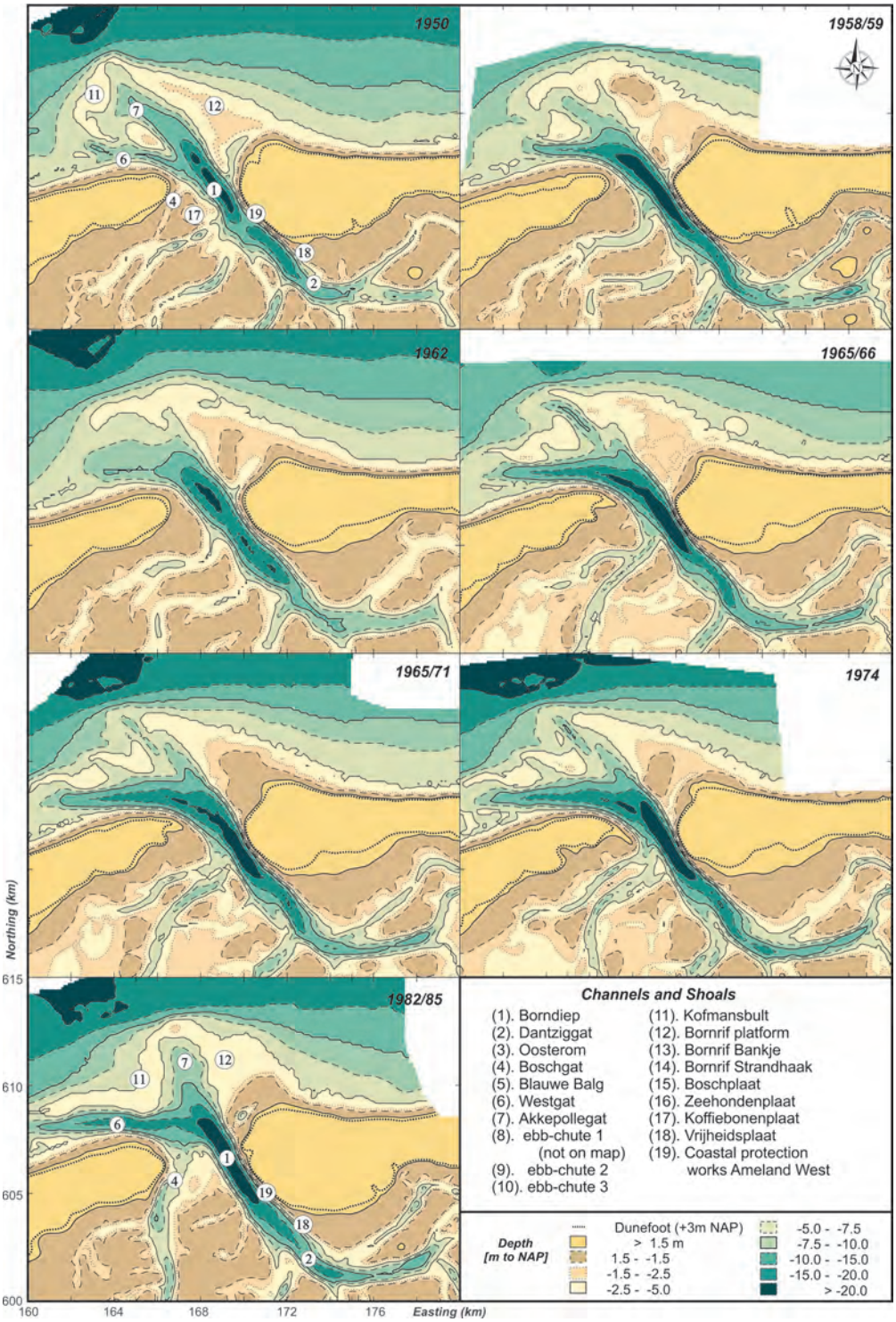

Figure 2.4: Bathymetric charts of Ameland Inlet for the period 1950-1982/85. Based on digitized contour lines of the bathymetric charts (*Verhoeff*, 2018). Major channels and shoals are indicated with numbers. Source: *Elias et al.* (2019).

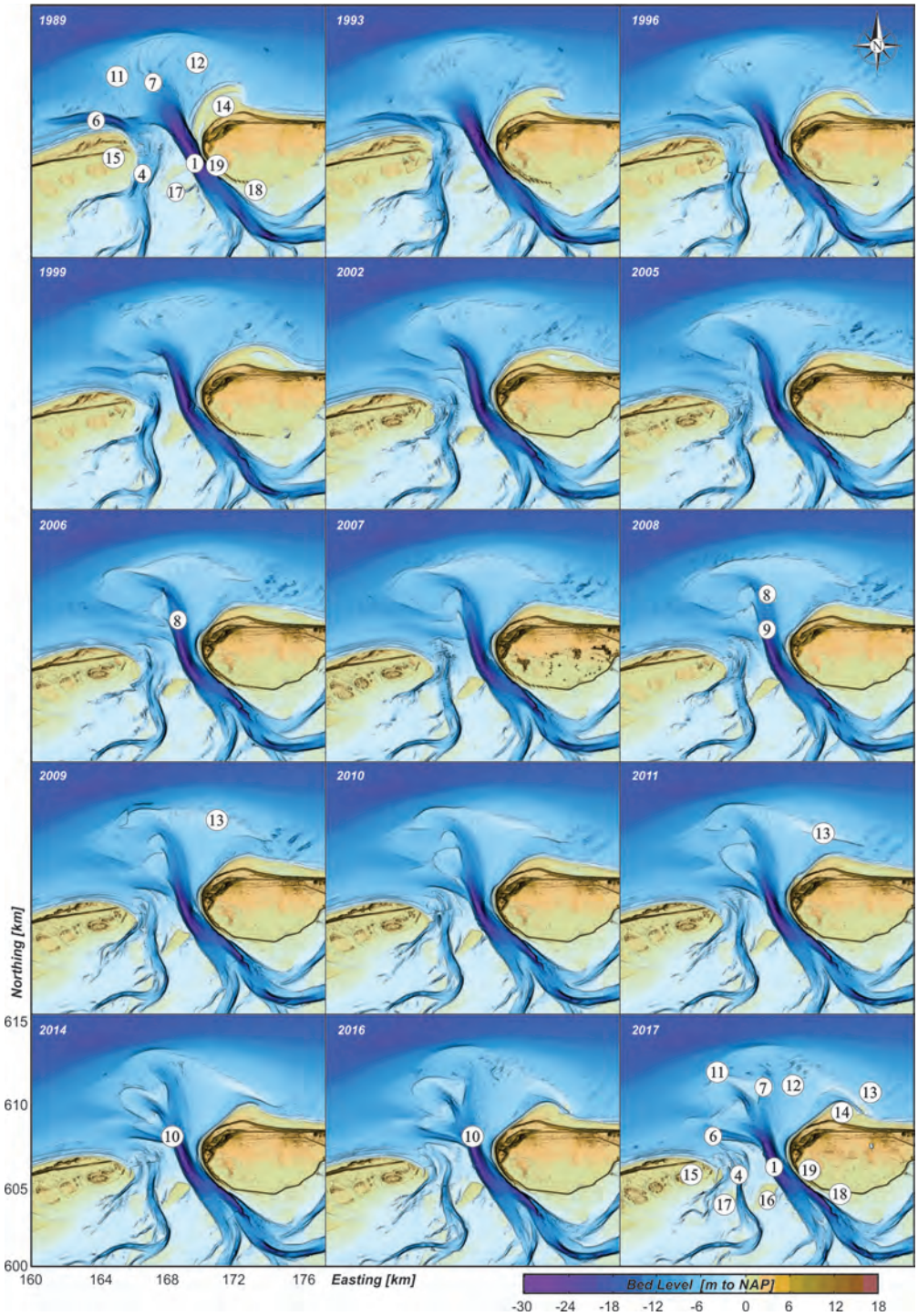

Figure 2.5: Complete digital elevation models of the ebb-tidal delta based on measurements from 1989-2017. Numbers corresponding to major channels and shoals are indicated in Figure 2.4. Source: *Elias et al.* (2019).

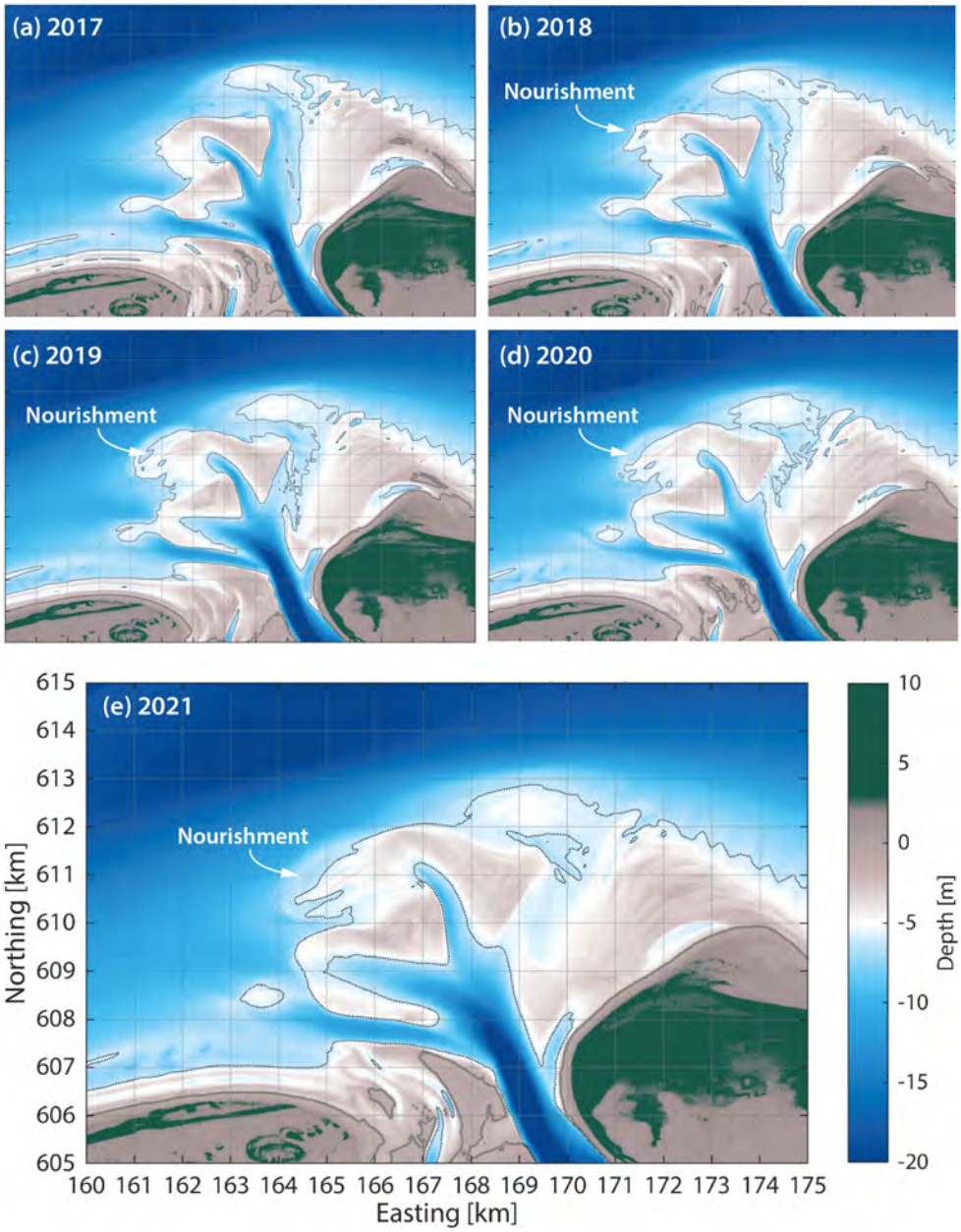

Figure 2.6: Complete digital elevation models of the ebb-tidal delta based on measurements from 2017-2021, featuring the ebb-tidal delta nourishment. The approximate mean low water level (MLW) contour of the z_{mean} at -1.4 m NAP (*Normaal Amsterdams Peil,* approximately mean sea level) is represented with a thick grey line, and the -6 m NAP depth contour is indicated with a thin dashed line. Modified from *Elias et al.* (2022).

2.3. SEDIMENT CHARACTERISTICS

2.3.1. EARLY SEDIMENT SAMPLES

Ameland Inlet has been subject to several grain size measurement surveys in the past three decades (*Rijkswaterstaat*, 1999; *Leopold and Baptist*, 2016; *Compton et al.*, 2013), which together paint a fairly consistent picture of the site's sediment composition.

The surface sediment of Ameland ebb-tidal delta is overwhelmingly composed of fine sand ($126 < d < 250\mu m$); the same is true for much of the nearby Wadden Sea and area immediately offshore. The seabed of the main channel (Borndiep) and the Boschplaat region largely consist of medium sand ($250 < d < 500\mu m$). This is reflective of the higher energy conditions observed there. A landward fining trend is observed, with the d_{50} decreasing towards the rear of the basin, where calmer conditions prevail.

The presence of mud (silt and clay, $d < 63\mu m$) influences the erodibility of seabed sediment. Mud content is highest in intertidal areas along the mainland coast of Friesland and Groningen, as well as along tidal divides. However, mud can also be found in deeper regions offshore and at the distal edge of the ebb-tidal delta where conditions are less energetic.

Observable differences in the median grain size between 1995 (*Rijkswaterstaat*, 1999) and 2001 (*Leopold and Baptist*, 2016) surveys may be related to bathymetric changes during the intervening period. The ebb-tidal delta is a highly dynamic region, and as it evolves, so too will the processes acting on a given location and its sedimentological response. Seasonal trends were not possible to discern because of low temporal resolution and inconsistencies in sample locations between datasets.

2.3.2. KUSTGENESE 2.0 SEDIMENT SAMPLES

In order to have an updated map of sediment characteristics coinciding with field measurements for the Kustgenese 2.0 project, additional samples were taken in September 2017. To determine seabed sediment composition and benthic ecological communities, boxcores were taken across the inlet and ebb-tidal delta. The locations were chosen based on a series of sixteen morphological units, defined by depth, slope, orientation and morphological activity (*Holzhauer et al.*, 2021). In such a way, morphologically representative coverage of the entire site was obtained, using a relatively limited (165) number of cores. Sampling of shallower locations took place with a circular Reineck box corer from September $4^{th} - 5^{th}$, and deeper locations from September $20^{th} - 21^{st}$, 2017. Sediment samples were taken from the surface of the box core and their grain size distribution analyzed with a Malvern Mastersizer, resulting in a sediment distribution with 67 bins ranging from $0.01\mu m - 2000\mu m$.

As in earlier surveys, the median grain size (d_{50}) of Ameland ebb-tidal delta is very homogeneous, with 79% of samples between $170 - 230\mu m$ (Figure 2.7a). When plotted on a polar grid (See Chapter 3), it becomes apparent that sediment fines in a clockwise direction (θ) and away from the inlet (ρ). The variance and envelope of d_{50} also decrease steadily in a clockwise direction and with distance from the inlet. The coarsest samples tend to be found in deeper channel areas near the inlet, where tidal currents are persistently strong ($> 1m/s$). The mud content is < 1% for 81% of samples, and the only samples with > 1% mud content are located in deeper channel areas and the distal edge of the ebb-tidal delta (Figure 2.7b). Visual inspection of boxcores suggests that the mud within samples from the channel consists of lumps of consolidated clay that were eroded from older deposits and transported as bed load. Conversely, mud in the distal samples was likely freshly deposited after Storm Sebastian (September 12-16, 2017), several days prior to their collection.

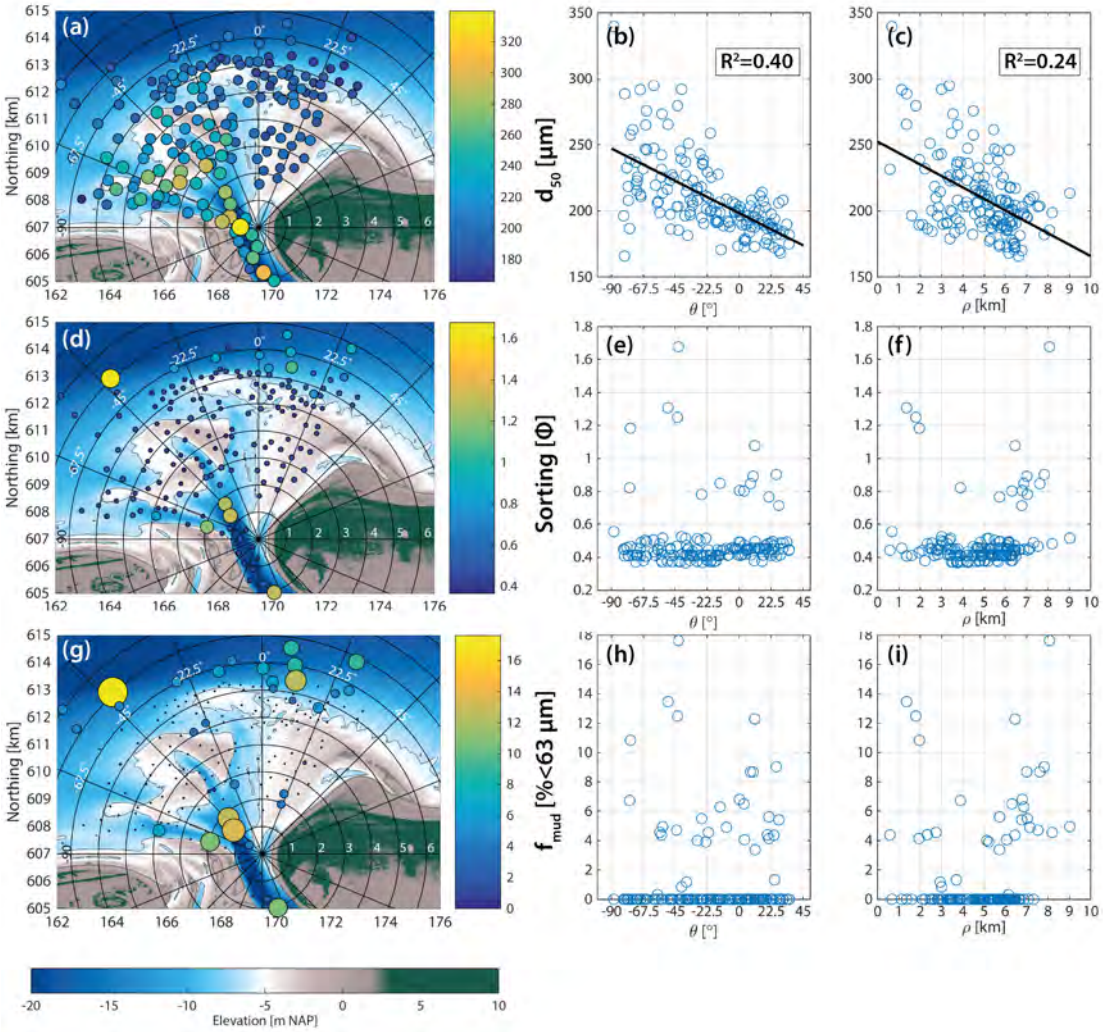

Figure 2.7: (a-c) Overview of the median grain size (d_{50}), (d-f) sediment sorting and (g-i) fraction of mud in the bed (f_{mud}, defined as sediment with $d_{50} < 63\mu m$). The right two columns indicate relation of the sediment parameter with clockwise direction relative to north (θ) and distance from inlet (ρ). Modified from *Elias et al.* (2022).

There is no trend in sorting with either ρ or θ (Figure 2.7ac), but 80% of samples are well-sorted ($0.35 < \sigma < 0.5$ based on the Logarithmic Folk and Ward graphical measure (*Blott and Pye*, 2001). Moderately sorted samples ($0.5 < \sigma < 1$) tend to be located on the distal edge of the delta, while the most poorly sorted samples ($\sigma > 1$) are mainly found in the channels. The body of the ebb-tidal delta is overwhelmingly well-sorted fine sand.

These observations may be explained by breaking waves, which promote sorting of the sand by the continuous resuspension, resulting in well-sorted deposits on the distal (wave-dominated) portion of the ebb-delta. In channels, all sizes are transported, from clay flocs to stones, and finer fractions settle on slack tide. These may get buried under new deposits, resulting in poor sorting there.

2.4. HYDROMETEOROLOGICAL CHARACTERISTICS

2.4.1. TIDE

Semi-diurnal tidal motion is the main driving force behind the water flow through Ameland Inlet (Figure 2.8). Long-term observations of water levels at the nearby West Terschelling station show that the semi-diurnal tide has a dominant M2 constituent with an amplitude of 0.77 m. Distortion of the M2 tide due to shallow water effects results in a significant asymmetry and faster rise than fall of the tide (flood dominance). A considerable spring-neap variation results from an S2 amplitude of 0.20 m. At the nearby Terschelling Noordzee station (Figure 2.1), the tidal range varies from 1.2 m at neap to 2.5 m at spring (Figure 2.8b). The tide is amplified within the Wadden Sea, increasing the maximum range to nearly 3 m at Nes.

The tidal signal represents only part of the measured water levels. Meteorological distortion due to air pressure variations and wind-generated setup or set-down can reach significant heights along the Dutch coast (Figure 2.8c). Setup gradients can drive complicated residual flow fields over the complex bathymetry of the Wadden Sea, generate shore-parallel velocities and throughflow between adjacent basins (*Duran-Matute et al.*, 2014; *Van Weerdenburg et al.*, 2021). In addition, the increased volume of water stored in the Wadden Sea due to the larger setup can considerably enhance the outflow velocities in the inlets following the storm events, thereby affecting channel dimensions, the ebb-tidal delta development and adjacent beaches (*Koch and Niemeyer*, 1978; *Krogel*, 1995; *Elias et al.*, 2006). Measurements of the mean sea level over the last 150 years reveal an increase of around 0.20 m at the nearby tidal gauge of West Terschelling.

Tidal motions drive a significant flow through the inlet gorge. Measurements of discharge have been taken frequently in transects across the inlet gorge by roving 13-hour ship measurements, and on average, ebb- and flood volumes through the inlet are approximately $400-500\times10^6 m^3$ (*Elias et al.*, 2019). The two most recent measurements have small ebb residuals that are less than 10 % of the gross ebb and flood volumes. The observed peak ebb- and flood-tidal velocities are around 1 m/s in the central Borndiep channel.

2.4.2. WAVE & WIND CLIMATE

The wave climate at Ameland Inlet is relatively mild, based on 10 years of measurements from a buoy located just northwest of the ebb-tidal delta (Figure 2.9b, see Figure 2.1 for location). Typically, significant wave heights (H_s) are below 2 m (83% of the record), and only during severe storms can wind-generated significant wave heights occasionally reach

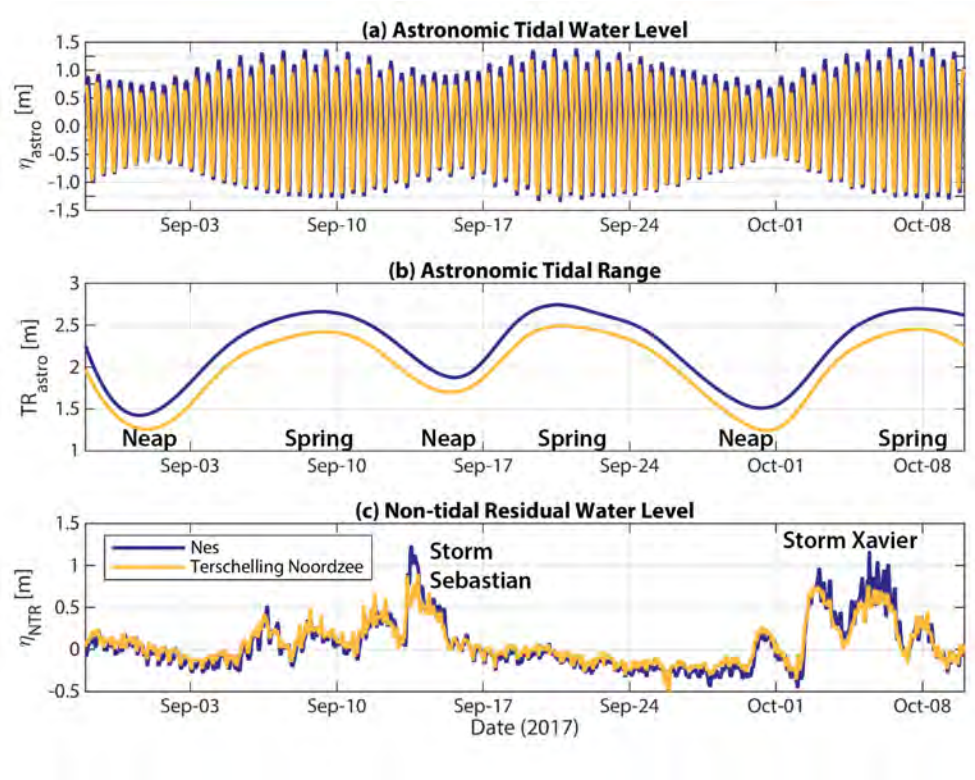

Figure 2.8: (a) Water surface elevation due to astronomic tide, (b) astronomic tidal range, and (c) non-tidal residual water levels in September 2017 near Ameland Inlet. Terschelling Noordzee is located 16 km west of the inlet on the North Sea coast of Terschelling, while Nes stations is located 15-20 km east of the inlet within the Wadden Sea (see Figure 2.1 for exact locations). All water levels are referenced with respect to NAP, approximately mean sea level.

values between 4.5 and 9.1 m (less than 1% of the record). The mean significant wave height is 1.37 m with a corresponding peak wave period of 7.2 s.

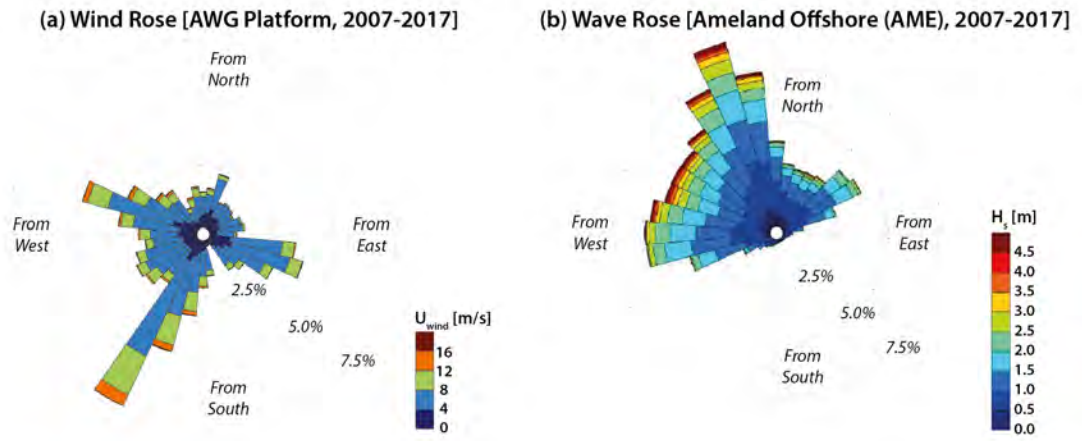

Figure 2.9: (a) Wind rose for AWG Platform based on data from 2007-2017. (b) Wave rose for Ameland Offshore station (AME) based on data from 2007-2017. See Figure 2.1 for measurement locations. Modified from *Elias et al.* (2019, 2022).

The dominant wind and wave directions differ considerably (Figure 2.9). The largest and most frequent winds occur from the southwest, a direction hardly present in the wave record due to the sheltering of the mainland and the barrier islands. Roughly 33% of the wave directions lie between west-southwest and north-northwest ($235^o - 305^o$). Most waves (62%) are from directions between north-northwest and east ($305^o - 90^o$). The remaining 4% is offshore directed and do not significantly contribute to sediment transport. Wave periods ($T_{1/3}$) typically vary between 3 to 6 seconds for lower wave conditions (89% of the measurements). For typical storm waves (H_s = 2-3 m) a mean wave period of 6.0 s occurs, increasing to 7.6 s for severe storms (H_s > 4m). Contributions of swell are minor. Wave periods over 9 seconds are only measured occasionally (0.1 % of the record). The short-wave periods indicate that the wave climate is dominated by wind waves generated in the North Sea basin.

In general, the shallow ebb-tidal delta is considered to act as a natural breakwater for the adjacent shorelines and effectively prohibits wave propagation from the North Sea into the basin. Refraction and wave breaking on the shoals (especially during the high wave-energy events with large morphodynamic impact) and wave blocking by the supra-tidal shoal areas modify and distort the nearshore wave climate (*Hine*, 1975; *FitzGerald*, 1988; *Elias and Hansen*, 2013). *Elias et al.* (2022) show that wave heights measured at the distal region of the ebb-tidal delta are noticeably reduced compared with offshore waves. Furthermore, they observe a strong tidal modulation in wave height associated with wave-current interaction (waves tend to be amplified by opposing ebb-currents (*Elias et al.*, 2012b; *Dodet et al.*, 2013)). Larger waves on the delta generally coincide with higher water levels.

2.4.3. FRESHWATER INFLOW

Owing to a long history of anthropogenic intervention, Ameland Inlet has been almost completely cut off from direct fresh water input. Several small sluices discharge water from polders on the Wadden Islands and mainland, but as a consequence of widespread dike construction (*van der Spek*, 1995) and tidal basin closures *de Jonge et al.* (1993), most nearby land drains into either Lake IJssel or Lauwersmeer. The Rhine River plume travels along the coast and is the primary, albeit indirect, contributer of fresh water to the Wadden Sea (*de Jonge et al.*, 1993).

Early research on discharge from Lake IJssel to the Wadden Sea concluded that most of the freshwater travels out via the Vlie and Marsdiep inlets (*Zimmerman*, 1976). However, numerical modelling studies by *Duran-Matute et al.* (2014, 2016a) suggest that there are actually significant wind-induced flows across these watersheds, leading to exchange of water between adjacent sub-basins.

Salinity was measured in 2017 at AZG Frame 3, 14 m deep in the main inlet channel (Figure 2.10a). Salinity typically varies between 25 to 33 PSU at the inlet, which is similar to the range of 22 to 35 PSU observed by *van Aken* (2008a) on the Dutch coast at Texel from 1976 to 2003. Semidiurnal (M2) variations in salinity were captured, corresponding with advection of slightly fresher water from the Wadden Sea to the saltier North Sea. This variation approximately doubles at spring tide. Salinity on the ebb-tidal delta (at AZG Frame 4, 8 m deep) varies much less, between 30 to 33 PSU.

Between September 11 to 14, there is a pronounced drop in salinity at the inlet to almost 20 PSU (Figure 2.10a). This decrease is uncorrelated with local rainfall or discharge from the nearest sluice at Kornwerderzand, 45 km away (Figure 2.10b,c). However, in the days before and during the salinity drop, it is spring tide (Figure 2.8b) and there is a sustained wind from the southwest (Figure 2.10c,d). This leads to a steady net flux of water over the Terschelling tidal divide towards Ameland (Figure 2.10e). On September 13, Storm Sebastian peaks and there is an abrupt increase in flux over the tidal divide, associated with a high storm surge (Figure 2.8c). At this point, the discharge sluices are shut, and much of the freshwater lingering in the Ameland basin appears to be flushed out. After September 14, salinity in the inlet resumes its oscillation between approximately 28-32 PSU.

Seawater temperature was also measured during this period at Frames 3 and 4 (Figure 2.10a). Over the month of September 2017, there is a steady decline in the average temperature from 19^oC to 16^oC, which is consistent with typical observations for September at the nearby Marsdiep (*van Aken*, 2008b). Superimposed on this is a semidiurnal (M2) variation in temperature associated with colder water from the Wadden Sea moving out and in of the inlet. The shallower Wadden Sea is much quicker to respond to changes in the ambient air temperature than the North Sea, so it tends to be relatively cooler at this time of year. There is almost no variation in the inlet for the first week of the deployment, but later temperatures varied semidiurnally by as much as 2^oC on a single tide. The observed variation nearly doubled at spring tide. Temperature on the ebb-tidal delta varies much less than in the inlet, seldom changing by more than 1^oC on a given tide.

To examine the potential for baroclinic conditions, the horizontal buoyancy gradient $\partial b/\partial x$ was calculated as per *Becherer et al.* (2015) from the time-varying difference between buoyancy $b = -g(\rho_w - \rho_0)/\rho_0$ measured at Frame 3 in the inlet and Frame 4 on the ebb-tidal delta (approximately 5.8 km apart). ρ_0 is the reference density estimated as $1000 kg/m^3$, and seawater density (ρ_w) was calculated from salinity, temperature, and pressure observations

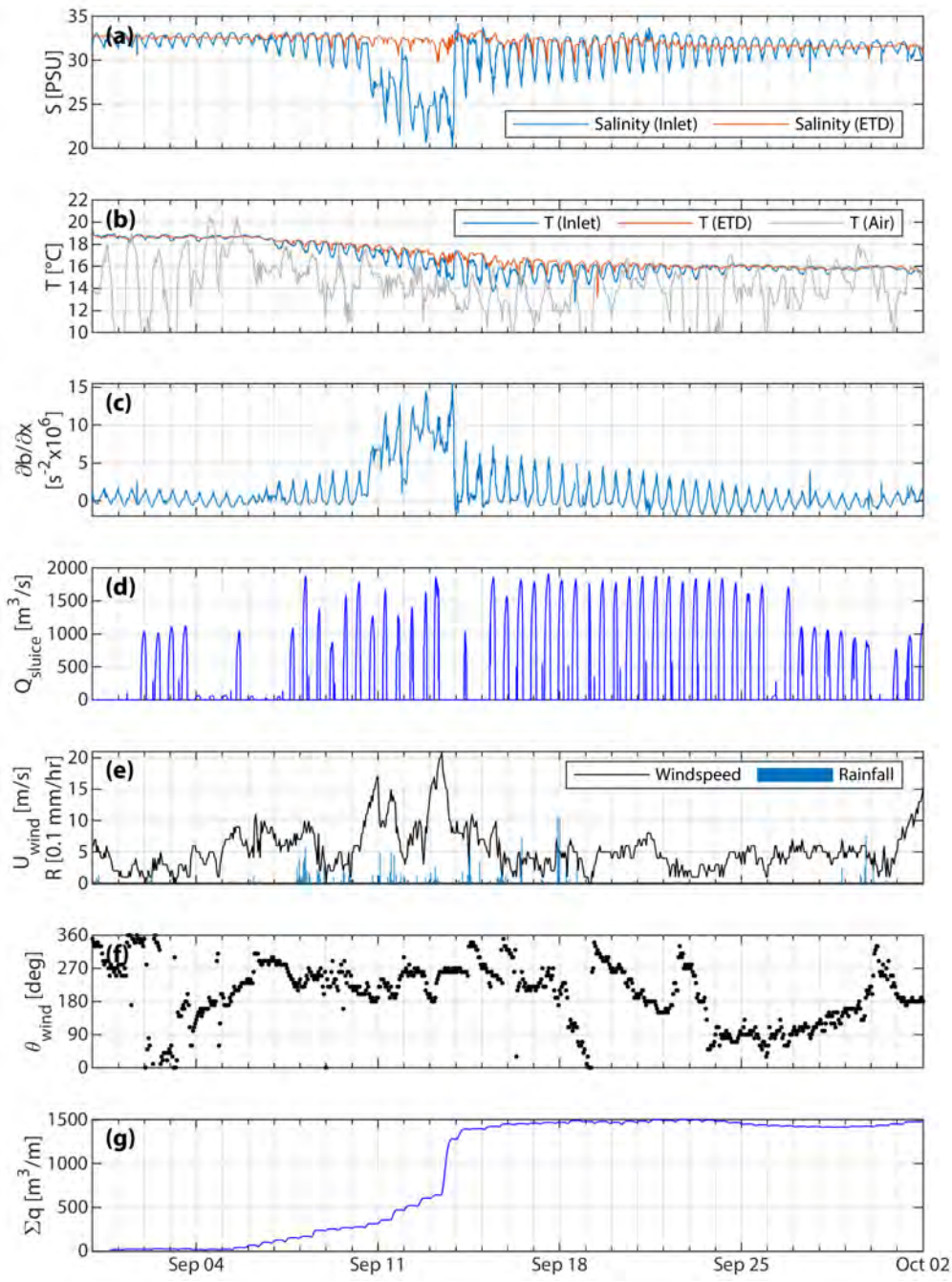

Figure 2.10: Relationship between salinity and meteorological forcing at Ameland Inlet. (a) Salinity (S) at AZG Frames 3 (14 m deep, on the west side of the main inlet channel) and 4 (on the ebb-tidal delta), Figure 2.1). (b) Water temperature (T) at AZG Frames F3 & F4 and air temperature at West Terschelling. (c) Horizontal buoyancy gradient $\partial b/\partial x$ between F3 and F4. Positive values indicate a "classical" estuarine configuration with less dense water on the landward side of the system. (d) Freshwater discharge from the sluices at Kornwerderzand, 45 km southwest of Ameland Inlet. (c) Windspeed and precipitation at West Terschelling. (d) Wind direction at West Terschelling. (e) Cumulative water flux q (depth × velocity) in principle flow direction (NW) over the Terschelling tidal divide, measured by Watershed ADCP 3 (Figure 2.1).

using the Gibbs Seawater Oceanographic Toolbox (*McDougall and Barker*, 2017). There is generally a positive gradient, which corresponds to "classical" estuarine conditions, where density is greater over the ebb-tidal delta than within the inlet. However, sometimes this gradient is reversed at flood tide.

$\partial b/\partial x$ is strongest during the period of freshwater inflow between September 11-13, but shows semidiurnal variations of up to $5s^{-2}$ in the weeks that follow. These values are comparable in magnitude with horizontal buoyancy gradients observed at other tidal inlets in the German and Danish Wadden Seas (*Becherer et al.*, 2011; *Purkiani et al.*, 2016). During the deployment period, $\partial b/\partial x$ largely responds to changes in salinity rather than temperature. However, this sensitivity may be seasonal, as the similar Otzumer Balje inlet in the German Wadden Sea showed a stronger dependency on temperature (*Becherer et al.*, 2016).

These data support the numerical simulations of *Duran-Matute et al.* (2014, 2016a), suggesting that the presence of freshwater is relatively minor at Ameland Inlet and strongly influenced by wind conditions. The exchange of fresh water with the Wadden Sea may lead to baroclinic exchange processes within the inlet. This hypothesis is supported by the presence of estuarine fronts, which are ubiquitous in aerial imagery (e.g., Figure 4.5) and appear as abrupt jumps in salinity on the ebb-tidal delta (Figure 2.10a). These fronts mark the transition between water masses with different properties (i.e., salinity, temperature, turbidity), and are symptomatic of processes that could modify sediment transport pathways through Ameland Inlet and across its ebb-tidal delta. However, measurements taken during the Kustgenese 2.0 campaign were insufficient to fully quantify these patterns, so investigating this remains a task for future research.

2.4.4. CIRCULATION PATTERNS

Lagrangian surface currents were measured using drifters equipped with GPS trackers. Positioning of the drifters were recorded at 1 Hz intervals using an internal logger. The drifters were designed as floating devices that follow the top layer velocities but are minimally influenced by wind. The main experiments were carried out in a series of experiments around Frame 4 and 5, at the location of the planned nourishment (*de Wit et al.*, 2018). In this section, we will consider the results of a single large-scale experiment conducted during spring tide on September 9, 2017. The goal of this experiment was to better understand the spatial variations in velocity on the ebb-tidal delta scale circulation patterns and flow pathways. During this experiment drifters were released at flood tide and retrieved after a full tidal cycle at ebb (Figure 2.11). From these experiments, velocity magnitudes and directions were determined.

Based on a series of numerical tracer experiments, *Elias* (2017) hypothesize that Westgat forms a transition area on the ebb-tidal delta. Particles located landward of Westgat mostly exchange with the southern part of the domain, while particles to the north exchange with Borndiep and are transported back onto the ebb-tidal delta. The drifter experiment confirms this hypothesis for surface currents (Figure 2.11). All drifters deployed along the Terschelling coast follow the Boschgat channels into the basin. Drifters that reach Borndiep are transported seaward into the ebb chutes or through Akkepollegat onto the ebb-tidal delta. These patterns may differ for sediment travelling along or near the bed, but still provide an additional line of evidence to explain likely suspended sediment pathways.

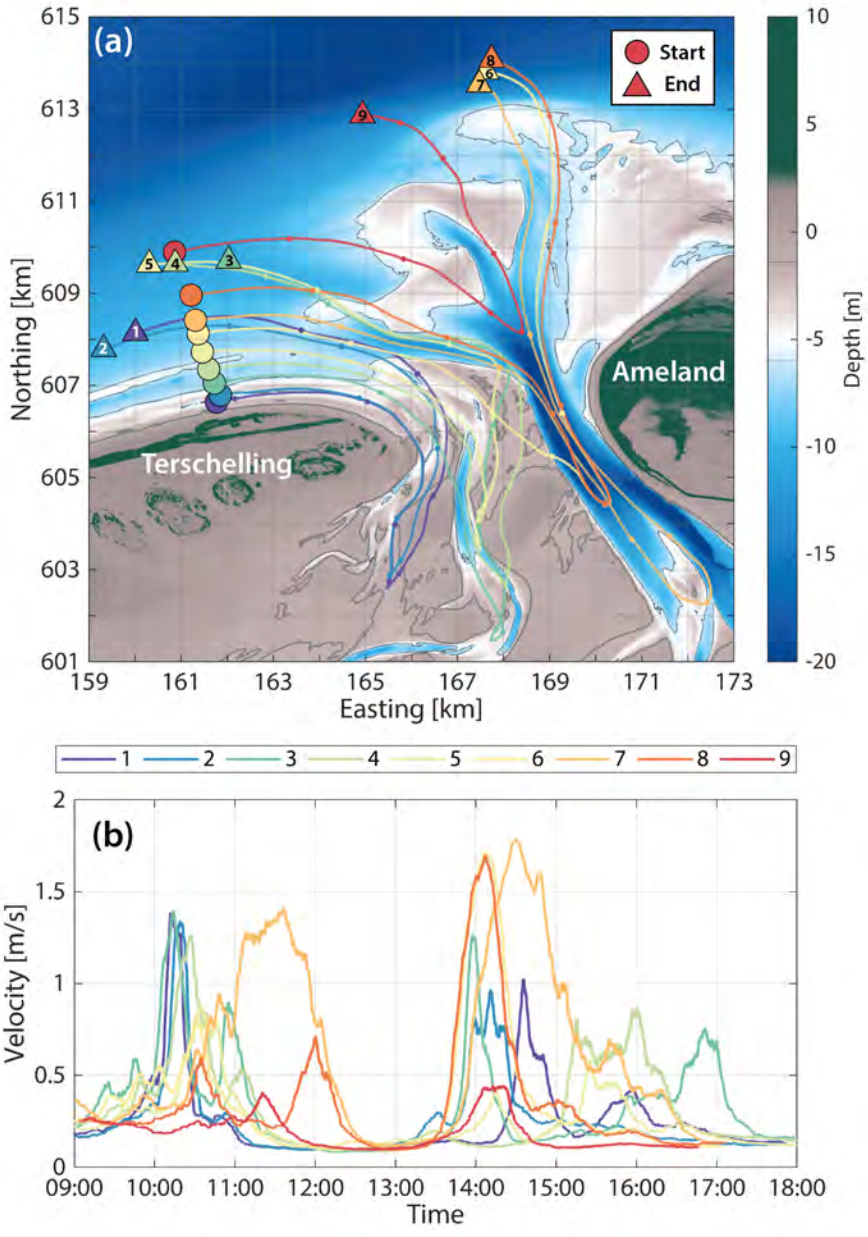

Figure 2.11: Lagrangian flow (drifter) measurements. (a) GPS tracks of the large-scale deployment on September 9th, 2017 during spring tide. Drifters were deployed in a 3 km long line north of Terschelling at flood tide (circles) and retrieved at different locations around the inlet at ebb tide (triangles). Small dots along the drifter paths indicate position every hour from 9:00 until it was retrieved. (b) Flow velocity magnitude of each drifter through time (5 minute moving average).

2.5. SEAWAD & KUSTGENESE 2 PROJECTS

The Kustgenese (*Coastal Genesis*) 2.0 and SEAWAD projects spawned numerous PhD and MSc research studies, covering a range of physical and ecological processes. Collectively, they enhance our understanding of ebb-tidal delta systems and how to nourish them.

Part of the challenge of predicting ebb-tidal delta morphodynamics stems from the non-linearity of waves as they evolve across the convoluted bathymetry. In addition, strong tidal currents modify the wave field and interact with wave-generated currents to produce complex sediment transport patterns. Using the array of pressure sensors mounted at the seaward edge of Ameland ebb-tidal delta (Figure 2.1), *de Wit et al.* (2019) investigated the evolution of near-bed velocity skewness and asymmetry. They determined that due to spatial variations in wave breaking, energy transfer, and tidal currents, wave shape varies significantly across the ebb-tidal delta. This means that accounting for the history of a given wave may be necessary for successful predictions of wave shape, instead of just relying on local parameters. Expanding on these findings, *de Wit et al.* (2020) found a clear relationship between bound superharmonic wave height and nonlinear wave shape. This presents opportunities for better numerical predictions of bound wave height and nonlinear wave shape. Since wave skewness and asymmetry are important determinants of wave-driven sediment transport, this work marks an important step forward in our ability to simulate the evolution of ebb-tidal deltas.

As the seabed is perturbed by waves and currents, it creates bedforms ranging in size from ripples ($\mathcal{O}(1cm)$) to shoals ($\mathcal{O}(1km)$). In turn, these bedforms also feed back and influence the hydrodynamic conditions and sediment transport. Predicting the formation and evolution of these bedforms is essential to making good predictions of sediment transport there, so numerous small and large-scale measurements of them were undertaken as part of the Kustgenese 2.0 and SEAWAD projects. Saw-tooth bars on the eastern side of Ameland ETD are several metres high and several hundred metres long, and migrate rapidly in the direction of littoral transport (*Brakenhoff et al.*, 2019b). Similar bars are also identified on most of the other Wadden ebb-tidal deltas, and seem to originate from instabilities forced by tidal and wave-driven currents. At a much smaller scale, *Brakenhoff et al.* (2020b) found that ripples were highly three dimensional and remarkably constant in size ($\sim 1.5cm$). In numerical simulations of the ebb-tidal delta, *Brakenhoff et al.* (2020b) found that changes in bedform-related roughness could modify current velocity by up to 20% and sediment transport magnitude by over 100%. Her findings underscore the ubiquity and importance of these features on the ebb-tidal delta.

In order to predict and mitigate the ecological impact of ebb-tidal delta nourishments, a clear understanding of the present ecosystem is first necessary. The number and variety of organisms living on a given part of the seabed (benthic species) are closely linked to the physical characteristics of that environment. In the nearshore zone of Ameland's central coast (20 km east of the ETD), *Holzhauer et al.* (2020) identified close relationships between benthic species distribution and morphological feature (i.e., slopes and bar crests or troughs). Extending this type of analysis to the more complex ebb-tidal delta, *Holzhauer et al.* (2021) classified the site into habitats based on the level, slope, orientation, and recent erosion or accretion of the seabed, and compared this with benthic samples. Smaller and more mobile burrowing organisms live fast and die young in the sites that are more exposed to strong waves and currents. Conversely, larger filter-feeding organisms tend to live out their days in more sheltered areas. Based on these traits, *Holzhauer et al.* (2021) ex-

pect that creatures living in the more exposed regions will recover from sand nourishments more quickly than those living in sheltered areas. This is essential guidance for avoiding more severe nourishment impacts on the ebb-tidal delta and its surroundings.

Nourishment dynamics were also explored in many KG2-affiliated projects. When the placement of hypothetical nourishments on the ebb-tidal delta was simulated, *Bak* (2017) determined that nourishment fate is highly dependent on its initial location and sediment composition. *Lenstra* (2020) demonstrated via idealized modelling that the placement timing with respect to channel configuration determined how a nourishment would develop and influence an ebb-tidal delta. When the Ameland pilot nourishment was constructed in 2018, frequent multibeam bathymetric surveys indicated that its initial development was largely shaped by waves (*van Rhijn*, 2019). This analysis was further extended by *Lambregts* (2021), who identified the shoreward and eastward dispersal of the nourished sand via a combination of modelling and bathymetry analysis. *Harlequin* (2021) successfully modelled the pre- and post-nourishment evolution of the ebb-tidal delta over a period of months to years. Their simulations showed that the 2018 nourishment behaved passively, remaining within the Coastal Foundation and having little effect on the overall development of the delta. Depending on their locations, hypothetical alternative nourishments either actively changed the natural dynamics of the ebb-tidal delta or merely contributed passively to its overall sediment budget (*Harlequin*, 2021). However, the model was unable to capture the initial formation of new ebb shoals or their longer-term development in wave-dominated areas. The goal of decadal-scale morphodynamic simulation of ebb-tidal deltas remains elusive.

Although Ameland Inlet features one of the most well-monitored and studied ebb-tidal deltas in the world, there are still gaps in our understanding of the pathways that sediment takes across it. The research summarized above provides a solid foundation on which the present dissertation builds. Via the example of Ameland, we can thus reach our goal of filling those gaps to better understand ebb-tidal delta dynamics.

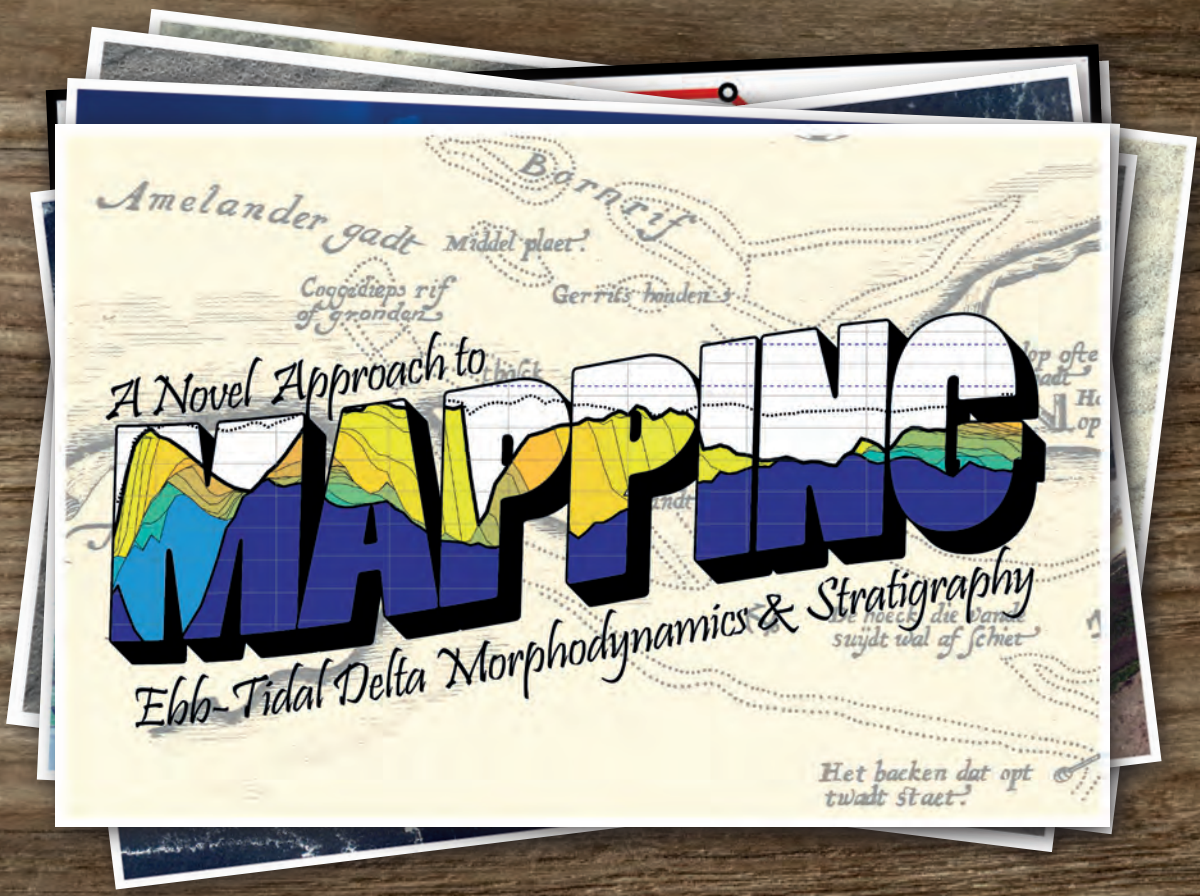
A Novel Approach to
MAPPING
Ebb-Tidal Delta Morphodynamics & Stratigraphy

Dear Reader

Dear Reader,

After spending all that time looking at old maps, we figured there must be a more effective way of analyzing so much data. We came up with some new techniques for combining all the old maps into a single diagram that makes it easier to see how the sand is moving around. We also used those maps to construct a picture showing how all the different layers of sand have piled up or eroded over the years. This is useful for figuring out where to put sand to protect the coast, but also handy for geologists and other people trying to understand ancient rocks made in the same kind of environment.

Stuart

Delft University of
Technology
Stevinweg 1
2628 CN Delft

3

A Novel Approach to Mapping Ebb-Tidal Delta Morphodynamics and Stratigraphy

Key Points:

- Conformal (polar) mapping of Ameland ebb-tidal delta improves the quantification and visualization of its morphodynamics.
- A stratigraphic model generated from bathymetry showcases the delta's depositional behaviour through time.
- These approaches provide new perspectives on ebb-tidal delta dynamics and preservation potential.

This chapter has been accepted for publication in *Geomorphology* pending minor revisions:

Pearson, S.G., Elias, E.P., van Prooijen, B.C., van der Vegt, H., van der Spek, A. & Wang, Z.B. A Novel Approach to Mapping Ebb-Tidal Delta Morphodynamics and Stratigraphy.

IN this chapter, we continue to investigate how ebb-tidal delta morphology varies in space and time in order to learn more about sediment pathways there. Part of the problem with understanding ebb-tidal delta evolution is compressing massive amounts of spatial and temporal data into pictures and metrics that are easier to understand and pick out important patterns from. In this chapter, we show two new mapping techniques that collapse the dozens of individual maps in Figures 2.4 to 2.6 into a single figure. The first technique makes it easier to track the motion of shoals and channels as they migrate across the ebb-tidal delta. The second is used to create a stratigraphic model that shows how sand deposits in layers through time. These techniques are useful for planning nourishments because they give us clues about sediment pathways and tell us where sediment is better preserved. This is even helpful for interpreting ancient ebb-tidal deltas that are preserved in the rock, making it a useful approach across many space and time scales.

ABSTRACT

Ebb tidal deltas (ETDs) are highly dynamic features of sandy coastal systems, and coastal management concerns (e.g., nourishment and navigation) present a pressing need to better describe and quantify their evolution. Here we propose two techniques for leveraging the availability of high-resolution bathymetric surveys to generate new insights into the dynamics and preservation potential of ebb-tidal deltas. The first technique is conformal mapping to polar coordinates, using Ameland ebb-tidal delta in the Netherlands as a case study. Since the delta tends to evolve in a clockwise direction around the inlet, this approach provides an improved quantification and visualization of the morphodynamic behaviour as a timestack. We clearly illustrate the sediment bypassing process and repeated rotational migration of channels and shoals across the inlet from updrift to downdrift coasts. Secondly, we generate a decadal scale (1975-2021) stratigraphic model from the differences between successive bathymetries. This stratigraphy showcases the delta's depositional behaviour through space and time, and provides a modern analogue for prehistoric ebb-tidal deltas. During the surveyed period, inlet fills form the largest and most stable deposits, while the downdrift swash platform is the most stable structure over longer periods. Together, these approaches provide new perspectives on ebb-tidal delta dynamics and preservation potential which are readily applicable to other sites with detailed bathymetric data. These findings are valuable at annual to decadal timescales for coastal management (e.g., for planning sand nourishments) and also at much longer timescales for interpreting stratigraphy in ancient rock records.

3.1. INTRODUCTION

CEASELESSLY shaped, shifted, and shuffled around by the complex interaction of waves and tides, ebb-tidal deltas (ETDs) are dynamic morphological features whose behaviour affects navigation, coastal safety, and ecosystems. They form an essential, connected part of the regional sediment budget for tidal inlets, basins, estuaries, and barrier coasts (*Rosati*, 2005; *Gelfenbaum and Kaminsky*, 2010). Due to the large volumes of sand contained within them, ETDs are commonly viewed as a resource to be mined (*Hicks and Hume*, 1997; *Fontolan et al.*, 2007). However, it has been recognized in the Netherlands that preserving ETDs (in part via sand nourishments) to maintain coastal sediment budgets is a potentially viable strategy for mitigating sea level rise and coastal erosion (*Elias et al.*, 2012a; *Lodder and Slinger*, 2021). Estimating the preservation potential of modern ETD and tidal inlet deposits is thus essential for present-day coastal management. However, the possible fate of nourishments placed in such a dynamic environment is still largely unknown. The stochastic nature of meteorological forcing, highly nonlinear character of sediment transport, and complex morphodynamic feedbacks make predicting ebb-tidal delta evolution an ongoing challenge (*Lenstra et al.*, 2019a; *Zhu et al.*, 2019a). Mapping the evolution and preservation of ebb-tidal deltas and tidal inlets in order to better understand and predict their behaviour across multiple space and time scales is therefore a key research priority in coastal engineering and geoscience (*Power et al.*, 2021).

Rising to meet such challenges demands new tools and techniques for interpreting ETD morphodynamics. This is difficult because it requires quantification and analysis of complex patterns in ever-changing bathymetry, which typically require numerical models, many measurements, and lengthy narrative descriptions to elucidate (*Elias et al.*, 2019, 2022; *Fortunato et al.*, 2021). Although the conceptual model of sediment bypassing around ebb-tidal deltas has been well-established for several decades (*FitzGerald*, 1983; *Kana et al.*, 1999a), the pathways that sediment takes across ebb-tidal deltas are still poorly understood (*Son et al.*, 2011; *Herrling and Winter*, 2018). We thus need techniques to distil the 4D (three spatial dimensions evolving through time) complexities of ETDs into more easily interpretable and comparable metrics and visualizations.

Just as we need new ways to characterize the dynamics of ETDs, we also need new approaches to quantify the sediment that remains deposited there. Early research on sediment preservation or stratigraphy in tidal inlets and ebb-tidal deltas was carried out principally in support of paleo-environmental reconstruction via modern analogues (*Hubbard et al.*, 1979; *Hayes*, 1980; *FitzGerald*, 1984; *Moslow and Tye*, 1985; *Imperato et al.*, 1988; *Sha and De Boer*, 1991; *Tye and Moslow*, 1993). In many of these cases, a key goal was to identify the potential for large sand deposits like tidal inlets and ebb-tidal deltas to be preserved as petroleum reservoirs. Sediment from ebb-tidal delta deposits typically survives in the ancient rock record as inlet channel fills (*Mulhern et al.*, 2021). A perennial challenge in sedimentology is that preserved stratigraphy is discontinuous and seldom completely matches the initially-deposited stratigraphy due to distortion and "shredding" of the complete geological record by sediment transport (*Jerolmack and Paola*, 2010; *Lazarus et al.*, 2019; *Straub et al.*, 2020). A model of modern sedimentary preservation potential in ETDs would thus aid in the interpretation of the ancient rock record.

However, it is not just at geological timescales ($\mathcal{O}(> 10^6$ years)) that preservation potential is relevant. ETDs form key components of barrier coastal sediment budgets (*Kaminsky et al.*, 2010; *Elias et al.*, 2012a; *Oost et al.*, 2012), so understanding the nature of sediment

preservation there on approximately decadal timescales ($\mathcal{O}(10^0 - 10^2$ years)) is essential for managing these coastal systems. What is the potential of ETDs to store sediment rather than bypassing it down the coast or importing it into the tidal basin? Which parts of the ETD are actively evolving on decadal timescales as opposed to remaining passively buried? Developing detailed stratigraphic models of modern ebb-tidal deltas may yield valuable scientific and coastal management insights into the nature of sediment storage there.

The age and preservation of ETD deposits can be estimated in numerous ways. Stratigraphy is preserved in the geological record and can be derived from cores or seismic data. However, such data (e.g., seismic surveys (*Sha*, 1989b; *Ronchi et al.*, 2019)) consider longer timescales of structural morphodynamic change caused by changing boundary conditions, and may not provide the temporal resolution required for coastal engineering and management. To achieve the necessary resolution, process-based numerical models can be used to develop synthetic stratigraphic models (*Kleinhans*, 2010; *Nicholas et al.*, 2016; *van der Vegt et al.*, 2020). Alternatively, stratigraphic models can be constructed directly from repeated bathymetric surveys (*Bridge*, 1993; *Sylvester et al.*, 2011), if they are sufficiently accurate and high in spatial and temporal resolution. Adopting a similar approach for ebb-tidal deltas would provide valuable insights into the sediment dynamics and preservation there.

Ameland ebb-tidal delta in the Netherlands has a long and rich history of bathymetric surveying, ranging from navigational charts made in the late 1500s to annual surveys in recent years (*Elias et al.*, 2019, 2022). This dataset thus makes Ameland an ideal candidate for such an investigation of modern ETD architecture. In this chapter, we present a novel analysis of high-resolution bathymetric surveys of Ameland ETD, constructing a decadal-scale stratigraphic model and projecting the bathymetry into polar coordinates that align with the dominant transport patterns. This technique can also be applied to bathymetric datasets computed by morphodynamic models. With this approach, we simplify the spatial and temporal complexity of ebb-tidal deltas and generate new perspectives on their dynamics and preservation.

3.2. SITE BACKGROUND: AMELAND EBB-TIDAL DELTA

Ameland Inlet lies between the barrier islands of Ameland and Terschelling in the northern part of the Netherlands (Figure 3.1). On the North Sea side of the inlet, there is a large ebb-tidal delta characterized by a dynamic system of channels and shoals on its west side, and a more stable swash platform to the east. The surface of the ebb-tidal delta consists predominantly of well-sorted fine sand (mean $d_{50} = 211\mu m$) with limited mud content (*Rijkswaterstaat* (1999), Chapter 2). The $4km$-wide inlet connects the North Sea to the shallow Wadden Sea backbasin, and features a $30m$ deep main channel (Borndiep) on the downdrift (east) side. On the updrift (west) side, the inlet consists of a shallow (approximately $5m$ deep) platform that is intersected by smaller, highly dynamic channels.

The tide propagates along the coast of Terschelling and Ameland in an easterly direction, and is predominantly semi-diurnal. Ameland is a mixed-energy tidal inlet with a tidal range varying from $1.5m$ at neap tide to $3m$ at spring tide, and a tidal prism of $400 - 500 \times 10^6 m^3$ (*Elias et al.*, 2022). This tidal prism did not vary substantially between 1968-2017, and there has been no clear trend in residual ebb or flood dominance (*Elias et al.*, 2022). Although other Dutch inlets have been dramatically changed in the past century by closure dams and other engineering works, Ameland has remained comparatively untouched during the 46-year period covered in this study. Although there are no major sources of

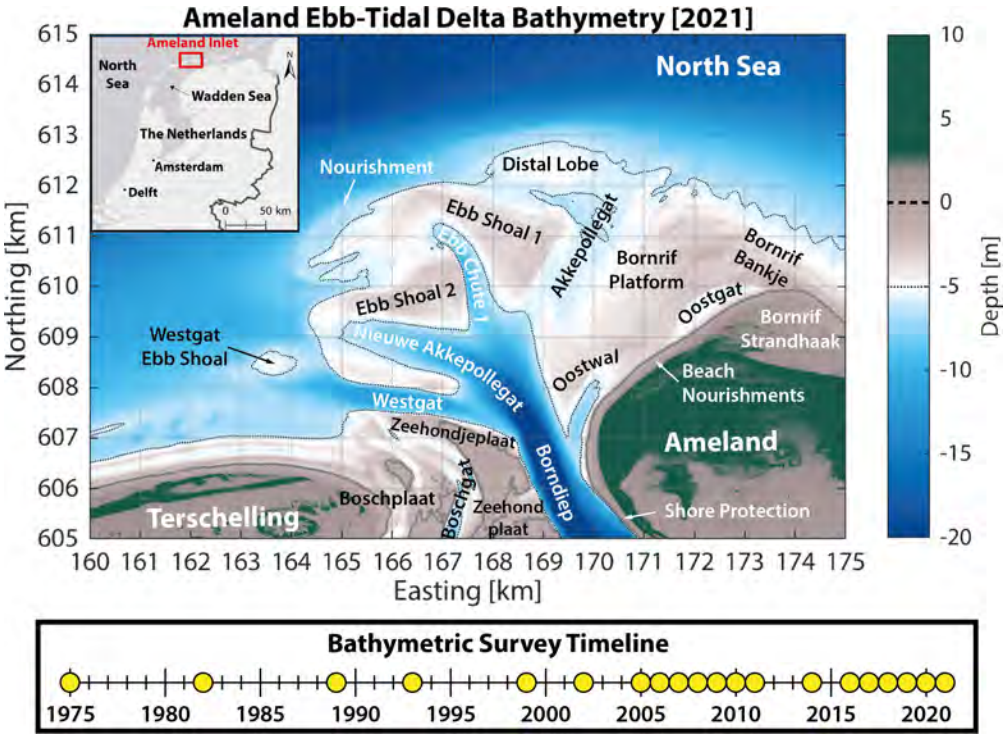

Figure 3.1: Overview Ameland inlet and ebb tidal delta (circa 2021), located between the Dutch Wadden Islands of Terschelling and Ameland, in the north of the Netherlands. Key morphological features like channels and shoals are indicated, along with human interventions (e.g., nourishments and shore protection). Yellow dots on the timeline beneath the map indicate the years in which the bathymetry of the delta was surveyed. Bathymetry source: Rijkswaterstaat Vaklodingen. Elevation source: Actueel Hoogtebestand Nederland (AHN), Rijkswaterstaat. Basemap sources: Esri, HERE, Garmin, ©OpenStreetMap contributors, and the GIS user community. *Translation of selected Dutch terms: "plaat" = shoal, "bankje" = (sand)bar, "gat" = channel or creek, "diep" = deep (channel), "strand' '= beach, "haak" = hook, "nieuwe" = new, "oost" = east, "zeehond" = seal, "zeehondje" = baby seal.*

fresh water within Ameland basin, episodic wind-driven flows lead to residual transport of fresh water from adjacent parts of the Wadden Sea into Ameland basin (*Duran-Matute et al.*, 2016a; *Van Weerdenburg et al.*, 2021).

The North Sea in the vicinity of Ameland has a mild wave climate dominated by locally-generated wind waves. The mean significant wave height H_s at the adjacent island of Schiermonnikoog is $1.37m$ (peak period T_p of $7.2s$), and H_s is less than $2m$ for 83% of the time (*Elias et al.*, 2022). Severe storms ($4.5 < H_s < 9.1m$) occur less than 1% of the time, and generally take place in the winter months. Although the mean wind direction is from the southwest, the dominant wave direction is from the northwest. This wave climate drives a net eastward longshore sand transport estimated at between 0.3 and $1.2 \times 10^6 m^3$/year (*Ridderinkhof et al.*, 2016; *Elias et al.*, 2019).

3.3. METHODOLOGY & DATA

3.3.1. POLAR ANALYSIS

To analyze the morphodynamic evolution of the ETD, we create a conformal map, an angle-preserving spatial transformation that allows complex geometries to be reprojected on a rectangular grid (*Schinzinger and Laura*, 2003). Since the delta tends to evolve in a clockwise direction around the inlet (*Elias et al.*, 2019), we plot the bathymetry in polar coordinates centred at the inlet. We can then stretch out the bathymetry and re-map it on a rectangular grid that is aligned with the main directions of shoal and channel migration. This approach enables the ebb-tidal delta's morphodynamic behaviour to be quantified more easily, since the grid can be further collapsed to a single spatial dimension. Although ETDs have often been simulated in process-based morphodynamic models along curvilinear and unstructured grids (*Elias et al.*, 2006; *Eelkema et al.*, 2012) and radial coordinates have been used in some river delta models (e.g., *Parker and Sequeiros* (2006)), this type of gridding has not yet been used in this way to analyze decadal-scale bathymetry.

First, the origin and properties of the polar grid were selected. For Ameland Inlet, 607 km N, 169.5 km E (RD coordinate system) was chosen subjectively as the origin based on prior knowledge of the site's dynamics (*Elias et al.*, 2019). This location is near the deepest part of the Borndiep, the main inlet channel, and remains stable throughout the surveyed period. A grid extent of 7 km from the origin was used because it lay within an area of consistent coverage area by the available bathymetric surveys. A 180°-wide swath from 260° (WSW) clockwise to 80° (ENE) was chosen as this extent was sufficient to capture the key morphodynamic processes of interest but excluded the inland portions of Terschelling and Ameland islands. Trial and error revealed that the dominant bathymetric migration patterns coincided best with this origin and grid extent. This step could be further quantified and optimized in future applications to minimize distortions and enable automated analysis of e.g., global datasets of remote sensing-derived bathymetry.

Next, the radial grid was overlain on the raw bathymetric data. An angular resolution ($d\theta$) of 1° and radial grid spacing of $40m$ were chosen, as this gave a good balance between having sufficient resolution in the coarser distal cells (approximately 40×120 m) and ensuring that there was at least one data point per cell in the proximal cells (approximately 40×20 m). To estimate the elevation of the polar grid cells (z_{polar}), all elevation points from the original rectangularly-gridded bathymetry (z_{rect}) lying within a given polar cell were averaged. Points within 1 km of the origin were neglected from the interpolation, since many

of the polar grid cells within that radius were smaller than the 20 m resolution of the original bathymetric datasets.

To monitor volumetric changes in the delta through time, the sediment volume anomaly $V_{a(t)}$ within a given cell was calculated by multiplying its surface area A with the difference in elevation from the mean bathymetric surface z_{mean}. Since the interval between surveys was not equally spaced, each survey in the calculation of z_{mean} was weighted by the interval preceding it.

This procedure was repeated for all available surveys to create a three-dimensional timestack of the delta's bathymetry. The evolution of the inlet can be further analyzed by collapsing the map along a single dimension, summing the volume anomalies $\sum V_{a(t)}$ along rows (ρ, distance from the inlet) or columns (θ, angular sector relative to $0°N$). This permits the creation of Hovmöller (*Hovmoller*, 1949) or timestack diagrams to illustrate the morphodynamics of the entire ETD in a single plot. This approach has been used at shorter timescales for specific regions of an ETD before (e.g., *Harrison et al.* (2017); *Humberston et al.* (2019)), but not yet for a whole delta or at decadal timescales.

3.3.2. STRATIGRAPHY

To develop the stratigraphic model, we compare elevation (z) differences in the bathymetry at sequential timesteps t and $t+1$ (e.g., Figure 3.2). At all grid cells i where $z_{t+1,i} > z_{t,i}$, there is deposition and $z_{t+1,i}$ becomes the new surface elevation. The difference between $z_{t+1,i}$ and $z_{t,i}$ becomes labelled as a deposit with a date of $t+1$, and $z_{t,i}$ remains the same for all previous values of t. At all grid cells i where $z_{t+1,i} < z_{t,i}$, there is erosion and $z_{t+1,i}$ becomes the new surface elevation. The elevation of z_t for all previous t is retroactively reset to $z_{t+1,i}$ and no deposition is recorded. This process is then repeated for all grid cells at all available timesteps.

The minimum bathymetric surface elevation across all surveys z_{min} defines the lower envelope of morphodynamic change during the total surveyed interval, which corresponds to the depth of reworking (e.g., *van der Spek* (1996); *Vonhögen-Peeters et al.* (2013)). Conversely, the maximum bathymetric surface elevation across all surveys z_{max} defines the upper envelope of morphodynamic change. The volume of sediment contained between z_{min} and z_t can be considered the "active" ETD (on the timescale of available surveys) V_{active}, while the volume of sediment beneath z_{min} can be considered the "passive" ETD ($V_{passive}$).

To estimate the age of a given surface deposit sample of depth Δz_{sample}, all deposit dates are first converted to an age from the most recent timestep. The mean deposit age across Δz_{sample} is estimated, weighted by the thickness of each deposit in the sample. This averaging is analogous to taking a surface core, but also reduces variability due to minor ($\mathcal{O}(0.1m)$) differences in survey elevations. Note that this calculation reveals the time since the sediment was deposited, not the actual age of the sediment particles in that deposit. This approach does not explicitly consider the influence of sub-grid scale bedforms on sediment reworking. We also cannot say anything about grain size characteristics of the deposits, since we lack sediment size data in equivalent spatial and temporal resolution to the bathymetry.

3.3.3. BATHYMETRY

The two analysis techniques proposed here exploit the opportunities presented by high spatiotemporal resolution bathymetry. The earliest bathymetric surveys of Ameland Inlet were

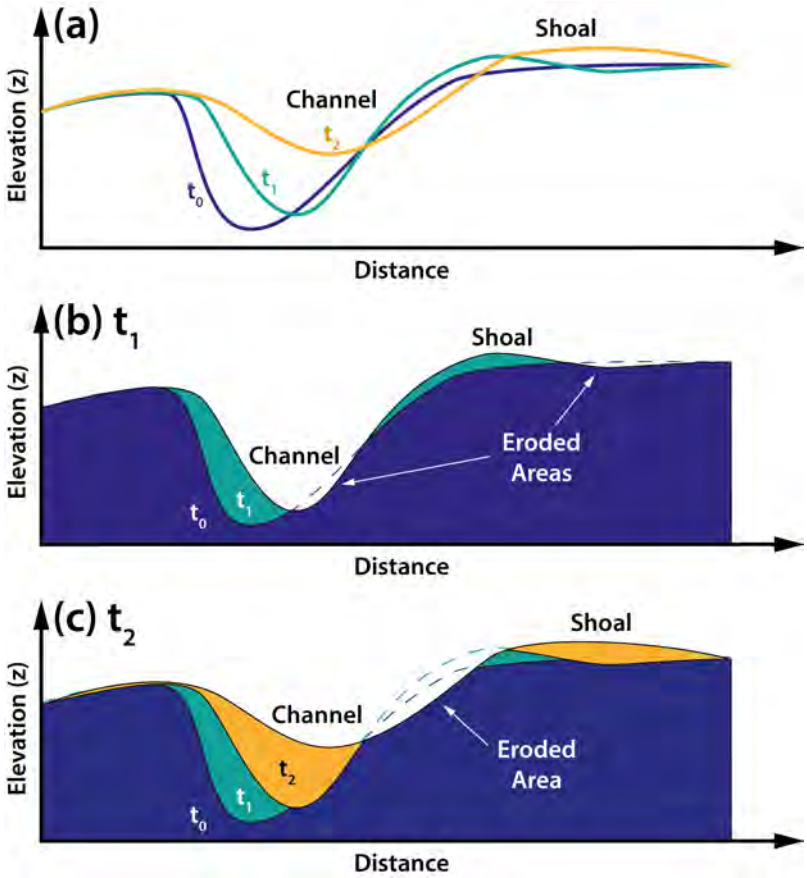

Figure 3.2: Schematic diagram indicating how the stratigraphy is computed from (a) bathymetry at three sequential timesteps, (t_0, t_1, t_2). For example, at t_1 (b), the channel migrates to the right and fills in slightly. The left part of the shoal accretes, but the right part erodes slightly below the t_0 elevation, z_0. The areas deposited at t_1 are shaded in teal. At t_2 (c), the channel continues to infill and migrate to the right, eroding into t_0 and t_1 deposits. Sediment is also deposited on the shoal, as is indicated by yellow shading. This process is repeated for all grid cells in the bathymetry at all available timesteps. Note that eroded and deposited volumes are not necessarily conserved along the transect because it represents a 2D vertical slice of 3D stratigraphy

conducted for navigational purposes in the 1500s, and the area has been closely monitored in the centuries since then (*Elias et al.*, 2019). These surveys were sporadic throughout the 20th century, but since 1989, Rijkswaterstaat (part of the Ministry of Infrastructure and Water Management) has measured the site at 3 to 6-year intervals and stored the data digitally as part of its *Vaklodingen* dataset (Figure 3.1). In 2007-2010 and 2016-2021, more frequent surveys of the site (semi-annual to annual) were carried out as part of the SBW-Waddenzee and Kustgenese2.0 projects, respectively (*Zijderveld and Peters*, 2009; *Van Prooijen et al.*, 2020; *van der Werf et al.*, 2019a).

Subtidal areas of the study site were measured with a single-beam echo sounder in transects with approximately $200m$ spacing. The data are reduced to $1m$ resolution along transects after quality control is performed, after which the bathymetry is combined with nearshore coastal profile measurements and LIDAR measurements of intertidal areas from the Dutch national elevation model, *Actueel Hoogtebestand Nederland (AHN)*. The integrated digital elevation dataset is interpolated to a $20 \times 20m$ grid ($dx = 20m$), which forms the basis of the analysis presented here. Much more extensive descriptions of the Ameland Inlet bathymetric dataset used in the present study are given in *Elias et al.* (2019) and *Elias et al.* (2022).

3.4. RESULTS

3.4.1. BATHYMETRY

Nearly 50 years of high-resolution bathymetric surveys are available for Ameland ETD, which provides a unique dataset that is well-suited to demonstrating our new analysis techniques. To characterize the delta, we first examine its average shape and its range of variability. The mean surface z_{mean} retains the key, persistent features of the ETD (e.g., Borndiep, Westgat, and Akkepollegat channels; Bornrif platform), but smooths out unique ephemeral features (Figure 3.3a). This surface can thus serve as a basis of comparison for investigating the variability of ETD morphology.

The minimum bathymetric surface is dominated by the wide and deep Westgat and Borndiep channels (Figure 3.3b). The western side of the delta is relatively deep ($< 6m$), since this region is repeatedly scoured down by migrating ebb-channels. Conversely, the Bornrif platform on the eastern side of the delta is relatively shallow and stable without intersections by deep channels.

The maximum bathymetric surface (Figure 3.3c) has a fairly uniform elevation of approximately $-3m$ across much of the ebb-tidal delta. This depth is subtidal (MLW $\approx -1.4m$) but still well within the breaking wave depth threshold for average wave conditions.

By computing the difference between the maximum and minimum bathymetric surfaces, we obtain the full envelope of observed morphological change (Figure 3.3d). The envelope is thickest in the channel areas, but also on the Boschplaat where erosion of the island tip was substantial. The volume of the envelope between the maximum and minimum surfaces is given by:

$$V_{envelope} = \sum_{i=1}^{n} (z_{max,i} - z_{min,i}) \cdot dx^2 = 440 \times 10^6 m^3 \tag{3.1}$$

where dx is the (fixed) rectangular grid cell width and n is the total number of rectangular grid cells within the boundaries of the polar grid defined in Figure **??**. The volume of

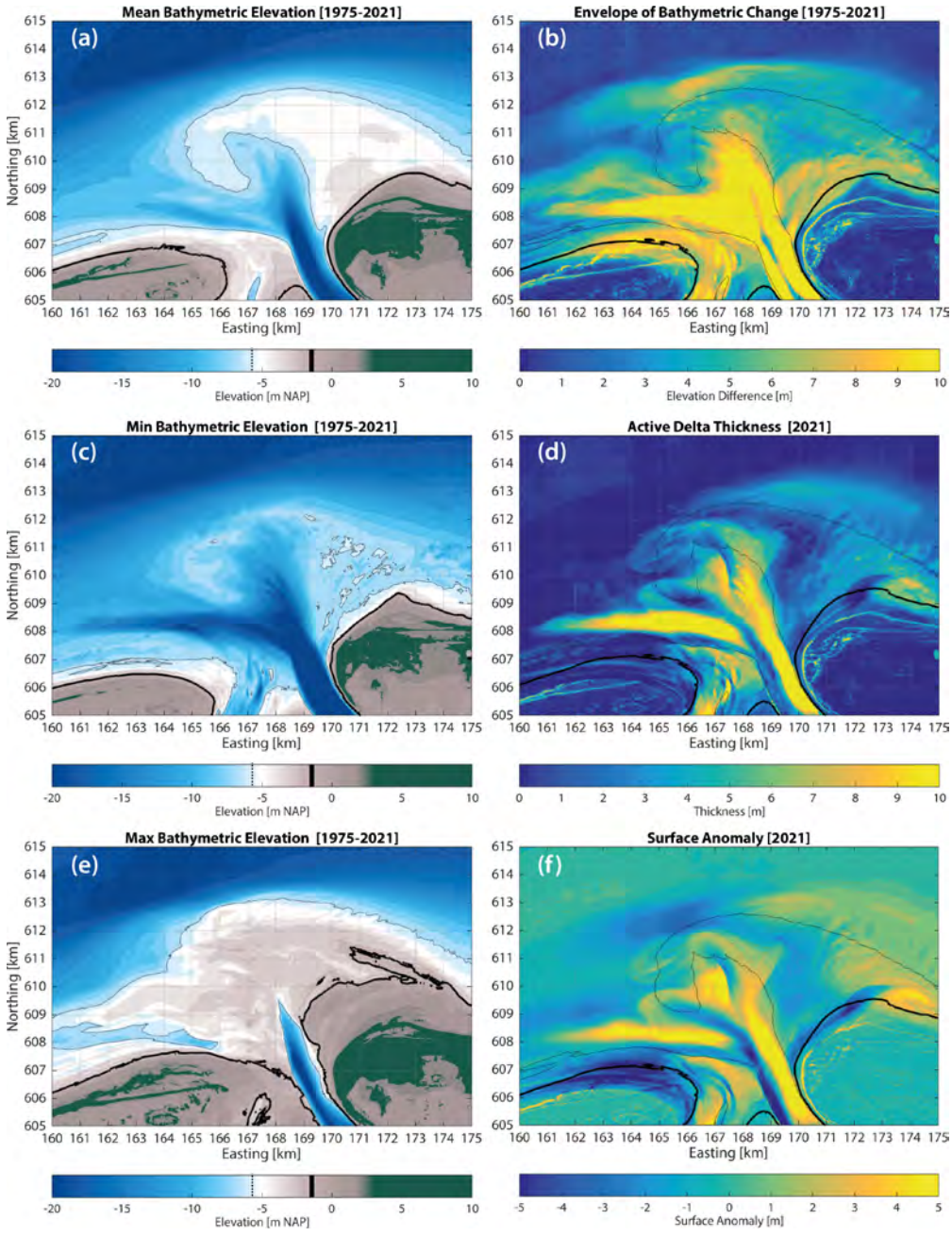

Figure 3.3: Bathymetric surfaces derived from stratigraphic analysis. (a) Mean bathymetric elevation (z_{mean}). (b) Minimum bathymetric surface (z_{min}). (c) Maximum bathymetric surface (z_{max}). (d) The envelope of bathymetric change ($z_{max} - z_{min}$). (e) Active delta (preserved deposit) thickness in 2021 ($z_{2021} - z_{min}$). (f) Surface anomaly in 2021 ($z_{a,2021} = z_{2021} - z_{mean}$). In (a,d,e,f), the approximate mean low water level (MLW) contour of the z_{mean} at -1.4 m NAP (*Normaal Amsterdams Peil*, approximately mean sea level) is represented with a thick black line, and the -6 m NAP depth contour is indicated with a thin dashed line. The MLW and -6m contours in (b,c) correspond to those of z_{min} and z_{max}.

sediment preserved in the active delta in 2021 is:

$$V_{active} = \sum_{i=1}^{n} (z_{2021,i} - z_{min,i}) \cdot dx^2 = 236 \times 10^6 m^3 \tag{3.2}$$

This accounts for the volume of sediment that was deposited since 1975 and preserved in its original location until 2021 (Figure 3.3e). Note that this is smaller than the volume of the envelope, indicating that the volume deposited and volume that is actually preserved differ by nearly a factor of 2. For comparison, (*Elias et al.*, 2022) computed the total net volume change $V_{net} = V_{2021} - V_{2005}$ and mean annual gross volume change $\bar{V}_{gross} = \bar{V}_{eroded} + \bar{V}_{deposited}$ of the delta from 2005 to 2021 as $18.3 \times 10^6 m^3$ and $47 \times 10^6 m^3/year$, respectively. These findings indicate that net changes in the size of the ETD are very small relative to the gross changes and that the morphodynamics of the delta are characterized by extensive reworking.

Lastly, we can compute the surface anomaly $z_{a(t)} = z_t - z_{mean}$ for each year, as indicated for 2021 in Figure 3.3f. This corresponds to the height of the bed above or below the mean bathymetry, which makes it easier to monitor the migration of shoals and channels across the delta through time. In 2021, the most anomalous features are the shallower Borndiep and Westgat channels, massively eroded tip of the island Terschelling, twin ebb spillover lobes, nourishment, and Bornrif Bankje shoal.

3.4.2. POLAR ANALYSIS

Plotting the ETD bathymetry in polar coordinates (Figure 3.4) aligns the grid with the principle sediment transport pathways (*Pearson et al.*, 2020; *Lambregts*, 2021): rotationally around the inlet (θ-axis), and radially out from the inlet (ρ-axis). The power of this conformal mapping approach arises when the complex geometry of the ETD (*Elias et al.*, 2019, 2022) can be collapsed to a single spatial dimension. To do so, we compute the volume of sediment above and below the mean bathymetric surface (Figure 3.3f). The computed volume anomaly $V_{a(t)} = z_{a(t)} \cdot dx^2$ is then summed across the θ and ρ directions for each surveyed year to produce a Hovmöller or timestack diagram (Figure 3.5c,d). In doing so, the essential morphological features of the ETD can be tracked in space and time.

Patterns in the volume anomaly with respect to θ correspond to rotational motion around the inlet (Figure 3.5c). This makes it an ideal means of investigating sediment bypassing from one side of the inlet to the other via shoals. Bright yellow ridges indicate the presence of shoals, and dark blue troughs indicate channels or other deeper areas. All of the ridges and troughs show a clear trend up and to the right, which corresponds to a mean clockwise rotation of between 14.4°/decade (see Appendix A for details). The migration of shoals and channels appears to speed up in the northern quadrant of the ETD, then slows down again as it approaches the downdrift coast. Several key patterns demonstrate this bypassing phenomenon (Figure 3.5c):

i - The persistent erosion of the Boschplaat at the tip of Terschelling ($\sim -90°$), which began around 1975.

ii - The infilling of the Westgat as its role changes from main ebb-channel to marginal flood channel.

iii - A large volume of sediment migrates from the Boschplaat beginning in the 1990s, and gradually moves around the inlet to approximately $-22.5°$ in 2021. This corresponds to the growth and migration of the Ebb Lobe 1 at 13.5°/decade ($R^2 = 0.95$).

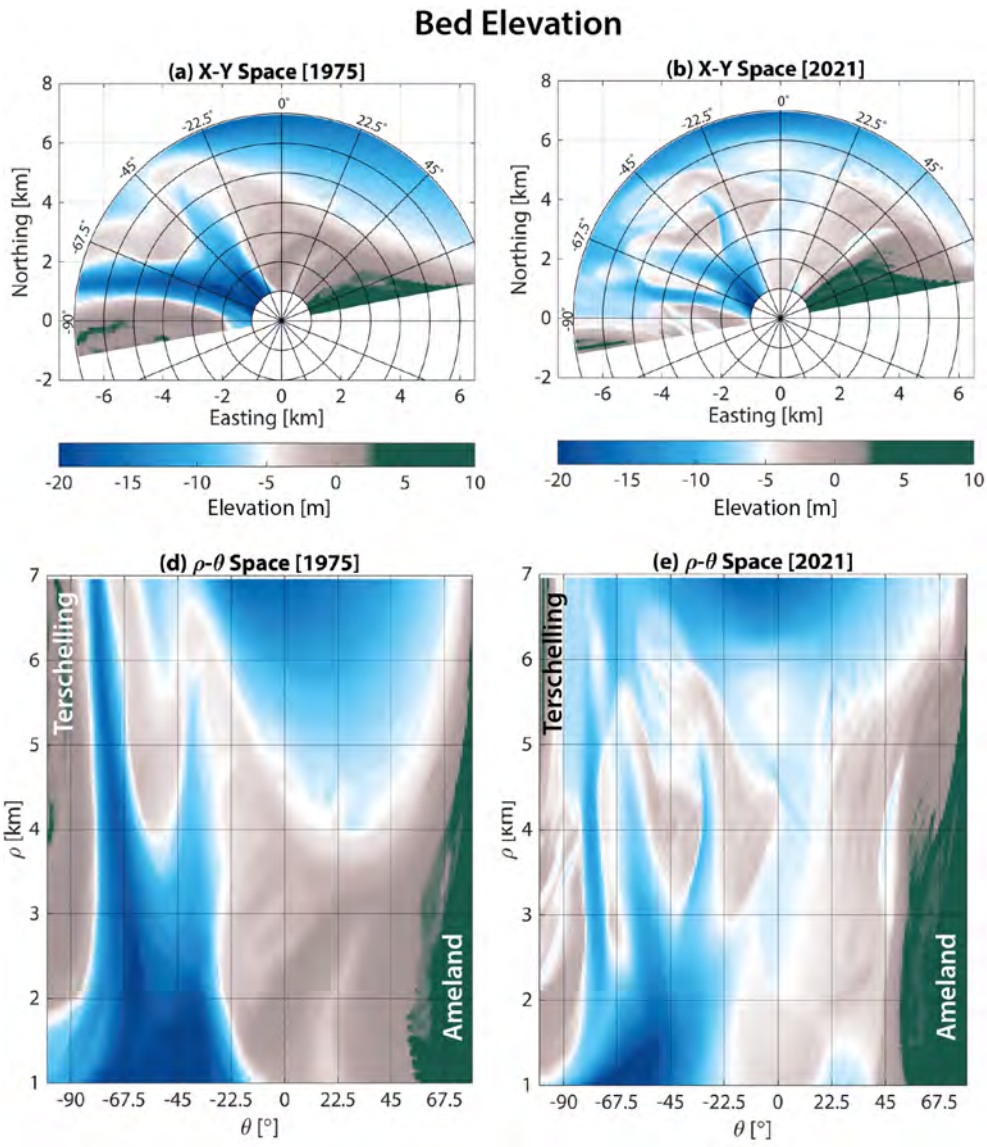

Figure 3.4: Bathymetry of the ebb-tidal delta in Cartesian space (top) and reprojected in polar space (bottom) for the years 1975 (a,c) and 2021 (b,d). Both coordinate systems are centred at 169.5 km E, 607 km N (RD coordinates).

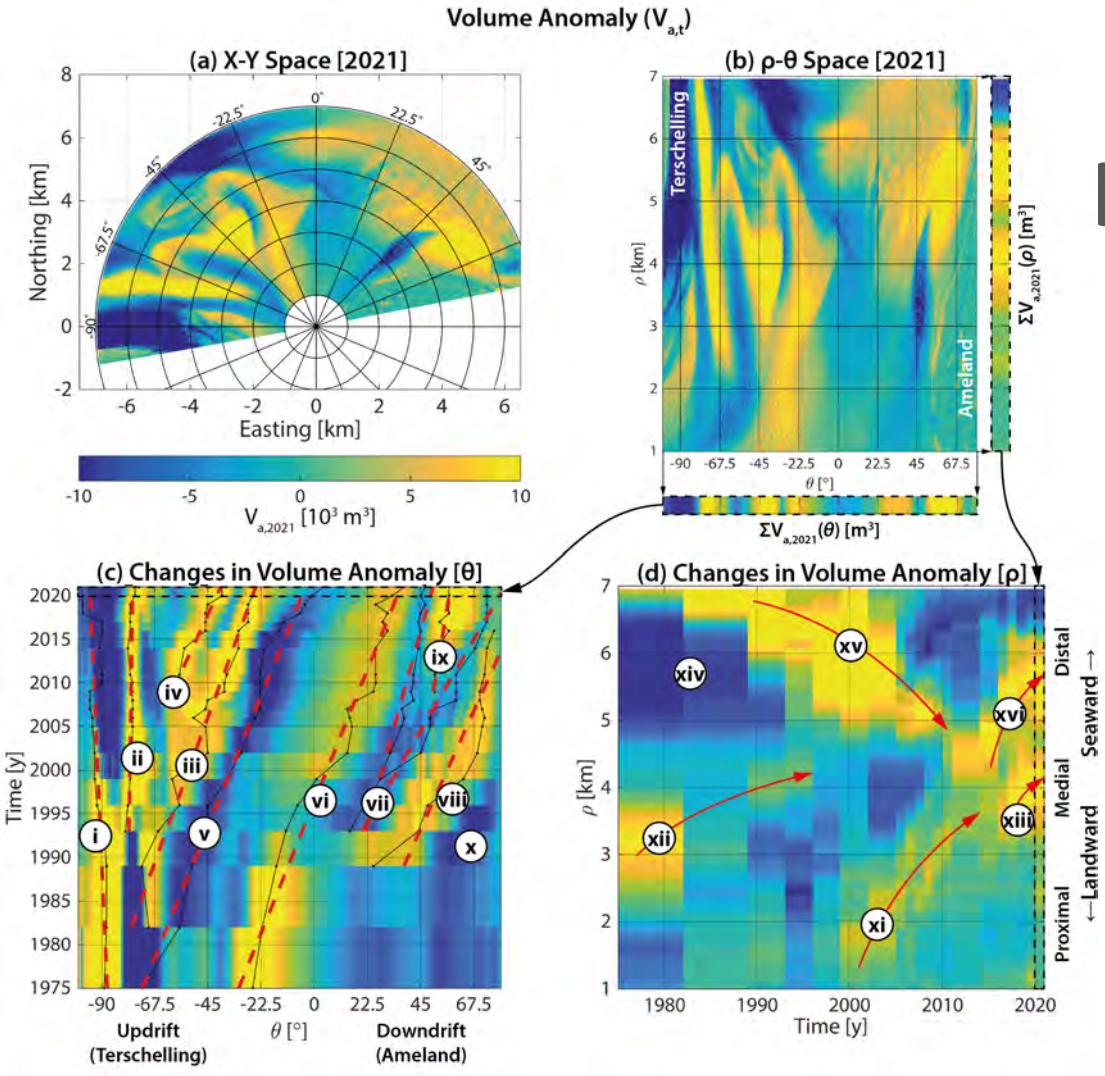

Figure 3.5: The volume anomaly $V_{a(t)}$ (volume of sediment in a given year (here 2021) above or below the mean bathymetric surface z_{mean}) in Cartesian (a) and polar space (b). Hovmöller diagrams indicate the change in volume anomaly for each year summed along the θ (c) and ρ axes (d), stacked in time. For example, the sum of each column in (b) is the top row of (c), and the sum of each row in (b) is the right-most column of (d). In (c), thin black lines denote the trajectory of shoals or depositional areas (yellow) and channels or eroded areas (blue) in space and time. Red dashed lines indicate linear fits through those trajectories. Trends up and to the right in $\theta - t$ space (c) indicate clockwise motion around the inlet. Trends up and to the right in $\rho - t$ space (d) indicate seaward expansion of the delta, and are qualitatively shown by red arrows.

iv - In 2005 at $\sim -55°$, there is a bifurcation in this ridge, which corresponds to the outgrowth of Ebb Chute 2. The ebb delta nourishment in 2019 is visible as a small increase at the end of this ridge. The average migration rate of this shoal complex is $17.2°$/decade ($R^2 = 0.94$).

v - The clockwise rotation of the Akkepollegat channel from 1989-2021 at $15.0°$/decade ($R^2 = 0.97$) and gradual infilling after 2015 as it loses its prominance as main ebb channel.

vi - The migration of shoals across the Bornrif platform at $14.9°$/decade ($R^2 = 0.95$).

vii - The migration of the proximal and distal parts of the marginal Oostgat channel at $10.1°$/decade ($R^2 = 0.88$) and $21.5°$/decade ($R^2 = 0.88$), respectively.

viii - Attachment and migration of the Bornrif Strandhaak at $16.6°$/decade ($R^2 = 0.81$).

ix - The gradual migration and attachment of the Bornrif Bankje shoal to the Ameland coast at $6.0°$/decade ($R^2 = 0.80$). The appearance of this shoal leads to an apparent bifurcation of the Oostgat channel (vii), although this is just an artefact of the chosen polar coordinate system.

x - Erosion of the Ameland coastline associated with the westward migration and diffusion of the attached Bornrif Strandhaak shoal.

Patterns in the volume anomaly with respect to ρ correspond to expansion and contraction of the ETD in a radial direction from the inlet (Figure 3.5d). We can divide the domain into three regions: proximal ($1-3km$), medial ($3-5km$), and distal ($5-7km$). This behaviour is exemplified by these notable patterns:

xi - The proximal region reflects the migration of a shoal complex from the tip of the Boschgat seawards, eventually becoming Ebb Lobe 1 and 2.

xii - The medial region has a large volume anomaly in 1975 associated with the Bornrif shoal, which then attached to the Ameland coast and moved away from the inlet.

xiii - The medial region increases in volume after 2010 due to seaward growth of Ebb Lobe 1 and 2 and attachment of Bornrif Bankje to the Ameland Coast

xiv - The distal region has a large negative volume anomaly in 1975 because the Bornrif platform is then located further westward and closer to the inlet than in later years.

xv - Prior to 1989, the distal region is dominated by the large volume of sand stored in the ebb lobe of the Westgat, which was then the main channel. Between 1989-2010, the distal region shows the landward contraction of the ETD associated with the migration of this mass of sediment from the distal lobe across the Bornrif.

xvi - After 2010, the distal region grows seaward as Ebb Lobe 1 continues to develop and migrate around the periphery of the delta. The addition of the ebb delta nourishment in 2018 is also visible. This growth in the distal region also reflects the eastward migration of sediment from the Bornrif Bankje and Strandhaak after attaching to the Ameland coast.

Collectively, these patterns strongly suggest that sediment bypasses Ameland Inlet (at least in part) via shoals that migrate around the medial and distal region of the ETD. In the 46 years encompassed by the present study, no individual shoal makes a complete cycle across the entire inlet.

3.4.3. STRATIGRAPHIC MODEL

To explore the stratigraphic model, we examine seven vertical cross-sections through the ebb-tidal delta (Figures 3.6 & 3.7), chosen to best illustrate key morphodynamic behaviours:

- **Section A-A'** spans the width of the inlet between the islands of Terschelling and Ameland. The Boschplaat (the eastern tip of the island Terschelling, $X = 2-5km$) eroded nearly 3 km westward in the past 50 years (*Elias et al.*, 2019). The shoal and channel complex left behind in its wake at the centre of the inlet ($X = 3-6km$) is highly dynamic. From $X = 2-4km$, the active depth reaches around $-4m$, whereas eastward ($X = 4-6km$) the active layer extends deeper to about -6 to $-10m$. This is a result of the dynamic secondary channels that continuously rework the sediment. Even though Zeehondjeplaat ($X = 5-6km$) retains its height, the deposit age indicates that it has been heavily reworked (to a considerable depth – down to $-10m$). This apparently stable shoal is actually highly morphodynamic.
  There is a clear channel fill sequence as the main ebb-channel (Borndiep) migrates westward at this location ($X = 6-7km$). Note, however, that south of this transect, the channel migrates eastward into the island, necessitating shore protection works and nourishments.
- **Section O-B'** extends northwest from the inlet across the Kofmansbult platform. There are extensive channel fills in the proximal part of the Borndiep ($1-2km$), but the distal parts of the profile are characterized by extensive recent deposition in subtidal ebb spillover lobes. The seaward growth of these lobes is evident from the steep lee slopes of progressively newer deposits (at $\sim 4km$), whereas the rear slope (at $1.5-3.5km$) is much milder and eroding into older deposits. The active deposits in this transect are typically $4-8m$ thick, since this cross-section roughly follows the former centreline of the Akkepollegat ebb channel. The maximum shoal height appears to decrease with distance, from $-2m$ between $2-3km$ to almost $-4m$ at $6-7km$. In 2018, a $5\times10^6 m3$ sand nourishment was placed at the seaward edge of the profile ($6-7km$).
- **Section O-C'** extends due north of the inlet through the Akkepollegat ebb channel. At the proximal end of the section there are deep deposits associated with infilling of the Borndiep ($0-2km$) and the growth of the Oostwal shoal. Recent deposits in the middle of the section are thin or non-existent, as in 2019 the Akkepollegat is migrating laterally and eroding into older sediment ($2-5km$). At the far end of the transect lies the distal lobe deposits of the delta ($5-7km$).
- **Section O-D'** cuts northeast past the tip of Ameland and across the Borndiep swash platform. In 2019, the beach of Ameland was nourished ($0.5-2km$) to limit coastal erosion there. This nourishment filled in part of a shallow marginal channel, the Oostgat, which persists in the middle of the transect ($2.5-4.5km$). The channel has been gradually squeezed against the Ameland coast, so there is relatively little deposition there. At the distal end of the profile lies the Bornrif Bankje, a large sandy shoal that began attaching to the Ameland coast in about 2016 (*Elias et al.*, 2019).
  A crucial difference between the Oostgat and the main channels to the west (i.e., Borndiep, Westgat, and Akkepollegat before 2011) is that it does not scour beneath the surface of the Bornrif platform. Its definition as a channel is mainly due to the development of shoals on either side of it (see also Section F- F') .
- **Section E-E'** is a 6 km long arc spanning the proximal part of the delta at a radius of 2 km from the origin. Recent shallow channel fills at $0-1km$ are associated with shoal

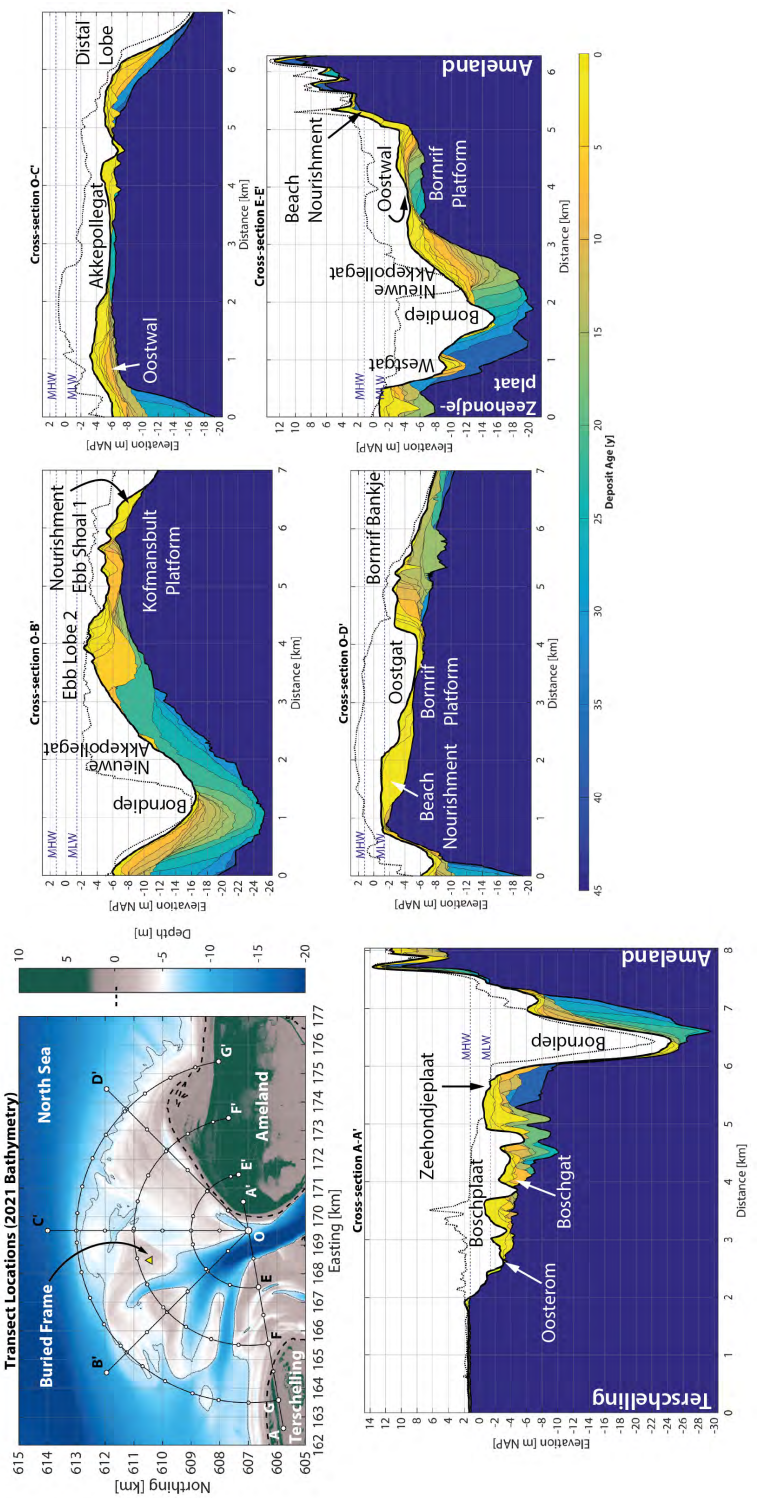

Figure 3.6: Ameland ebb-tidal delta bathymetry and stratigraphic sections. The maximum surface elevation across all surveys is given by a thick dotted line. Mean Low Water (MLW, $-1.4m$ NAP) and Mean High Water (MHW, $+1.2m$ NAP) are indicated with blue dotted lines. Small white circles on the transect location map correspond to the $1km$ intervals on the x-axes of the accompanying cross-sections. See Figure 3.2 for an explanation of how to interpret the transects. The small triangle in the map represents the approximate location of a measurement frame that was buried beneath the migrating Ebb Lobe 1 during a storm in October 2017.

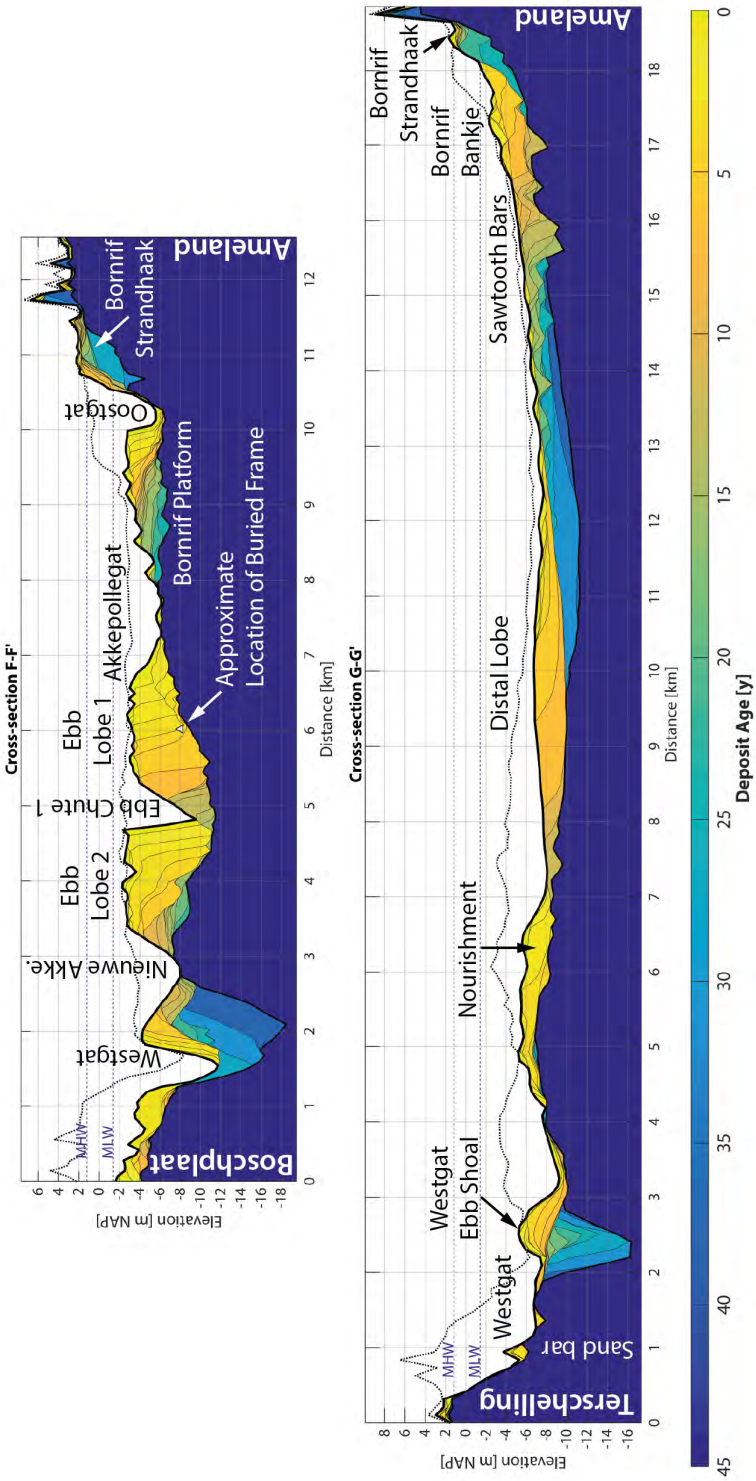

Figure 3.7: Figure 3.6, continued. Stratigraphic sections derived from historical bathymetry, with older deposits in blue and more recent deposits in yellow. The maximum surface elevation across all surveys is given by a thick dotted line. Mean Low Water (MLW, $-1.4m$ NAP) and Mean High Water (MHW, $+1.2m$ NAP) are indicated with blue dotted lines. See Figure 3.2 for an explanation of how to interpret the transects. The small triangle in F-F' represents the approximate location of a measurement frame that was buried beneath the migrating Ebb Lobe 1 during a storm in October 2017.

development at the tip of the Zeehondjeplaat. The much older and deeper channel fills between $0.8-1.5km$ are connected with the infilling of the Westgat, which used to be the primary ebb channel from the 1950s-1980s (*Elias et al.*, 2019). Channel fill between $1.5-3km$ corresponds to the switch of the main ebb-channel from the Westgat to the Akkepollegat, beginning in the 1980s. The Akkepollegat migrated laterally with a fairly persistent base of $-19m$ until approximately 2007, at which point it began to diminish in importance and accrete vertically. In contrast to the steeper-banked active channels (e.g., A-A' at $7km$), infilling channels on the ETD tend to have more gradual side slopes, and are deposited in much thinner layers (e.g., at $2.5km$). At $3-5km$, the gradual progradation of the Oostwal shoal can be seen. At $5km$, the 2019 beach nourishment fronts the Ameland coast, on which high dunes extend above the intertidal zone.

- **Section F-F'** cuts across the medial part of the delta (4 km from the origin) and spans from the Boschplaat to Ameland, clearly demonstrating the shoal bypassing process illustrated in Figure 3.5. Between $1-3km$, the extensive channel fill of Westgat seen in Section E-E' continues. Westgat has continued to narrow in recent years as the Nieuwe Akkepollegat channel ($2-3km$) widened and encroached southward ($\sim 2km$). Ebb Lobe 2 emerged at the tip of Nieuwe Akkepollegat, outbuilding laterally on both sides and migrating clockwise around the inlet, encroaching on Ebb Chute 1. Ebb Chute 1 and Ebb Lobe 1 are migrating clockwise and encroaching on Akkepollegat, the former main ebb channel. This migration tends to occur most rapidly during fall and winter storms (*Elias et al.*, 2022). Vividly illustrating this process, a measurement frame placed at 168.46 km N, 610.44 km E (53.48^oN 5.59^oE) on September 19, 2017 was irretrievably buried beneath the migrating Ebb Lobe 1 during a large northwesterly storm on October 3-7, 2017.[1]
  The minimum surface along F-F' between approximately $4-8km$ corresponds to the former and current base of the Akkepollegat channel and Ebb Chute 1. Section F-F' shows the fate of a former main ebb channel – as Akkepollegat migrated eastward, more and more flow was diverted to the western channels (*Elias et al.*, 2019). Akkepollegat still scours the main platform, but only a shallow channel forms – it does not have the strength to carve a pronounced channel here (see also O-C'). The western channel embankment only forms as Ebb Lobe 1 pushes eastward.
  On the eastern bank of the Akkepollegat, a shallow shoal steadily accretes vertically and migrates shoreward across the Bornrif platform, encroaching on the Oostgat marginal channel ($2-3km$). The maximum surface elevation reveals that the ETD at this radius from the inlet has remained completely subtidal, at an average depth of 3 m. At the coastline ($11km$), the remnants of the Bornrif Strandhaak (a shoal which attached to Ameland in the 1990s) are visible, although it has been eroded and subsequently re-deposited by the Oostgat.
- **Section G-G'** spans a 17 km transect along the distal end of the delta, $6km$ from the origin. The shoreline of Terschelling has retreated by over $1km$, encroached by Westgat ($0-2km$). Between $2-3km$, the vertical infilling of the formerly-dominant Westgat is evident, and this area is now capped by an ebb-tidal shoal at the end of the present-

[1] Given the apparent migration rate of Ebb Chute 1, I suspect that the frame could re-emerge in as little as 5 years. However, if the channel fills up (as Nieuwe Akkepollegat becomes the dominant ebb-channel), Ebb Chute 1 may simply pass over top of the frame without uncovering it. In that case, it might be much longer before before it resurfaces – hopefully by the time I retire...

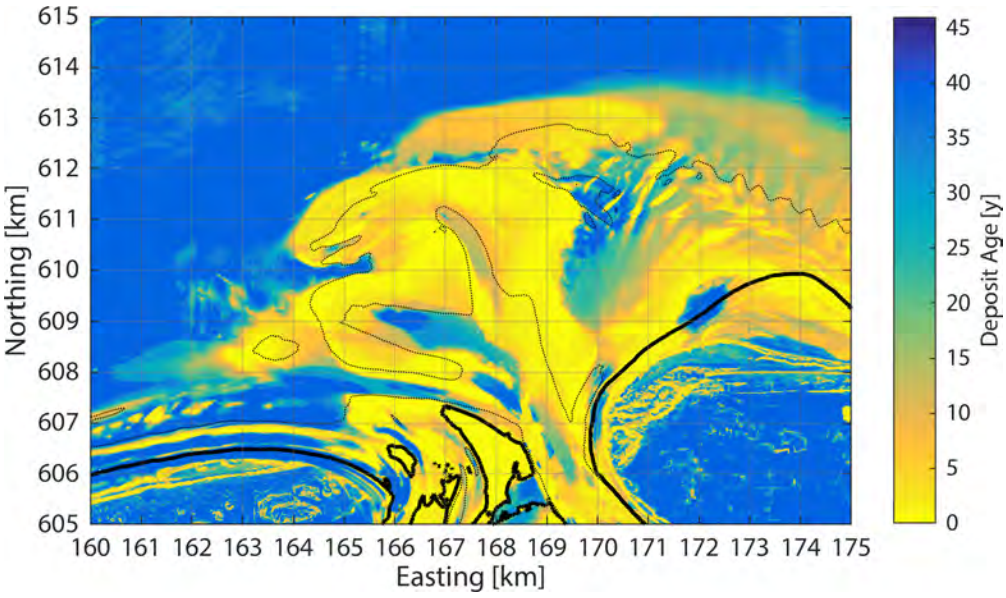

Figure 3.8: Surface deposit age, calculated using the average age of deposits in the top 1.0 m of the seabed. The approximate mean low water level (MLW) contour at -1.4 m NAP (*Normaal Amsterdams Peil*, approximately mean sea level) in 2021 is represented with a thick black line, and the -6 m NAP depth contour is indicated with a thin dashed line.

day channel. The 2018 ETD nourishment sits between $4-7km$ atop the seaward edge of Ebb Lobe 1. The relatively recent distal lobe spans from $7-12km$, and migrates in a clockwise (locally, eastward) direction. The eastern edge of the delta ($12-17km$) is characterized by a series of onshore-migrating sawtooth bars, discussed in greater detail by *Brakenhoff et al.* (2019b). At the Ameland coast, the more recent Bornrif Bankje (circa 2015) abuts against the older deposits of the Bornrif Strandhaak (circa 1989).

The stratigraphic model provides an additional perspective on the ebb-tidal delta dynamics revealed by the polar analysis. The arc transects of E-E', F-F', and G-G' depict the same clockwise migration patterns demonstrated in Figure 3.5c. Similarly, the radial transects O-B', O-C', and O-D' indicate sedimentary structures that correspond to the seaward growth of the delta observed in recent years (Figure 3.5d).

In addition to the delta's dynamic behaviour, the stratigraphic model shows much about the less mobile sedimentary deposits that remain preserved. The surface deposits of Ameland ebb tidal delta circa 2019 are generally young (< 5 years), which reflects the continuous reworking of the system (Figure 3.8).

The oldest areas of exposed sediment correspond to channel incision and migration in Ebb Chute 2, Westgat, the seaward tip of Akkepollegat, and Oostgat. Older material is exposed on the shoreface west of the delta, whereas the shoreface east of the delta is more freshly deposited. Bar migration on the upper shoreface of Terschelling reveals alternating patterns of older and younger sediment.

Beneath the present-day surface, large portions of the ebb-tidal delta have remained undisturbed for at least the last 46 years. These are indicated by the oldest, dark blue sed-

iment in Figures 3.6 & 3.7 and the shallowest regions of the minimum bathymetric surface in Figure 3.3b. The most stable parts of the ebb-tidal delta appear to be the Bornrif platform to the east and the deeper parts of the Kofmansbult platform to the west. The majority of shoals on the ETD are continuously reworked on timescales of less than 10 years.

3.5. DISCUSSION

In this study, we developed a combination of techniques for mapping and analyzing the decadal scale morphodynamics and stratigraphy of a mixed-energy ebb-tidal delta. This approach leverages bathymetric data in ways that provide new insights into the dynamics of present-day ETDs or the strata left behind by ancient ETDs. The conformal mapping (polar) analysis collapses large amounts of spatiotemporal bathymetric data into a single figure that clearly shows key morphodynamic behaviour like ebb-tidal delta bypassing. The combination of conformal mapping and stratigraphic modelling provides greater interpretive value than either approach in isolation. Our approach also gives useful information for dealing with contemporary coastal management issues like nourishment planning, by indicating where deposited sediment is more likely to migrate or persist. This methodology is generally applicable to any coastal or submarine landscape where high resolution (in space and time) digital elevation models or numerical model output are available. We demonstrated this technique by applying it to 46 years of bathymetric surveys from Ameland ebb-tidal delta in the Netherlands. Together with the narrative explanation of morphological evolution from studies like *Elias et al.* (2019, 2022), these techniques provide a powerful set of tools for analyzing and interpreting ebb-tidal delta dynamics.

3.5.1. PRESERVATION POTENTIAL

The stratigraphic model developed here provides insight into the preservation potential of Ameland ebb-tidal delta on yearly and decadal timescales. Deposits are eroded rapidly at first, and then more gradually after several years. Surficial sediments are extensively reworked, indicative of the large gross but small net changes observed there (*Elias et al.*, 2022). The thickest deposits with the greatest preservation potential over the observed timescale are channel fills (Figures 3.6, 3.7, and 3.3e). With the exception of some deeper channel fills, the majority of sediment deposited in the 1970s to 1990s has already been reworked by the 2021 (Figures 3.6 & 3.7).

Via this approach, we can clearly demarcate the active and passive parts of the ebb-tidal delta on decadal timescales. The passive (blue) part and the ebb-tidal delta as a whole are governed largely by the tidal prism (*Walton and Adams*, 1976). Conversely, we hypothesize that the active (yellow) part fluctuates in response to the sediment bypassing process. This distinction is particularly useful in the case of features that appear relatively stable but are in fact continuously reworked (e.g., Zeehondjeplaat in Figure 3.6 Section A-A').

Our analysis does not consider regions which are stable over much longer periods than the 46 years analyzed here. *Elias et al.* (2019) indicate that the Bornrif platform has been very stable for the past two centuries with no major channel bisections since 1831, when a channel extended northeast across it to depths greater than 7 m. The Bornrif is a remarkably persistent feature, present in its familiar form as far back as the first available nautical charts in 1585. Conversely, the main ebb-channel nearly always occupies the northwest quadrant of the delta, and although deposits there tend to be thick, this area is subject to frequent reworking. Ages of preserved deposits derived using our method could be further verified

in the field with geochronological methods (e.g., *Reimann et al.* (2015); *Fruergaard et al.* (2015)).

3.5.2. SEDIMENT DYNAMICS

Sediment bypassing across the delta in shoals can now be more accurately quantified with the techniques shown here. The clockwise migration of shoals and channels around the inlet is corroborated by both the polar analysis and stratigraphic model (e.g., Figure 3.5c and Cross Section F-F' of Figure 3.7). Although this is perhaps unsurprising given that their underlying datasets are the same, it demonstrates their combined usefulness for interpretation of complex patterns.

The utility of the polar/conformal mapping approach extends to sediment properties like grain size. Projecting sediment samples from Ameland ebb-tidal delta into polar coordinates illuminates a clear decreasing trend and reduction of variability in median grain size (d_{50}) clockwise around the inlet (*Elias et al.*, 2022). This coincides with the direction of shoal migration and channel rotation mapped in Figure 3.5c. *van der Vegt* (2018) also demonstrated spatial variation in grain size of river deltas using polar mapping.

It is not possible to conclusively estimate the duration of a full bypassing sequence from the present data, since the longest continuous ridges or troughs in Figure 3.5c traverse no more than halfway around the inlet. Previous estimates of Ameland's bypassing period estimated a cycle duration of 50 to 60 years (*Israel and Dunsbergen*, 1999; *Ridderinkhof et al.*, 2016; *Cheung et al.*, 2007). The timescale of main ebb channel switching appears to be on the order of 50 years, given that the primary ebb channel (Nieuwe Akkepollegat) in 2021 is west-aligned for the first time since 1975. *Elias et al.* (2019) suggest that multiple small bypassing events may be necessary to create sufficient shoal volume on the downdrift platform to trigger a major shoal bypassing event.

The results of Figure 3.5c make it apparent that the definition of a bypassing cycle needs clarification: is it just the time between shoal attachments on the downdrift coast, or is it about tracking a discrete plug of sand from one side of the inlet to the other? Multiple forms of shoal bypassing can exist, with differently-sized shoals migrating along different pathways and at varying timescales. These shoal migrations may be due to the migration of the main ebb channel (e.g., on the Bornrif Figure 3.5c (v)) or may arise from local instabilities (e.g., the initial formation of ebb chutes Figure 3.5c (iii)). We hence advocate for using the term bypassing "sequence" (as per *Elias et al.* (2012a)) in lieu of "cycle" to better reflect the often nonlinear, discontinuous, and aperiodic nature of the process.

Furthermore, bar migration is not completely representative of the sediment bypassing process since part of the transport is in suspension. A recent tracer study at the Ameland ETD nourishment site indicated that individual grains of sand can migrate several kilometers in just a few tidal cycles (Chapter 6), which is more indicative of gross transports than the net transport represented by shoal migration. The adoption of Lagrangian sediment transport models (e.g., *MacDonald and Davies* (2007); *Soulsby et al.* (2011); Chapter 8) could be used to identify the transport pathways connecting eroding and depositional regions of the ETD.

3.5.3. COASTAL MANAGEMENT IMPLICATIONS

Coastal management and policy makers require new tools and approaches in order to make informed decisions (*Lodder and Slinger*, 2021). Our new mapping approaches show the

storage potential of ETDs for sediment on annual to decadal timescales. Understanding the changes in the active volume of the ETD may lead to better estimates of when it is acting as a net sediment source or sink. This knowledge can inform nourishment strategies by indicating where and when to nourish, depending on the location and longevity of existing deposits. Placing a nourishment in an (comparatively) inactive zone will lead to less dispersive behaviour than placing it a highly dynamic zone. The choice depends on the goal of the nourishment (preserving volume versus increasing sand fluxes in a specific location).

For instance, the clockwise migration of shoals at approximately 15° / *decade* (Figure 3.5c) suggests that the bulk of the nourishment placed in 2018 will likely take several decades before reaching the downdrift Ameland coast. If the goal is to directly feed Ameland, it should be placed closer to the shore (e.g., at the location of the beach nourishment in Figure 3.6 Section E-E'). However, for a goal of increasing the total sediment budget of the ebb-delta on longer timescales, the location of the 2018 nourishment was likely a good choice.

Equilibrium models are frequently used to predict the evolution of ETDs at timescales of 10 to 100+ years (*Stive and Wang*, 2003; *Lodder et al.*, 2019; *Wang et al.*, 2020). These models typically schematize ETDs as homogeneous deposits that directly exchange sediment with neighbouring coasts and basins. Recent numerical modelling studies (*Herrling and Winter* (2018); Chapter 7) reveal complex sediment pathways across ETDs and their surroundings, which are also reflected by the patchiness of sediment deposition presented here (Figure 3.6 & 3.7). This calls into question the assumption of perfect, symmetric sediment connectivity between the ebb-tidal delta and other components of the coastal system. Understanding the actual spatial heterogeneity of ETD deposits and the resulting implications for sediment connectivity is essential to making good long-term predictions of these systems.

In addition to planning nourishments, understanding where stable and unstable areas of ETDs are located is important for protecting coastal and submarine infrastructure (e.g., cables and pipelines), as eroding coasts and nearshore regions pose hazards for these (*Eide et al.*, 1992; *Pearson et al.*, 2016). In this regard, the minimum surface and envelope of morphodynamic change (Figure 3.3b,c) provide valuable metrics for planning.

Ebb-tidal deltas are often perilous for navigation and frequently lead to shipwrecks (*McNinch et al.*, 2001, 2006; *Wells and McNinch*, 2003; *Torres*, 2015). Knowledge of the maximum historic surface and envelope of morphodynamic change are thus valuable for safe navigation, since they indicate the shallowest and most dynamic regions of the ETD. In the event of a shipwreck or other such maritime incident, the stratigraphic modelling approach demonstrated here is also valuable for marine archaeology and salvage operations (e.g., the buried measurement frame in Figure 3.7 F-F'). Our techniques are useful for any application where it is necessary to understand the burial and re-emergence of objects and infrastructure on ETDs.

3.5.4. COMPARISON WITH GEOLOGICAL MODELS

ETD stratigraphy has been well-explored and classified in previous studies, so here we present a comparison with our own technique. *Imperato et al.* (1988) and *FitzGerald et al.* (2012) identify three main elements of ebb-tidal delta architecture at mixed-energy tidal inlets:

1. *Marginal flood channel deposits*, characterized by steep, sharp erosional contact with adjacent barrier sand and upper shoreface deposits (e.g., Figure 3.6 Cross Sections A-A', E-E'), as well as infilled channels topped by swash bar deposits. *Imperato et al.* (1988) notes that the shoreward migration of swash bars usually reworks deposits

from previous bars, so that the complete sequence of a single bar is seldom preserved. This reflects what we see on the Bornrif: thin layers sediment gliding over the underlying platform without substantial vertical accretion.

2. *Proximal delta deposits*, formed primarily by migration of the main ebb channel, thick and with a sharp contact with underlying Pleistocene sediment. Ameland Inlet is underlain by a highly resistant Pleistocene potclay layer between approximately -25 and $-30 mNAP$ (*van der Spek*, 1994). This layer restricts the inlet channel depth and thus leads to a thinner inlet sequence compared to what would be expected in a completely sandy case. The thickest parts of the active delta are along the margins and bed of the former and current main ebb-channels (Figure 3.3d). This is consistent with *Moslow and Tye* (1985), *Imperato et al.* (1988), and *Sha* (1989b) who note that ebb-channel deposits tend to be the thickest, most preservable ETD facies on longer timescales. The repeating sigmoidal downdrift-dipping surfaces observed in Cross-Section F-F'(Figure 3.7) are consistent with migrating inlet/spit systems (*FitzGerald et al.*, 2012).

3. *Distal delta deposits*, which are 1-4 m thick and interweave with seaward shoreface sediment. These are evident in Cross Sections O-B', O-C', and G-G' (Figure 3.6 & 3.7), and have been confirmed with vibrocore samples offshore of the present study area by *van der Spek et al.* (2021).

Our results thus provide a clear explanation of the layering and sedimentary structures that are typically observed in the geological record. Previous studies mentioned above have largely relied on core samples, numerical models, and sparse surveys to construct stratigraphic models of ebb-tidal deltas, but the approach presented here provides a new way to find this information, and provides a novel perspective on the genesis of these architectural features. Future research should also consider relating the stratigraphy developed with this approach to observations of bed sediment particle size (e.g., *Elias et al.* (2022)).

3.5.5. OUTLOOK

Having demonstrated our approach for Ameland ebb-tidal delta, the logical next steps for future research are to apply and extend these techniques at other tidal inlet systems. For instance, future studies could investigate more advanced techniques for optimizing the choice of origin or even use a conformal mapping layout that better reflects a given site's morphology than a fixed polar grid. Ameland is a somewhat ideal case in that like many stabilized tide-dominated inlets (*FitzGerald*, 1984; *Sha and De Boer*, 1991; *Tye and Moslow*, 1993; *Smith and FitzGerald*, 1994; *Elias et al.*, 2006; *Son et al.*, 2011; *Eelkema et al.*, 2013), it pivots around its inlet, so its dynamics map remarkably well to a polar grid. However, a polar coordinate system may not be the best choice for analyzing all ETDs, particularly multi-inlet systems or less stable wave-dominated inlets that migrate rapidly or close intermittently (*Morales et al.*, 2001; *Nienhuis and Ashton*, 2016).

Our method for developing a stratigraphic model from bathymetric surveys is applicable regardless of a system's dynamics, though. The main requirement is sufficiently high temporal resolution to capture the true reworking of sediment (*Vonhögen-Peeters et al.*, 2013). For shallower ETDs, the necessary frequency of measurement could be obtained via remote sensing (e.g., *Pianca et al.* (2014); *Harrison et al.* (2017); *Ford and Dickson* (2018); *Humberston et al.* (2019); *Zhang et al.* (2020a); *Heimhuber et al.* (2021)). Together, polar

and stratigraphic analyses give researchers new means of simplifying and quantifying ETD dynamics, which could be used to quantitatively generalize ETD behaviour by examining other sites.

Although the temporal resolution of the Ameland dataset is high enough to resolve most decadal-scale morphodynamic changes, it is not sufficient to resolve seasonal patterns or the influence of specific storm events. To shed more light on these matters, the stratigraphic modelling approach could be further extended to process-based numerical model output. There are still many unresolved challenges in morphodynamic modelling of ebb-tidal deltas (*Elias et al.*, 2015a; *Lenstra et al.*, 2019a), and the results of this study can help in their analysis and interpretation by providing new types of information to validate against. Numerical models could also conceptually extend the present approach to look at the role of grain size, sorting, and provenance in depositional processes, similarly to *van der Vegt et al.* (2020).

The approach demonstrated here is also likely to be applicable on other diverging sedimentary systems, such as alluvial fans, submarine fans, river-dominated deltas, or fan deltas. Distributary channels in these systems tend to radiate from a single outlet, which suggests that a radial collapse of the data could be an effective way to represent major morphodynamic trends.

3.6. CONCLUSIONS

We demonstrated the development and application of new approaches to mapping and analyzing ebb-tidal delta (ETD) dynamics, using the high resolution, frequent bathymetric surveys of Ameland Inlet in the Netherlands. Conformal mapping (polar) analysis provides a novel perspective on the analysis of ETD bypassing, by aligning the coordinates of analysis with the principle directions of sediment transport and morphodynamic evolution. In doing so, we transform the complex geometry of the ETD into a more convenient format for analyzing the morphologic patterns and sediment transport pathways that are of interest to coastal scientists and managers. With this approach, the bypassing behaviour described by *Elias et al.* (2019) and *Elias et al.* (2022) can be collapsed into fewer dimensions and the patterns expressed more simply as a timestack. This enables the concept of ETD shoal bypassing and the rotational migration of ebb-tidal deltas to be investigated more continuously and quantitatively than previous efforts on the topic. There is a clear clockwise motion of shoals and channels of approximately 14°/*decade*, which corresponds to the dominant direction of longshore drift and offshore tidal dominance.

The interpretation made from the polar analysis is complemented by a decadal-scale stratigraphic model of Ameland ETD that we produced from the differences between repeated bathymetric surveys from 1975-2021. This approach permits the detailed analysis of deposit thickness, spatial distribution, age, and preservation potential. The majority of shoals in the active part of the ETD are continuously reworked on timescales of less than 10 years. These findings provide insight into the most stable regions of the ebb-tidal delta, which is important information for predicting how these features are likely to evolve in the future. This also provides a new and valuable approach for interpreting modern and ancient ETD stratigraphy.

Our analyses are permitted by the wealth of frequent, high-resolution bathymetric surveys conducted at Ameland Inlet. This method can be applied to any coastal system, but is best used where the data spans the dominant timescale of morphological change for the site, and with sufficiently high resolution in space and time to capture detailed phenomena.

As such, the approach can also be applied to numerical model output. Together, the techniques presented here give researchers a new means of simplifying and quantifying ETD dynamics, and can lead to more generalized depictions of ETD behaviour. Furthermore, the approach can be applied to validate and interpret outcomes from numerical models. The improved understanding and practical techniques provide coastal managers with useful tools for sediment management and optimizing nourishment strategies in such complex environments. This will better prepare them to tackle future challenges posed by climate change and human interventions.

ACKNOWLEDGEMENTS

This work is part of the research programme 'Collaboration Program Water' with project number 14489 (SEAWAD), which is (partly) financed by NWO Domain Applied and Engineering Sciences. Special thanks to the Dutch Ministry of Infrastructure and Water Management (Rijkswaterstaat and Rijksrederij) for their ongoing support as part of the Kustgenese2.0 project. We thank David Hoyal and an anonymous reviewer for their positive and constructive feedback. A special thank you is extended to Anna-Maartje de Boer who originally asked, "where is the oldest sand on the ebb-tidal delta?", the question that inspired this analysis. The *Vaklodingen* bathymetric data used in this study are publicly available at: https://waterinfo-extra.rws.nl/monitoring/morfologie/. *Actueel Hoogtebestand Nederland* (AHN) topographic data are available at https://www.ahn.nl/.


Observations of
SUSPENDED PARTICLE SIZE
on an Energetic Ebb-Tidal Delta

Dear Reader,

I am really excited because we have a fancy sand laser that lets us see how big the sand particles floating through the water in Ameland are. This will be important information for understanding where, how much, and what size of sand is moving around out there. Hopefully we can link the wave and tidal conditions with what we observe floating around in the water. Did I mention we get to play with a sand laser?

Stuart

Delft University of
Technology
Stevinweg 1
2628 CN Delft

4

OBSERVATIONS OF SUSPENDED PARTICLE SIZE DISTRIBUTION ON AN ENERGETIC EBB-TIDAL DELTA

KEY POINTS:

- *In situ* suspended particle size distributions and hydrodynamics were measured on Ameland ebb-tidal delta
- There are two distinct populations of suspended sediment: locally resuspended fine sand and mud exported from the Wadden Sea.
- Additional techniques are needed to distinguish suspended sand from mud in mixed sediment environments.

This chapter has been presented as part of *Coastal Sediments 2019: Proceedings of the 9th International Conference*:

Pearson, S.G., van Prooijen, B.C., de Wit, F.P., Holzhauer-Meijer, H., de Loof, A.P., & Wang, Z.B. (2019). Observations of suspended particle size distribution on an energetic ebb-tidal delta. *Coastal Sediments 2019: Proceedings of the 9th International Conference*, May 27-31, 2019, St. Petersburg, Florida. [Link].

IN the previous two chapters, we examined snapshots of Ameland ebb-tidal delta as it evolved over the decades. Millions of cubic metres of sand shift between each map, but we did not measure the physical processes leading to these changes, only the effects. In this chapter, we begin to examine how sediment transport in suspension across the ebb-tidal delta varies as a function of grain size and under the influence of different wave and tidal conditions. We focus on the particle size distributions of suspended sediment (obtained using a device called a LISST) during a period of several weeks. We then compare these measurements with the particle size characteristics of the seabed. The aim of this chapter is to quantify the details of sediment transport processes on the scale of individual particles, in order to inform the larger-scale analyses elsewhere in this dissertation.

ABSTRACT

Sustainable management of barrier islands and tidal inlet systems requires a knowledge of sediment transport pathways throughout the system. this chapter places in situ suspended sediment observations (obtained using a LISST) in context with seabed sediment samples and hydrodynamic measurements to identify such pathways. The results indicate two distinct populations of sediment in suspension on the ebb-tidal delta: locally resuspended fine sand and (largely flocculated) mud exported from the Wadden Sea on ebb tide. This reinforces the notion of the strong dependence of sediment pathways on particle size. Future work will combine additional lines of evidence to better distinguish suspended sand from sand-sized flocs and provide a more robust definition of these pathways.

4.1. INTRODUCTION

SUSTAINABLE management strategies for barrier island coasts and tidal inlets require robust predictions of their morphological evolution. These systems play a key role in flood safety, navigation, fisheries, and form a living environment for numerous mammals, birds, fish, and benthic species. To predict the response of such systems to human interventions (e.g., dredging or nourishments) or sea level rise and other climate change effects, it is necessary to quantify the pathways that sediment takes as it moves through the system. Sediment transport pathways at tidal inlets are governed by complex interactions between tides, waves, wind, and density-driven forcing, and may vary significantly as a function of particle size.

The current coastal safety policy of the Netherlands hinges around maintaining sufficient sediment supplies in the coastal zone. Understanding and predicting the long-term infilling trends of the Wadden Sea and the consequent source or sink from the adjacent coastline is thus of critical importance (*Wang et al.*, 2018). Furthermore, it is necessary to quantify this net import and export behaviour of sediment as a function of grain size.

This chapter links in situ observations of suspended sediment particle size to the composition of the seabed and concurrent hydrodynamic conditions in order to estimate sediment sources, pathways, and receptors across the Ameland Inlet system.

4.2. METHODOLOGY

From August to October 2017, an extensive field measurement campaign was carried out at Ameland Inlet in the Dutch Wadden Sea (Figure 4.1). Hydrodynamics, suspended sediment, and water quality were measured at 11 stations across the inlet, ebb-tidal delta, and tidal watersheds of the basin. This chapter focuses on the measurements obtained by a frame located on the distal end of the ebb-tidal delta (AZG Frame 4, Figure 2.1). Suspended particle measurements were contextualized with in situ measurements of hydrodynamic conditions and seabed sediment.

4.2.1. HYDRODYNAMIC ANALYSIS

Near-bed current velocities, water level, and wave heights during the monitoring period were measured using a downward-facing Nortek Aquadopp HR, a high-resolution Acoustic Doppler Current Profiler (ADCP). It was mounted $0.5m$ from the base of the frame, although actual height above the seabed varied due to field conditions. The ADCP sampled at a rate of 4 Hz in 30 minute bursts. These measurements were first depth-averaged and then averaged over the 30 min burst intervals. Each burst was classified into four tidal stages (flood, high water slack (HWS), ebb, and low water slack (LWS)) using the velocity measurements (Figure 4.2). At the measurement frame, the mean flood current is approximately eastward-directed, and the mean ebb current approximately westward.

4.2.2. BED SEDIMENT ANALYSIS

In addition, 165 box cores were obtained from the seabed in order to characterize the bed sediment composition (Figure 4.3). To obtain a sedimentologically representative coverage of the entire ebb-tidal delta, the locations of these cores were chosen based on a series of 16 benthic habitat zones, defined by their depth, slope, orientation, and degree of recent morphological change (*Holzhauer et al.*, 2021). Subsamples of $8cm$ depth were taken from

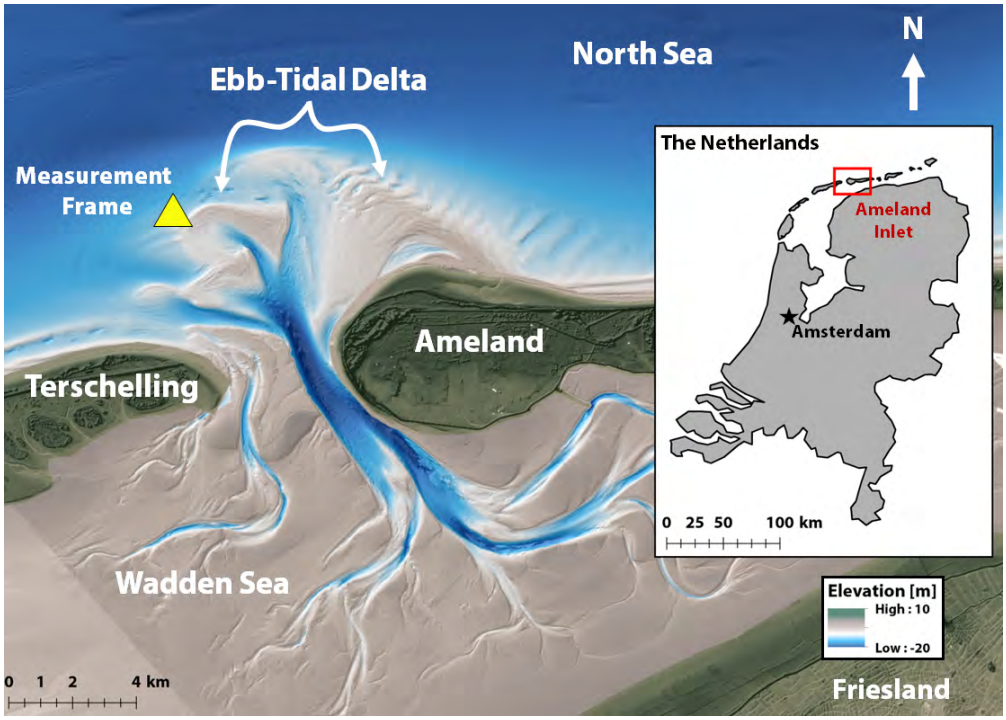

Figure 4.1: Site overview of Ameland Inlet, the Netherlands. The inlet sits between the islands of Ameland and Terschelling, and connects the North Sea with the shallow Wadden Sea. The yellow triangle indicates the location of the measurement frame on the western part of the ebb-tidal delta (8m depth).

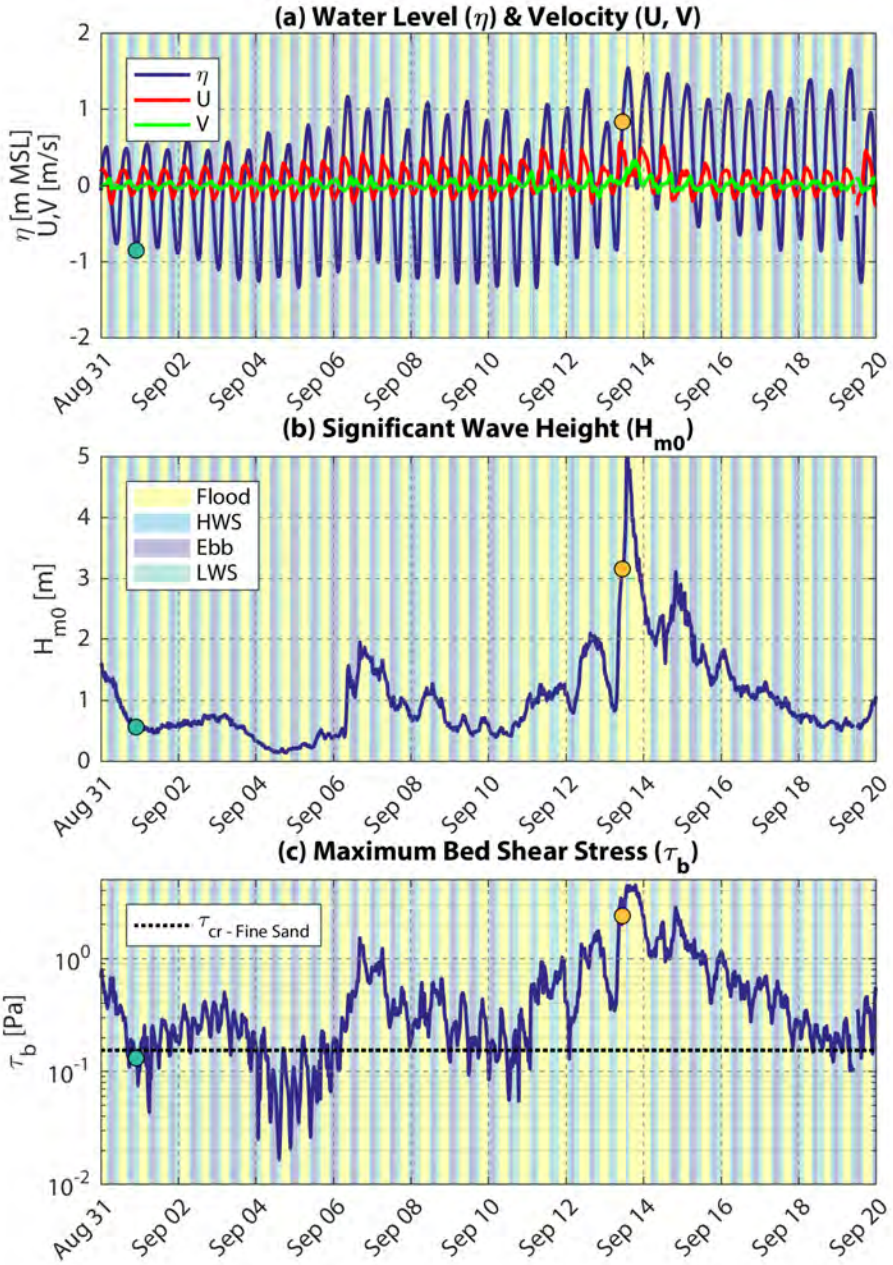

Figure 4.2: In situ measurements of 30 min burst-averaged (a) water level (η), near-bed velocity (U is positive eastward and V is positive northward) and (b) significant wave height (H_{m0}). Vertical stripes in (a-b) correspond to stages of the tidal cycle. (c) Maximum bed shear stress under waves and currents is calculated using the method of *Soulsby* (1997). The dashed black line in indicates the critical bed shear stress threshold for mobility of fine sand (125 μm) as calculated using *Soulsby* (1997). Coloured dots in (a-c) indicate sample times for *S*1 and S2 in Figure 4.4d.

the surface of the box cores and analyzed using a Malvern Mastersizer to obtain particle size distributions. This dataset was supplemented with additional samples from the Wadden Sea Sediment Atlas (*Rijkswaterstaat*, 1999; *TNO*, 2017) to provide additional context and greater spatial coverage (i.e., within the Wadden Sea).

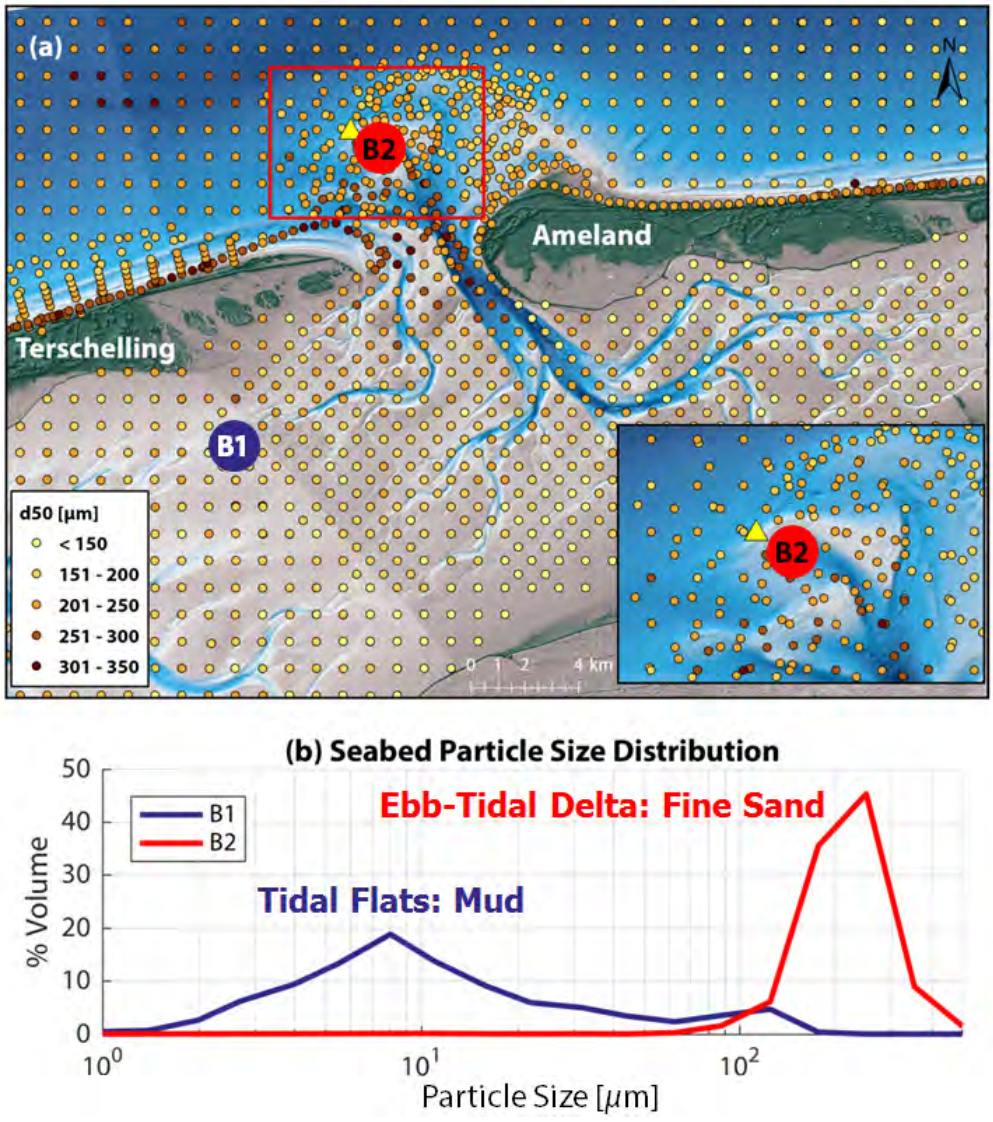

Figure 4.3: (a) Median bed sediment grain size (d_{50}). Ebb-tidal delta sediment was obtained from box cores for this study, and basin/offshore areas were obtained from the Wadden Sea Sediment Atlas (*Rijkswaterstaat*, 1999). The yellow triangle indicates the measurement frame. (b) Particle size distribution in the bed at key locations.

4.2.3. SUSPENDED PARTICLE ANALYSIS

Particle size distributions (PSD) of suspended sediment were obtained using a Laser In-Situ Scattering and Transmissometry (LISST-100X) instrument (*Sequoia Scientific*, 2015) mounted $0.6m$ above the seabed on Frame FED. Differently-sized spherical particles scatter laser light in characteristic patterns across 32 detector rings, enabling the calculation of volumetric particle concentration ($\mu L/L$) for 32 unique particle sizes ranging logarithmically from 2.5 to 500 μm. Bulk particle size statistics (i.e. d_{50} and sorting) were calculated using the Logarithmic Folk and Ward graphical measures (*Blott and Pye*, 2001).

The quality of the LISST measurements is highly dependent on the strength of the transmitted laser beam through the water column. If the optical transmission dropped beneath 10% (indicating extremely turbid water) or exceeded 99.5% (indicating extremely clear water), then the measurements were removed from consideration, as per Sequoia Scientific (2015). This amounted to 3% of the time series at the measurement frame. The LISST sampled at $1Hz$ for 15 seconds every minute; these samples were also averaged over the same 30 minute intervals as the ADCP.

4.3. RESULTS

4.3.1. HYDRODYNAMIC FORCING

The tide at Ameland Inlet is semidiurnal with a spring tidal range of approximately $2.3m$ at Frame FED (Figure 4.2a). During the monitoring period, three storms were observed; two on August 31^{st} and September 7^{th} with significant wave height $H_{m0} > 1.5m$, and the much larger Storm Sebastian on September 14^{th} with H_{m0} of approximately $5m$ (Figure 4.2b). The storms also had a significant influence on the water level and flow velocities. For instance, a significantly longer flood period is found during Sebastian. Bed shear stress due to the combined influence of waves and currents was calculated using the method of *Soulsby* (1997) to give an indication of the potential for local bed material to be resuspended at the measurement frame (Figure 4.2c). The critical motion threshold for the fine sand composing much of the local sediment is exceeded during all three storms and at spring tide, which suggests that the seabed of the ebb-tidal delta is highly mobile.

4.3.2. BED SEDIMENT CHARACTERISTICS

The bed of the ebb-tidal delta primarily consists of well-sorted fine sand (mean $d_{50} = 211\mu m$, standard deviation $d_{50} = 30\mu m$, $n = 165$), while the deeper parts of the inlet channel bed consist of medium sand (mean $d_{50} = 289\mu m$) and shell lags (Figure 4.3a). Mud content ($< 63\mu m$) of the ebb-tidal delta areas is typically $< 1\%$ by volume, although a slightly muddier patch exists at its northeastern edge. Conversely, the mud content is up to 20% in the bed at the landward edge of the Wadden Sea and along the tidal watersheds separating Ameland Inlet from its neighbouring basins.

4.3.3. SUSPENDED SEDIMENT CHARACTERISTICS

The total volumetric suspended particle concentration measured by the LISST varies by several orders of magnitude during the measurement period, from a base level of approximately $50\mu L/L$ during calmer periods to approximately $1700\mu L/L$ following Storm Sebastian (Figure 4.4). During periods with wave heights $< 1m$, a clear semidiurnal tidal signature is visible in the concentrations. Under calm conditions at LWS, total concentrations can ex-

ceed $1000 \mu L/L$.

The size of suspended sediment particles varies with ebb and flood currents, spring-neap cycles, and the impact of storms. The median suspended particle size (d_{50}) typically increases towards the end of flood, suggesting a dominance of sand-sized particles. The d_{50} then decreases during ebb, reaching a minimum at LWS, suggesting a greater contribution by mud-sized particles. Particles are generally best-sorted at the end of flood under calm conditions, whereas they tend to be poorly sorted after ebb or during storms.

Bed sediment closest to the measurement frame is mainly composed of fine sand (d_{50} = $186 \mu m$), and a sediment tracer study carried out on the site confirmed the transport of such sand particles in suspension across the ebb tidal delta (Chapter 6). The high concentrations of sand-sized suspended particles ($63 - 500 \mu m$) observed by the LISST would seem to reflect this; however, many of these particles appear at times when the bed shear stress is insufficient to suspend sand particles (Figure 4.4a), or beyond expected settling timescales for sand. However, such particle size distributions could be explained by the additional presence of flocculated mud and organic particles advected from a remote location, rather than solely locally-resuspended sand.

Suspended sand tends to be lognormally distributed and unimodal (*Sengupta*, 1979), whereas flocculated fine sediment and sand/silt/clay mixtures are often characterized by multimodal PSDs (*Lee et al.*, 2012). Suspended sediment in the inlet and on the ebb-tidal delta are usually multimodal (89% of 30 minute sample bursts, n = 1035), with peaks suggesting a combination of fine and medium sand, silt and clay particles (e.g., Figure 4.4d). Changes in the median particle size and sorting reflect the hydrodynamic forcing, but the multimodal nature of the PSDs mean that these statistics alone are insufficient to describe sediment dynamics on Ameland ebb-tidal delta.

Flocs can be distinguished by examining concurrent hydrodynamic measurements. High-concentration bursts of sediment (e.g., S1 in Figure 4.4d) frequently coincide with calm conditions at LWS. This suggests that the fine sediment has been ejected from the Wadden Sea during ebb tide past the measurement frame (e.g., Figure 4.5). Conversely, PSDs corresponding to flood tide and under high waves are more likely to contain higher proportions of sand (e.g., S2 in Figure 4.4d). Thus, there are two distinct populations of sediment in suspension on Ameland ebb-tidal delta: locally-resuspended sand, and mud originating from within the Wadden Sea. Both may be present simultaneously, but the dominance of a particular type depends on the hydrodynamic conditions.

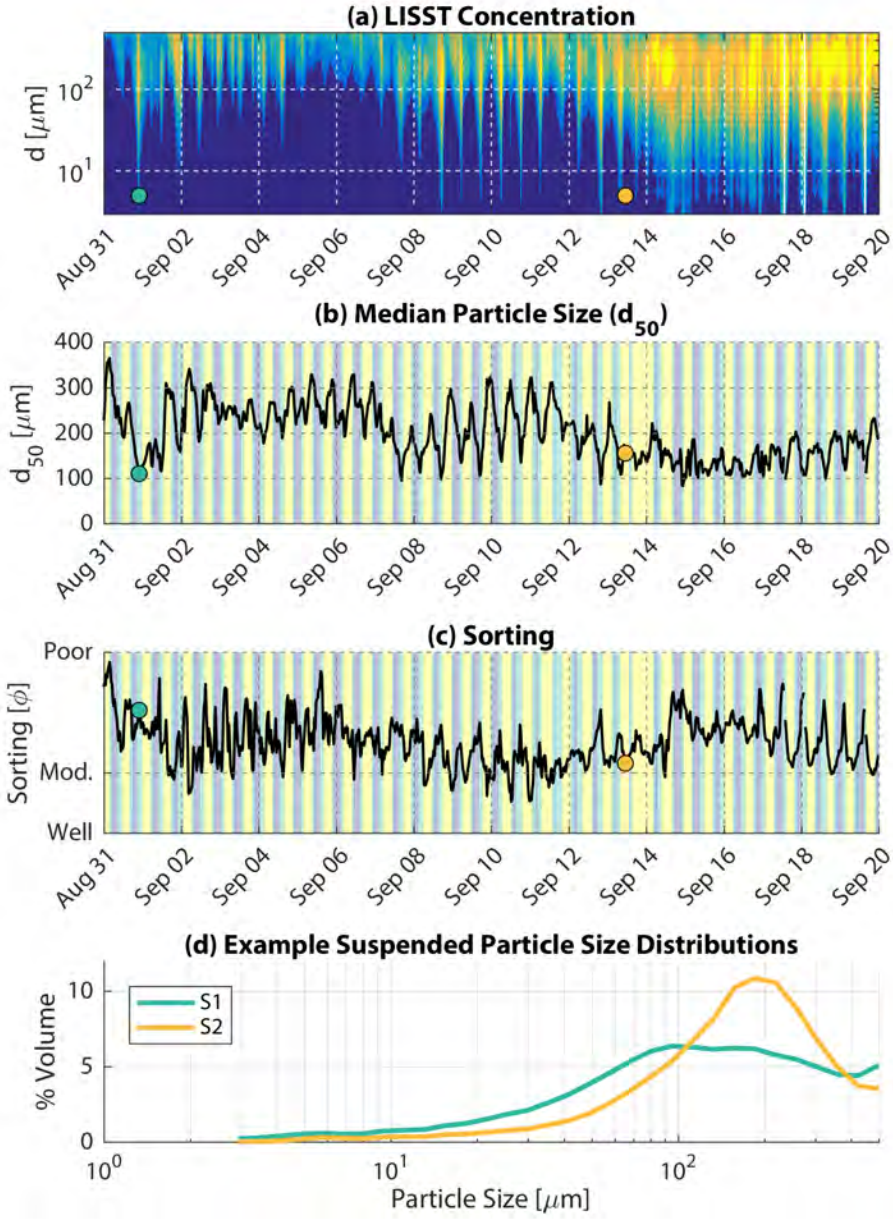

Figure 4.4: In situ measurements of (a) suspended particle size distribution and concentration measured using LISST at the measurement frame. (b) Median particle size (d_{50}) and (c) sorting coefficient (standard deviation) from 0.5 (well-sorted) to 2.0 (poor) using the Logarithmic Folk and Ward graphical measures (*Blott and Pye*, 2001). Vertical stripes in (b-c) correspond to stages of tidal cycle, see Figure 4.3 for legend. (d) Example particle size distributions at key moments. Coloured dots in (a-c) indicate sample times for *S*1 and *S*2 in (d)

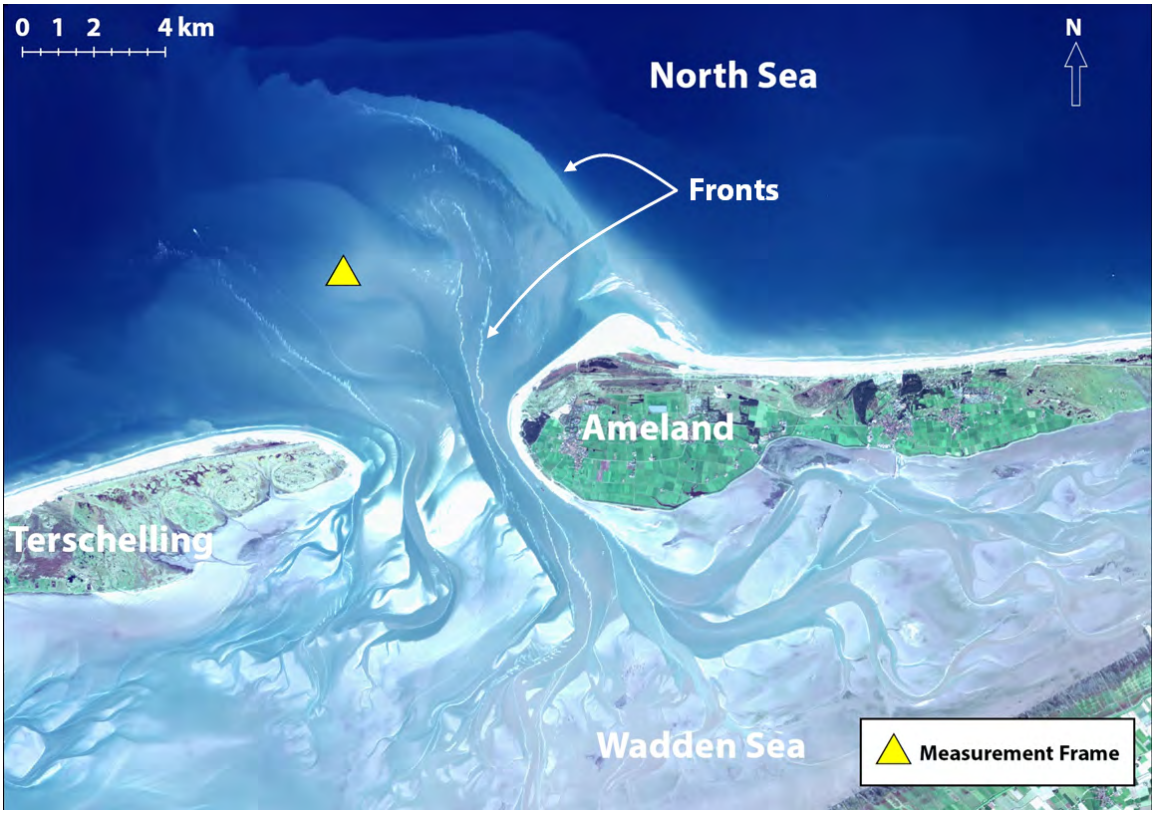

Figure 4.5: Satellite image of Ameland Inlet on October 15th, 2017 (outside the measurement period). Taken towards the end of low water slack (10:40am, a highly turbid plume of suspended matter is ejected from the Wadden Sea, across the ebb-tidal delta and several km into the North Sea. Fronts are visible as white lines of foam and zones with sharp colour contrast, suggesting abrupt spatial gradients in suspended sediment composition. The yellow triangle indicates the measurement frame used in this chapter. Sentinel-2 image courtesy of satellietbeeld.nl: ©NEO B.V. Amersfoort, ©ESA 2015-2018.

4.4. DISCUSSION

There are two distinct populations of sediment in suspension on Ameland ebb-tidal delta, and their presence depends on the hydrodynamic conditions. Locally resuspended sand at flood tide reflects the predominantly fine sand of the ebb-tidal delta, whereas the presence of flocculated mud at ebb and LWS reflects the Wadden Sea's much higher mud content. This reinforces the notion of different pathways and connectivity as a function of grain size. This study uses a unique set of field observations of suspended sediment transport on an energetic ebb-tidal delta in a mixed sediment environment. These findings demonstrate the challenge of measuring and interpreting suspended sediment mixed sand/mud environments.

Although we can derive detailed PSDs from the LISST data, the simultaneous presence of both sand and sand-sized flocs makes it impossible to confidently describe sand and

mud transport using the LISST alone.[1] Furthermore, a spherical particle inversion method was used to interpret the LISST results, and the anisotropy of flocs or other suspended organic matter may influence the measured PSDs. Furthermore, the LISST's accuracy may be affected by variations in particle composition (e.g., solid grains of sand vs. flocs).

The measurements used in this study are limited in their scope, both temporally and spatially. The 21 day period captured here encompasses a full spring-neap tidal cycle with a mix of calm and stormy conditions (including the largest storm of 2017), but do not capture seasonal variations which may affect suspended organic matter. Furthermore, here we measured a single point in a highly dynamic area, and as such may not be completely representative of the entire ebb-tidal delta. In addition, the results from this study can be used to calibrate and validate a multi-fraction sediment transport model and extend the analysis over larger spatial extents and periods of time.

4.5. OUTLOOK

To increase confidence in the classification of suspended sediment, additional support is required. Ambiguity in the composition of sand-sized particles may be resolved by analyzing the differential response of acoustic and optical signals from ADCP and OBS measurements on the ebb-tidal delta as per (*Fugate and Friedrichs*, 2002). Multimodal PSDs can also be broken down into constituent distributions using Gaussian Mixture Models (e.g., *Lee et al.* (2012)), and measured chlorophyll levels can be used to estimate the effect of suspended organic matter on flocculation (e.g., *Shen et al.* (2018)).

Antecedent wind conditions may also be a predictor for high mud concentrations on the ebb tidal delta, if mud is resuspended from intertidal areas in the Wadden Sea by wind-driven waves and currents, then discharged on the ebb tide. For instance, the turbid plume captured in Figure 4.5 was preceded by 5 days of persistent wind from S/SW directions (*KNMI*, 2019). Such trends in local versus remote sources of suspended sediment may also be revealed by examining hysteresis behaviour of sediment concentrations (e.g., *Jalón-Rojas et al.* (2015)).

[1] And now a poem about the LISST:
It is a great solution
To measure stuff that's floating
And its grain size distribution

"We have an awful lot of sand!"
Is this hallucination?
There's no bed shear! We should have guessed:
A muddy concentration

When processing your measurements
You must beware the floc!
Since if you don't account for it
You're in for quite a shock

The grains of sand in Ameland
Are pretty much the size
Of sticky, silty clumps of goo
That daily twice whiz by

So from the depths of the North Sea,
A lesson that does matter:
When working with a fancy LISST
Don't blindly trust your data!

Data collected from other instruments located around Ameland Inlet during the field campaign should be used in the interpretation of the particle size distributions to provide greater spatial context for the behaviour observed at this measurement frame (AZG Frame 4, Figure 2.1). The results of a sediment tracer study carried out on the ebb-tidal delta (Chapter 6) can also be incorporated to shed light on the transport of sand particles there.

The last step will be to examine these measurements in the context of a numerical model. This allows us to expand the scope of the present study from limited observations at a single point to larger spatial and temporal scales. The suspended particle size distribution data obtained here can also be used to improve the schematization of sediment in multi-fraction numerical models. By combining additional lines of evidence, we will obtain a more robust description of sediment pathways in Ameland Inlet.

4.6. CONCLUSIONS

Suspended particles on Ameland ebb-tidal delta are mainly fine sediment and flocs during calm conditions, but locally resuspended sand dominates during more energetic conditions. The western part of the ebb tidal delta functions as a source, pathway, and receptor for fine sand, but merely as a pathway for mud. Although there are large quantities of mud in suspension, they do not persist in the seabed there. The results suggest a variation in sediment connectivity between the ebb-tidal delta and other sources or receptors in the Ameland system as a function of grain size and hydrodynamic forcing.

These findings are essential for the development of numerical models with multiple sediment fractions, for predicting the evolution of nearby sand nourishments, and for the description of ecological habitats. Future research will focus on integrating additional measurements into the present analysis, numerical modelling of sediment transport in Ameland Inlet, and predicting the potential effects of nourishments and climate change on sediment pathways there.

ACKNOWLEDGEMENTS

This work is part of the research programme 'Collaboration Program Water' with project number 14489 (SEAWAD), which is (partly) financed by NWO Domain Applied and Engineering Sciences. Special thanks to the Dutch Ministry of Infrastructure and Water Management (Rijkswaterstaat and Rijksrederij) for organizing the field campaign and for their ongoing support as part of the Kustgenese2.0 project. Thanks also to Rieneke van Noort, Erik Hendriks, Ad Reniers, Marion Tissier, Alejandra Gijón, Claire Chassagne, and Romaric Verney for their fruitful discussions.

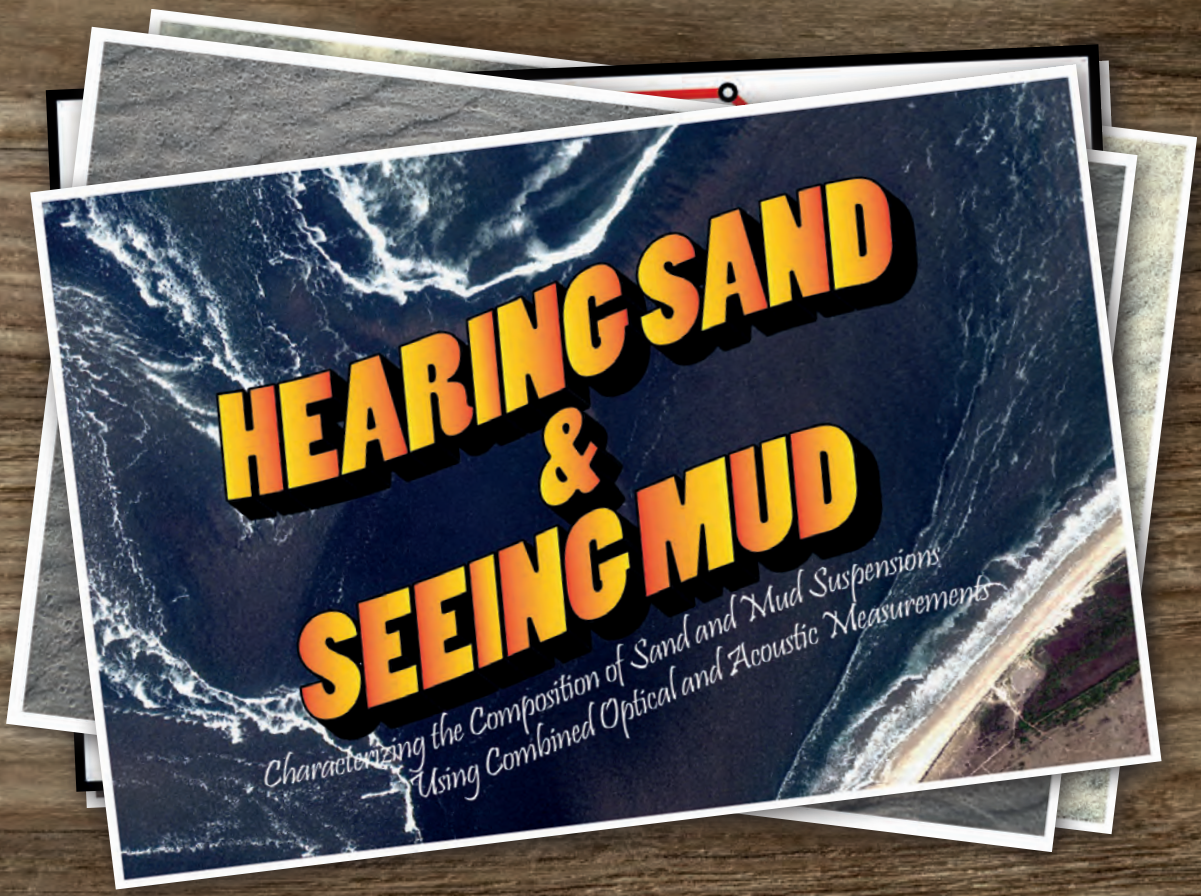
HEARING SAND
&
SEEING MUD
Characterizing the Composition of Sand and Mud Suspensions
Using Combined Optical and Acoustic Measurements

Dear Reader,

Un bonjour de Bretagne!

So, the sand laser didn't work out quite as expected... There is a lot of mud floating around, and it forms clumps about the same size as the sand grains, making them hard to tell apart using only one tool. We decided to try other tools that use sound and light to measure the sand and mud. We can "hear" the sand better than mud and "see" the mud better than sand, which helps us tell them apart. I came to Ifremer in Brest, France to do some laboratory tests and try out our theory. When we tried it on our Ameland data it worked pretty well. Things are looking up!

Stuart

Delft University of Technology
Stevinweg 1
2628 CN Delft

5

CHARACTERIZING THE COMPOSITION OF SAND AND MUD SUSPENSIONS IN COASTAL & ESTUARINE ENVIRONMENTS USING COMBINED OPTICAL AND ACOUSTIC MEASUREMENTS

KEY POINTS:

- Suspended sand and mud can be distinguished by their different optical and acoustic backscatter signatures
- We define a sediment composition index (SCI) from relative optical and acoustic backscatter and verify it with lab and field measurements
- SCI can be used to estimate the fraction of suspended sand, adding interpretive value to measurements in mixed sediment environments

This chapter has been published in *Journal of Geophysical Research: Oceans*:

Pearson, S.G., Verney, R., van Prooijen, B.C., Tran, D., Hendriks, H.C.M., Jacquet, M., Wang, Z.B. (2021). Characterizing Mixed Sand and Mud Suspensions using Combined Optical and Acoustic Measurements in Estuarine Environments. *Journal of Geophysical Research: Oceans*, 126, e2021JC017354. [Link].

SAND and mud particles are the building blocks of our coastlines. Counting and describing sand and mud particles floating through the water is essential to managing coasts. In the previous chapter, we tried to investigate how does sediment transport on the ebb-tidal delta varies as a function of grain size using a single instrument that measures suspended particle size. However, it was too difficult to tell the sand or mud apart from its particle size alone, since the mud at our site tended to stick together in sand-sized clumps. We also commonly measure sediment in the water with devices that send out a sound (acoustic) or light (optical) signal into the water. The sensors measure the strength of the signal reflecting back off of any sand and mud particles passing by. Optical instruments are better at "seeing" mud than sand, and acoustic instruments are better at "hearing" sand than mud. If both sand and mud are present, a single instrument will not accurately estimate the total amount of sediment because of these different sensitivities. Instead, we can use both types of instrument together and compare what we "see" with what we "hear". This comparison allows us to estimate whether there are more sand or mud particles floating through the water. The relationship between "seeing" and "hearing" can be described in a single number, the sediment composition index (SCI). We successfully tested this approach in laboratory experiments and then applied it to Ameland. This approach gives us a new way to understand environments that are both sandy and muddy, which provides valuable understanding of the small-scale processes shaping the ebb-tidal delta.

ABSTRACT

Quantifying and characterizing suspended sediment is essential to successful monitoring and management of estuaries and coastal environments. To quantify suspended sediment, optical and acoustic backscatter instruments are often used. Optical backscatter systems are more sensitive to mud particles ($< 63\mu m$) and flocs, whereas acoustic backscatter systems are more responsive to larger sand grains ($> 63\mu m$). It is thus challenging to estimate the relative proportion of sand or mud in environments where both types of sediment are present. The suspended sediment concentration measured by these devices depends on the composition of that sediment, thus it is also difficult to confidently measure concentration with a single instrument when the composition varies and extensive calibration is not possible. The objective of this chapter is to develop a methodology for characterizing the relative proportions of sand and mud in mixed sediment suspensions by comparing the response of simultaneous optical and acoustic measurements. We derive a sediment composition index (SCI) that is used to directly predict the relative fraction of sand in suspension. Here we verify the theoretical response of these optical and acoustic instruments in laboratory experiments, and successfully apply this approach to field measurements from Ameland ebb-tidal delta (the Netherlands). Increasing sand content decreases SCI, which was verified in laboratory experiments. A reduction in SCI appears during more energetic conditions when sand resuspension is expected. Conversely, the SCI increases in calmer conditions when sand settles out, leaving behind mud. This approach provides crucial knowledge of suspended sediment composition in mixed sediment environments.

5.1. INTRODUCTION

5.1.1. BACKGROUND

ESTUARIES and coastal seas are characterized by strong morphological and sedimentary gradients, from shallow beaches and intertidal shoals or flats, to deeper foreshore and channel areas or other subtidal features. Furthermore, the sediment composition at a given site may vary widely in both particle size and mineralogy (*Winkelmolen and Veenstra*, 1974; *Flemming and Ziegler*, 1995; *Son et al.*, 2011). The size and material properties of mud (a.k.a. "fines" or "fine sediment") and sand are different: sand particles are individual quasi-spherical grains (with typical density $\rho_s = 2{,}650 kg/m^3$ for quartz particles), between 63 and $2{,}000 \mu m$ in diameter, d. Muddy sediments, especially clay particles ($d < 2\mu m$), have the ability to flocculate and often bond with organic matter. The resulting flocs vary widely in diameter (from 10 to $1{,}000 \mu m$) and have relatively low densities ($\rho_{floc} = O(1{,}100 - 2{,}000 kg/m^3)$) with irregular shapes and lower settling velocities than sand (*McCave*, 1984; *Eisma*, 1993; *Milligan and Hill*, 1998; *Hill et al.*, 2000; *Fugate and Friedrichs*, 2002; *Khelifa and Hill*, 2006; *Manning et al.*, 2006; *Dankers and Winterwerp*, 2007; *Chapalain et al.*, 2019; *Many et al.*, 2019). The spatial distribution of these different types of sediment is a function of morphology, supply, and hydrodynamic conditions.

Due to episodic (storms and floods) and persistent (tides) hydro-meteorological forcing and human influences, estuarine and coastal sediment are highly dynamic. Bed sediments are mobilized and transported, through bed load (rolling, sliding, and saltating near the surface of the seabed) or suspended load (held aloft in the water column by turbulence). In this chapter we focus on transport in suspension, dealing with mud ($d < 63\mu m$) and very fine to medium sand $d = 63 - 500\mu m$, the latter being found in suspension (relatively close to the bed) during energetic conditions. Depending on local and remote bed composition and hydrodynamic forcing, the concentration, characteristics, and fluxes of suspended particulate matter (SPM) will drastically change.

The morphological changes resulting from these fluxes may threaten or enhance coastal infrastructure and ecosystems. Quantifying these sediment fluxes is critical for sustainable coastal management (*Mulder et al.*, 2011; *Hanley et al.*, 2014; *Hendriks et al.*, 2020). Measurements of these fluxes can be used to derive sediment budgets (*Wang et al.*, 2018), better understand the physical processes underlying sediment transport (*White*, 1998), and quantify sediment pathways and connectivity (Chapter 7). They also allow us to calibrate and improve numerical sediment transport models (*Amoudry and Souza*, 2011; *Roelvink and Reniers*, 2012). Of critical importance is not just quantifying total sediment fluxes, but also sediment fluxes as a function of particle size. For example, overestimating sand concentration could lead to underestimates of an estuary's ability to import sediment and evolve in equilibrium with accelerating sea level rise (e.g., *Lodder et al.* (2019).

The main challenge faced in understanding coastal sediment dynamics and quantifying associated fluxes is to make continuous observations of total (sand and mud) suspended sediment and their related mass concentration (*SSC*). Continuous *in situ* measurements are possible with acoustic or optical instruments (*Fettweis et al.*, 2019). Optical backscatter sensors have been used successfully to measure suspended sediment in a wide range of environments, from estuaries and embayments (*Lunven and Gentien*, 2000; *Green et al.*, 2000; *Bass et al.*, 2002; *Fugate and Friedrichs*, 2002; *Bass et al.*, 2007; *Li et al.*, 2018; *Fettweis et al.*, 2019; *Lin et al.*, 2020) to mud flats and salt marshes (*Voulgaris and Meyers*, 2004; *Guo et al.*, 2018) to sandy beaches (*Downing et al.*, 1981; *Aagaard et al.*, 2002). Acoustic backscatter

sensors have also been successfully used to measure suspended sediment in many different coastal and estuarine settings (*Thorne et al.*, 1993; *Green et al.*, 2000; *Fugate and Friedrichs*, 2002; *Voulgaris and Meyers*, 2004; *Hoitink and Hoekstra*, 2005; *Bass et al.*, 2007; *Chanson et al.*, 2008; *Li et al.*, 2018; *Lin et al.*, 2020) and beyond (*Hill et al.*, 2003; *Hawley*, 2004).

The measurement capabilities of optical and acoustic backscatter instruments are inextricably tied to the material properties of the sediment they observe. Each type of instrument responds with different sensitivity to muddy or sandy sediment because of a dependence on particle size and density. Hence, in practice, empirical calibration models for optical or acoustic sensors are built via regression against laboratory or *in situ* samples, the latter providing reference gravimetric concentrations (*Gray and Elliott*, 2009; *Fettweis et al.*, 2019). Once the calibration for a given instrument has been developed, the calibrated relationship can be applied to the recorded signal from the field (e.g., voltage, NTU, counts, or SNR) and translated into a time series of mass concentration. This concentration can then be interpreted in light of other measurements such as velocity.

However, these calibration models are representative of a given condition (e.g., calm, moderate tidal flows with SPM dominated by mud), and may not be well-adapted for observing a succession of low- and high-energy conditions when the SPM sand and mud content (f_{sand} and f_{mud}) can vary strongly in time (*Bass et al.*, 2007). The most appropriate methodology would require sampling and re-calibrating sensors as fast as SPM composition changes, but this is neither easily predictable nor realistic. A library of population-adapted calibration models could be built following *Green and Boon* (1993), but knowledge about SPM composition dynamics is a prerequisite for their application.

In this chapter, we develop an original sediment composition index (SCI) derived from optical and acoustic measurements to quantitatively and dynamically evaluate the relative fraction of sand or mud in suspension. The concept is first validated using laboratory measurements, and then applied to field measurements. SCI provides researchers with a way to more accurately quantify SSC, especially during high energy events when calibration with physical samples is not possible.

5.1.2. OPTICAL BACKSCATTER MEASUREMENTS

Optical Backscatter (OBS) sensors are widely used to indirectly measure suspended sediment concentration. Near-infrared light (typical wavelength $\lambda = 0.780-0.865\mu m$) is emitted from the instrument, backscattered by suspended particles, and then recorded by photoreceptors. In a Mie scattering regime, backscatter is strongest when the light wavelength and particle size are similar, so OBS are more sensitive to mud particles $O(1\mu m)$ than sand particles $O(100\mu m)$ (*Green and Boon*, 1993; *Conner and De Visser*, 1992; *Voulgaris and Meyers*, 2004). According to *Sutherland et al.* (2000), the photon flux received by the sensor is given as:

$$F = VNE\frac{\pi d^2}{4}Q_s \tag{5.1}$$

Where F is photon flux $[W]$, V is scattering volume $[cm^3]$, N is the number concentration of scatters $[cm^{-3}]$, E emitted irradiance $[W/cm^2]$, d is the particle diameter $[\mu m]$, Q_s the (back)scattering efficiency of the particles $[-]$. Relating the number concentration to the mass concentration SSC $[mg/L]$, this relationship can be modified as follows (*Sutherland et al.*, 2000):

$$F = \frac{3}{2}\frac{V(SSC)E}{\rho_s d}Q_s \tag{5.2}$$

Where ρ_s is the particle (dry) density $[kg/m^3]$. This flux is then translated to a voltage output by the sensor.

Equation 5.2 can then be reworked as:

$$OBS = \alpha_{OBS}\frac{Q_s}{\rho_s d}SSC \tag{5.3}$$

Where OBS is the optical backscatter signal $[V]$ and α_{OBS} is approximated as a constant for the range of SSC investigated.

Due to the dependency on $1/(\rho_s d)$, for the same concentration of sediment, the flux observed for $200\mu m$ sand ($\rho_s \approx 2600 kg/m^3$) will be 10 times smaller than for muddy flocs of the same size ($\rho_{floc} \approx 1100 kg/m^3$), and even smaller in presence of microflocs. However, this sensitivity to size may be as low as a factor of 2 when intercomparing floc particles with a continuous size distribution from micro to macrofloc, rather than the sandy and muddy end members considered in this study (*Boss et al.*, 2009a,b; *Hill et al.*, 2011).

5.1.3. ACOUSTIC BACKSCATTER MEASUREMENTS

Analogously to OBS devices, an acoustic signal is emitted and backscattered by particles in suspension, then recorded by transducers. The estimation of SSC from acoustic measurements depends on the properties of sediment in suspension. For well-characterized particles (e.g., a well-sorted sand population) and electronically/acoustically calibrated sensors, backscattering models and representative diameters can be used to evaluate SSC from the theory (*Thorne and Hanes*, 2002). Otherwise, similarly to optical sensors, the acoustic response can be calibrated against samples from field or laboratory experiments, with similar limitations regarding calibration representativity.

Acoustic devices typically used in coastal sediment studies can loosely be grouped into (i) single-frequency Acoustic Doppler Velocimeters (ADVs) which measure at a single point; (ii) single-frequency Acoustic Doppler Current Profilers (ADCPs) which measure over multiple points in the water column; and (iii) multi-frequency acoustic backscatter devices. Only the latter is specifically designed to measure suspended sediment concentration; ADCPs and ADVs were originally intended to measure velocity, but their operating principles mean that inferring sediment concentration from acoustic backscatter is a useful side benefit. In this study, we mainly consider acoustic backscatter from ADVs, which are widely used to measure suspended sediment concentrations (*Fugate and Friedrichs*, 2002; *Öztürk*, 2017; *Lin et al.*, 2020).

We can mathematically describe acoustic backscatter using the sonar equation, which balances the difference between energy emitted and received by the sensor with energy lost on the return trip of an acoustic pulse (*Hoitink and Hoekstra*, 2005). The sonar equation is presented here in form similar to (*Hoitink and Hoekstra*, 2005; *Salehi and Strom*, 2011; *Chmiel et al.*, 2018):

$$SNR = C - \underbrace{20\log_{10}(\psi R^2)}_{Spherical\,Spreading} - \underbrace{\int_0^R (\alpha_w(r) + \alpha_s(r))\,dr}_{Attenuation} + BI \tag{5.4}$$

SNR $[dB]$ is the Signal-to-Noise Ratio recorded directly by the ADV, which indicates the intensity of acoustic backscatter. C $[dB]$ is a constant including instrument-related and geometrical terms. The spherical spreading term ($20\log_{10}(\psi R^2)$) is a function of R $[m]$, the one-way distance that the acoustic pulse travels from the transmitter to the measurement volume. The attenuation of the acoustic pulse can be decomposed into absorption by the water α_w $[dB/m]$ and attenuation by sediment α_s $[dB/m]$, integrated over the travel distance. BI is the volume backscatter strength $[dB]$ and is a function of SSC and particle characteristics:

$$BI = 10\log_{10}(\frac{SSC\bar{\sigma}}{\rho_s \bar{V}_s}) \tag{5.5}$$

Where $\bar{\sigma}$ is the mean backscattering cross section $[m^2]$, ρ_s is the dry particle density $[kg/m^3]$, and $\bar{V}_s$ is the scattering volume $[m^3]$.

The attenuation terms (α_s and α_w) are higher at larger concentrations and greater distances (*Thorne et al.*, 1993), but can be neglected below $1{,}000 mg/L$ (*Chmiel et al.*, 2018) and $O(10cm)$ from the sensor (*Pomázi and Baranya*, 2020). In this study we thus neglect attenuation, given the small distance between source and measuring volume (15 cm) and low concentrations expected at our study site in Ameland ($< 1{,}000 mg/L$). All terms except BI can be reorganized and set in a global constant C' $[dB]$. Equation 5.5 then becomes:

$$SNR = 10\log_{10}(SSC) + 10\log_{10}\left(\frac{\bar{\sigma}}{\rho_s \bar{V}_s}\right) + C' \tag{5.6}$$

Equation 5.6 can be further simplified as:

$$SNR = 10\log_{10}(SSC) + b' + c' \tag{5.7}$$

where c' is a constant depending on instrument characteristics and b' is a variable depending on suspended particle properties (e.g., size, shape, density, elasticity). The log-linear relation between SNR and SSC is only valid for concentrations less than $1{,}000 mg/L$ (*Salehi and Strom*, 2011; *Chmiel et al.*, 2018); beyond this threshold particle absorption losses reduce the recorded backscattering signal.

The interaction between an acoustic pulse and particles (scattering) is optimal for coarser individual (unflocculated) particles, with a dependency on the acoustic frequency such as $kd/2 \approx 1$ (or $< d$) where k is the wave number ($2\pi/\lambda$, and λ is the wavelength) and d the diameter of the particle (*Salehi and Strom*, 2011). Hence for a $1 Mhz$ acoustic signal, the optimal backscattering size (diameter) is around $480\mu m$, while for a $6 Mhz$ signal, the optimal size is around $80\mu m$. Flocculated particles are characterized by lower backscattering efficiency (1 to 2 order of magnitude lower) (*Thorne and Hurther*, 2014). Acoustic instruments are thus more sensitive to fine to coarse sands than flocculated mud particles (*Salehi and Strom*, 2011): for similar concentrations, the SNR will be stronger for sand than for mud.

5.1.4. COMBINING OPTICAL AND ACOUSTIC MEASUREMENTS: TOWARDS THE SEDIMENT COMPOSITION INDEX (SCI)

In coastal and estuarine environments where suspended particles are often characterized by a mixture of mud (including flocs) and sand particles, *SSC* measurements relying on a single technique (optical or acoustic) are ambiguous with respect to sediment composition. This can lead to misestimates of particle size and concentration (*Thorne et al.*, 2021), and limits the interpretability and representativeness of the recorded signal. The objective of the present paper is to combine the use of optical and acoustic backscatter sensors to estimate the relative fraction of sand in suspension.

Bass et al. (2007) note that although optical and acoustic backscatter systems are routinely used together, few studies have taken advantage of using them together to estimate suspended sediment composition in mixed environments. There is a salient difference in the response of optical and acoustic instruments to changes in suspended particle size (*Ha et al.*, 2009), which may be exploited to resolve ambiguities.

In some cases, it has been assumed that optical or acoustic instruments only observe a single class of sediment. *Bass et al.* (2002) disregard locally resuspended sand in their OBS measurements of mud. In studies of tidal channels flanked by intertidal mud flats, both *Green et al.* (2000) and *van de Kreeke and Hibma* (2005) assumed that optical sensors detected only silt, while acoustic sensors detected only sand. The interpretation of a single instrument depends on the assumptions behind its calibration (e.g., an OBS calibrated to sandy sediment will overestimate total SSC when mud is also present). However, instead of ignoring the presence of sand in optical measurements or the presence of mud in acoustic measurements, paired instruments can more beneficially be used concurrently and compared (*Conner and De Visser*, 1992; *Green and Boon*, 1993; *Hawley*, 2004). In this study, we take advantage of these paired instruments to derive a Sediment Composition Index (*SCI*) that quantitatively discriminates the presence of suspended sand from mud.

This relative optical-acoustic backscatter response can be analyzed by combining Equations 5.3 and 5.7 to obtain:

$$SNR = 10\log_{10}(OBS) + b_{particle} + c_{instr} \tag{5.8}$$

where $b_{particle}$ is a variable parameter function of SPM characteristics and c_{instr} is a global (optical/acoustic) instrument-related constant. In our study, as instruments were not calibrated, $b_{particle} + c_{instr}$ are considered as a single constant, the Sediment Composition Index (*SCI*). *SCI* is therefore dependent on the characteristics of the sediment particles being measured and of the instruments being used. Equation 5.8 can be rearranged to present *SCI*:

$$SCI = 10\log_{10}(OBS) - SNR \tag{5.9}$$

Considering the high sensitivity of the acoustic sensor to sand and of the optical sensor to mud, *SCI* is relatively smaller when suspended sand particles dominate, and relatively larger when mud dominates suspensions. *SCI* can thus be used as an indicator of sand or mud dominance.

5.2. METHODS

Laboratory measurements were used as a proof of concept for the *SCI*, and to quantify the relationship between *SCI* and the fraction of sand in suspension (f_{sand}). The fraction of

mud in suspension can also be directly calculated via $f_{mud} = 100\% - f_{sand}$. We then analyze *in situ* measurements to demonstrate the added value of SCI for investigating the dynamics of mixed-sediment environments. We compared optical/acoustic signals measured on Ameland ebb-tidal delta in the Netherlands during a 40 day period featuring storms and calm conditions. From these signals we calculated SCI and f_{sand}, and put them into context with other simultaneous measurements (tidal stage) and derived parameters (bed shear stress due to waves and currents). By interpreting these measurements, we can test whether SCI is a valid and useful indicator of relative suspended sand or mud dominance in estuarine environments.

5.2.1. LABORATORY EXPERIMENTS

We used the DEXMES (*Dispositif EXpérimental de quantification des Matières En Suspension*) tank for our experiments. DEXMES is operated by Ifremer and managed together with Géosciences Océan, Géosciences Rennes, and SHOM (French Hydrographic Service). The glass-walled tank has a volume of approximately $1 m^3$ and internal diameter of $0.97 m$ (Figure 5.1), and was filled with fresh water.

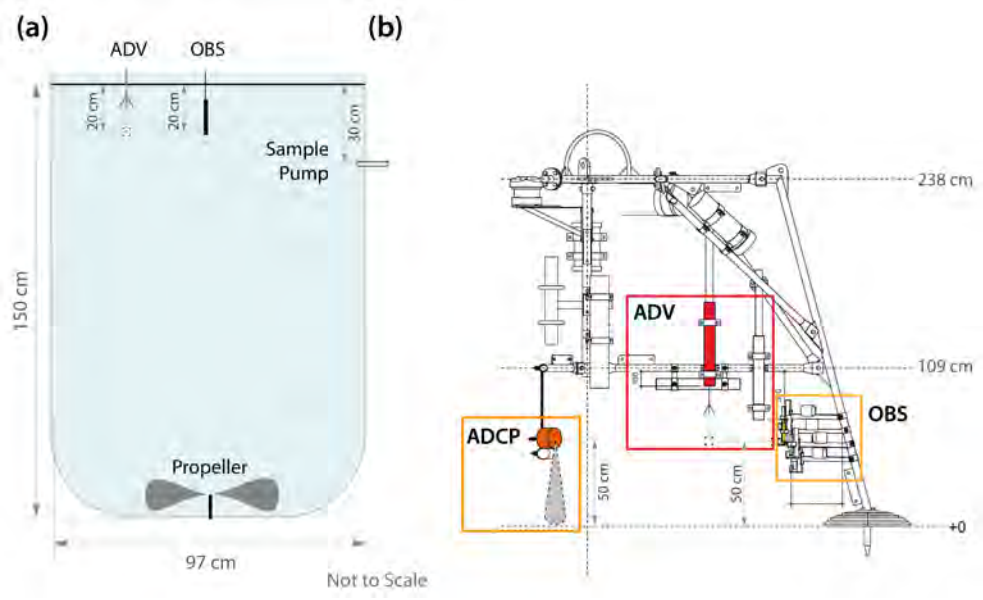

Figure 5.1: Overview of the DEXMES tank used in the laboratory experiments. (a) Schematic of instrument setup. During the experiments, the tank contained an Acoustic Doppler Velocimeter (ADV) and an Optical Backscatter Sensor (OBS) mounted just below the surface. An external pump was connected to the tank to extract suspended sediment samples. (b) Frame used to conduct field measurements (AZG F4), featuring ADVs, OBSs, and an downward-facing Acoustic Doppler Current Profiler (ADCP) sensors. The ADV and OBS measured sample volumes 50 cm above the base of the frame, and the ADCP measured a 50 cm profile between the instrument and the bed.

Two sets of similar experiments were conducted to evaluate SCI at various total sediment concentration ranges and sand/mud contents. In Experiment 1, pure bentonite (d_{50} = $17 \mu m$) and two classes of well-sorted pure quartz sand ($\rho_s = 2{,}650 kg/m^3$) with median grain sizes $d_{50} = 100 \mu m$ and $220 \mu m$ were used. Conversely, Experiment 2 used estuarine

mud ($d_{50} = 15\mu m$) instead of bentonite, and the same sources of sand but without further sieving ($d_{50} = 93\mu m$ and $210\mu m$). The estuarine mud contained organic matter, but this was not quantified. For simplicity, we hereafter refer to $d_{50} \approx 100\mu m$ and $d_{50} \approx 200\mu m$ sand for both experiments. In the context of these experiments, "mud" refers to bentonite and estuarine mud ($d_{50} < 63\mu m$), while "coarse sediment" or "sand" refers to both size classes of sand ($d_{50} > 63\mu m$).

Five sediment composition conditions were investigated for both 100 and $200\mu m$ sand in Experiment 1: pure bentonite, pure sand, and 3 intermediate mixtures: 25%, 50% and 75% sand content (f_{sand}). For each condition, 6 total concentrations were tested stepwise from $15mg/l$ to $200mg/l$ (See Appendix A). In Experiment 2, the (estuarine mud) concentration was held constant at approximately $130mg/l$ and sand concentration (100 or $200\mu m$) incrementally varied between 0 and $1,460mg/l$ (See Appendix A), in order to approximate an estuarine environment with a sandy local bed composition and steady background presence of mud (e.g., *Green et al.* (2000); *van de Kreeke and Hibma* (2005)). Concentrations of both classes of sediment were kept within the linear range of response for each instrument ($< 5,000mg/L$ of mud and $< 50,000mg/L$ of sand for the OBS (*Downing*, 2006) and $< 5,000mg/L$ for the ADV (*Salehi and Strom*, 2011)) to avoid ambiguity in the readings. Precise details of the suspended sediment concentrations and sand fractions in each experiment are provided at the end of this chapter and experimental protocols are outlined in Appendix B.

Vertical concentration gradients were observed within the tank for $200\mu m$ sand, but all instruments and samples measured within 10 cm of the same elevation, leading to comparable sample and sensor data. The propeller at the bottom of the tank was set to a speed of $175rpm$ to provide high turbulent shear between $G = 30$ and $100s^{-1}$, maximizing resuspension and mixture homogeneity while minimizing the formation of bubbles.

In Experiments 1 and 2, acoustic backscatter was measured using a Nortek Vector Acoustic Doppler Velocimeter (*Nortek AS*, 2005), operating at a frequency of 6 MHz, and sampling at 32 Hz (8 Hz in Experiment 2), 20 cm beneath the water surface (25 cm in Experiment 2). Optical backscatter was measured in Experiment 1 using a Wetlabs FLNTU *WET Labs Inc* (2019), sampling at 1 Hz, 20 cm beneath the water surface. In order to exclude data points below the sensor's detection limits for coarser particles, turbidity data below $0.9NTU$ are discarded from the study. In Experiment 2, a Campbell OBS 3+ (*Campbell Scientific Inc.*, 2014) was used instead, with similar properties to the Wetlabs FLNTU. To calibrate the optical and acoustic measurements, an external pump was connected to the tank 30 cm beneath the surface to extract suspended sediment samples. The instruments were arranged to avoid mutual interference but while sampling a similar elevation and hence similar sediment concentrations. All sensors were operated in continuous recording mode for the duration of each experiment, and statistics were computed over a 10-11 min period at each sediment concentration level. The median signal-to-noise ratio (SNR) of the three ADV beams and median OBS output were then used to calculate the relative optical-acoustic backscatter index SCI from Equation 5.9.

5.2.2. *In Situ* MEASUREMENTS

Ameland Inlet is located in the Netherlands between the sandy barrier islands of Terschelling and Ameland, connecting the North Sea with the Dutch Wadden Sea (Figure 5.2). The inlet is characterized by a 30 m deep main channel (the "Borndiep") on its eastern side, and a

shifting complex of shoals and channels on its west side. There is a large and highly dynamic ebb-tidal delta complex on the seaward side of the inlet, and a shallow backbarrier basin environment of intertidal shoals and flats on the landward side (the Wadden Sea) (*Elias et al.*, 2019; *Lenstra et al.*, 2019a). The seabed of the ebb-tidal delta of the inlet is mainly well-sorted sand (mean $d_{50} = 211\mu m$, $n = 165$) with mud content generally < 1%, whereas the Wadden Sea has a mud content up to 20% at its landward edge and on the intertidal flats separating Ameland Inlet from adjacent tidal basins (*Rijkswaterstaat*, 1999; *Pearson et al.*, 2019). Samples with mud content of ~ 5% can also be found on the North Sea bed beyond the distal end of the ebb-tidal delta.

Figure 5.2: Overview of measurements during the September 2017 field measurement campaign at Ameland Inlet, including the frame (AZG-F4) bearing the instruments used in this study. Bathymetry source: Rijkswaterstaat Vaklodingen. Elevation source: Actueel Hoogtebestand Nederland (AHN), Rijkswaterstaat. Basemap sources: Esri, HERE, Garmin, ©OpenStreetMap contributors, and the GIS user community.

A field measurement campaign was carried out from August 29th to October 9th 2017, with the goal of characterizing hydrodynamic and sediment transport processes in the inlet and on its ebb-tidal delta (*de Wit et al.*, 2019; *Reniers et al.*, 2019; *Brakenhoff et al.*, 2019b; *van der Werf et al.*, 2019a; *Van Prooijen et al.*, 2020). Measurements of flow, waves, suspended particulate matter, bedform dynamics, and water quality were made at 4 locations across the site. Measurements considered in this study were obtained at frame AZG-F4 (Figure 5.2), at the distal end of the ebb-tidal delta, approximately $8m$ deep.

As with the laboratory experiments in Section 5.2.1, acoustic backscatter was measured using three Nortek Vector Acoustic Doppler Velocimeters (ADVs) (*Nortek AS*, 2005), operating at a frequency of 6 MHz, and sampling at 16 Hz, 20, 50, and 78 cm above the seabed.

The median SNR of acoustic backscatter was taken over 30 minute bursts for the deployment period as per *Ha et al.* (2009).

Optical backscatter was measured using four Campbell OBS 3+ (*Campbell Scientific Inc.*, 2014), sampling at $16Hz$, 20, 30, 50, and $78cm$ above the seabed. The OBS was initially calibrated using sandy sediment obtained from the seabed adjacent to the measurement frame, as is frequently done in practice (*Paphitis and Collins*, 2005; *Fettweis et al.*, 2019). However, there is still concern that calibration using bed material can be inappropriate and error-prone if there are significant differences between the bed sediment and material in suspension (*Kineke and Sternberg*, 1992; *Beamsley et al.*, 2001; *Bass et al.*, 2007; *Su et al.*, 2016; *Öztürk*, 2017), as expected at our field site. On this basis, the original calibration was discarded when it was recognized that the additional presence of suspended sediment significantly finer than the bed sediment made interpretation ambiguous. Thus, the uncalibrated OBS signal is presented here in volts. The median OBS signal over 30 minute bursts was used.

Near-bed hydrodynamic conditions during the monitoring period were measured using a high-resolution downward-looking Nortek Aquadopp Acoustic Doppler Current Profiler (ADCP-HR) (*Nortek AS*, 2008). The ADCP sampled at a rate of 4 Hz in 30 minute bursts. These measurements were averaged over the water column between the sensor and the bed (approximately 0.5 m, depending on field conditions) and then median velocities were calculated for each 30 min burst interval. Bed shear stresses due to the influence of waves and currents were calculated separately using the method of *Soulsby* (1997) (with default parameter settings) to give an indication of the potential for local bed material to be resuspended at the frame. For simplicity, we do not consider the effect of combined wave-current bed shear stresses here, which likely underestimates the frequency of sediment resuspension.

To assess the intratidal variation of the field measurements, we classified each 30 minute burst into flood tide, high water slack (HWS), ebb tide, and low water slack (LWS) based on an analysis of tidal currents (*Pearson et al.*, 2019). At the measurement site, the major axis of flow is almost exactly in an east-west direction. Thus, eastward ($0-179$ deg) currents exceeding $0.1m/s$ were classified as flood, and westward ($180-359$ deg) currents exceeding that threshold as ebb. Velocities below that threshold with positive water surface elevations (with respect to MWL) were classified as HWS, and with negative water surface elevations as LWS.

5.3. RESULTS

5.3.1. LABORATORY EXPERIMENTS

OPTICAL AND ACOUSTIC BACKSCATTER

We consider the joint response of the optical and acoustic sensors to various sand/fine sediment mixtures: from purely mud suspensions to purely sand suspensions, and with varying total concentrations (Figure 5.3). Optical turbidity values are recorded in NTU or Volts (Experiment 1 and 2, respectively) depending on the instrument deployed. Readings in Volts are first normalized in equivalent NTU using an offset value in log space (constant for all Experiment 2 OBS data), so that their values are aligned in Experiments 1 and 2 for purely mud suspension conditions.

Results from Experiment 1 for $100\mu m$ sand (Figure 5.3a,c) show that the sensors' response is linear in $log_{10}(OBS)/ADV\ SNR$ space. This is valid for a range of total sediment

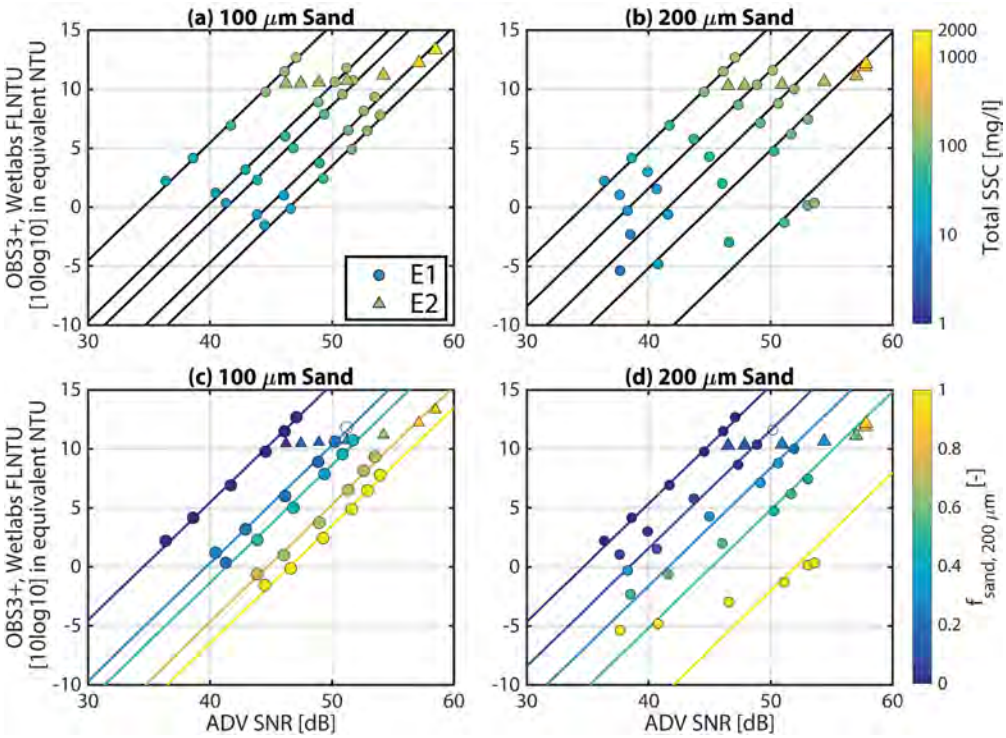

Figure 5.3: Median acoustic (ADV SNR) and optical backscatter (OBS) as a function of total suspended sediment concentration (a,b) and suspended sand fraction (f_{sand}) in the laboratory experiments (c,d). (a,c) Experiments with 100μm sand. (b,d) Experiments with 200μm sand. Data from Experiment 1 (E1) measured with a Wetlabs FLNTU, are marked with circles ($n = 30$), while data from Experiment 2 (E2), measured with an OBS3+, are marked with triangles ($n = 7$). Black and coloured lines indicate constant f_{sand} contours.

concentration (from 15mg/l to 200mg/l), such that $10log_{10}(OBS) = SNR + SCI$, confirming the theoretical relationship (Equation 5.9). Increasing the sand fraction (f_{sand}) leads to a shift in the data alignment for the different conditions, but lines are still parallel (Figure 5.3c). That is, for a given $ADV\ SNR$ value, the optical turbidity value increases as SPM becomes finer. Conversely, for a given optical turbidity value, $ADV SNR$ increases as SPM become sandier. Experiment 2 independently tested a larger total SSC gradient, increasing the sand content from 0 to 100% and total sediment concentration from 135mg/l to 1603mg/l, while progressively adding sand (Figure 5.3a,c). These results are in full agreement with Experiment 1, with their data points matching the corresponding sand/mud ratio contours as sand content increases.

Similar results are observed for 200μm sands: $log_{10}(OBS)/ADV$ pairs are aligned for a given sand content, and these lines are organized parallel to each other (Figure 5.3b,d). For similar turbidity values, the SNR signal is stronger for 200μm sand than for 100μm sand (Figure 5.3a,b). However, deviations from alignment are observed when sand content dominates (i.e., $f_{sand} > 50\%$) and total concentration is low (i.e., $SSC <= 50mg/l$) (Figure 5.3b,d). This bias corresponds to the poor sensitivity of the optical sensor to detect low 200μm particle concentrations, when there are few scatterers in suspension. In such con-

ditions, recorded NTU values range from 0.1 to 0.9NTU, close to the sensor resolution and lower detection limit.

The measurements in Figure 3 are time-averaged values (see Supporting Information for full protocols), and we describe signal variability using the coefficient of variation ($CV = \sigma/\mu$). In Experiment 1, Wetlabs FLNTU signals are more variable when sand particles get coarser (from $CV = 2-3\%$ for pure mud to $3-16\%$ for pure $100\mu m$ sand and $5-22\%$ for pure $200\mu m$ sand), and $2-9\%$ for sand-mud mixtures. ADV SNR variability is less ($CV < 6\%$ for mud, $100\mu m$ sand, and $100\mu m$ sand-mud mixtures), and generally decreases with increasing concentration. The highest ADV SNR variability was seen for low concentrations of pure $200\mu m$ sand (CV up to 20%). $200\mu m$ sand-mud mixtures have CV ranging from $5-13\%$ in Experiment 1 . For sand-mud mixtures in Experiment 2, OBS signal variability is between $6-12\%$ and ADV SNR variability is between $2-5\%$. As with Experiment 1, mixtures with $200\mu m$ sand showed higher signal variability than mixtures with $100\mu m$ sand in Experiment 2.

SEDIMENT COMPOSITION INDEX (SCI)

We derived the sediment composition index SCI for the laboratory measurements using Equation 5.9, and it is shown to be an appropriate proxy for evaluating the sand content (Figure 5.4a). As a first step towards a generic SCI, we propose to normalize SCI such that $SCI = 0$ in purely muddy conditions.

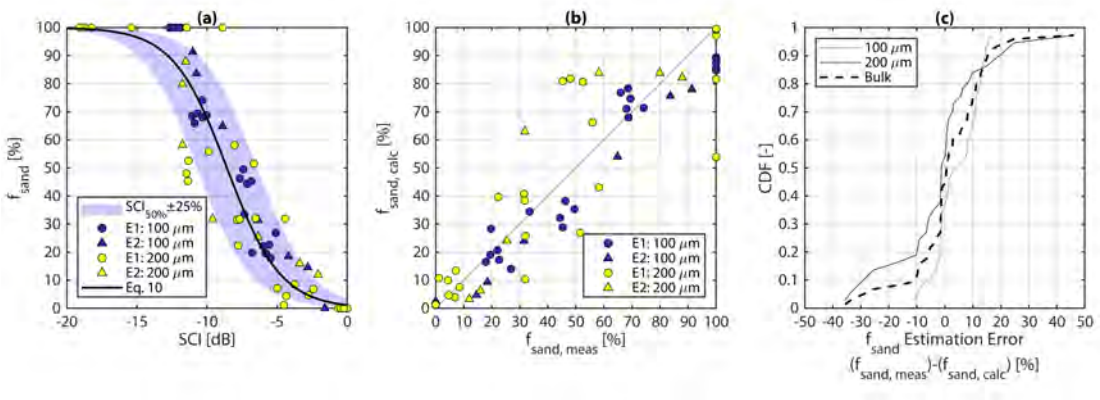

Figure 5.4: Fraction of sand in total suspended sediment (f_{sand}), calculated from the sediment composition index (SCI). (a) f_{sand} as a function of SCI, with Equation 5.10 fit to both grain sizes in bulk ($SCI_{50\%} = -8.58$). Blue bands indicate the envelope of uncertainty in f_{sand}, varying $SCI_{50\%}$ by ±25%. Experiments 1 and 2 (E1 and E2, respectively) are indicated, along with the sand grain size used in each experiment ($R^2_{100} = 0.957$; $R^2_{200} = 0.806$; $R^2_{bulk} = 0.884$). (b) Comparison of experimentally measured $f_{sand,meas}$ with $f_{sand,calc}$ determined using Equation 5.110. (c) Cumulative distribution function (CDF) of sand fraction estimation error ($f_{sand,meas} - f_{sand,calc}$) for each sand grain size class and for all classes combined in bulk.

To understand the relationship between the derived SCI and the actual sediment composition, we compare f_{sand} with SCI from both experiments and grain size classes, and find a negative correlation (Figure 5.4a). A hyperbolic tangent was fit to the data (Equation 5.10) because f_{sand} should asymptotically reach 0% for maximum SCI (minimum acoustic response, maximum optical response, no sand, only mud), and should tend asymptotically

towards 100% for minimum SCI (maximum acoustic response, minimum optical response, only sand, no mud).

$$f_{sand} = \left(\frac{1}{2} + \frac{1}{2}\tanh\left[\frac{(SCI - SCI_{50\%})}{\Delta SCI}\right]\right) \cdot 100\% \tag{5.10}$$

Where $SCI_{50\%}$ is a constant corresponding to a mixture of 50% sand and 50% mud. It is equal to -8.03 when fitting only $100\mu m$ sand ($R^2_{100\mu m} = 0.954$), -9.63 for $200\mu m$ sand ($R^2_{200\mu m} = 0.848$), and -8.58 when both grain sizes are fit in bulk ($R^2_{bulk} = 0.884$). For the analyses in the rest of this study, we consider $SCI_{50\%} = -8.58$. $\Delta SCI = 3.85$, and indicates the width in variation. Equation 5.10 allows us to deepen the interpretation of SCI by directly predicting f_{sand} (and by extension, $f_{mud} = 1 - f_{sand}$). It shows good predictive skill when compared with measured f_{sand} for both experiments and grain size classes ($R^2_{100} = 0.957$; $R^2_{200} = 0.806$; $R^2_{bulk} = 0.884$) (Figure 5.4b). The bulk prediction is accurate for $200\mu m$ sands, as 70% of the calculated sand fractions are associated with an absolute error lower than ±10%. Results are the best for $100\mu m$ sand, with more than 85% of the samples estimated with an absolute error below ±10%. In case the sand distribution is not known, we also investigated the SCI response to sand content when merging all experimental data (Figure 5.4c). This bulk index still performs well, with 70% of the calculations with errors within ±10%, although the error range is slightly larger, between −30% and +20%.

5

5.3.2. IN SITU MEASUREMENTS

HYDRODYNAMIC CONDITIONS

The measurements from Ameland ebb-tidal delta span 40 days (August 29 to October 8, 2017), or approximately 2.5 spring-neap cycles (Figure 5.5a). There are two minor storms ($H_s \approx 1m$) on August 30th and September 7th, and two major storms ($H_s > 4m$), *Sebastian* (September 14th, during neap tide) and *Xavier* (October 6th, during spring tide).

Spring tide occurs around September 10th, 20th, and October 7th (corresponding to the larger tidal range in Figure 5.5a). Under calmer conditions, bed shear stresses due to currents ($\tau_{b,c}$) exceed the critical threshold for local sand ($\tau_{cr,211\mu m} = 0.18Pa$, derived using *Soulsby* (1997)) only during spring flood tides (Figure 5.5c and Figure 5.6f). These periods with currents strong enough to resuspend or advect sand correspond to flood and ebb stages of the tidal cycle (Figure 5.5a and Figure 5.6b).

Wave-induced bed shear stress $\tau_{b,w}$ is greatest during the storms (Figure 5.5b and Figure 5.6c), exceeding $\tau_{cr,211\mu m}$. High bed shear stresses due to currents ($\tau_{b,c}$) are also observed during the two major storms, likely due to wind-induced storm surge and wave-driven currents (Figure 5.5b). During *Storm Sebastian* on September 14th, eastward currents during the peak of the storm were so strong and persistent that the tide did not reverse (no ebb occurred for nearly 24 hours). During storm periods, $\tau_{b,w}$ is greatest at low tide.

OPTICAL AND ACOUSTIC BACKSCATTER

Over the total deployment period, OBS measurements show strong tidal variation and a response to individual storm events (Figure 5.5d and Figure 5.6h). The largest ADV readings occur during spring tide and the peaks of the two largest storms (Figure 5.5e and Figure 5.6i,j), while the lowest ADV SNR readings tend to correspond to calmer periods with low wave stress (Figure 5.5e and Figure 5.6j).

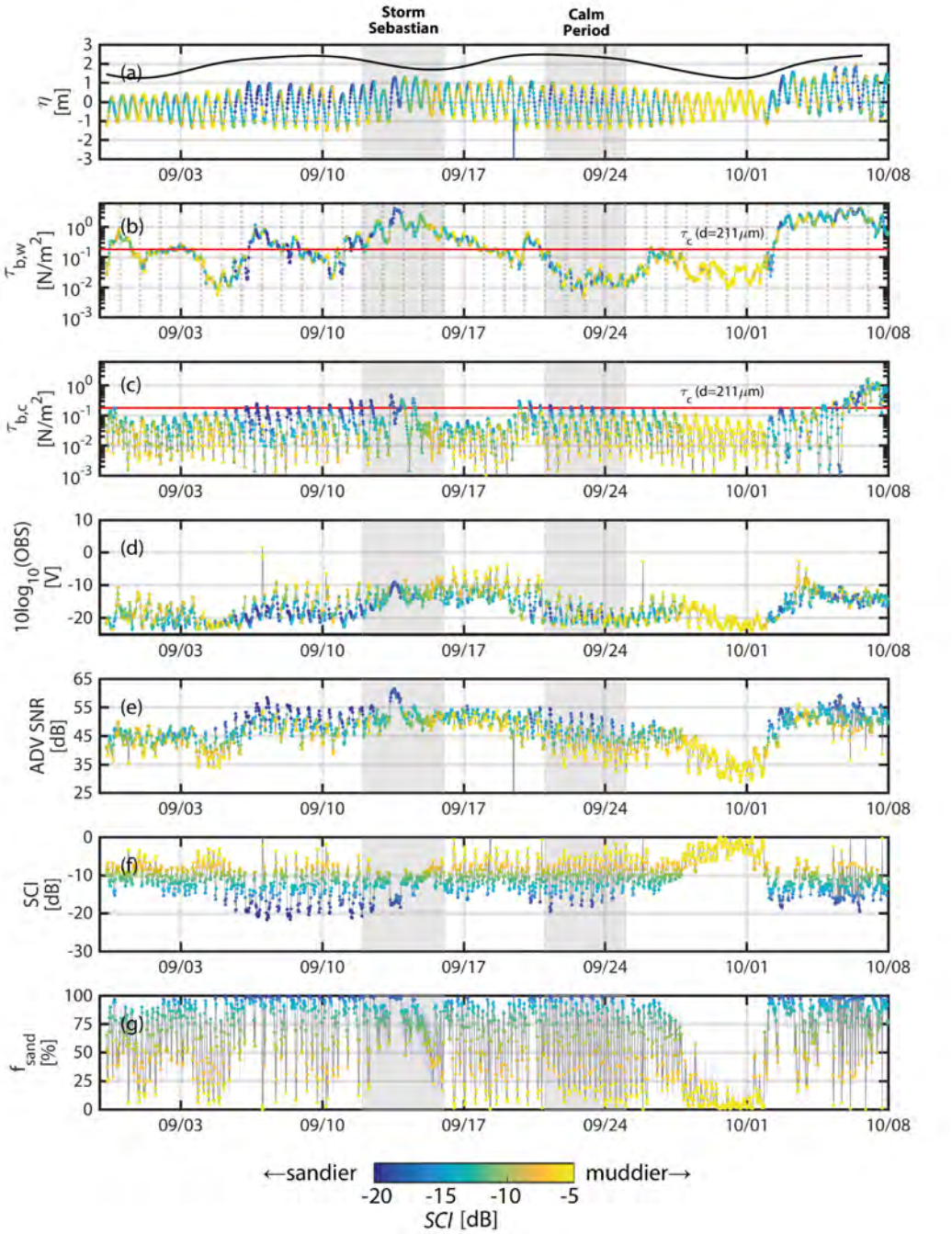

Figure 5.5: Time series of hydrodynamic conditions and backscatter at Ameland ebb-tidal delta Frame 4, with dot colour indicating relative optical-acoustic backscatter index SCI. Higher SCI (lighter yellow colours) suggest relatively higher mud content, and lower SCI (darker blue colours) suggest relatively higher sand content. (a) Water level relative to the mean depth during the deployment period ($8.3m$). The tidal range (indicated with a solid black line) shows spring tide (high values) and neap tide (low values). (b) Bed shear stress due to waves ($\tau_{b,w}$). The critical shear stress for local sand ($\tau_{cr,211\mu m} = 0.18Pa$) is indicated with a solid red line. (c) Bed shear stress due to currents ($\tau_{b,c}$). (d) Log of optical backscatter measured 50 cm above the bed. (e) Acoustic backscatter (signal-to-noise ratio, SNR) measured 50 cm above the bed. (f) Relative optical-acoustic backscatter index SCI. (g) Fraction of sand in total suspended sediment (f_{sand}), calculated from SCI using Equation 5.10.

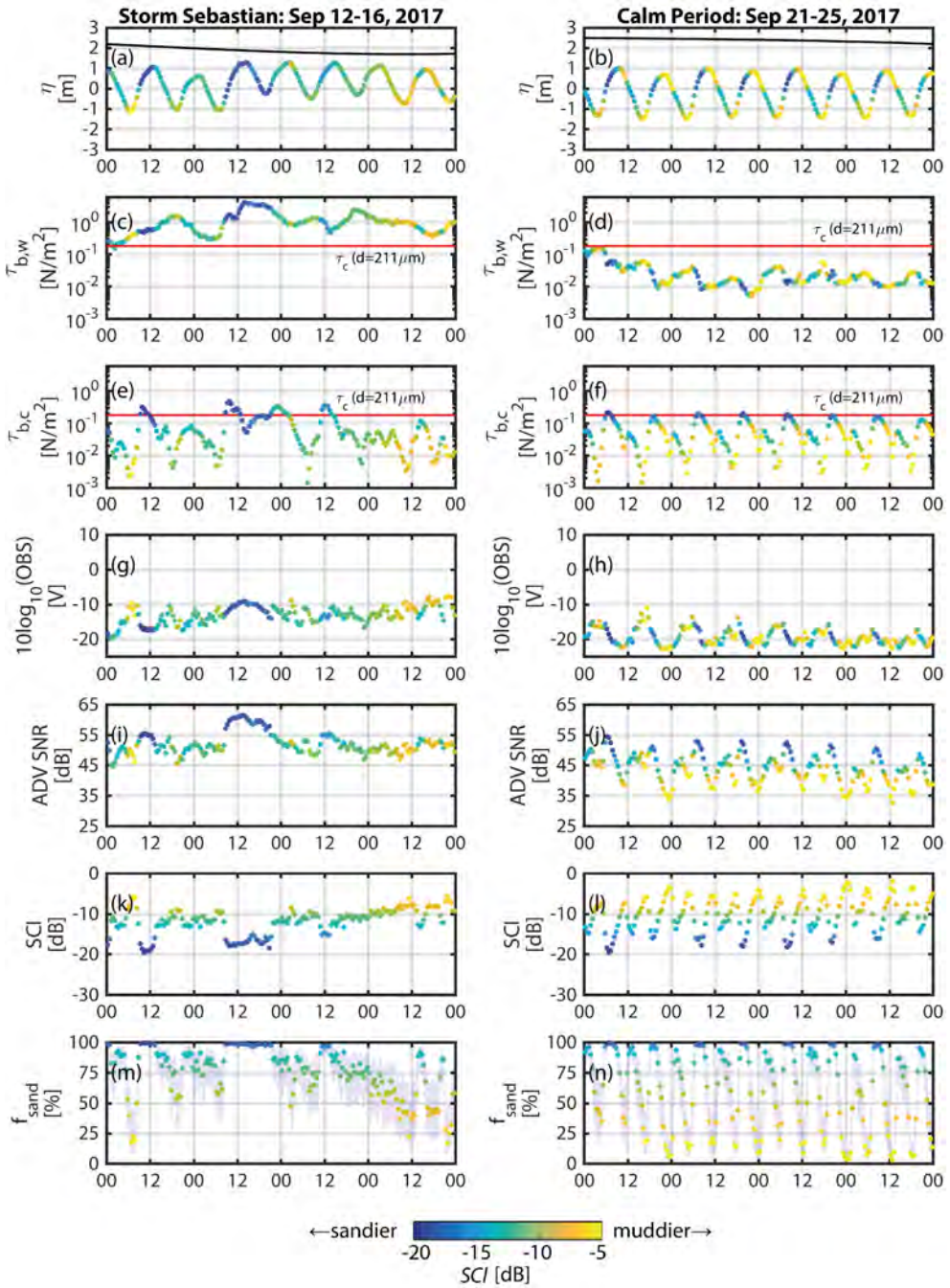

Figure 5.6: Time series of hydrodynamic conditions and backscatter at Ameland ebb-tidal delta Frame 4, focusing on Storm Sebastian (Sept 12-16) and a calmer period during spring tide (Sept 21-25). Dot colour indicates relative optical-acoustic backscatter index SCI. Higher SCI (lighter yellow colours) suggest relatively higher mud content, and lower SCI (darker blue colours) suggest relatively higher sand content. (a,b) Water level (η) relative to the mean depth during the deployment period ($8.3m$). The tidal range (indicated with a solid black line) shows spring tide (high values) and neap tide (low values). (c,d) Bed shear stress due to waves ($\tau_{b,w}$). The critical shear stress for local sand ($\tau_{cr,211\mu m} = 0.18Pa$) is indicated with a solid red line. (e,f) Bed shear stress due to currents ($\tau_{b,c}$). (g,h) Log of optical backscatter. (i,j) Acoustic backscatter (signal-to-noise ratio, SNR). (k,l) Relative optical-acoustic backscatter index SCI. (m,n) Fraction of sand in total suspended sediment (f_{sand}), calculated from SCI using Equation 5.10.

During Storm Sebastian on September 12th-16th, both SNR and OBS signals strongly increase and tidal variation is weak for the next 2 tidal cycles (Figure 5.6g,i). Both signals remain relatively high but noisy, and higher background (minimum) readings persist for about a week after the storm.

During the calm spring tidal period from September 21st-25th, the influence of waves is minimal and the intratidal dynamics are clear (Figure 5.6h,j). The OBS signal shows strong M2 (semi-diurnal) tidal oscillations peaking around low water slack. Conversely, ADV SNR shows mixed M2 and M4 (quarter-diurnal) tidal variation, peaking at flood tide and to a lesser degree at ebb. ADV SNR is lowest at high water slack. The calm period from September 28th to October 2nd coincides with neap tide and exhibits similar dynamics to the pre-storm period at the beginning of the monitoring period, albeit with lower background OBS and ADV SNR levels and reduced intratidal variability.

SEDIMENT COMPOSITION INDEX (SCI) AND f_{sand}

Suspended sediment composition was estimated from the optical and acoustic backscatter readings. SCI was calculated with Equation 5.9, using the OBS and ADV SNR measurements 50 cm above the bed. SCI was offset to zero by subtracting its 99^{th} percentile value. As in the laboratory experiments, this corresponds to a condition when sand is not likely present. This assumption is corroborated by the calm hydrodynamic conditions during moments of high SCI. We then applied Equation 5.10 with $SCI_{50\%} = -8.58$ (fit to both 100 and 200μm sand) to the SCI time series including the confidence bands to approximate the fraction of sand in suspension (f_{sand}).

At subtidal timescales, SCI is lower during storms and spring tides (e.g., Figure 5.6k,l). SCI reaches its lowest observed values during spring tide, during both calm and stormy periods (Figure 5.5b). By contrast, it is highest during calm conditions and neap tide (e.g., Figure 5.5f from Sep 28 to Oct 2). SCI is much more dynamic at spring tide, its standard deviation nearly doubling when compared to neap tide.

Over the course of a tidal cycle, SCI typically followed a mixed M2 and M4 pattern. The M4 signal has minima at flood and ebb tide, and is especially pronounced during spring tidal conditions. Superimposed on this is an M2 variation with its peak centred at ebb tide. The combination of these two signals results in minimal SCI at flood tide when $\tau_{b,c}$ is high, then a peak at high water slack when $\tau_{b,c}$ is low (Figure 5.6l). This is followed by a sharp drop to a secondary minimum at ebb tide (when $\tau_{b,c}$ increases again), and then a gradual rise to another peak at low water slack. The cycle completes with another rapid decline in SCI at flood tide as currents strengthen. Although SCI nearly always peaks at slack water, the maximum varies between low water slack (e.g., Sep 8-10) and high water slack (e.g., Sep 21-25).

SPM composition varied throughout the tidal cycle, with distinct differences observed between periods of higher flow (i.e., ebb and flood) and periods of lower flow (i.e., slack water). SPM is dominated by sand at ebb and flood tide, when $f_{sand} > 75\%$ (Figure 5.6n). Conversely, the suspension consists primarily of mud at high and low water slack ($f_{sand} < 25\%$). f_{sand} follows an M4 signal, with only weak M2 variations compared to SCI.

The presence of waves (indicated by higher wave-induced bed shear stress $\tau_{b,w}$) was often associated with lower SCI (Figure 5.5b). During Storm Sebastian on September 13th, SCI drops during the peak in the storm, and loses its characteristic M2-M4 tidal variation for several days (Figure 5.6k). This corresponds to a period of mainly sand in suspension ($f_{sand} > 75\%$), with f_{sand} approaching 100% at the peak of the storm (Figure 5.6m). The

proportion of mud in suspension increases towards the end of the storm, and tidal variations in f_{sand} begin to return.

To further explore the influence of waves on tidal variations in relative optical-acoustic response, SCI is plotted as a function of wave ($\tau_{b,w}$) and current-related bed shear stresses ($\tau_{b,c}$) at each stage of the tidal cycle (Figure 5.7). We summarize the variability of SCI relative to wave and current forcings (shear stresses), separating results into flood and ebb tidal phases. In this shear stress space, the dynamics of SCI are clearly structured. During calm flood tides ($\tau_{b,w} < \tau_{cr,211\mu m}$), SCI ranges from $0dB$ during weak currents to $-22dB$ during stronger currents. A similar pattern is observed during ebb, although generally $SCI > -15dB$. This can be explained by the weaker $\tau_{b,c}$ during maximum ebb compared with during maximum flood. Both high and low water slack are characterized by relatively high SCI ($> -10dB$). SCI reaches $< -12dB$ during slack periods during wavy conditions. Larger wave-induced stresses are generally associated with $SCI < -5dB$, although brief peaks in SCI can sometimes be observed during storms (Figure 5.5).

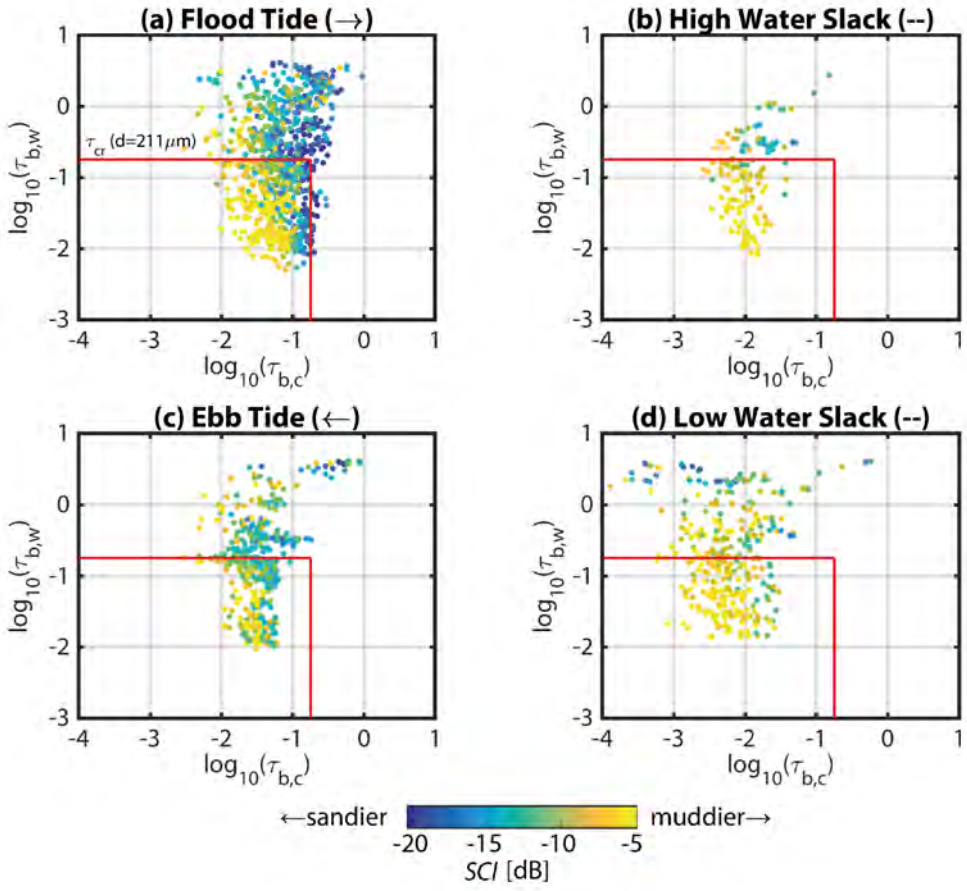

Figure 5.7: Sediment composition index SCI (in color) as a function of wave shear stress (vertical axes) and current shear stress (horizontal axes), at four different stages of the tidal cycle. (a) Flood tide ($u > 0.1 m/s$ and to the east); (b) high water slack ($u < 0.1 m/s$ and at high water); (c) ebb tide ($u > 0.1 m/s$ and to the west); (d) low water slack ($u < 0.1 m/s$ and at low water). The critical shear stress for local $211 \mu m$ sand ($0.18 Pa$) is plotted for reference as a solid red line. Bed shear stresses were computed using *Soulsby* (1997).

5.4. DISCUSSION

5.4.1. INTERPRETING THE DYNAMICS OF THE SEDIMENT COMPOSITION INDEX (*SCI*)

The sediment composition index (*SCI*) is a useful indicator of the relative fractions of sand and mud in suspension, as validated in laboratory experiments. Application of this index was demonstrated by interpreting the sediment dynamics on Ameland ebb-tidal delta in light of two main processes: resuspension of local sandy bed material by waves and strong tides, and tidal advection of mud from locations outside the ebb-tidal delta. These processes explain the response of optical and acoustic backscatter measurements, and hence the corresponding dynamics of *SCI*.

At subtidal timescales (> 24 hours), the dynamics of *SCI* can be explained in part by a fortnightly spring-neap cycle. The larger intratidal variation of *SCI* at spring tide is likely due to the increased resuspension of sand by stronger currents (Figure 5.5c) and to the greater advection of mud from nearby intertidal flats at late ebb and LWS, similarly to the observations of *Weeks et al.* (1993) and *Fettweis et al.* (1998) at other sites. Conversely, high *SCI* (and thus higher relative proportions of mud in suspension) coincides with the neap tide (e.g., Sep 28-Oct 1) and with lower values of $\tau_{b,w}$ and $\tau_{b,c}$. Without sufficiently strong forcing to resuspend local sand ($\tau_b < \tau_{cr,211\mu m} = 0.18Pa$, derived using *Soulsby* (1997)), only mud can remain in suspension (Figure 5.5c).

The observed intratidal variation in *SCI* (Figure 5.6l) can be explained by the local hydrodynamics and sedimentary environment, and is summarized conceptually for a generic sandy tidal inlet or ebb-tidal delta with a muddy inner basin in Figure 5.8. At flood and ebb tide, strong currents are capable of resuspending sand from the local seabed or advecting it from elsewhere nearby, so the corresponding *SCI* values decrease. Conversely, when sand settles out at slack water, only the suspended mud remains in the water column, explaining the increase in *SCI* value at that time. The result is an M4 signal with minima at flood and ebb tide. This relationship between local resuspension and local current velocities is also observed by (*Lavelle et al.*, 1984; *Weeks et al.*, 1993; *Bass et al.*, 2002; *van de Kreeke and Hibma*, 2005).

Modulating the M4 *SCI* signal is an M2 signal with its maximum centred at ebb tide. This M2 signal can be explained by the semidiurnal migration of a strong landward mud concentration gradient in the channels of Ameland basin (*Postma*, 1961). Remote sensing indicates that this turbid water mass can be ejected several kilometres seaward of the inlet and across the ebb-tidal delta at ebb (*Pearson et al.*, 2019), which causes the corresponding *SCI* to increase. This muddy water mass is then displaced by less turbid oceanic water on the flood tide, so *SCI* decreases again. This semidiurnal transport pattern is widely observed at other sites where there is a persistent gradient in suspended mud concentration (*Weeks et al.*, 1993; *Green et al.*, 2000; *Bass et al.*, 2002; *van de Kreeke and Hibma*, 2005).

To fully explain the *SCI* dynamics at Ameland, the episodic influence of storms must also be accounted for. If waves are sufficiently large ($\tau_{b,w} > \tau_{cr,211\mu m}$), then the majority of local sand can be mobilized, which can result in low values of *SCI* regardless of the tidal stage. Conversely, the periods with the lowest *SCI* (suggesting lower proportions of sand in suspension and relatively more mud) coincide mainly with periods of low wave action (e.g., Sep 28-Oct 1).

During periods with large waves, *SCI* may be influenced not just by an increased capacity for local resuspension of sand, but also by wind and wave-induced mud resuspension.

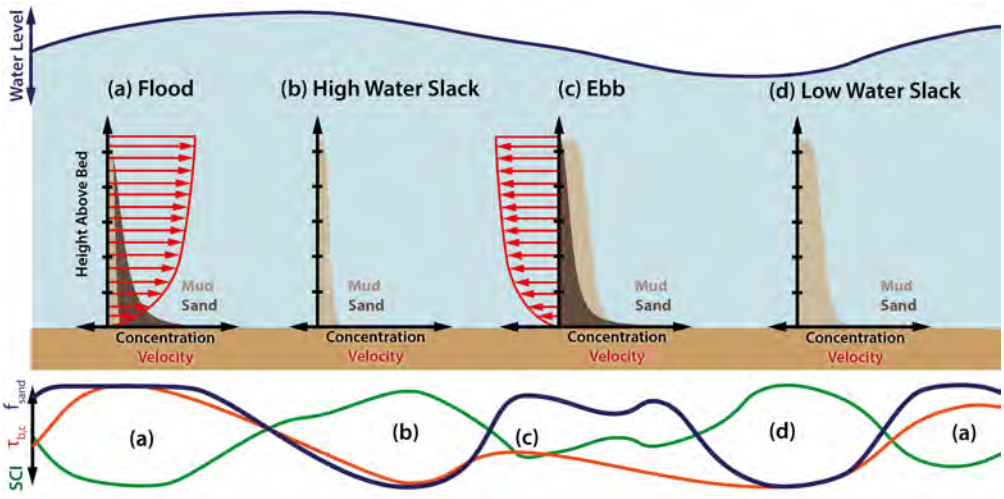

Figure 5.8: Conceptual model of tidally-driven mixed sand-mud sediment transport at a sandy tidal inlet or ebb-tidal delta with a muddy inner basin. A normalized example time series of sediment composition index (SCI), bed shear stress due to currents ($\tau_{b,c}$), and fraction of sand in suspension (f_{sand}) over a tidal cycle are indicated below. (a) At flood tide, strong currents locally resuspend sand, but carry few mud particles from the sea, so SCI is low. (b) At high water slack, currents are too weak to mobilize sand, so total concentrations are relatively low and consist only of mud, so SCI is higher. (c) At ebb tide, strong currents locally resuspend sand, though less than at flood tide, so SCI decreases again. These ebb currents also carry with them mud particles from the muddy and biologically productive inner basin. (d) At low water slack, currents are too weak to mobilize sand, leaving only the mud advected from the inner basin at ebb, which begins to settle, resulting in higher SCI.

This is reflected in the SCI signal during Storm Sebastian (Figure 5.6). Even when bed shear stresses due to waves and currents greatly exceed $\tau_{cr,211\mu m}$, SCI seldom drops below $-15dB$ and f_{sand} remains between $50-90\%$ for most of the storm. In the latter half of the storm, f_{sand} decreases as sand settles out, while mud remains in suspension. This mud can originate from two locations: the Wadden Sea tidal basin or the bed of the North Sea. During storms, tidal flats in Ameland basin may easily lose the surface layers of sediment deposited in calm periods (*Postma*, 1961). In a similar case study, *Green et al.* (2000) found that wave activity on nearby intertidal flats was the principal determinant of suspended mud load advected through a tidal channel. However, storms may also remobilize mud which accumulates in the bed of the North Sea (*van der Hout et al.*, 2017; *Flores et al.*, 2017; *Hendriks et al.*, 2020). Instantaneous bed shear stress does not tell the whole story of suspended sediment composition: it is also necessary to account for spatial and temporal variations in the supply of mud.

Our interpretation of SCI based on theoretical considerations and the laboratory results are fully supported by the local hydrodynamics and sedimentological context. SCI thus provides a novel and valuable characterization of the suspended sediment dynamics on Ameland ebb-tidal delta. This metric is especially useful for mixed-sediment environments like Ameland where optical and acoustic measurements are otherwise ambiguous when viewed in isolation.

5.4.2. LIMITATIONS & OUTLOOK

Having been conceptually validated by laboratory and field measurements, there are many opportunities for further developing the SCI and improving its applicability. The next steps towards a more quantitative evaluation of sediment composition lie in the accumulation of larger datasets and in quantifying the component of SCI specific to the instruments being used (the c_{instr} term of Equation 5.8, which is invariant with SPM).

For a more generic SCI, we propose a reference calibration of optical and acoustic sensors to evaluate the instrument constant c_{instr} (Equation 5.8), using NTU/BTU (formazin calibration) for optical systems, and monodispersed glass beads for acoustic particles, similarly to the calibration procedure for an ABS system (e.g., *Thorne and Meral* (2008)). With calibrated scatterers, the sonar equation (Equation 5.4) can be fully evaluated, the instrument constant c_{instr} is the only unknown. Acoustic backscatter is sensitive to the acoustic frequency of the transducers: the SCI dynamics will be different from 1 MHz to 6 MHz sensors, because each sensor will respond differently to sediment of a given grain size and concentration. Similarly, optical sensors will provide different NTU values depending on whether the optical sensor is based on backscatter (e.g., OBS 3+ (*Campbell Scientific Inc.*, 2014), Seapoint *Seapoint Sensors Incorporated* (2013), or Wetlabs (*WETLabs*, 2010)) or sidescattering (e.g., YSI 6600 (*YSI Incorporated*, 2012)). Many additional laboratory experiments would be required in order to determine c_{instr} and make a full set of conversion factors for each type of instrument. By applying these calibrations, SCI could become generic, at least for similar instruments. However, even without quantifying c_{instr} directly, SCI provides useful information on suspended sediment composition when its dynamics are considered in the context of local hydrodynamic and sedimentological conditions.

Additional laboratory experiments must be carried out with a wider variety of sediment mixtures and concentrations. We expect that most of the variability of SCI is caused to first order by the presence of sand in suspension, because sand has a relatively stronger influence on acoustic backscatter than flocs of comparable size (*Thorne and Hurther*, 2014). However, the influence of flocculation on the variability of SCI requires further investigation. Estimating how SCI would change in response to organic matter also remains an open question. Organic matter has different optical and acoustic backscatter characteristics from inorganic sediment (*Hoitink and Hoekstra*, 2005; *Boss et al.*, 2018), so its presence will potentially affect SCI.

Field measurements should also be collected from sites with different sedimentary characteristics under a range of hydrodynamic conditions in order to generalize the conclusions of the present study and $SCI - f_{sand}$ relationships like Equation 5.10. Samples pumped at regular intervals (e.g., *Beamsley et al.* (2001)) or better yet, at moments triggered by specific turbidity levels, would provide a more representative basis for calibrating optical and acoustic measurements. Fortunately, analyzing SCI dynamics of additional field sites is already possible, since optical and acoustic instruments are frequently paired together in the field (e.g., *Fugate and Friedrichs* (2002); *Voulgaris and Meyers* (2004); *Moura et al.* (2011); *Flores et al.* (2018); *Zhu et al.* (2019b); *Lin et al.* (2020); *de Vet et al.* (2020); *Colosimo et al.* (2020); *Pomeroy et al.* (2021)). Our approach thus gives added value to existing datasets by providing an additional, simple-to-calculate metric for interpreting sediment dynamics.

These additional efforts to make SCI more general and to better understand the underlying physics will strengthen the usefulness and applicability of the metric. This will lead to new insights into the dynamics of mixed sediment environments where ambiguity due

to suspended sediment composition previously limited the information that could be obtained from optical and acoustic measurements.

This approach is most valuable in settings where it cannot be assumed that suspended sediment always has the same properties as the seabed. The majority of the world's coasts are heterogeneous sedimentary environments where these conditions may be found (*Holland and Elmore*, 2008). Even if ADV and OBS measurements are not available, the general principle of using differential optical and acoustic backscatter to disambiguate mixed sediment suspensions should still apply to pairs of other similar instruments. This would however require SCI-specific calibration experiments with the dedicated pair, similar to those performed in the present study. If applied in conjunction with instruments using different measurement principles (e.g., Laser In-Situ Scattering and Transmissometry (LISST) (*Agrawal and Pottsmith*, 2000; *Mikkelsen and Pejrup*, 2001; *Hill et al.*, 2011; *Chapalain et al.*, 2019) or multifrequency acoustic backscatter sensors (*Gray and Gartner*, 2009; *Moate and Thorne*, 2009, 2012; *Wilson and Hay*, 2015)), SCI could yield even more insight into suspended sediment composition.

5.5. CONCLUSIONS

The sediment composition index (SCI) derived in this study quantifies the suspended sediment composition in mixed-sediment environments. It does so using the relative intensity of optical and acoustic backscatter signals, as these two measurement techniques have different sensitivities to sand and mud (Equation 5.9). SCI can be used to estimate the fraction of sand and mud in suspension (f_{sand} and f_{mud}) in marine environments. Here, we verify the theoretical response of these optical and acoustic instruments in laboratory experiments. SCI is negatively correlated with the fraction of sand in suspension (Equation 5.10).

The SCI approach was successfully applied to *in situ* measurements on the ebb-tidal delta of Ameland Inlet in the Netherlands. SCI shows a clear M4 variation associated with suspension of local sand, modulated by an M2 variation associated with suspended mud advected from the nearby Wadden Sea. Lower values of SCI (indicating a stronger acoustic response) and higher f_{sand} are observed under more energetic conditions when sand is expected to dominate the suspension (e.g., spring flood tide or strong wave conditions). Conversely, SCI increases (indicating a stronger optical response) and f_{sand} reduces in calmer conditions and at slack water, when the suspended sediment consists mainly of mud.

This approach reduces the ambiguity of suspended sediment composition in mixed sediment environments. Furthermore, it adds value to existing sets of measurements since simultaneous optical/acoustic measurements have frequently been carried out together in sediment transport studies. Being able to discern between different types of sediment in suspension will increase confidence in the interpretation of suspended sediment concentration measurements. This can ultimately improve estimates of sediment fluxes, leading to deeper understanding of coastal systems and enable better-informed coastal management decision-making.

ACKNOWLEDGMENTS

This work is part of the research program "Collaboration Program Water" with project number 14489 (SEAWAD), which is (partly) financed by NWO Domain Applied and Engineering Sciences. Special thanks to the Dutch Ministry of Infrastructure and Water Management (Rijkswaterstaat and Rijksrederij) for their ongoing support as part of the Kustgenese2.0 project. This work was also supported by ISblue project, Interdisciplinary graduate school for the blue planet (ANR-17-EURE-0015) and cofunded by a grant from the French government under the program "Investissements d'Avenir". DT was partly funded by the research project PHRESQUES 2, coordinated by the GIP Seine Aval and financed by the CPIER Vallée de Seine program. We are grateful to the two anonymous reviewers for their positive and constructive feedback, which has improved the quality of the manuscript.


Tracking fluorescent and ferrimagnetic sediment
TRACERS
to monitor grain size-selective dispersal

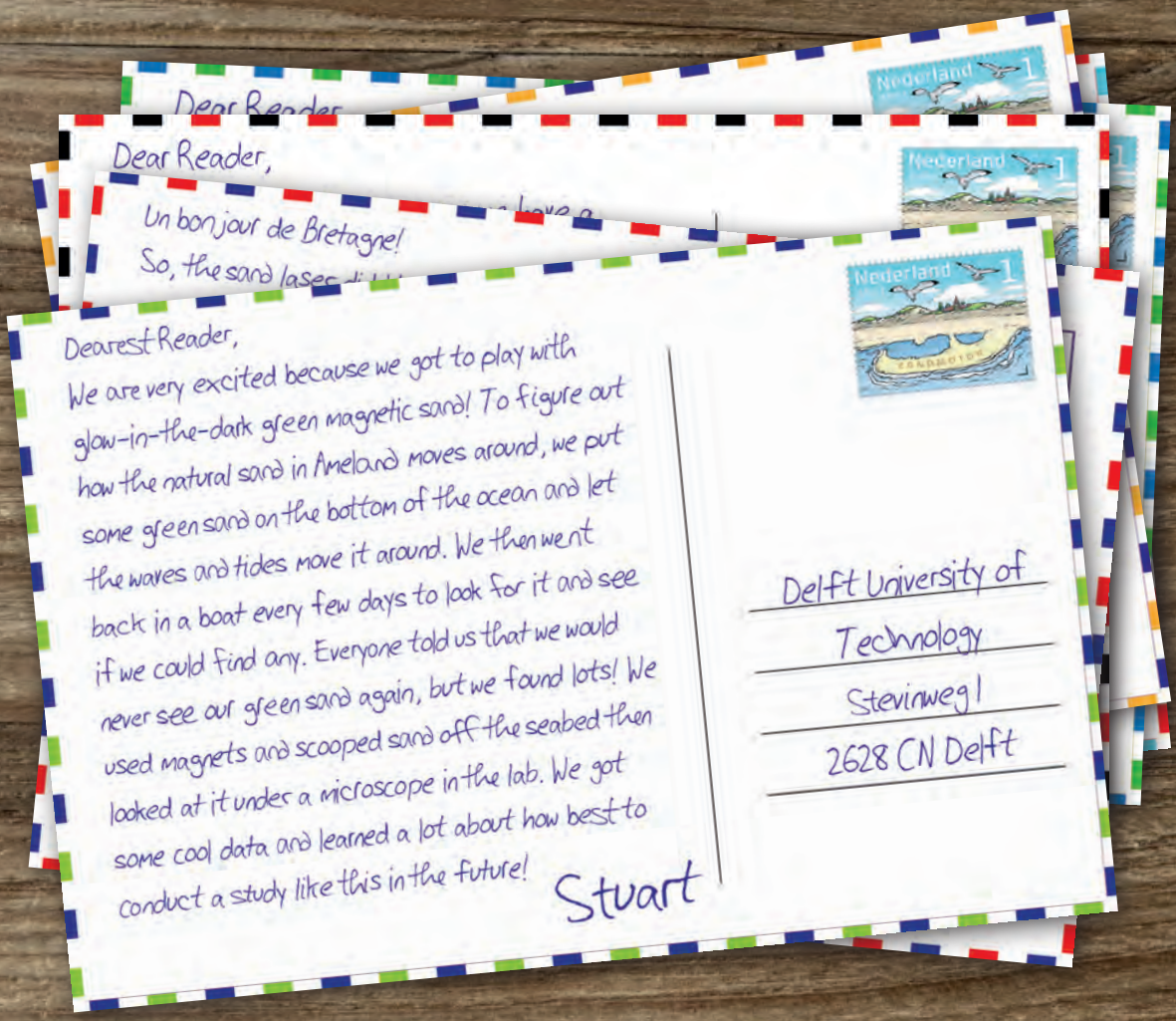
Dear Reader,
Un bonjour de Bretagne!
Dear Reader,
Nederland
Nederland
Nederland
Dearest Reader,
We are very excited because we got to play with glow-in-the-dark green magnetic sand! To figure out how the natural sand in Ameland moves around, we put some green sand on the bottom of the ocean and let the waves and tides move it around. We then went back in a boat every few days to look for it and see if we could find any. Everyone told us that we would never see our green sand again, but we found lots! We used magnets and scooped sand off the seabed then looked at it under a microscope in the lab. We got some cool data and learned a lot about how best to conduct a study like this in the future!
Stuart
Delft University of
Technology
Stevinweg 1
2628 CN Delft

6

TRACKING FLUORESCENT AND FERRIMAGNETIC SEDIMENT TRACERS ON AN ENERGETIC EBB-TIDAL DELTA TO MONITOR GRAIN SIZE-SELECTIVE DISPERSAL

KEY POINTS:

- Large-scale sediment tracer study conducted on a highly dynamic ebb-tidal delta, and despite the challenges presented by such an energetic setting, tracer was recovered
- Tracer recovery and processing were enhanced by its fluorescence and ferrimagnetism
- Tracking grain size of recovered tracers is essential for interpretation
- Tracers prove to be useful tool for sand nourishment planning and monitoring

This chapter has been published in *Ocean & Coastal Management*:

Pearson, S.G., van Prooijen, B.C., Poleykett, J., Wright, M., K. Black, K., & Wang, Z.B. (2021). Tracking fluorescent and ferrimagnetic sediment tracers on an energetic ebb-tidal delta to monitor grain size-selective dispersal. *Ocean & Coastal Management*, 212, p.105835. [Link].

IN the previous chapters, we examined sediment transport processes in an Eulerian frame of reference, considering only measurements at a fixed point on the ebb-tidal delta over a period of several weeks. However, such measurements provide an incomplete picture of how sediment moves across the ETD ($\mathcal{O}(100m-1km)$), so an alternative approach to monitoring sediment transport is necessary. In contrast, a Lagrangian frame of reference is one that moves with the thing being measured. For example, we measure the velocity at a fixed point in Chapters 4 & 5, but follow drifters around the entire inlet in Chapter 2.11. In this chapter, we do something similar, using fluorescent and magnetic tracers to follow grains of sand around the delta. These measurements complement the Eulerian sediment transport measurements in Chapters 4 & 5, and yield useful insights into the sorting behavior of sand on the ebb-tidal delta. Furthermore, the tracer experiment acts as a proxy for sand nourishments and provides guidance on nourishment strategies for ebb-tidal deltas.

ABSTRACT

Sediment tracer studies use uniquely identifiable particles to track the pathways and fate of individual sand or silt grains in marine environments. These techniques are best applied to assess connectivity between potential sediment sources and sinks, such as between a sand nourishment and an ecologically sensitive area. Significant challenges exist when applying sediment tracing techniques to further understanding of systems with complicated hydrodynamic, sediment, and morphological regimes. Ebb-tidal deltas are highly dynamic coastal environments shaped by the complex interplay of waves and tides, but have been under-explored. In this study, we use dual signature (fluorescent and ferrimagnetic) sediment tracers to simulate the dispersal of dredged sediment placed as a sand nourishment on an energetic ebb-tidal delta (at Ameland Inlet, the Netherlands). After deployment, sediment dispersal and grain size sorting behaviour were monitored via the collection of seabed grab samples and magnetic sampling of sediment transported in suspension. The tracer content within collected samples were put in context with hydrodynamic conditions observed during the study period. Here we show that the use of such dual signature tracers, in addition to novel tracer recovery and analysis techniques, enables the dispersal of sediment to be monitored even in such complex settings and energetic conditions as an ebb-tidal delta. Our observations show that tracers transported in suspension are significantly finer than tracers that accumulated in the seabed. These suggest that preferential transport as a function of grain size is a key process in shaping the morphology of ebb-tidal deltas and thus governing the dispersal of sand nourishments there. The findings of this study and the approach used here provide valuable tools for assessing the baseline conditions of complex coastal environments today, and for planning the interventions which may be necessary in future responses to climate change. Lessons learned from the application of sediment tracers in this study are provided to assist future researchers and practitioners in the application of this technique in dynamic coastal environments.

6.1. INTRODUCTION

SAND nourishments have proven to be an effective management strategy for reducing coastal erosion and are widely positioned as a means of coping with sea level rise (*de Schipper et al.*, 2021; *Lodder et al.*, 2019). While they are most common at beaches and foreshores (*Hanley et al.*, 2014; *Hanson et al.*, 2002; *Liu et al.*, 2019; *Stive et al.*, 2013), they are now also applied in other coastal settings like tidal flats (*Baptist et al.*, 2019; *van der Werf et al.*, 2019b).

Existing tools to predict and monitor the processes influencing the fate of a nourishment are however not yet sufficient. Seemingly trivial questions like: "Where, how much, when, and how to nourish?", or “Where does the nourished sediment go?” are challenging to answer, but crucial for effective and efficient coastal management. This is especially the case for nourishments in complex settings like ebb-tidal deltas. Only a few examples of nourishments on ebb-tidal deltas are known (*Bishop et al.*, 2006; *Foster et al.*, 1994); on the contrary, ebb-tidal deltas have often historically been viewed instead as a source for nourishments (*Fontolan et al.*, 2007; *Hicks and Hume*, 1997). However, nourishing ebb-tidal deltas is now being proposed as a key component of the Dutch coastal management strategy (*Lodder et al.*, 2019; *Wang et al.*, 2018). There is thus a pressing need to answer these basic questions.

A large-scale research program (Kustgenese2.0/SEAWAD) was initiated in the Netherlands to provide insights for designing nourishment on ebb-tidal deltas. The project included numerical modelling (*Brakenhoff et al.*, 2020a; *de Wit et al.*, 2019; *Reniers et al.*, 2019) and field measurement campaigns (*Van Prooijen et al.*, 2020). Point measurements of hydrodynamics and suspended sediment characteristics were carried out at five locations across the delta. Bathymetric mapping provided snapshots of the ebb-tidal delta’s morphological evolution in high spatial and temporal resolution (*Elias et al.*, 2022). However, none of these methods tell us anything about the dispersal of sediment from a specific location, as in a nourishment. These methods also do not reveal sediment transport pathways, nor do they differentiate between pathways of different grain sizes. This type of information is necessary to predict the longevity of a nourishment, as well as its ecological impact.

Particle tracking or tracing is a method that can be used to obtain more insights into the pathways that sediment particles take. The former involves taking uniquely identifiable "tracer" particles, injecting a known quantity at a particular location, and then monitoring the dispersal of this tracer across space and through time (*Black et al.*, 2007). This approach has been successfully employed to monitor nourishments by *Smith et al.* (2007). Unlike Eulerian measurements (at a fixed point in space), Lagrangian techniques like particle tracking can provide information about the fate and provenance of sediment. Most previous tracer studies have focused on using tracers to quantify transport rates and directions. For example, *Ciavola et al.* (1998); *Oliveira et al.* (2017); *Silva et al.* (2007) used tracers to monitor alongshore transport rates. *Komar* (1978) and *Wilson* (2018) have used tracers to examine the relative degree of bed load and suspended load transport in coastal settings. By examining core samples of the seabed, *Kraus* (1985) and *Sunamura and Kraus* (1984) used tracers to monitor burial depths and quantify the mixing depth or "active layer" thickness.

Tracers can also be used to quantify grain size-dependent sediment transport and sorting processes. *Allison et al.* (2017) tracked the fate of tracer with multiple grain sizes, using differently-coloured tracers to represent different particle sizes. *Robin et al.* (2009) assumed that tracer particle size was uniform, and most previous studies focused only on match-

ing the particle size distribution of the initial tracer to the native sediment, not how that distribution changes after being transported. A few studies have challenged this assumption and examined grain-size selective transport using tracers on straight, sandy beaches (*Blackley and Heathershaw*, 1982; *Duane and James*, 1980; *Ribeiro*, 2017). However, the potential of tracers to better understand sediment sorting and grain size-selective transport on ebb-tidal deltas is relatively under-explored, even though knowledge of such processes is essential to the design of effective nourishments there.

Execution of tracer studies in coastal settings is challenging due to the variety of physical processes influencing sediment transport and the numerous potential pathways that the tracer can take. Unlike in rivers where transport is driven mainly by unidirectional currents, the influence of waves or wind-induced currents must also be considered on open coasts (*Hanes*, 1988; *Wilson*, 2018). Even in relatively well-constrained coastal settings (e.g., straight, sandy beaches), there may be bidirectional tidal currents, stirring by waves, and wave-induced alongshore or cross-shore currents (*Duane and James*, 1980; *Komar*, 1978; *Oliveira et al.*, 2017; *Silva et al.*, 2007). Tracer studies have also been carried out at other coastal sites such as tidal flats (*Kato et al.*, 2014), harbours (*Khalfani and Boutiba*, 2019; *McComb and Black*, 2005; *Vila-Concejo et al.*, 2003), and navigation channels (*Smith et al.*, 2007). The challenges of conducting and interpreting tracer studies are perhaps greatest in estuaries and tidal inlets, where complex interactions between waves, tides, and rivers may act in multiple directions.

Few studies have considered sediment tracers at coastal locations as dynamic and complex as tidal inlets (e.g., *Moritz et al.* (2011); *Li et al.* (2019)). Most tracer studies conducted at tidal inlets have focused on intertidal shoals and beaches, where it is easier to deploy and sample the tracer material at low tide (*Balouin et al.*, 2001; *Oertel*, 1972; *Robin et al.*, 2009; *Vila-Concejo et al.*, 2004). These studies were principally concerned with the migration of shoals and swash bars or sediment transport at the margins of the inlet. However, to the authors' knowledge, no tracer studies have considered transport on the distal lobe of an ebb-tidal delta. Sediment pathways here may be extremely convoluted and grain size-dependent (*Elias et al.*, 2019; *Herrling and Winter*, 2018; *Pearson et al.*, 2020; *Son et al.*, 2011), which greatly increases the uncertainty involved in designing a sampling plan to recover tracer placed there. Effectively monitoring the dispersal of sediment tracer on the outer limits of a highly energetic ebb-tidal delta at subtidal depths thus presents a daunting challenge and requires the use of new recovery and analysis techniques.

There are numerous techniques available to uniquely "tag" sediment to make it distinguishable from native background sediment. Natural geochemical properties of the sediment can be used (*Clemens and Komar*, 1988). Radioactive tracers were commonly used in the 1960s, but have since fallen out of favour due to their environmental impact (*Courtois and Monaco*, 1969; *Duane and James*, 1980; *White*, 1998). Radio frequency identification (RFID) tags can be used for larger gravel and cobble-sized particles (*Miller and Warrick*, 2012), although this approach is not feasible for sand-sized grains. Luminescence is also frequently used to trace sediment in geomorphological applications (*Gray et al.*, 2019; *Reimann et al.*, 2015). The most popular approach in recent years has been to apply a fluorescent coating to grains of sand, as the tracer can be identified visually or through automated image analysis (*Gallaway et al.*, 2012; *Komar*, 1978; *Kraus et al.*, 1982; *McComb and Black*, 2005; *Miller and Warrick*, 2012; *Oliveira et al.*, 2017; *Robin et al.*, 2009; *Silva et al.*, 2007; *Smith et al.*, 2007; *Sunamura and Kraus*, 1984). It may also be possible to trace parti-

cles via a comparative measure of the relative ease with which a material can acquire a magnetic field (i.e., the magnetic susceptibility of grains (*Gallaway et al.*, 2012)). However, the risk of using tracer with a single unique identifying characteristic (termed a mono-signature tracer) is that it can limit the techniques which can be applied to sample tracer in the field and determine tracer content within samples in the laboratory. The solution to these issues may be the use of tracers that can be detected and distinguished via multiple properties.

In this chapter, we explore the potential of particle tracking in energetic marine areas for monitoring the dispersal of nourishments. We aim to answer questions such as: "*Is it possible to recover tracer particles in such dynamic environments?*"; "*What are efficient and effective ways to collect the particles?*"; and finally: "*What can we conclude from a particle tracking experiment that we cannot conclude from other monitoring techniques?*". To simulate and predict the potential dispersal of sand from an ebb-tidal delta nourishment, we conducted a sediment tracer study at Ameland Inlet in 2017. Such a dynamic environment necessitated novel techniques for recovery and analysis of the tracer. A dual-signature (fluorescent and ferrimagnetic) tracer (manufactured by Partrac Ltd) was used, enabling samples to be collected from both the water column and seabed via a combination of suspended high-field magnets and seabed grab samples. Our approach afforded the opportunity to sample tracer deposited on the bed and transported as suspended load. The characteristics and location of recovered tracer provide useful information for understanding sediment sorting processes and differential transport as a function of grain size on ebb-tidal deltas from strategically placed sediment, as from a nourishment.

6.2. BACKGROUND

6.2.1. REGIONAL SETTING

Flood safety and vital ecosystems in the northern Netherlands depend on the fate of the Wadden Sea and Islands. Their morphodynamic response to sea level rise and sand nourishments is closely tied to the evolution of the ebb-tidal deltas between them. To understand the fate of these ebb-tidal deltas and effectively plan nourishments there, we must quantify the transport and dispersal of sediment as it moves across them.

The tracer study was conducted as part of a larger field measurement campaign which included simultaneous measurements of hydrodynamics, suspended sediment, bed sediment, seabed morphology, and benthic ecology across Ameland ebb-tidal delta, inlet, and Wadden Sea (Figure 6.1). The location was chosen because it was the proposed site of a future sand nourishment project. Prior to this study in 2017, human interventions to the inlet had been relatively minor compared to other inlets on the Dutch coast (*Elias et al.*, 2003; *Wang et al.*, 2015). Ameland Inlet has been widely studied before (*Cheung et al.*, 2007; *Lenstra et al.*, 2019a; *van der Spek*, 1996; *Wang et al.*, 2016), and there are over 400 years of historical bathymetric data available (*Elias et al.*, 2019). The abundance of both historic and present-day data makes Ameland Inlet the ideal location for such a study.

Historical bathymetry analysis by *Elias et al.* (2019) indicates that the recent evolution of Ameland ebb-tidal delta has been dominated by a pattern where the main ebb channel alternates positions and rotates in a clockwise direction. As the ebb-channel moves, shoals develop on the delta's periphery, and gradually move eastward where they eventually merge with the island of Ameland. The position of the ebb-tidal delta and main ebb-channel also determines the position of the eastern tip of the island of Terschelling. This morphodynamic evolution suggests the existence of eastward sediment transport pathways across

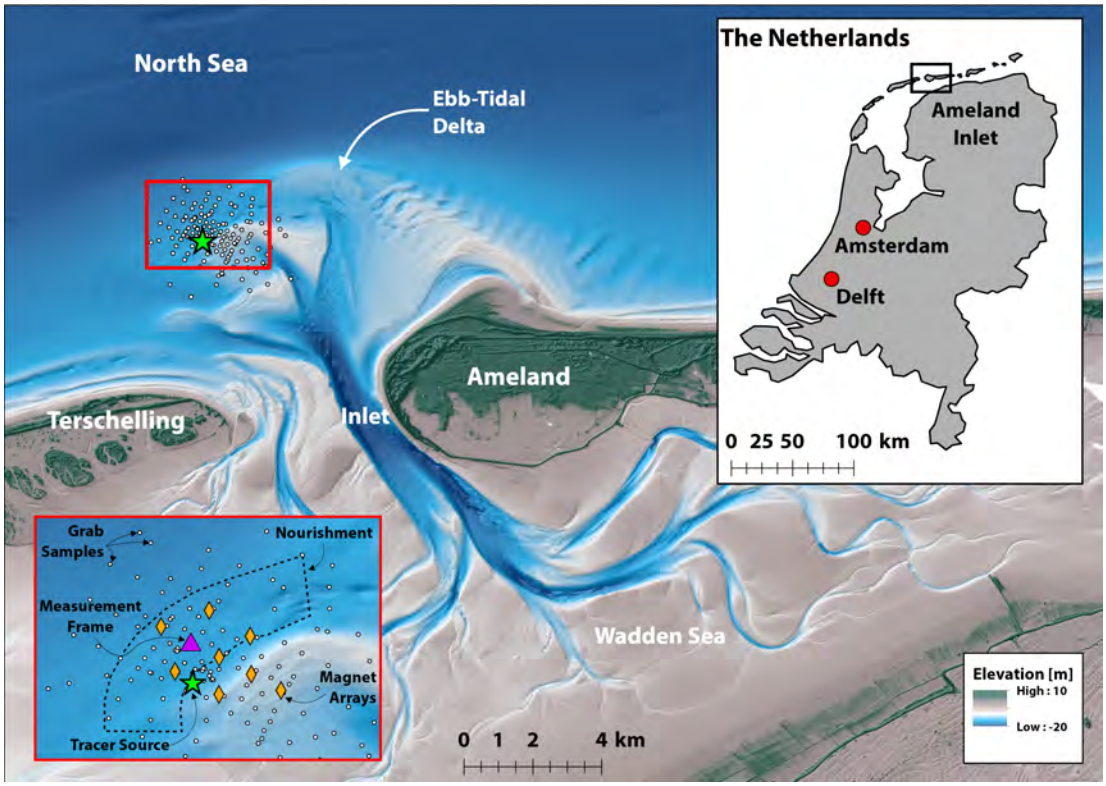

Figure 6.1: Location of project site at Ameland Inlet, the Netherlands. The deployment site or source of the tracer is denoted by a green star. Orange diamonds indicate the location of suspended magnets, and yellow dots indicate seabed Van Veen grab sampling locations. The magenta triangle corresponds to Frame 4 of the Kustgenese2 measurement campaign (*Van Prooijen et al.*, 2020), with which measurements of hydrodynamic conditions were made during the field experiment.

the inlet and ebb-tidal delta. Mapping out these pathways and quantifying rates of sediment transport is essential to the design of nourishments on the ebb-tidal delta.

6.2.2. HYDRODYNAMIC CONDITIONS

To provide context for the tracer measurements, we examine measurements of hydrodynamics and suspended matter carried out simultaneously during the deployment period. *Van Prooijen et al.* (2020) and *van der Werf et al.* (2019a) provide a general overview of the field campaign at Ameland Inlet, which took place over 41 days from August 29 to October 9, 2017. Henceforth, dates in this chapter are given as $T+n$, where n is the number of days since the tracer release on August 29, 2017 (Section 6.3.2).

Water level, wave height, and near-bed current velocities were measured using a downward-facing high resolution Nortek Acoustic Doppler Current Profiler (ADCP-HR) mounted $0.50m$ above the seabed (*Nortek*, 2008). From the wave characteristics and near-bed velocity, the maximum bed shear stress under combined wave and currents was computed using the method of *Soulsby* (1997). Changes in seabed level and acoustic backscatter were monitored using the altimeter on Nortek Acoustic Doppler Velocimeters (ADV) (*Nortek AS*, 2005) mounted 0.35 and $0.50m$ above the bed. Together, these measurements provide additional information to assist in the interpretation of the observed behaviour of the tracer.

Hydrodynamic conditions at the outer lobe of the Ameland ebb-tidal delta during the measurement period were highly energetic, featuring two major ($H_s > 4m$) and three minor ($H_s > 1.5m$) storms (Figure 6.2b). The spring tidal range at the measurement frame is approximately 2.3 m, and current velocities can reach 0.5 m/s, predominantly flowing along an axis oriented east – west. The net displacement at the measurement frame was computed by integrating the measured velocities over time (Figure 6.2f). These show a net eastward displacement from the vicinity of the tracer deployment site during the measurement period. In the 24 hours after release, maximum tidal excursion from the measurement site is approximately 2 km westward and 4 km eastward (Figure 6.2f). There is generally a strong eastward net displacement, with north or southward currents only dominating during the storms on $T+15$ and $T+40$ days.

Acoustic backscatter is frequently used as a proxy for suspended sand concentration (*Green et al.*, 2000; *van de Kreeke and Hibma*, 2005). Although fine sediment is abundant in suspension on Ameland ebb-tidal delta, acoustic backscatter measurements here show stronger correspondence with sand (Chapter 5). The acoustic backscatter signal (measured with the ADV) shows clear semidiurnal peaks during ebb and flood currents, with higher peaks during flood and greater variability during spring tides. This corresponds to resuspension of local sand from the seabed. Relatively higher backscatter is also observed during the storms (e.g., $T+16$ and $T+35$ to 40).

Regular fluctuations of the seabed between August 31 (T+02) and September 5th (T+06) are on the order of $1-3cm$ Figure 6.2d, which matches the findings of *Brakenhoff et al.* (2020b), who found that wave-current ripples on Ameland ebb-tidal delta are consistently between $1-2cm$ in height. The bed then continues to accrete episodically but erodes gradually during the intervening periods. The frame was repositioned following servicing on T+21, and the bed altimetry measurements become sparse thereafter.

These findings demonstrate that the seabed around the tracer deployment site is highly dynamic, even on the timescale of days to weeks. Combined with the energetic hydrodynamic conditions observed during the measurement period, there is strong potential for widespread tracer dispersal and/or burial.

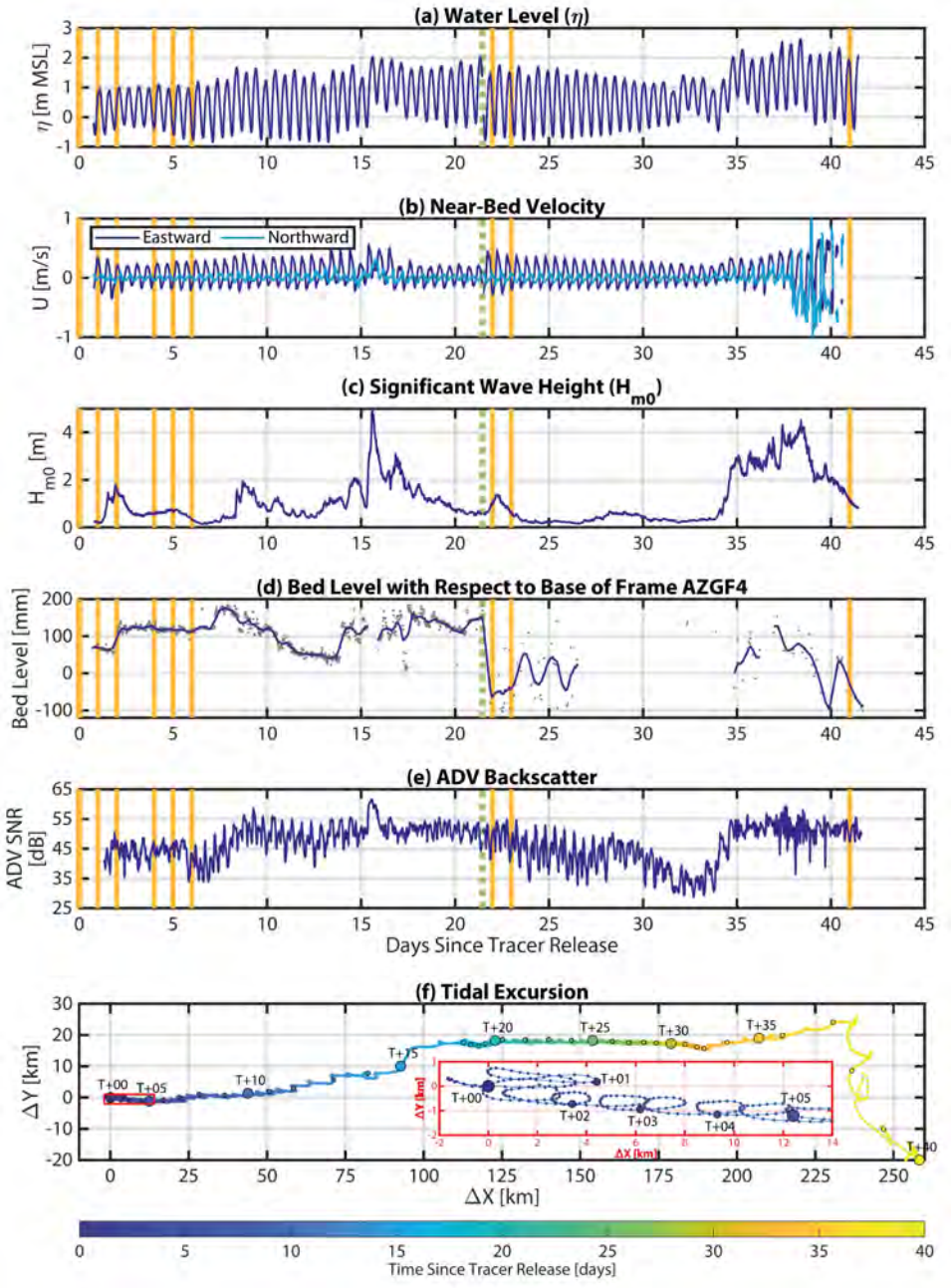

Figure 6.2: Overview of hydrodynamic and seabed conditions measured near the tracer deployment site (AZG-F4) during the field campaign. (a) Water level with respect to mean sea level. Vertical yellow lines indicate days when tracer sampling occurred, and the green dashed line on day $T+21$ indicates when the frame was serviced. (b) Near-bed current velocity measured with a downward-facing ADCP-HR and averaged over a $0.5m$ profile to the bed; (c) significant wave height (H_{m0}); (d) Bed level measured with ADV mounted $0.35m$ above the bed. Note that position of frame shifts after being serviced on T+21, and bed level readings are sparse thereafter; (e) Acoustic backscatter measured using an ADV mounted at $0.5m$ from the bed. Acoustic backscatter is given here as a proxy for suspended sediment concentration, with greater sensitivity to sand than fine sediment (*Pearson et al.*, 2021a); (f) Progressive vector diagram indicating total tidal excursion during the deployment period based on the near-bed current velocity measured by ADCP-HR during the 40-day deployment period. The red inset zooms in on the first 5 days ($T+00$ to $T+05$) after tracer release (August 29, 2017). Circles indicate the displacement at a given number of days after release, with larger markers indicating every fifth day.

6.3. METHODS

To investigate sand transport processes on ebb-tidal deltas using sediment tracers, we broadly followed the methodological framework described by *Black et al.* (2017). This includes seven key steps:

1. Manufacture an appropriate tracer to match local sediment characteristics.
2. Perform a background survey of the site.
3. Release tracer in the field.
4. Recover tracer via sampling of the seabed and water column.
5. Separate tracer from background sediment in the laboratory.
6. Determine tracer content within samples.
7. Determine particle size of recovered tracer and background sediment.

6.3.1. TRACER PREPARATION

A dual signature sediment tracer was manufactured by Partrac Ltd. for use in this study (Figure 6.3). The coated mineral tracers have two signatures (fluorescent colour and ferrimagnetic character) applied as part of the coating process. These signatures are used to identify the particle unequivocally following introduction into the environment. In this study, each natural minerogenic kernel within the tracer batch was coated using a green fluorescent dye pigment with magnetic inclusions. The dye pigment is characterized by specific excitation and emission wavelengths, which facilitates a targeted sample analysis procedure. The tracer is consistently reactive upon exposure to ultraviolet (UV–A, $\sim 400nm$) or blue light ($\sim 395nm$). The tracer grain will also adhere to any strong permanent or electro-magnet that comes into close proximity with it. This enables a simple separation of tracer within environmental (water, sediment) samples, a process which can also be exploited in situ through the use of submerged magnets (e.g., *Guymer et al.* (2010)).

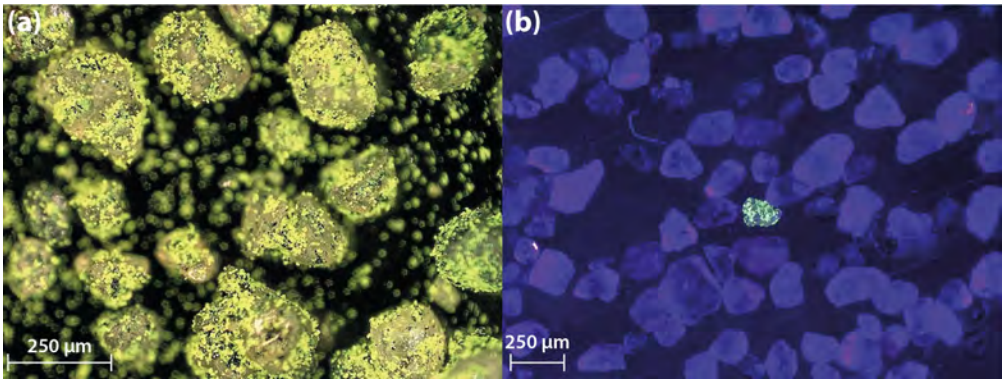

Figure 6.3: (a) Tracer sediment particles with fluorescent and ferrimagnetic coating under normal lighting. (b) Seabed sample illuminated under $395nm$ blue light. The fluorescent green tracer particles are unequivocally distinguishable from native sand grains and other types of particle in this lighting. Photos obtained using a Keyence VHX-5000 digital microscope (*Keyence Corporation*, 2014).

A key requirement of tracer studies is that the tracer sediment needs to have similar physical and hydraulic properties to the native sediment it is intended to mimic (*White*, 1998), and that the properties of the tracer do not significantly change through time (*Foster*,

2000). This ensures that the tracer will be eroded, transported, and deposited in a similar manner to native sediments. A historic sample from the nearest available point to the proposed tracer release site served as a basis for the tracer (*Rijkswaterstaat*, 1999). Typically, differences of 10-15% from the native grain size have been deemed acceptable in the peer-reviewed literature (*Black et al.*, 2007; *Robin et al.*, 2009; *Vila-Concejo et al.*, 2004).

The sediment of Ameland ebb-tidal delta is largely composed of fine to medium sand (125 to 500μm), grain size characteristics reflected by the available sample ($d_{50,native}$ = 271μm) (Figure 6.4). Sediment composition on the nearby beaches of Ameland is approximately 84% quartz, 10% feldspar, 6% heavy minerals, and has specific gravity (grain density) of $\rho_{s,native} = 2700 kg/m^3$ (*Veenstra and Winkelmolen*, 1976). An assessment of the physical and hydraulic equivalence between the manufactured sediment tracer and the native sediment on Ameland was performed. The tracer's physical characteristics ($d_{50,tracer} = 285\mu m$, $\sigma_{1,tracer} = 0.48\Phi$, $\rho_{s,tracer} = 2628 kg/m^3$) closely matched those of the available pre-study native sediment sample ($d_{50,native} = 271\mu m$) (Figure 6.4). Approximately 60% of the deployed tracer consisted of medium sand ($250 < d < 500\mu m$), 35% of fine sand ($125 < d < 250\mu m$), and <5% of very fine sand ($63 < d < 125\mu m$). Although particles < 63μm were present in the deployed tracer, they are not considered for particle size analysis in this study, given the difficulty of optically identifying, counting, and sizing any recovered particles that small, and the project's overall focus on sand transport. Based on these data, it is reasonable to conclude that the manufactured tracer will form an effective tracer for use within the study.

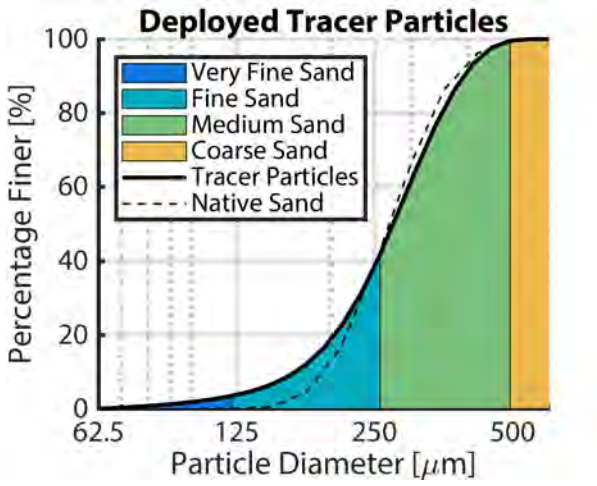

Figure 6.4: Particle size distribution of deployed tracer sediment and native seabed sediment (from available pre-study data (Rijkswaterstaat, 1999)). Deployed tracer and native sediment largely consist of fine (125-250 µm) and medium (250-500 µm) sand.

6.3.2. TRACER RELEASE

To simulate the dispersal of sand as part of an ebb-tidal delta nourishment, tracer was released below the water surface and monitored across the period from August to October 2017. Immediately prior to the release of the tracer in August 2017, a background survey of

the seabed sediment was carried out in the vicinity of the placement site to determine the presence and/or absence of particles with the same or similar characteristics as the tracer. Subsequent laboratory analysis revealed no presence of tracer-like fluorescent, magnetic particles in the bedded sediment prior to tracer deployment.

Based on the local grain size and typical local hydrodynamic conditions, it was expected that sand would be partly transported in suspension through the water column. To sample tracer particles travelling as suspended load, 8 arrays of suspended magnets were installed across the monitoring site in the hours before releasing the tracer (orange diamonds in Figure 6.1). High field, Ne-Bn 11,000 Gauss bar magnets ($30cm$ in length and $2.5cm$ in diameter) were covered in clear acrylic sheaths to facilitate the separation of recovered tracer from the magnet surface (e.g., *Guymer et al.* (2010)). These magnets were affixed to mooring lines at elevations of $1m$, $2m$, and $5m$ above the seabed.

On August 29 2017 (T+00), $2000kg$ of tracer was released at 14:52 CEST on the northwest distal lobe of Ameland ebb-tidal delta ($53.485°N$, $5.5358°W$, at the green star in Figure 6.1) over a period of 14 minutes. A PVC pipe was affixed to the side of the ship (MS Schuitengat) and tracer poured down in buckets, with water sprayed down it to ensure continuous discharge and disaggregation of the tracer while in the release zone. The release technique was also intended to, as best as possible, mimic the placement of nourishment sand from a dredge hopper via a rapid release.

Successful tracer studies require that the tracer is introduced to the target site with minimal loss and redistribution. The timing was selected to correspond with high water slack during a neap tide, which would minimize dispersal of the tracer by ambient currents before it reached the seabed. Offshore waves were small during the deployment procedure ($H_{s0} = 0.4m$, $T_{m02} = 2.8s$, $\theta = 270°$), and thus offered fairly benign conditions for tracer settling. The depth of the water at the time and location of deployment was $6.9m$, which means that 95% of the sand-sized tracer should have reached the bed within 11.2 minutes of deployment ($w_{s,d05=137\mu m} = 0.010m/s$ based on (*Soulsby*, 1997)). Current velocity measurements did not begin until 2 hours after the release (Figure 6.2), but based on the drift of the ship (MS Schuitengat) during the release period ($< 100m$, Figure 6.5a), currents were minimal.

6.3.3. TRACER RECOVERY

The sampling scheme for recovering tracer was designed to maximize the chances of retrieving tracer particles in a dynamic environment where widespread dispersal was likely. Over the next 41 days, the spatiotemporal distribution of the tracer was monitored via the collection of 209 seabed grab samples. A sampling grid was initially defined in an approximately radial pattern surrounding the proposed tracer source site, with higher sampling density towards the point of tracer release and sparser coverage further away. The assessment of tidal excursion indicates that after 5 days, tracer grains mobilized under tidal flows could be dispersed on the order of $10km$ away (Figure 6.2f). This is beyond the bounds of the area within which it is practically possible to focus sampling resources ($\sim 3km$ radius). If we assume that tracer with a d_{50} of $285\mu m$ was uniformly distributed across this area, sufficient tracer was released ($\mathcal{O}$(1010 grains)) to ensure an average of 22 grains per grab sample. This suggests that a large enough quantity of tracer was placed to ensure a meaningful prospect of recovery. Due to several practical issues (discussed in Section 5), post-release sampling was limited.

Seabed samples were obtained from the *MS Siege* using a Van Veen grab to a maximum depth of $8cm$, with an average mass of $1.7kg$ ($n = 190$). Once on deck, excess water was slowly drained from the grab sampler, and handheld blue flashlights ($\sim 395nm$) were used to assess the initial presence or absence of tracer particles. Grab samples were double-bagged in $2L$ plastic bags, labelled, and stored in plastic crates out of direct sunlight.

Suspended magnets were recovered on August 30^{th} ($T+01$) by the *MS Terschelling*, although adverse weather conditions meant that the recovery of two sets of magnets (K and L) was delayed until September 2nd ($T+04$). The $5m$ magnet at location I was lost during recovery after it became attracted to the hull of the ship. Once lifted on deck, the magnets were removed from their mooring lines and visually inspected with blue light to determine the presence or absence of tracer. The plastic sheath was then carefully removed and its contents washed through a funnel into a $1L$ sampling jar. Magnet samples typically weighed $0.1-1g$ ($n = 21$), but sample masses between $16-27g$ were obtained in three cases. All sampling equipment was carefully washed between samples to reduce the risk of cross-contamination between samples.

6.3.4. QUANTIFYING TRACER CONTENT WITHIN ENVIRONMENTAL SAMPLES

To quantify the tracer content (particle counts) within environmental samples, each sample was first processed. Each sample was dried in an oven at 180^oC until no further change in mass was observed. The material was smoothed to an approximately granular monolayer on a large black board, and then a preliminary visual inspection for tracer particles was performed using a handheld blue light ($\sim 395nm$). Samples revealing fluorescent particles were then magnetically screened to further distinguish tracers from other fluorescent matter (i.e., microplastics, which were commonly observed). A permanent, high field Ne-Bn 11,000 Gauss magnet was then passed across the sample at a distance of $2-3mm$, facilitating separation of magnetic particles, or sifted through the sample where samples were larger. This procedure was repeated, with intermittent cleaning and recovery of the particles from the surface of the magnet, until no further magnetic particles were extracted and no further fluorescent particles were found within the sample.

Once separated, the number of tracer gains were counted by eye; the error from visual counting should be below 5-10% (*Carrasco et al.*, 2013). To do this, the samples were systematically scanned with the aid of a hand tally counter. Where high tracer counts were observed, the sample was sub-sampled and the data extrapolated.

6.3.5. PARTICLE SIZE ANALYSIS

To investigate sorting behaviour of the tracer material as it dispersed in the environment, we measured the particle size distributions of the recovered tracer and native background sediment. Magnetically-separated samples containing visible tracer particles were examined using a Keyence VHX-5000 digital microscope (*Keyence Corporation*, 2014). Whilst illuminating the sample using blue light ($395nm$), high resolution photographs at $40-100\times$ magnification were captured and stitched together into a mosaic of the entire sample. The microscope's automated image processing tools were used to obtain the equivalent circular diameter of each tracer particle in the sample (similarly to *Ribeiro* (2017)). Each grain was visually checked to ensure that the particles were accurately identified. Under $100\times$ magnification, the bright green tracer particles were unequivocally distinguishable from native sand grains and other types of particle (Figure 6.3b). Where there was a discrepancy

in tracer count from the visual analysis, the count obtained via microscope prevailed. After each analysis, the sample was shaken to redistribute the position of the grains, and the procedure repeated to reduce potential biases in the image analysis.

The particle size distributions of native non-tracer sediment separated from the tracer samples were measured using a Malvern Mastersizer 3000 (*Malvern Instruments Limited*, 2017). At least 4 measurements were made per sample and then averaged together to provide a representative distribution.

6.4. RESULTS

Tracer particles were recovered from 45 of 190 seabed grab samples (24%) and 23 of 23 recovered magnetic samples (100%), despite the occurrence of conditions capable of mobilizing 99% of the deployed particles (Figure 6.10). Although hydrodynamic measurements indicate an eastward tidal residual flow (Figure 6.2f), the spatial pattern of the recovered tracer indicates that transport dispersed the tracer in all directions relative to the release site, likely due to a combination of tidally driven transport and wave action.

Tracer material was recovered from the grab samples taken in the first week after deployment, up to $1325m$ away from the source (Figure 6.5). Although the majority of samples are clustered within $500m$ of the release site, there is no distinct trend in their spatial distribution. Most of these samples were recovered between August 30^{th} ($T+01$) and September 4th ($T+06$), but some tracer was even recovered from the tracer source on October 9th ($T+41$), after two large storms had passed. In total, 14 of the tracer samples contained a single tracer particle, 13 had $2-10$ particles, 14 had $11-100$ particles, 14 had $101-1000$ particles, and 11 samples contained more than 1000 particles. All but one of the latter were obtained via suspended magnets.

The tracer particles recovered from the seabed (mean $d_{50} = 212.8\mu m$, $\sigma_{d50} = 74.3\mu m$, $\sigma_1 = 0.48\Phi$) were finer and better sorted on average than the original tracer ($d_{50} = 274.4\mu m$, $\sigma_1 = 0.34\Phi$) (Figure 6.6). The samples recovered by the magnets (mean $d_{50} = 81.9\mu m$, $\sigma_{d50} = 6.0\mu m$) are significantly finer than both the original tracer sample and the samples recovered from the bed (Figure 6.6).

On average, tracer particles are largest closer to the bed ($d_{50} = 83.9\mu m$ at $1m$ above the bed), decreasing slightly with elevation ($d_{50} = 80.6\mu m$ at $2m$ above the bed) (Figure 6.7). The particle size is negligibly different at $5m$ above the bed ($d_{50} = 81.0\mu m$). All suspended samples are well sorted ($\sigma_1 < 0.5\Phi$) based on Folk & Ward Logarithmic Graphical measures (*Blott and Pye*, 2001), where increased sorting corresponds to reduced spread around the mean particle size. Sorting is poorest at 1 m above the bed ($\sigma_1 = 0.41$), but improves slightly at $2m$ and $5m$ above the bed ($\sigma_1 = 0.38\Phi$ and $\sigma_1 = 0.39\Phi$, respectively).

Although there is a marked difference between the original tracer and the material recovered in the water column, the particle size distributions of suspended tracer samples do not vary substantially with elevation from the bed. This is consistent with *Beamsley et al.* (2001), who observed that although median particle size decreases with height above the bed, the modal peak of suspended sand grain size distributions stays relatively consistent. They attribute upward fining to an inverse relationship between concentration profile gradient and grain size, with finer particles being more dominant at higher elevations.

The particle size distribution of recovered tracer particles can also be considered spatially (Figure 6.8). Among samples with more than one grain (it is not meaningful to compute d50 and sorting from a single particle), there is a weak negative correlation between

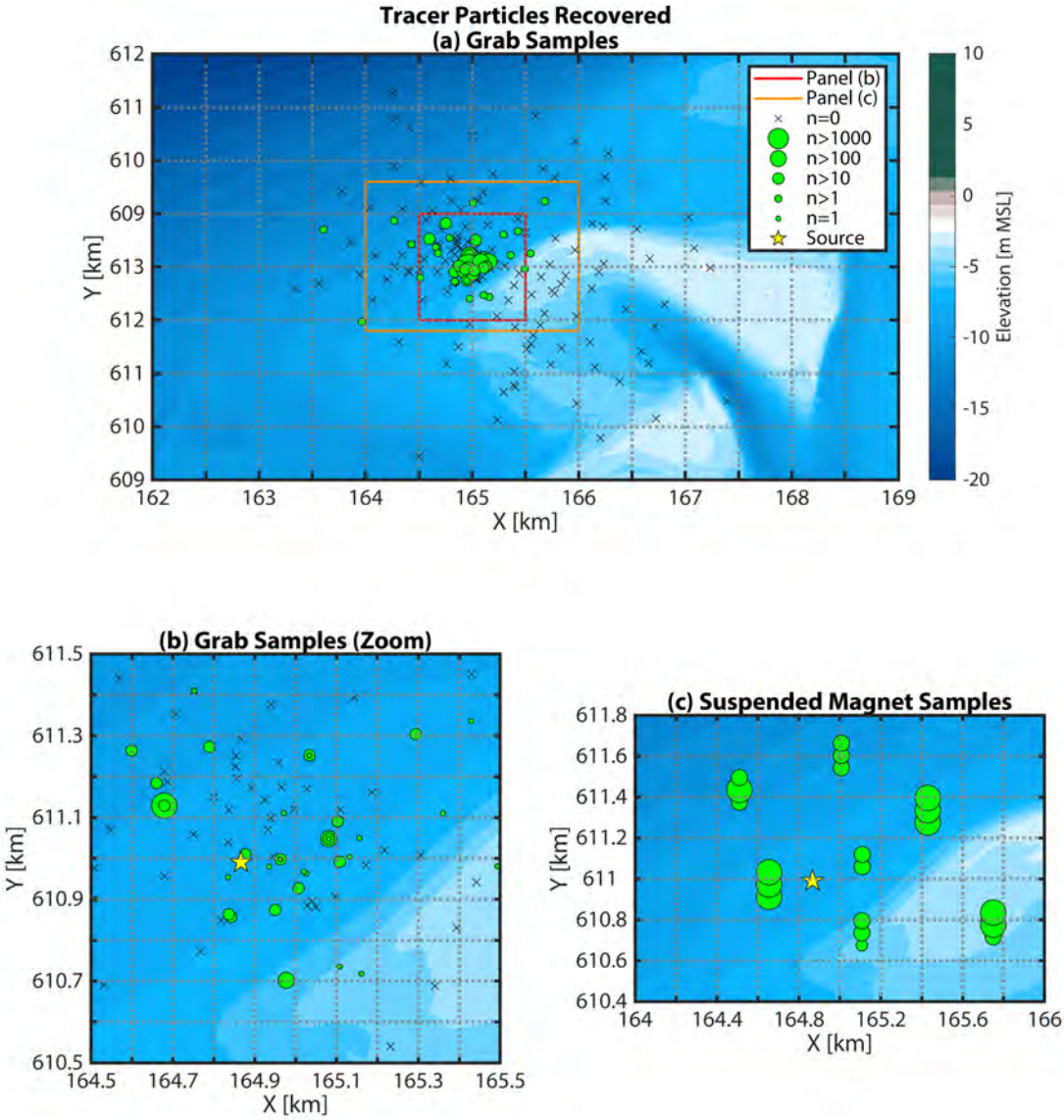

Figure 6.5: Spatial distribution of tracer recovered in the first 41 days after deployment, indicating the number of tracer grains recovered from each sample. (a) Tracer samples obtained via seabed grab samples. (b) Tracer samples obtained via seabed grab samples, zoomed in on central area with denser sampling. (c) Samples obtained using suspended magnets. The tracer release location is indicated by a yellow star. X-symbols indicate samples in which no tracer particles were found.

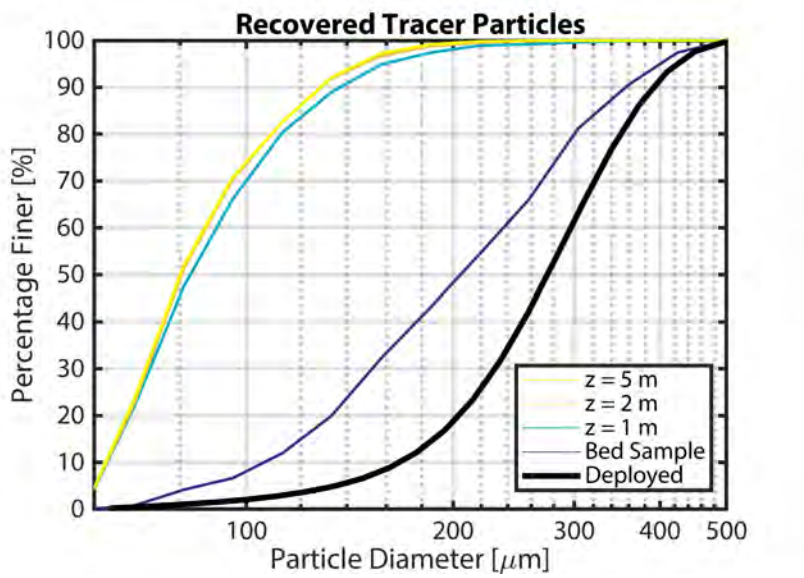

Figure 6.6: Mean particle size distributions of tracer recovered from the seabed and suspended magnets at z=1, 2, 5 m above the seabed. Magnetically-recovered tracers were significantly finer than those acquired via grab sample from the seabed.

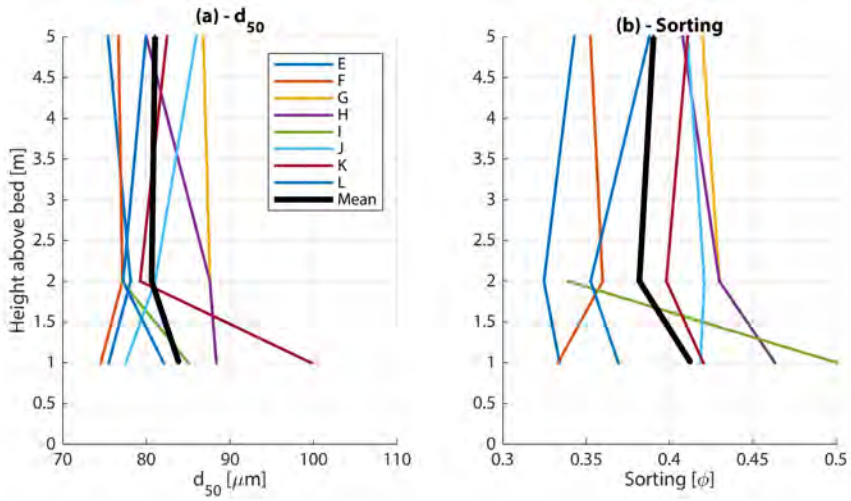

Figure 6.7: Particle size statistics of tracer recovered from the seabed and suspended magnets at $z = 1, 2, 5m$. (a) Median particle diameter (d_{50}); (b) Sorting coefficient. Thin lines correspond to individual magnet locations, and thick black lines are averaged across all samples.

median grain size (R^2 = 0.224) and increasing distance from the source (Figure 6.9). Furthermore, the mean d_{50} of the magnet samples is <100 µm, with all seabed samples consistently coarser. The envelope of grain size variability shrinks with distance from the source: the variation in d_{50} decreases further away. A very weak negative correlation is observed between sediment sorting coefficients of multi-grain samples and distance from the source (R^2 = 0.082), which implies that the tracer become slightly better sorted with distance. These patterns are consistent with the frequently-observed trend of fining and better sorting along transport pathways in complex marine environments (*Le Roux and Rojas*, 2007; *Poizot et al.*, 2008).

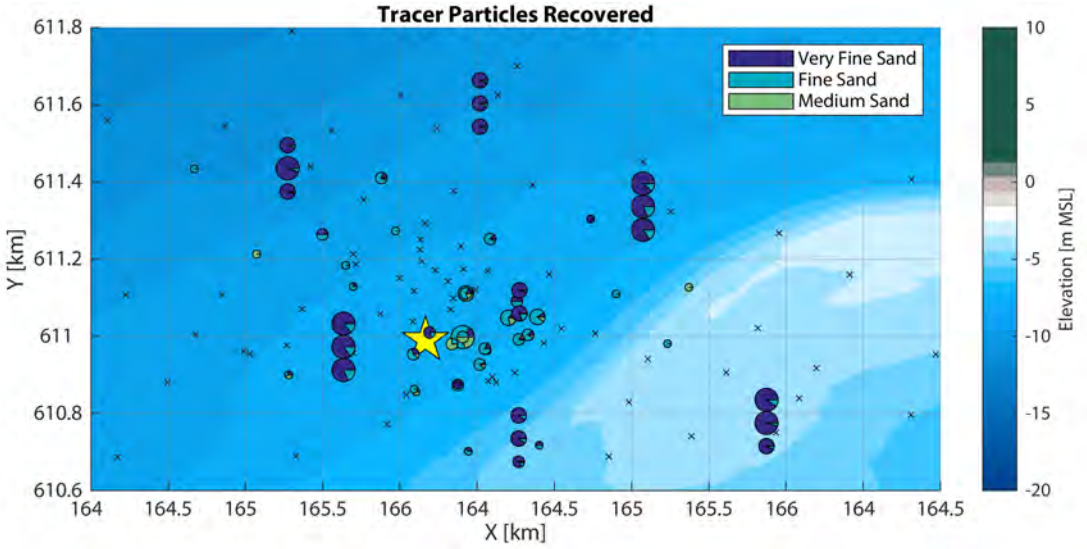

Figure 6.8: Spatial distribution of tracer with pie charts indicating the relative fraction of a particular sediment class. The yellow star denotes the tracer source location. The size of the pie chart is proportional to the number of particles found in a given sample. X-symbols denote samples in which no tracer particles were found.

To better visualize the influence of the hydrodynamic conditions on the potential transport modes of tracer particles and explain the observed differential transport, we computed the inverse Rouse number ($\kappa u_* / w_s$) of four grain size classes using the method of *Soulsby* (1997) (Figure 6.10). The medium sand ($250-500\mu m$) comprising most of the tracer travels mainly as bed load, only moving into suspension during the two largest storms (September 13^{th} & October 3^{rd}). This could explain its absence on the suspended magnets, which were all collected by September 2^{nd}. Fine sand ($125-250\mu m$) travels in suspension during minor storms and also at spring tide, whereas very fine sand grains ($63-125\mu m$) are nearly always travelling as suspended load.

These estimates are consistent with existing numerical model simulations of Ameland Inlet (*Reniers et al.*, 2019). Modelled daily averaged sediment transport of 200 µm sand near the tracer deployment site is principally tidal suspended transport in calm conditions, whereas suspended transport due to wave skewness dominates during storms. *Huisman et al.* (2016) found that grain size-selective sediment transport at a sand nourishment on the Dutch coast was most prevalent during mild and moderate conditions when some but

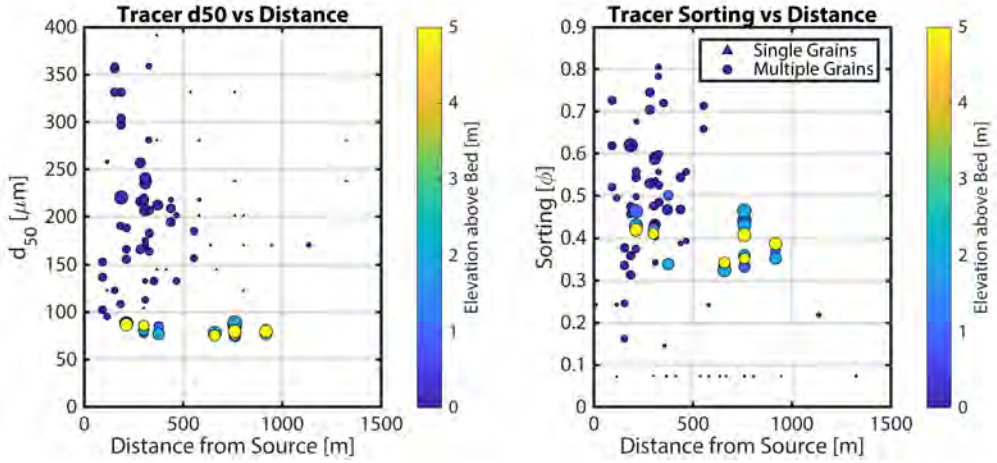

Figure 6.9: Comparison showing distance from the tracer source vs (a) d50 and (b) sorting of recovered tracer. Triangular markers indicate single grains, whereas circles indicate samples with multiple grains. The size of the symbol is proportional to the number of particles found in a given sample, and the colour of the markers indicates sample elevation above the bed.

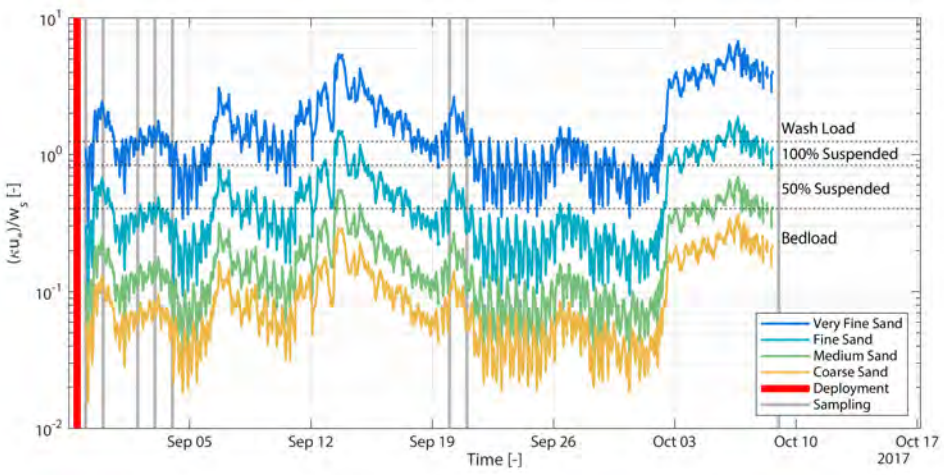

Figure 6.10: Inverse Rouse number ($\kappa u_* / w_s$) and transport mode for each sediment class. Calculated using the method of *Soulsby* (1997) from wave and near-bed velocity measurements taken by a downward-facing ADCP-HR near the tracer source (mounted $0.5m$ above the seabed). Tracer sampling dates are indicated by grey bars.

not all of the bed material is mobilized. Finer sand classes will thus be entrained more frequently into the water column (Figure 6.10). In more intense conditions, sorting behavior is still present but to a lesser degree, since all size classes are mobilized, including coarser particles. However, it is mild and moderate conditions that prevail during the first 6 days of tracer sampling

We can quantify the potential impact of a nourishment on the native grain size distribution by analogy using recovered tracers. We compared the grain size characteristics of each tracer sample with the native sediment that it was recovered in. The native background sediment samples containing tracer are overwhelmingly homogeneous, well-sorted fine (F) sand, with a mean d_{50} of 200.2μm (σ_{d50} = 21.7μm), and mean sorting coefficient of 0.50Φ (Figure 6.11). Conversely, the recovered tracer shows a wide variation in d_{50} from 100 to 400μm (mean d_{50} of 212.8μm, σ_{d50} = 74.3μm), and is on average 12.6μm coarser than the native sediment in which it was recovered. The recovered tracer is negligibly better-sorted on average, but shows more variation in sorting than the native sediment. Comparing the particle size analysis of recovered tracer and the native sediment in which it was found reveals clear signs of grain size-selective transport.

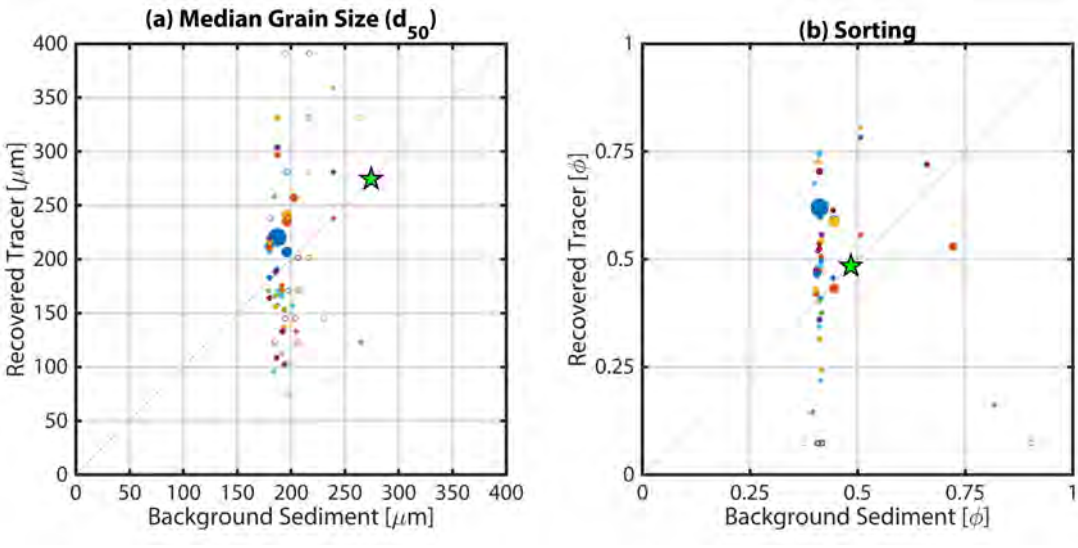

Figure 6.11: Particle size statistics of native background sediment vs recovered tracer. (a) Median particle size (d_{50}) and (c) sorting coefficient (Φ). Hollow circles represent samples with only single tracer grains, and solid circles represent samples with multiple tracer grains. The size of the circles is proportional to the number of tracer grains found in the sample. The green star indicates the properties of the tracer that was initially released.

6.5. DISCUSSION

We recovered tracer sediment on a highly dynamic ebb-tidal delta as part of a study to understand the potential spreading of nourishments there. The high recovery rates of tracer on an energetic subtidal ebb-tidal delta in spite of sampling limitations are a proof of concept for using tracers to monitor sediment dispersal in such environments. In particular, the suspended magnets were revealed to be an effective means of capturing tracer particles suspended throughout the water column. Furthermore, microscopy analysis enabled the

determination of different grain sizes within the collected samples, facilitating the assessment of differential transport (per grain size) following tracer release.

Grain size influences both the persistence and ecological impact of sand nourishments. Nourished sand will tend to disperse more quickly if its grain size is smaller than native sediment, which thus determines how long it will persist at its placement site (*Dean*, 2002). As such, grain size of placed material relative to native sediment is often a key parameter in nourishment design (*Hanson et al.*, 2002). Grain size also influences benthic habitat (*McLachlan*, 1996), and the recovery of benthic ecosystems after a nourishment can be impeded if nourished sand grain characteristics do not closely match the native sediment (*Bishop et al.*, 2006; *Defeo et al.*, 2009; *Peterson et al.*, 2014). Tracer particle size analysis like that carried out in this study is thus a useful technique for understanding the grain size-specific evolution of nourishments. By releasing tracers in conjunction with nourishments (e.g., *Smith et al.* (2007)) and then tracking tracer particle size, coastal managers can improve the efficacy of nourishments and monitor potentially negative ecological impacts.

Our study's findings are summarized in a conceptual diagram (Figure 6.12). Finer grains become preferentially resuspended and transported further than coarser grains. The coarser grains are mobilized less frequently and travel more as bedload, which leaves them more susceptible to burial (e.g., Figure 6.2d) or integration into bedforms. Material travelling in suspension travels more quickly than material moving as bedload, so finer tracer particles are also found further from the source. Superdiffusive behaviour due to correlated grain motion and grain size heterogeneity may explain the solitary coarser grains of sand found farthest away from the source (*Martin et al.*, 2012).

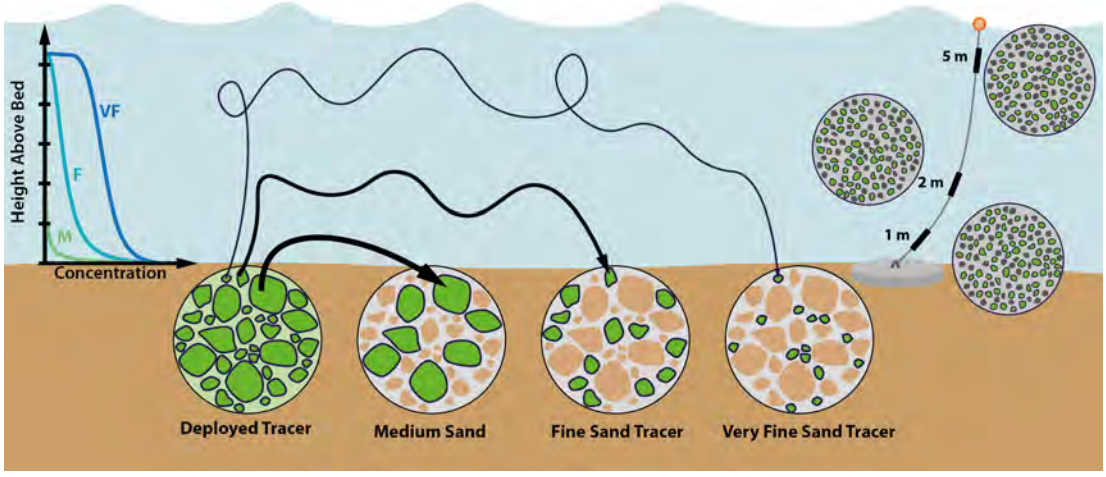

Figure 6.12: Conceptual diagram indicating dispersal of tracer on the seabed and in the water column. Finer grains are preferentially resuspended and transported further than coarser grains, which travel more often as bedload and are more susceptible to burial. Suspended sand grains observed on the magnets were overwhelmingly very fine, with little difference as a function of height above the bed.

Two days after the tracer release ($T+02$), the bed accretes by approximately $8.5cm$ in 7 hours, mostly during flood tide following the peak of a small storm (Figure 6.2d). It is therefore possible that tracer particles deposited on the seabed within this area could have been buried beyond the reach of the Van Veen grab sampler used to extract the sediment (approximately $8cm$). This is consistent with the historical bathymetry analysis of *Elias et al.* (2019) and *Elias et al.* (2022), which shows this region of the ebb-tidal shoal to be prograding and hence depositional. Sampling via deeper cores may yield greater insight into the burial of tracers and sediment balance in future studies.

The tracer dispersal pattern in Figure 6.8 does not appear to coincide with the eastward direction of net tidal excursion (Figure 6.2f). This may be explained by the difference between residual (net) transport and gross transport. If the tidal flow is bi-directional, the residual is a small difference between the much larger gross flood and ebb transports. In open water, sediment transport vectors form an open ellipse over the course of a tidal cycle, just like the flow velocity vectors (Figure 6.2f, inset). Where the tracer can be found back is not determined by the residual transport field, but by the gross transport field, which is highly variable in direction during a tidal cycle. This may be evidence of chaotic stirring, which is known to occur at tidal inlets similar to Ameland (*Ridderinkhof and Zimmerman*, 1992). Ridderinkhof & Zimmerman showed that after just a few tidal cycles, particles can be dispersed in highly spatially heterogeneous patterns that do not necessarily coincide with the direction of net transport. This hypothesis could be tested via Lagrangian sediment particle modelling (e.g., *Soulsby et al.* (2011), Chapter 8).

One of the key findings of this study was the effectiveness of magnets mounted on mooring lines through the water column at capturing suspended tracer particles. The magnets in this study typically recovered several orders of magnitude more tracer particles than grab samples taken from the seabed. Tracer particles found in grab samples were deposited on the seabed, and hence give an indication of sediment accumulation there. However, tracer recovered by the suspended magnets is indicative of grains that are actively moving as suspended load. Very fine grains of tracer ($63-125\mu m$) made up a small fraction of the tracer particles recovered in the bed but were abundant on the suspended magnets. This supports the expected theory that sorting due to differential suspended transport by grain size is a key process on the ebb tidal delta.

Although tracer studies are a well-established tool in the arsenal of coastal scientists and engineers, challenges associated with their deployment have typically limited their application to more well-constrained settings like alongshore uniform beaches. Previous applications to tidal inlets and ebb-tidal deltas have tended to focus more on intertidal areas which could be more easily sampled, whereas this study investigates a fully subtidal site. In this study we also successfully employ innovative methods for both recovery (e.g., suspended magnets) and analysis (e.g., particle size analysis of recovered tracer via microscopy) in a very dynamic setting, demonstrating that these techniques can be used in such environments. However, the purpose and method of application must be carefully considered in study planning. These advances expand the range of environments in which tracer studies can be conducted, but also increase the amount of data that can be gained from such a study. Since tracer studies can be labour-intensive, time-consuming, and challenging to execute (*Ciavola and Grottoli*, 2017; *White*, 1998), it is important to find new ways to add value to them, both in terms of practicalities but also in terms of expanding their scientific worth. The following section provides lessons learned from the study, which we hope will be

useful for future researchers/practitioners interested in utilizing sediment tracers in highly dynamic environments:

- Dual tracer signatures (fluorescence and ferrimagnetism) were very beneficial, increasing the ease of tracer recovery in the field and analysis in the laboratory. In particular the suspended magnets placed on mooring lines were both an effective means of recovering tracer and potentially offer a route to sampling the suspended sediment load in deeper water or environments where it is challenging to sample frequently, but also an afforded an "opportunistic" measurement: the magnets were place on marker buoys of pressure sensors mounted on the seabed as part of a different experiment (*de Wit et al.*, 2019; *Reniers et al.*, 2019).
- Magnets were highly effective at recovering tracer, with large quantities of tracer particles (> 1000) found on all of the recovered magnets. In addition, magnetic non-tracer particles were found within the seabed grab samples and especially attached to the suspended magnets. The high recovery rates of tracer from the magnets indicates that some of the tracer particles travelled in suspension, for at least part of the measurement period, which is consistent with hydrodynamic conditions (Figure 6.10). It is unlikely that the sediment captured by the magnets is from the initial tracer release, given that deployment took place at high water slack, and that deposition of all sand-sized tracer would have occurred within half an hour. This is especially true for magnets located east (upstream) of the ebb currents that followed release (i.e., Figure 6.2f). Tracer recovered on the magnets is thus likely indicative of resuspended sand.
- The use of a digital microscope expanded our tracer analysis capabilities significantly beyond what is possible with only the naked eye. The microscope allows for unequivocal identification of tracer particles, automated particle enumeration, and estimation of tracer particle size distributions. This reduces the likelihood of human error in tracer particle characterization and enables topics such as sediment sorting to be investigated. *Robin et al.* (2009) assumed that the grain size distribution of the tracer is identical throughout the entire plume. However, the spatial variations in particle size relative to the original tracer particles observed in this study challenge this assumption. Future tracer studies should thus consider microscopy analysis to investigate grain size characteristics.
- The primary study limitation was our inability to perform frequent, spatially repeated sampling due to challenging sea conditions and practical issues such as vessel availability. Sampling resources prioritized maximum potential recovery of tracer within the available ship time, rather than keeping a regular sample grid in space and time. Further possibilities for tracer sampling were eliminated by the placement of a $5Mm^3$ sand nourishment directly on top of the tracer release site beginning in March 2018. Collectively, these conditions led to a disparate sampling campaign which prevented the meaningful derivation of general spatial statistics (e.g. tracer plume centroid movement in time and space), and application of the spatial integration method (e.g., *Robin et al.* (2009); *Vila-Concejo et al.* (2004); *White* (1998)) to account for the dispersed tracer mass. This kind of analysis is achievable on a beach face, for example, but on a highly dynamic ebb-tidal delta spanning several kilometers in size, the extrapolation of particle counts may be dubious.

- Tracer studies with similar logistical constraints should prioritize consistent sampling at fewer sites over attaining wider spatial coverage with limited repetition in time. It is essential to clearly identify the purpose of deploying sediment tracers, so that a considered, targeted and achievable, sampling plan can be developed and implemented. When working in an open system where significant dispersion is likely, it is necessary to focus sampling resources on tracer recovery and balance that against the goals of the project. In highly dynamic environments, the use of tracers to monitor sediment transport pathways over extended temporal periods is not advised. Careful consideration of site data prior to tracer deployment to determine the best positions for release and sampling is essential.
- The sample selected from *Rijkswaterstaat* (1999) to serve as a model for the tracer particle size distribution was coarser (d_{50} = 270.7μm) than most of the native sediment samples obtained during the tracer study (mean d_{50} = 200.2μm) (Figure 6.11). Even though the tracer closely matched the target sample, that sample was not very representative of the present-day conditions on that part of the ebb-tidal delta, likely due to the shifting position of channels and shoals (e.g., *Elias et al.* (2019)). This shows the importance of using recent reference sediment samples for tracer studies in such dynamic areas. However, this problem was circumvented by performing optical grain size analysis on the recovered tracer, which permitted analysis of tracer particles that were closer in size to the native sediment. In addition, the relative absence of recovered medium-sized tracer compared with the amount that was initially placed strengthens the case for differential transport as a key mechanism.

This study also provides guidance for carrying out nourishments on ebb-tidal deltas in the future. The behaviour observed in this field experiment suggests that fine nourishment sand applied to Ameland ebb-tidal delta will also be highly dispersive, which may be important for estimating the lifetime and ecological impact of a nourishment. Tracer studies do not account for indirect effects of the nourishment on sediment transport (e.g., due to modification of local flow and transport fields), but they do enable unequivocal identification of sediment from a particular source. Thus, a useful application of tracers for nourishment design and monitoring would be to combine the tracers with the nourished sediment as it was placed, similarly to *Smith et al.* (2007). In this way, the performance of the nourishment could be monitored using conventional bathymetric surveys, but it would also be possible to differentiate nourished sediment from native sediment using tracer as a proxy. If the goal of a tracer study is to establish whether particles from a given source (e.g., nourishment) reach a given location (e.g., an ecologically-sensitive area), then the target site could be surrounded by suspended magnets as a means of intercepting tracer. This would give an indication of the quantity and characteristics of nourished sediment reaching the target site.

The results obtained in this study also fill a need for high-quality data to further validate models of grain size-specific transport of nourished sediment (*de Schipper et al.*, 2021), particularly Lagrangian models (*MacDonald and Davies* (2007); *Soulsby et al.* (2011), Chapter 8). These models can be used to predict the pathways, receptors, and system-wide connectivity of nourished sediment (Chapter 7), providing coastal researchers and managers with additional tools for analysis and design.

6.6. CONCLUSIONS

In this study, we presented the results of a sediment tracer study carried out on the energetic ebb-tidal delta of Ameland Inlet in the Netherlands. We aimed to answer the questions: "*Is it possible to recover tracer particles in such dynamic environments?*"; "*What are efficient and effective techniques to collect the particles?*"; and finally: "*What can we conclude from a particle tracking experiment that we cannot conclude from other monitoring techniques?*"

The use of a dual-signature tracer (fluorescent and magnetic) aided both recovery in the field and analysis in the laboratory. Despite the very energetic and open environment, we found tracer particles in 45 of 190 grab samples (24%) and on 23 of 23 recovered suspended magnets (100%). Generally, only small numbers of particles ($\mathcal{O}(1-100)$) were found using grab samples. The suspended magnets provided a much more effective tracer recovery technique than the seabed grab samples: $\mathcal{O}(1000-10000)$ particles were retrieved in this manner. The higher efficiency of suspended magnets boosts the chances of tracer recovery and could lead to cost savings by requiring less tracer sediment to be deployed or fewer seabed grab samples. Furthermore, the application of suspended magnets for recovering tracer opens new possibilities for measuring sediment pathways, as it is an indication of the sediment in suspended transport, instead of an indication of sediment deposition (as measured by grab sampling). Analysis of tracer particle size via digital microscopy enabled additional data to be extracted from the recovered tracer than merely counting the amount observed within the sample.

The methodology in this study expands the range of environments in which tracer studies can be completed by demonstrating successful tracer recovery in a setting characterized by dramatic morphodynamic changes and convoluted sediment transport pathways. In doing so, we increase the potential knowledge yield that can be gained from such field experiments. We also offer a series of lessons learned and recommendations for the use of sediment tracers in highly dynamic environments to support future research and coastal management practice. Particle tracking is the only technique that can directly measure the provenance of sediment, but its full potential is seldom realized due to common challenges in recovery and analysis. The techniques explored here (e.g., magnetic tracer retrieval and separation, microscopic analysis of tracer) provide additional means of generating value from tracer studies. These approaches increase our ability to tap into the unique perspective on sediment transport that tracers offer.

ACKNOWLEDGEMENTS

This work is part of the research programme 'Collaboration Program Water' with project number 14489 (SEAWAD), which is (partly) financed by NWO Domain Applied and Engineering Sciences. Special thanks to the Dutch Ministry of Infrastructure and Water Management (Rijkswaterstaat and Rijksrederij) for organizing the field campaign and for their ongoing support as part of the Kustgenese2.0 project. Thanks also to the crew of the *MS Schuitengat*, *MS Siege*, and *MS Terschelling* for their assistance with the fieldwork. Thank you to Claire Chassagne, Mohammed Jafar, and Saskia Huisman for their help with the laboratory equipment. Data from the 2017 Kustgenese2.0/SEAWAD field measurement campaign are available at the 4TU Centre for Research Data:
https://doi.org/10.4121/collection:seawad, and tracer data are available here:
https://doi.org/10.4121/15057378

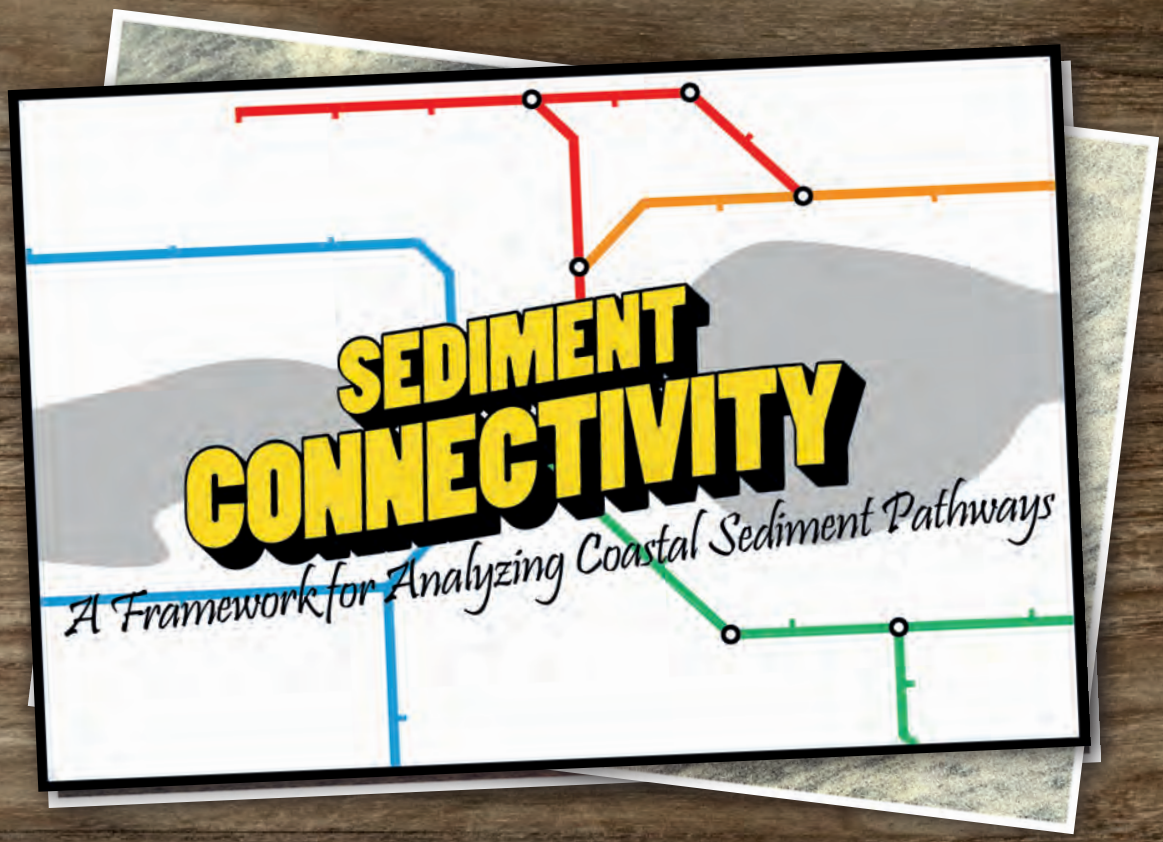
SEDIMENT
CONNECTIVITY
A Framework for Analyzing Coastal Sediment Pathways

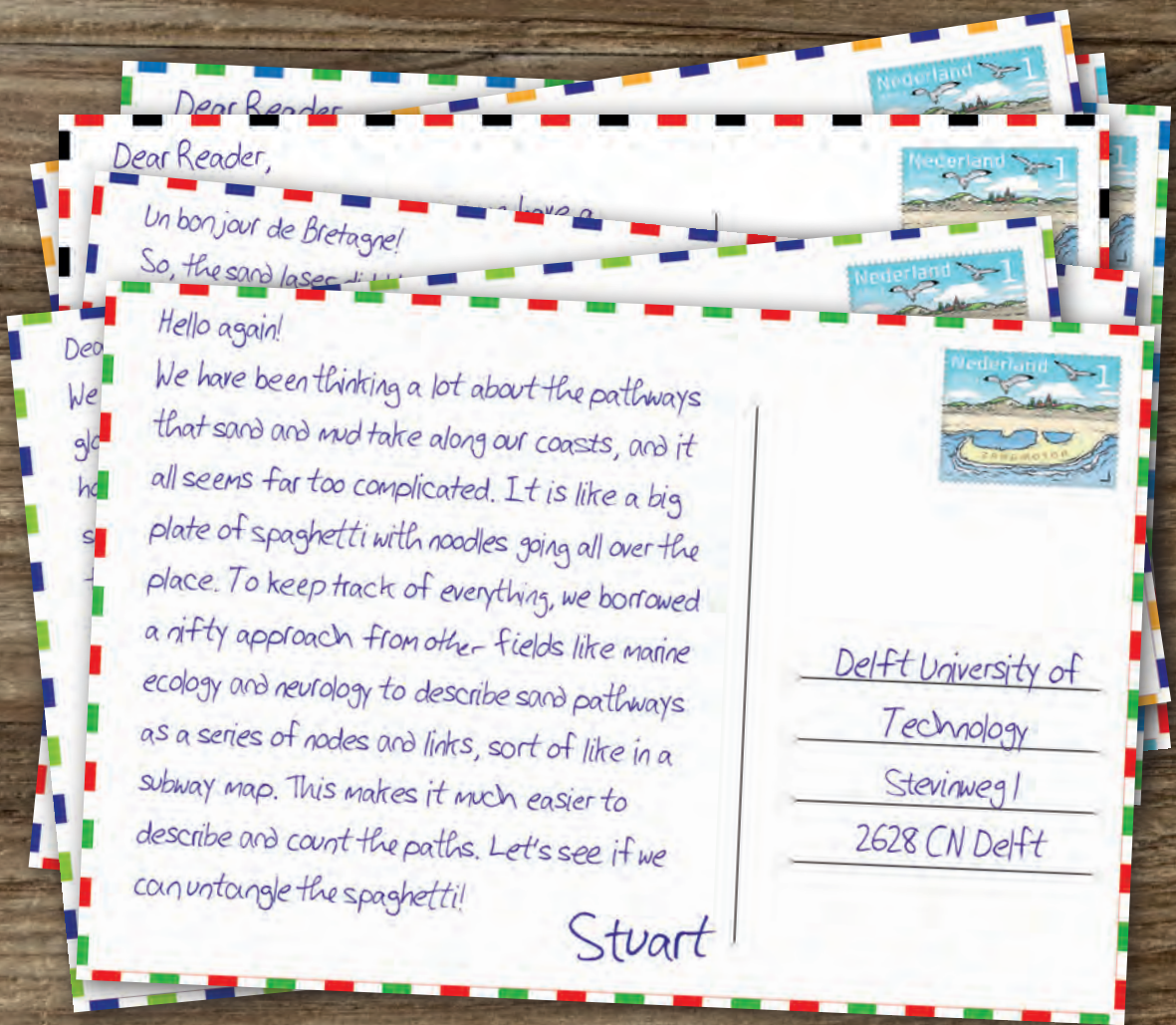
Dear Reader,
Un bonjour de Bretagne!
Hello again!
We have been thinking a lot about the pathways that sand and mud take along our coasts, and it all seems far too complicated. It is like a big plate of spaghetti with noodles going all over the place. To keep track of everything, we borrowed a nifty approach from other fields like marine ecology and neurology to describe sand pathways as a series of nodes and links, sort of like in a subway map. This makes it much easier to describe and count the paths. Let's see if we can untangle the spaghetti!
Stuart
Delft University of Technology
Stevinweg 1
2628 CN Delft
Nederland

7

SEDIMENT CONNECTIVITY: A FRAMEWORK FOR ANALYZING COASTAL SEDIMENT TRANSPORT PATHWAYS

KEY POINTS:

- Connectivity schematizes sediment transport pathways as a directed graph (series of nodes & links)
- Novel application of graph theory and network analysis to characterize complex coastal systems
- Example of Ameland Inlet demonstrates usefulness of connectivity in real-world applications

This chapter has been published in *Journal of Geophysical Research: Earth Surface*:

Pearson, S.G., van Prooijen, B.C., Elias, E.P., Vitousek, S., Wang, Z.B. (2020). Sediment Connectivity: A Framework for Analyzing Coastal Sediment Transport Pathways. *Journal of Geophysical Research: Earth Surface*,125(10), e2020JF005595. [Link]

IN the previous chapters, we considered three types of measurements: (1) large-scale bathymetric measurements spanning decades ($\mathcal{O}(100m-10km)$), (2) point measurements of hydrodynamics and suspended sediment over a period of several weeks, and (3) the dispersal of a Lagrangian sediment tracer across the ebb-tidal delta ($\mathcal{O}(100m-1km)$). To paint a more complete picture of sediment transport pathways on ebb-tidal deltas, we need to integrate these disparate sources in a common framework. In this chapter, we aim to systematically manage and quantitatively interpret complex datasets of sediment pathways. These pathways can be challenging to analyze and predict using existing approaches, so we turn to the concept of connectivity. Connectivity represents the pathways that sediment takes as a series of nodes and links, much like in a subway or metro map. This approach is well-used in other scientific fields, but in this study we apply these techniques to a new research field: coastal sediment dynamics. To demonstrate the sediment connectivity approach, we use it to map sediment pathways at a coastal site in the Netherlands. The statistics computed using connectivity let us quantify and visualize these sediment pathways, revealing new insights into the coastal system at multiple scales. We can also use this approach to address practical engineering questions, such as where to place sand nourishments for coastal protection.

ABSTRACT

Connectivity provides a framework for analyzing coastal sediment transport pathways, building on conceptual advances in graph theory from other scientific disciplines. Connectivity schematizes sediment pathways as a directed graph (i.e., a set of nodes and links). This study presents a novel application of graph theory and connectivity metrics like modularity and centrality to coastal sediment dynamics, exemplified here using Ameland Inlet in the Netherlands. We divide the study site into geomorphic cells (i.e., nodes), and then quantify sediment transport between these cells (i.e., links) using a numerical model. The system of cells and fluxes between them are then schematized in a network described by an adjacency matrix. Network metrics like link density, asymmetry, and modularity quantify system-wide connectivity. The degree, strength, and centrality of individual nodes identify key locations and pathways throughout the system. For instance, these metrics indicate that under strictly tidal forcing, sand originating near shore predominantly bypasses Ameland Inlet via the inlet channels, whereas sand on the deeper foreshore mainly bypasses the inlet via the outer delta shoals. Connectivity analysis can also inform practical management decisions about where to place sand nourishments, the fate of nourishment sand, or about how to monitor locations vulnerable to perturbations. There are still open challenges associated with quantifying connectivity at varying space and time scales, and the development of connectivity metrics specific to coastal systems. Nonetheless, connectivity provides a promising technique for predicting the response of our coasts to climate change and the human adaptations it provokes.

7.1. INTRODUCTION

7.1.1. CHALLENGES POSED BY COASTAL SEDIMENT TRANSPORT

COASTS and estuaries are complex geomorphic systems formed by connected fluxes of water and sediment. Tides, wind, and waves steer the development of coastal systems, and non-linear transport processes shape them. Tight feedback loops between morphology and hydrodynamic processes lead to dynamic landscapes in a wide range of coastal environments, from sandy beaches (*Masselink et al.*, 2006) to coral atolls (*Barry et al.*, 2007) or mudflats (*Friedrichs*, 2012). Sediment transport pathways become particularly dynamic and convoluted in the vicinity of tidal inlets or estuaries (*Oertel*, 1972; *Hayes*, 1980; *Sha*, 1989c; *Kana et al.*, 1999b; *Elias et al.*, 2006; *Barnard et al.*, 2013a), as indicated conceptually in Figure 7.1. Sediment may be exchanged between the lagoon or estuary and the adjacent coastlines. For example, it may bypass the inlet via bar migration on an outer (ebb-tidal) delta (*FitzGerald*, 1983; *Sexton and Hayes*, 1983; *Gaudiano and Kana*, 2001; *Elias et al.*, 2019) or recirculate at the mouth (*Smith and FitzGerald*, 1994; *Hicks et al.*, 1999; *Son et al.*, 2011; *Herrling and Winter*, 2018). The net import or export of sediment through the inlet system and changes to the ebb-tidal delta can have a profound influence on the morphological evolution of the adjacent coastline (*FitzGerald*, 1984; *Elias et al.*, 2006; *Ranasinghe et al.*, 2013; *Hansen et al.*, 2013; *Warrick et al.*, 2019).

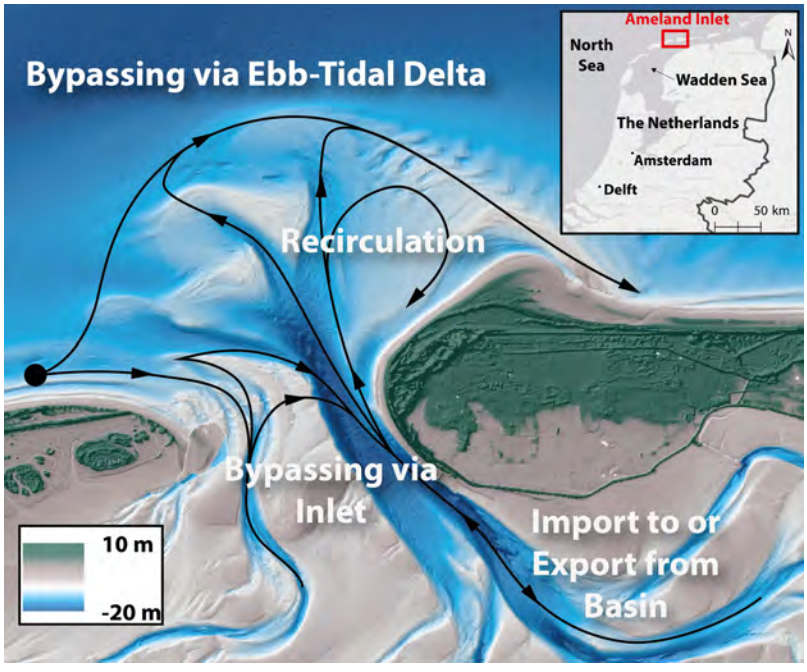

Figure 7.1: Conceptual diagram identifying key questions about sediment transport pathways, using Ameland Inlet as an example. 1. Via which pathways (black arrows) does sediment from a given origin (black dot) bypass the inlet? 2. Is there a net import or export of sediment to/from the basin? 3. Are there strong recirculations or opposing gross transports, or are transports largely unidirectional? 4. Where is the optimal location for a sand nourishment? 5. How do these patterns change with grain size? 6. Can the domain be grouped into distinct sediment-sharing cells? The inset map indicates the location of Ameland within the Netherlands. Bathymetry (circa 2017) and topography source: Rijkswaterstaat.

Effective management of coastal sediment is vital for sustainable protection against flooding and erosion (*Mulder et al.*, 2011; *Hanley et al.*, 2014; *Van Wesenbeeck et al.*, 2014). In order to reliably predict coastal evolution, improved understanding of sediment transport pathways is necessary at multiple scales (*Ruggiero et al.*, 2016; *Vitousek et al.*, 2017a). Interruptions to the flow of sediment may degrade coastal systems, causing socioeconomic and ecological damage (*Roelvink*, 2015). Furthermore, human interventions such as nourishments, protective structures, or basin closures can also affect coastal sediment transport pathways by interrupting existing paths, or by creating new ones (*Davis and Barnard*, 2000; *Fontolan et al.*, 2007; *Elias et al.*, 2012a; *Eelkema et al.*, 2013; *Luijendijk et al.*, 2017; *Wang et al.*, 2015, 2018). Understanding how human interventions change sediment pathways is important for gauging the effectiveness of the intervention, predicting potential consequences of that intervention, or assessing its environmental impact (*Hendriks et al.*, 2020).

Where does the sediment from a given location go to? Furthermore, where does the sediment at that same location come from? These two questions are fundamental to sediment transport. Yet rarely, if ever, are answers to these questions available, owing to the complexity of coastal sediment transport dynamics. Numerical models begin to answer these questions: at a given location, sediment goes to and comes from neighbouring grid cells over a single timestep. However, sediment transport pathways over large spatiotemporal scales are observed. Hence, the framework of sediment connectivity is critical to bridging the gap between geomorphic coupling among neighbouring regions (e.g., *Harvey* (2001)) and system-wide connections. In this study we show that connectivity is a useful framework for analyzing sediment transport pathways in coastal environments and for addressing challenges in sediment management.

7

7.1.2. CONNECTIVITY: A TRANSFORMATIVE CONCEPT

In its most general sense, connectivity is a framework for representing the connections and flows between the different parts of a system. It has been widely adopted in other fields such as neurology (*Honey et al.*, 2007; *Rubinov and Sporns*, 2010), biology (*Maslov and Sneppen*, 2002), epidemiology (*Read et al.*, 2008), computer science (*Bassett et al.*, 2010)), transportation (*Derrible and Kennedy*, 2009; *Sperry et al.*, 2017), ecology (*Cantwell and Forman*, 1993; *Urban et al.*, 2009), and sociology (*Scott*, 2011; *Krause et al.*, 2007). Connectivity has proven itself to be a "transformative concept" for describing and understanding complex dynamic systems in these disciplines (*Turnbull et al.*, 2018). *Wohl et al.* (2019) identifies the value of connectivity in geomorphology, since it can illuminate interactions between seemingly-disparate and/or distant components of a system. *Keesstra et al.* (2018) argue that connectivity is useful for designing better measurement and modelling schemes for water and sediment dynamics.

Increasing attention has been paid to the topic of sediment connectivity in recent years, although the concept has seen limited application in coastal sediment transport contexts (*Tejedor et al.*, 2015a,b; *Passalacqua*, 2017; *Anthony and Aagaard*, 2020). On the other hand, advances made in non-coastal fields like neurology and hillslope geomorphology have led to the development of techniques for assessing connectivity using graph theory and network analysis (*Newman*, 2003; *Csárdi and Nepusz*, 2006; *Rubinov and Sporns*, 2010; *Phillips et al.*, 2015; *Franz et al.*, 2016).

The major advance in connectivity analysis in recent years has been the adoption of techniques from network science, a broad field concerned with the analysis of complex sys-

tems. Within network science, graph theory conceptualizes a complex system as a series of nodes and the links between them, referred to as a graph (*Newman*, 2003; *Phillips et al.*, 2015). The terms 'network' and 'graph' are often referred to synonymously in literature (*Newman*, 2018). Graph theory provides a strong mathematical framework for analyzing geomorphic systems and quantifying sediment connectivity (*Heckmann and Schwanghart*, 2013). With this approach, sources and receptors of sediment are defined as a series of n nodes interconnected by m links (Figure 7.2a). These links can have both magnitude (i.e., a weighted graph) and direction (i.e., a directed graph). They can represent fluxes between nodes (e.g., sediment transport rates) or some other spatial relationship (e.g., distance).

Nodes and links can be compiled into an $n \times n$ adjacency matrix, A, with sources i and receptors j (Figure 7.2b). The matrix entry a_{ij} indicates the presence or absence of a connection (1 or 0, respectively), or alternatively, a probability, or the magnitude of the flux. The adjacency matrix lies at the heart of network analysis, since many different algebraic techniques can be applied to it. In this form, there are numerous statistical and algebraic techniques available for analyzing and interpreting the network (*Newman*, 2003; *Rubinov and Sporns*, 2010; *Phillips et al.*, 2015). These approaches can be used to quantify the propagation of disturbances through a system, to identify vulnerabilities or critical nodes, or to test sensitivity of transport across a system to changes in network structure (*Callaway et al.*, 2000; *Tejedor et al.*, 2015a). Furthermore, connectivity is a relatively accessible technique, as numerous open-source software libraries and packages are already available (e.g., Pajek (*Batagelj and Mrvar*, 1998), iGraph (*Csárdi and Nepusz*, 2006), the Brain Connectivity Toolbox (*Rubinov and Sporns*, 2010), and Cytoscape (*Franz et al.*, 2016)).

Within geomorphology, the use of graph theory for analyzing connectivity has grown in popularity (*Heckmann et al.*, 2015; *Phillips et al.*, 2015; *Heckmann et al.*, 2018), for applications including sediment delivery in catchments (*Heckmann and Schwanghart*, 2013; *Cossart et al.*, 2018) and the development of sand bars in rivers (*Koohafkan and Gibson*, 2018). Graph theory has also been used effectively for studying channel networks in river deltas (*Tejedor et al.*, 2015a,b, 2016, 2017; *Passalacqua*, 2017; *Hiatt et al.*, 2020) and sea level rise impacts on drainage networks in coastal regions (*Poulter et al.*, 2008). Aggregated morphodynamic models like ASMITA (*Stive et al.*, 1998; *Lodder et al.*, 2019), the reservoir model of *Kraus* (2000), and BRIE (*Nienhuis and Lorenzo-Trueba*, 2019) represent sediment pathways at tidal inlets using a series of reservoirs and the fluxes between them, but do not explicitly analyze connectivity in a graph theoretic framework.

A key strength of graph theory is the assessment of sediment cascades, the succession of different pathways from sources to sinks via a series of temporary storage landforms, in a sort of 'jerky conveyor belt' (*Burt and Allison*, 2009; *Heckmann and Schwanghart*, 2013). In coastal or estuarine contexts, this cascade begins with sediment supplied from fluvial sources, reworking of marine deposits, or coastal erosion (*Spencer and Reed*, 2010), and can end in a wide range of sinks from estuaries to submarine canyons (*Cowell et al.*, 2003). Graph theory provides a mathematical means of identifying and quantifying the structure of these individual connections in the context of a larger cascade or network (*Newman*, 2003). Furthermore, assessing connectivity in this way can reveal emergent patterns not evident in other approaches (e.g., *Rossi et al.* (2014)), such as sediment transport vector fields produced from numerical models.

In spite of its widespread adoption for connectivity studies, graph theory has its limitations. Chiefly, delineating complex natural systems into a limited number of nodes,

patches, or cells (e.g.,*Galpern et al.* (2011)) requires simplifications which can lead to a significant loss of information (*Moilanen*, 2011). Thus, the initial schematization of a network is a step requiring careful attention and scrutiny, in order to ensure that important signals and patterns are not oversimplified.

Schematizing open coastal systems (exposed to the open ocean and whose flows are unconfined by channels like in river catchments or deltas (*Li et al.*, 2006)) into networks is a non-trivial geomorphological mapping task. Nonetheless, graph theory has been embraced for connectivity analysis by the marine ecology and physical oceanography communities, primarily for analyzing larval dispersal, planning marine reserves, or quantifying the spread of pollutants (*Treml et al.*, 2008; *Cowen and Sponaugle*, 2009; *Grober-Dunsmore et al.*, 2009; *Gillanders et al.*, 2012; *Burgess et al.*, 2013; *Kool et al.*, 2013; *Paris et al.*, 2013; *Rossi et al.*, 2014; *Rogers et al.*, 2016; *Storlazzi et al.*, 2017; *Hock et al.*, 2017; *Condie et al.*, 2018; *van Sebille et al.*, 2018). Since graph theory has already proven its usefulness for describing transport processes in marine environments, it is therefore also well suited to analyzing sediment connectivity there. However, feedbacks between topography or structure and transport processes are less critical in marine ecology than in coastal geomorphology, so additional considerations must be taken to successfully adapt this approach for coastal sediment transport (Section 7.2).

7.1.3. OBJECTIVES & OUTLINE

The objective of this chapter is to demonstrate that connectivity analysis using graph theory is a useful framework for understanding sediment transport pathways in coastal environments and solving related sediment management problems. We summarize the relevant advances in connectivity analysis made in other fields and highlight their utility for coastal applications. The remainder of this chapter is presented in four sections. In the following section, we lay out a general methodology for applying connectivity (Section 7.2). To demonstrate the use of connectivity in coastal settings, we apply the concept to a case study of Ameland Inlet in the Netherlands (Section 7.3). We then discuss the utility and limitations of this approach, and provide an outlook for future research into how connectivity might be further adapted and improved for use in coastal environments (Sections 7.4 & 7.5).

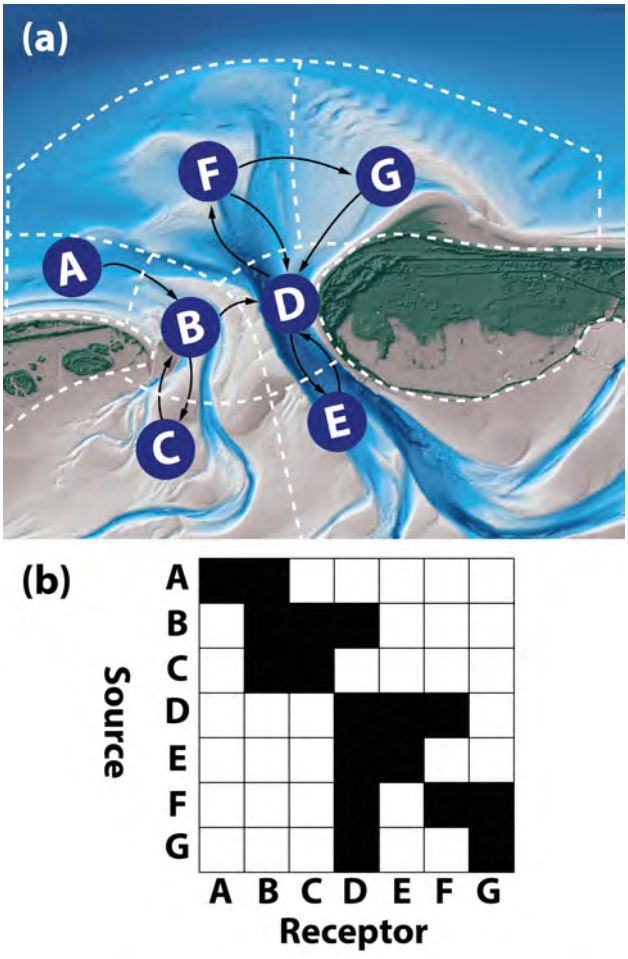

Figure 7.2: Conceptual diagrams explaining how graph theory can be used to quantify sediment connectivity. (a) Hypothetical sediment pathways at Ameland inlet, represented as an unweighted, directed network diagram. Blue nodes (A-G) are representative of the geomorphic cells defined with white dashed borders. Black arrows represent links or fluxes between the nodes. (b) An unweighted, directed adjacency matrix A, the algebraic representation of the network graph presented in (a). Black squares (represented numerically as a "1") indicate the existence of a pathway from a given source node i to a given receptor node j, while decoupled pairs of nodes are white (represented numerically as a "0"). For instance, row B shows that node B acts as a source for nodes C and D, while column B shows that node B receives sediment from node A and node C. The main diagonal of the matrix corresponds to self-self connections, i.e., sediment that stays in or returns to the node where it originated.

7.2. METHODOLOGY

We consider three main questions in order to apply connectivity to a coastal system:

1. **Defining connectivity**: what is the fundamental unit of connectivity, and are we concerned with structural or functional connectivity?
2. **Developing a network**: how can available data or model output be schematized in a network?
3. **Analyzing connectivity**: how can we measure the connectivity and emergent patterns of a network at different scales?

Answering these questions provides a framework with which connectivity can be assessed for coastal systems.

7.2.1. DEFINING CONNECTIVITY

FUNDAMENTAL UNITS

In order for the concept of connectivity to be applied, we must first define the entities or *fundamental units* between which connections exist. In neurological connectivity, the fundamental unit could be neurons or different parts of the brain, and in social networks it could be an individual person (*Turnbull et al.*, 2018). Ecologists often use the concept of the *habitat patch* (*Calabrese and Fagan*, 2004) or ecosystem (*Turnbull et al.*, 2018). For geomorphological applications, *Poeppl and Parsons* (2018) propose the concept of the *geomorphic cell* as the fundamental unit of connectivity, comparable to the landforms or units in a geomorphological map. Within a geomorphic cell, morphology and sediment transport processes remain relatively uniform.

Known sources and sinks of sediment (e.g., sea cliffs or submarine canyons) or criteria like depth, sediment transport patterns, or morphological characteristics can be used to define these cells (e.g., *Jeuken and Wang* (2010); *Stive et al.* (1998); *Stive and Wang* (2003); *Lodder et al.* (2019)). Geomorphic cells can also be defined without any reference to their function or position. *In extremis*, the cells of a high-resolution digital terrain model (DTM) could be used. However, *Poeppl and Parsons* (2018) discourage the "thoughtless adoption of DTM cells at whatever resolution happens to be available", since those cells do not necessarily have a meaningful relationship to the sediment transport within them. Geomorphic cells can be derived more effectively by combining geomorphological maps and high-resolution DTM cells (*Heckmann et al.*, 2015). If no information about sediment fluxes is known *a priori*, then expert judgment may be used for identifying appropriate geomorphic cells.

The spatial definition of geomorphic cells depends on the timescale under consideration. Regions delineated as geomorphic cells based on morphological characteristics or relatively constant sediment and water fluxes may cease to be representative as the landscape evolves. For example, on a long enough timescale, a shallow shoal could develop in a cell originally defined as a deep channel. Thus the spatial scale of geomorphic cells can affect the connectivity observed in a given period (*Poeppl and Parsons*, 2018).

STRUCTURAL & FUNCTIONAL CONNECTIVITY

Once the fundamental unit is defined, we must consider which type of connectivity is relevant: structural or functional. Structural connectivity concerns the spatial anatomy or form of the network (i.e., how the units are spatially arranged relative to one another), whereas

functional connectivity concerns the dynamic fluxes passing within the network (e.g., how much material passes between cells).

Structural connectivity is often defined in terms of adjacency: two neighbouring units not separated by physical barriers are structurally connected. For example, we can consider an open tidal inlet and the adjacent sea, or a river channel and its tributary. However, just because two units are adjacent, this does not mean that they will be functionally connected with fluxes between them. This is why it is important to distinguish between structural and functional connectivity.

Two units are functionally connected if there is some flux between them, such as sediment, water, or organisms. Units need not have strong structural connections to be functionally connected: fluxes may exist between adjacent units, but there may be teleconnections, wherein spatially remote cells can still influence one another (e.g., *Phillips et al.* (2015)). For functional connectivity, it is also necessary to define the dimensions and units of the fluxes under consideration (e.g., mass of sediment, number of particles, discharge, number of organisms in a given time period). Furthermore, functional connectivity can be derived using either Eulerian input (i.e., measured or modelled fluxes at fixed locations) or Lagrangian input (i.e., by tracking a given particle as it moves through the system (*van Sebille et al.*, 2018). Consensus on how to definitively measure and quantify connectivity is currently lacking (*Wohl et al.*, 2019).

As with defining geomorphic cells, the inherent feedback between structural and functional connectivity complicates matters. Sufficient gradients in sediment fluxes will eventually modify the landscape or seascape, which will in turn modify the sediment fluxes. For example, high alongshore sediment transport can lead to the closure of a tidal inlet, which then disconnects the associated basin from the sea (e.g., *Duong et al.* (2016)). Morphodynamics are essentially the relationship between form and process, between structural and functional connectivity.

Transport pathways have a wide range of timescales (*Tejedor et al.*, 2018a), so functional connectivity therefore has a temporal dimension (*Defne et al.*, 2016). Functional connectivity should thus be determined over a sufficiently long interval that areas of interest can be connected, but not so long that the structural connectivity changes (*Heckmann et al.*, 2018). At longer timescales, length scales of connectivity increase, and the likelihood of larger magnitude, highly connective events also increases (*Heckmann et al.*, 2018). Spatial and temporal scales determine connectivity and vice versa. *Keesstra et al.* (2018) argue that structural connectivity has no temporal dimension, as it is a snapshot of the system's architecture at a given moment. This suggests that it would be better to analyze connectivity at a fixed moment in time, if the timescale of sediment fluxes is smaller than the timescale of observable morphologic change at the considered spatial scale. This interdependency between structural and functional connectivity is still regarded as an intractable problem across the literature (*Turnbull et al.*, 2018; *Wohl et al.*, 2019).

To investigate the temporal dynamics of connectivity, multi-layer or multiplex networks can be used (*Kivela et al.*, 2014; *Pilosof et al.*, 2017). These networks can be represented as a three-dimensional tensor A^{α}: a stack of adjacency matrices, with each layer representing connectivity at a different timestep α (*Newman*, 2018). Multi-layer networks can also be used to incorporate connectivity of different processes or transport of different sediment classes simultaneously (e.g., *Tejedor et al.* (2018b)).

Also important to consider is the notion of disconnectivity: the absence or removal of a

given connection. Blockages in a system may inhibit sediment fluxes and thereby change the structural and functional connectivity of a given network (*Fryirs*, 2013). Such disconnections may be natural (e.g., the closure of a seasonal tidal inlet) or anthropogenic (e.g., the construction of a storm surge barrier or tidal energy barrage across an estuary).

7.2.2. DEVELOPING A NETWORK

Numerous qualitative and quantitative metrics have been developed to estimate connectivity (*Calabrese and Fagan*, 2004; *Kindlmann and Burel*, 2008; *Heckmann et al.*, 2018), but the most powerful means of quantifying connectivity is via graph theory (*Newman*, 2003; *Rubinov and Sporns*, 2010; *Phillips et al.*, 2015; *Heckmann et al.*, 2015). To develop a network, geomorphic units can be represented as nodes, and the sediment fluxes or structural connections between them as links. Coastal sediment connectivity networks can be populated using field measurements, numerical model output, or a combination of the two. The possibility to integrate and compare multiple sources of data in a unified framework is an advantage of the connectivity approach.

Sediment transport can be estimated using Eulerian measurements at a single point, based on current velocities and suspended sediment concentrations (e.g., *Gartner et al.* (2001); *Erikson et al.* (2013)). However, it is expensive and impractical to measure continuously for long periods of time at a sufficient number of points to reveal connectivity. While analyzing the differences between repeated bathymetric surveys can yield insight into the rates of morphological change (e.g., *Jaffe et al.* (1997); *Elias et al.* (2012a)), it does not give sufficient information to attribute directional transport.

Sediment tracer studies (both artificial (*Black et al.* (2007); *Elias et al.* (2011); *Bosnic et al.* (2017), Chapter 6) and natural (*Rosenbauer et al.*, 2013; *Hein et al.*, 2013; *McGann et al.*, 2013; *Wong et al.*, 2013; *Reimann et al.*, 2015)) offer a Lagrangian technique for identifying pathways, but are challenging to execute and recover (*Elias et al.*, 2011). Grain trend analysis (*McLaren and Bowles*, 1985; *McLaren et al.*, 1998; *Duc et al.*, 2016; *McLaren*, 2013; *Gao and Collins*, 1991; *Le Roux and Rojas*, 2007; *Velegrakis et al.*, 2007; *Poizot et al.*, 2006, 2008) and analysis of bedform asymmetry (*Sha*, 1989c; *Bartholdy et al.*, 2002; *Velegrakis et al.*, 2007; *Barnard et al.*, 2013a) offer additional techniques for identifying sediment pathways. However, field measurements alone are generally too limited to quantify sediment connections on the timescales of typical interest for engineering and policy decisions.

As an alternative or complement to field measurements, numerical models provide a convenient way of inferring connectivity, since they can calculate fluxes at every point in a system (*Wohl et al.*, 2019). The mean sediment transport vector field generated by a model can be used to visualize residual transport pathways (e.g., *Elias and Hansen* (2013); *Herrling and Winter* (2014); *Gelfenbaum et al.* (2017)). Alternatively, Lagrangian approaches to analyzing modelled sediment transport can be used. *Elias et al.* (2011), *Nienhuis and Ashton* (2016), and *Beck and Wang* (2019) used an approach where sediment originating from a particular location was labelled as a unique sediment class in a morphodynamic model, and then followed as it dispersed throughout the model domain.

Lagrangian particle tracking models (e.g., *MacDonald and Davies* (2007); *Soulsby et al.* (2011); *van Sebille et al.* (2018), Chapter 8) are also a useful tool for tracking sediment and defining transport pathways. One can either consider the final resting place of a given sediment particle at a given time (a depositional approach) or instead track the complete history of that particle. The disadvantage of a depositional approach to connectivity is that a path-

way with zero transport gradient may be very well connected, and yet leave no trace of the sediment it is transporting (*Wohl et al.*, 2019). For example, the main channel of a tidal inlet near morphological equilibrium may convey large volumes of sediment, but this sediment does not necessarily accumulate there, which would give the erroneous impression of low connectivity. Hence, the choices made in how sediment transport or particle trajectories are tabulated from numerical model output can significantly affect the conclusions drawn from connectivity analysis.

Once the data source has been chosen and organized into cells and fluxes, the network can be compiled. The contribution from a given source cell to every other possible receptor cell in the system constitutes one row of an adjacency matrix. By carrying out this calculation for each source in the system, we arrive at a fully populated adjacency matrix representing all the sediment fluxes in our system (e.g., Figure 7.3g). Thus, these large and complex datasets can be reduced to a relatively simple form, all visualized as a network diagram (e.g., Figure 7.3a). Once the adjacency matrix has been defined, it can be analyzed using a variety of algebraic and statistical techniques.

7.2.3. ANALYZING CONNECTIVITY

With the coastal system reduced to a adjacency matrix of sediment fluxes, we can begin to quantify and analyze connectivity. This is where connectivity has added value as a framework over existing approaches: an abundance of analytical metrics and statistics can be used once the data has been organized into a network. Here, we focus on a selection of connectivity metrics that lead to useful insights for coastal sediment management, both at a system level and for individual units.

SYSTEM LEVEL

System-level connectivity metrics (at the scale of the entire network) are important to consider because in a complex network, the overall structure and connectivity will influence the connections between individual nodes at smaller scales. The applicability of these indices depends on the temporal scale at which the system's structural connectivity undergoes significant change (*Heckmann et al.*, 2018).

Link Density

To gain insight into the overall connectivity of a given system, we can consider the link density (D), which is the number of connected links relative to the total number of possible links. If self-self connections are neglected, the maximum possible connections m_{max} is $(n^2 - n)$ for directed networks and $(n^2 - n)/2$ for undirected networks, where n is the number of nodes in the network (*Phillips et al.*, 2015). A fully connected network is one in which each node is connected to every other node ($D = m/m_{max} = 1$). A system without any transport between nodes corresponds to a fully disconnected network ($D = m/m_{max} = 0$) (*Cowen and Sponaugle*, 2009). In reality, most networks will lie somewhere in between (e.g., Figure 7.3a, with $D = 0.33$). Link density is a function of the observation or simulation time, since longer periods may allow sediment to travel greater distances and hence connect with additional receptors. This may be useful for comparing the general behaviour of a system at different time scales or in different scenarios.

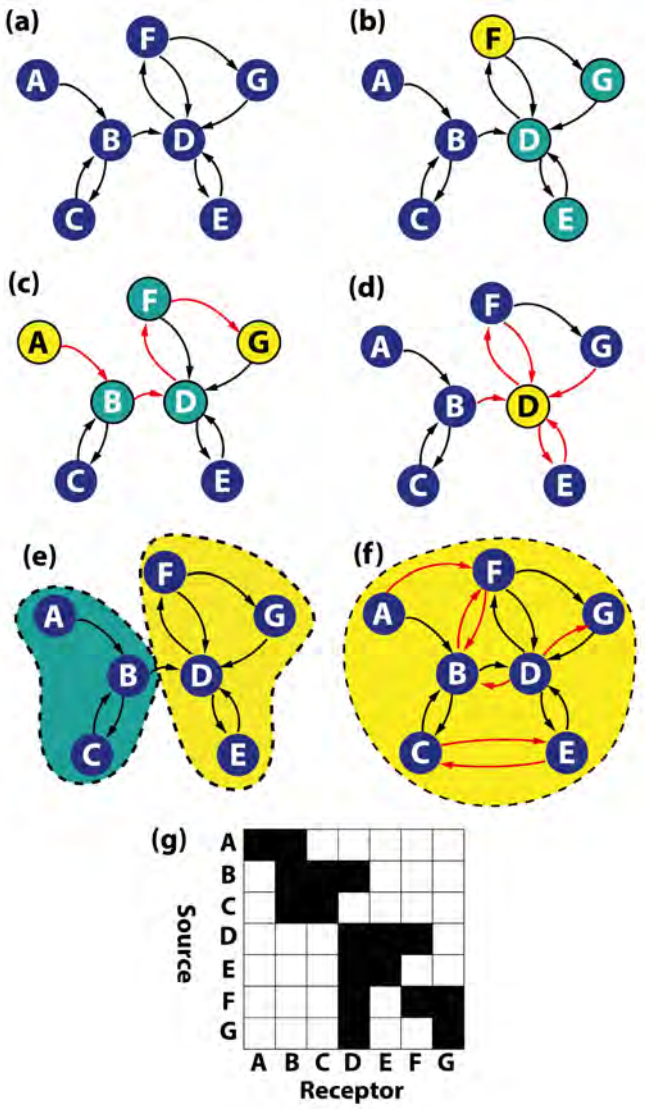

Figure 7.3: Examples of questions that can be answered via connectivity. (a) Simple unweighted directed network diagram from Figure 3(c); (b) What are the possible receptors for sediment from Source F? Nodes that cannot be reached from F are dark blue, and possible receptors are in teal; (c) What is the shortest pathway between A & G? The shortest pathway is indicated by red arrows and teal nodes (A-B-D-F-G); (d) Which node is the most interconnected (has the highest degree) in the system? Connections with this node are indicated by red arrows. (e) Can the system be easily separated into distinct modules? (yes: one green module of three nodes (ABC), and one yellow module of four nodes (DEFG)); (f) If additional links are added, can the system still be easily separated into modules? (no: there is now a single yellow module containing all nodes). (g) Adjacency matrix for the simple network shown in (a-e). Black squares indicate that a given source and receptor pair are connected.

Asymmetry

By definition, undirected networks have symmetric adjacency matrices. For directed networks like in Figure 7.3, asymmetry implies a net flux: more material is going to a given node than coming from it, or vice versa. In coastal systems, the sediment transport is often characterized by large opposing gross fluxes due to reversing ebb and flood tides (*Gatto et al.*, 2017) or variable wave climates (*Harley et al.*, 2011). Net fluxes are a consequence of small asymmetries between these ebb and flood fluxes or gross alongshore transports. These net fluxes are coupled with the morphological behaviour of a coastal system or feature. The asymmetry of connectivity is thus a direct measure of these fluxes and their interactions with the coastal system.

Asymmetry can be revealed by decomposing an adjacency matrix A into its symmetric A_{sym} and skew-symmetric A_{sk} components (*Kundu and Cohen*, 2008):

$$A = A_{sym} + A_{sk} = \frac{1}{2}(A + A^T) + \frac{1}{2}(A - A^T) \tag{7.1}$$

Where A^T is the transpose of the adjacency matrix. The skew-symmetric matrix A_{sk} should directly correspond to the net sediment transport of a system, and the symmetric matrix A_{sym} to the gross transports that cancel each other out. Decomposing a matrix in this way can be useful for understanding the transport pathways that drive morphological changes.

The degree of symmetry s in the network can be summarized using the approach of *Esposito et al.* (2014):

Where s is the symmetry index, u is the number of completely unconnected node pairs ($a_{ij} = a_{ji} = 0$). When $s = 1$, the network is fully symmetric, and when $s = 0$, there are no reciprocated connections in the network (fully asymmetric). High symmetry indicates relatively small net transports (and hence relatively small morphological changes), even if gross transports and connectivity are large. Conversely, low symmetry indicates relatively large net transports (and hence relatively large morphological changes), even if gross transports and overall connectivity are small.

Modularity

Modules or communities are densely-interconnected clusters of nodes with limited external connection. The degree to which a network can be be divided into such clusters is known as modularity, Q (*Leicht and Newman*, 2008):

$$Q = f_{mod} - f_{rnd} \tag{7.2}$$

Where f_{mod} denotes the fraction of links within a module and f_{rnd} denotes the expected fraction of such links based on random chance. These modules can be determined using a variety of cluster optimization techniques such as the Infomap (*Rossi et al.*, 2014) or Louvain (*Rubinov and Sporns*, 2010) algorithms.

Networks that can be clearly delineated into non-overlapping clusters have high modularity $Q > 0$ (Figure 7.3e), whereas networks with few coherent groups have low modularity $Q < 0$ (Figure 7.3f). For instance, *Rossi et al.* (2014) uses modularity to identify 'hydrodynamic provinces', regions that are internally well connected but are poorly linked to each other. This procedure could be used to delineate geomorphic cells (as per *Poeppl and Parsons* (2018)) or to examine emergent behaviour. Such grouping may be the result of similarities in morphology, initial sediment distribution, or hydrodynamic forcing.

INDIVIDUAL NODES & LINKS

Graph theory also offers numerous metrics with which to gauge the influence of individual nodes and links in a network. These statistics may provide practical insights into the role of a given node or link in transmitting sediment, and identify key vulnerabilities in the system.

Connectivity between Specific Nodes

Most simply, a network can be directly queried to examine the connectivity between specific nodes or groups of nodes. For example, we see in Figure 7.3b that Node F is directly or indirectly a source for Nodes D, E, and G. However, there are no possible pathways leading from Node F to Node C. Hence, if this were a coastal sediment system where the goal was to eventually nourish Node C with sand, Node F would not be an optimal location. In another example, we can consider the shortest path between two nodes (e.g., Figure 7.3c), where path length is calculated in topological space (rather than geographical space) as the inverse of the sediment flux between those nodes ($d_{ij} = 1/a_{ij}$) (*Rubinov and Sporns*, 2010). The total path length is defined by the sum of the lengths between any intermediate nodes, and the shortest path is then defined as the path with the minimum total length. That is, nodes connected by large fluxes are considered closer together in the topology of the network, and nodes with weak connections are more distant, irrespective of actual geographic distances. This metric may thus be useful for identifying the dominant transport pathways and quantifying processes like inlet bypassing. Asymmetry of connections between individual nodes or specific groups of nodes may also provide useful insight into net transport patterns.

Degree

Degree quantifies the number of links connected to a given node. For directed networks, this can further be decomposed into an in-degree k_{in} and an out-degree k_{out} (Figure 7.3b). For example, Node D in Figure 7.3d has an in-degree of 4 and an out-degree of 2. Degree provides insight into the diversity of different sources or sinks that a given node has. A network's degree distribution ($P(k) = n_k/n$, where n_k is the number of nodes of degree k and n is the total number of nodes in the network) can provide an indication of the overall network structure or topology (*Phillips et al.*, 2015). If each node has a similar degree, the network will have a relatively uniform, distributed structure. However if the degree distribution is exponential, the network will be more centralized with a few dominant hubs or clusters. This relationship highlights how connectivity at the level of individual nodes can cascade upwards to shape connectivity at the overall system level.

Strength

Strength is the sum of all fluxes in and out of a given node for weighted networks, and can be computed directly from the adjacency matrix. For weighted, directed networks, this can be further decomposed into in-strength and out-strength. Nodes with a relatively higher in-strength than out-strength are sinks, which is useful for identifying zones of sediment accumulation or convergence. Nodes with a higher out-strength than in-strength are sources, so material will tend to disperse there. Ultimately, it is the balance between in- and out-strength that determines morphological change. Knowledge of these key nodes can inform dredging/nourishment strategies.

This may be more insightful than degree, since high degree does not necessarily equal

high strength, especially where fluxes are unevenly distributed throughout the system. For example, even though Node D in Figure 7.3d has a higher in-degree than out-degree, if the out-strength is higher than in-strength, it will be a net source rather than net sink.

Centrality

Centrality quantifies how important or “central" a given node or link is within the context of the system as a whole. There are numerous ways of quantifying centrality (*Newman*, 2018), including degree-, closeness-, eigenvector-, and betweenness-, which we focus on here. Betweenness centrality B refers to the proportion of all shortest paths in a network that pass through a given node or link (*Phillips et al.*, 2015), where the “distance" along paths is calculated in terms of inverse sediment flux between nodes ($d_{ij} = 1/a_{ij}$). Hence, nodes with high betweenness centrality represent crucial nodes that may more efficiently transmit sediment through the rest of the system. This could translate to a greater vulnerability to disruptions, or could be used identify strategic locations for more dispersive nourishments. Thus, betweenness centrality gives more insight into the relationship between network structure as a whole and individual nodes than just degree or strength.

The comparison metrics in this section examine connectivity at the system or network-wide level, as well as at the scale of individual nodes or links. To illustrate their ease of application and usefulness in answering practical questions about coastal sediment systems, these metrics are applied to a case study of a Dutch tidal inlet in the following section.

7.3. CASE STUDY: AMELAND INLET

To illustrate the principles and analysis techniques discussed in previous sections, we apply the sediment connectivity approach to Ameland Inlet, a tidal inlet located in the Wadden Sea to the north of the Netherlands (Figure 7.1). The safety of the Dutch coast against coastal flooding is directly linked to the volume of sand contained in its dunes and beaches, so there is a strong need for sediment management there (*Hanson et al.*, 2002; *Stive et al.*, 2013). The beaches and shoreface are regularly nourished with sand, so connectivity provides an approach that can be used for optimizing those nourishments and improving our understanding of the underlying natural system. Since ebb-tidal deltas represent a key component in the sediment budget of the Wadden Sea and its adjacent coasts, quantifying sediment pathways across them is of critical importance (*Elias et al.*, 2019). This knowledge gap prompts the research questions outlined in Figure 7.1, which we will answer using the concept of connectivity.

Based on our general understanding of tidal inlets and our prior knowledge of Ameland, we can make a hypothesis about the system’s connectivity. Connectivity of a given grain size class should depend on its mobility threshold, the energy available to transport it, and its initial spatial distribution. We thus expect higher connectivity for finer sand and lower connectivity for coarser sand, because the lower critical shear stress threshold for fine sand means that it will be more easily mobilized and transported longer distances. Conversely, the higher threshold for mobilization of coarse sediment means that only the most energetic conditions can transport it. In addition, fine sand has a wider initial spatial distribution in this model, whereas coarser sand is only found in the deepest channels (Figure 7.4).

We also expect higher connectivity in regions with greater hydrodynamic energy to mobilize sediment, like the main channels and ebb-tidal delta. Conversely, deeper areas offshore and calmer areas at the periphery of the inner basin are expected to have low con-

nectivity. We also expect the main channels to function as transport bottlenecks, since they represent the only routes from the ocean to the inner basin (i.e., no transport through the islands in this model), whereas there are many possible pathways between different points on the ebb-tidal delta (e.g., *Herrling and Winter* (2018)).

To illustrate the coastal sediment connectivity framework, we used the Delft3D process-based numerical sediment transport model to assess the fate of sediment as it moved between specific morphological units defined in the model domain. For a detailed description of the Delft3D model formulations see (*Lesser et al.*, 2004). Delft3D has been widely used for simulating coastal sediment transport (*Elias et al.*, 2006; *Herrling and Winter*, 2014; *Nienhuis and Ashton*, 2016; *Huisman et al.*, 2018). We used an existing Delft3D model (*de Fockert*, 2008; *Elias et al.*, 2015b; *Wang et al.*, 2016; *Bak*, 2017) as a basis for this example. A link to model input files used in this study and a brief description of their contents have been included in Appendix C. The model is 2D and represents a 40×30 km domain, with a maximum resolution of $\approx 80m$ (Figure 7.4). Data from the 2016 Vaklodingen survey (*Rijkswaterstaat*, 2016) was used to create the bathymetry.

The existing model was simplified to demonstrate the concepts of connectivity, featuring a schematized morphological tide (e.g., *Latteux* (1995)) that propagates eastward along the offshore and seaward lateral boundaries. The morphological tide represents the equivalent net transports observed in the main channel during a full spring-neap tidal cycle as two semi-diurnal tides using the M2, M4, M6, and artificial C1 diurnal components, as per *Lesser* (2009). The lateral boundaries within the Wadden Sea are considered closed in these simulations. Ameland Inlet has a tidal range of between 1.5-3 m, and tidal prism of $400-500 Mm^3$ (*Elias et al.*, 2019). The tide drives currents of approximately 1 m/s in the main channel of the inlet at ebb and flood. Waves and inter-basin wind-driven flows are known to be important processes for Ameland Inlet (*Duran-Matute et al.*, 2014; *Van Weerdenburg*, 2019; *Lenstra et al.*, 2019a; *Elias et al.*, 2019; *Brakenhoff et al.*, 2019b; *de Wit et al.*, 2019), but are neglected here for simplicity.

Seabed sediment at Ameland Inlet is typically fine to medium sand, so four sediment grain size classes were chosen to simulate the influence of grain size variation (100, 200, 300, 400 μm). The sediment was initially distributed according to measured samples (*Rijkswaterstaat*, 1999), after which a bed composition generation run was carried out to redistribute the sediment in equilibrium with the model bathymetry, as per *van der Wegen et al.* (2011). The model has a 12 hour spinup period to limit the effect of initial instabilities. An equilibrium concentration condition is specified at the boundaries, which sets the sediment load there equal to the sediment load in the interior of the model and ensures that there is little erosion or accretion at the boundaries. A transport or surface bed layer thickness of $0.5m$ and maximum underlayer thickness of $1m$ (for bookkeeping of subsurface sediment layers) are used to describe vertical variations in bed composition.

We adopted a morphostatic (fixed bed) modelling approach, but permitted sediment exchange between the bed and water column. We ran the model for 6 months (360 tidal cycles), which ensures that the modelled timescale is smaller than the timescale of observable morphologic change at the chosen spatial scale, based on annual bathymetric surveys (*Elias et al.*, 2019). This is also long enough to ensure that the network is well-connected with few separate subsystems or *components*.

This model output (a spatial map of sediment mass in the bed and water column at every model grid cell, for each timestep) was used to populate a network (Sections 7.3.1 &

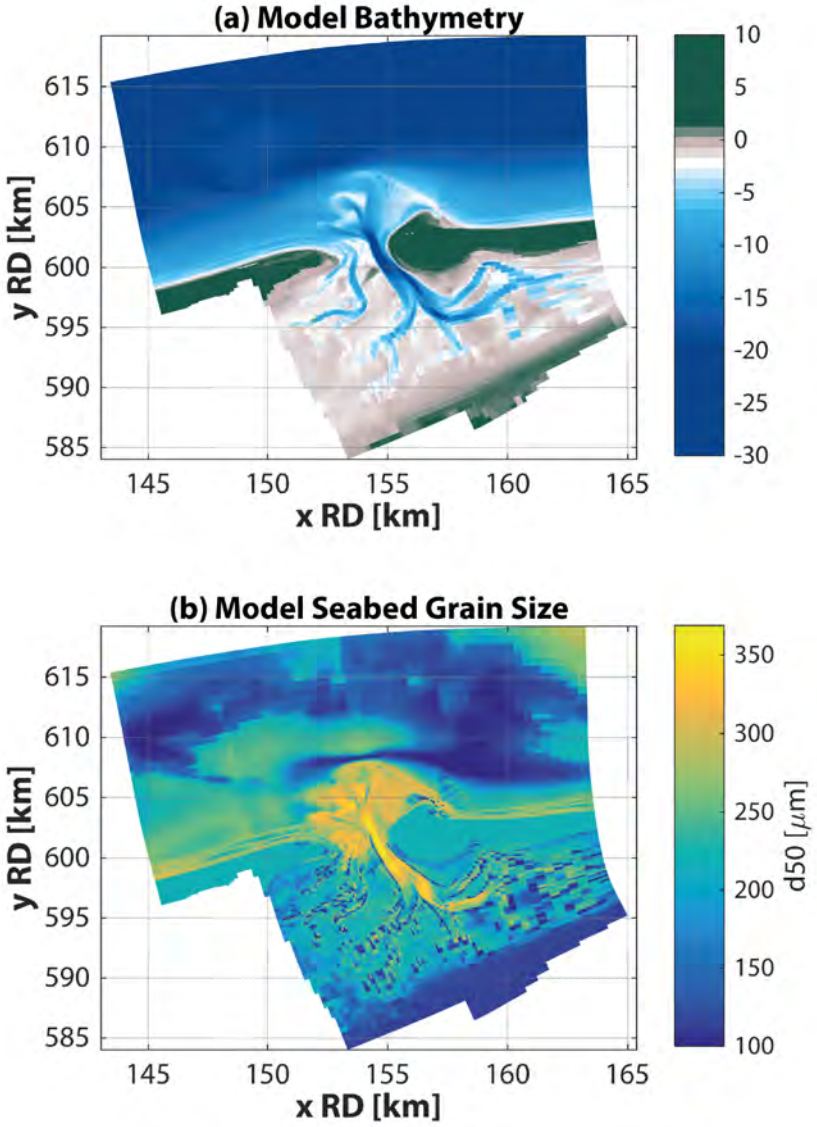

Figure 7.4: (a) Initial bathymetry of Delft3D numerical model used to calculate connectivity, based on *Rijkswaterstaat* (2016). The maximum resolution of the grid is approximately 80 m at the inlet. (b) Initial sediment distribution in Delft3D model. Median grain size (d_{50} [μm]). The coarsest sediment can be found in the deepest parts of the channel where tidal currents are strongest, whereas the finest sediment is located offshore, on intertidal flats inside the basin, and seaward of the ebb-tidal shoals. Coordinates are given in Amersfoort/RD New system.

7.3.2). We then used graph theory to analyze connectivity at different space and time scales (Section 7.3.3).

7.3.1. DEFINING CONNECTIVITY

For this example, we examine the functional connectivity of Ameland Inlet by looking at sediment fluxes between different parts of the system. To determine this functional connectivity, we started by defining 25 geomorphic cells, (Figure 7.5a). These cells were delineated subjectively on the basis of depth contours but also of their functionality. For instance, shallow parts of the ebb-tidal delta may occur at similar depths to the inner basin, but are morphologically distinct, with different hydrodynamic forcing and sediment composition. As such, the model domain was broken into offshore regions, ebb-tidal shoals, channels, beaches, and intertidal flats.

25 model simulations were prepared, one for each geomorphic cell (Figure 7.5b). In each simulation, a different cell served as the source node, and the remaining 24 cells were receptors. Similarly to *Elias et al.* (2011) and *Nienhuis and Ashton* (2016), we track the motion of sediment (and hence functional connectivity) from source to receptor by using a series of unique sediment classes. A total of eight sediment classes were included in the model: four “tracer" classes and four “background" classes. In each simulation, sediment within the source node was labelled as a tracer, while the sediment elsewhere in the model domain was labelled as “background" sediment. All the sources are activated simultaneously, although the analysis only focuses on tracking a single source in each run. In this way, it is possible to follow the movement of the tracer sediment and distinguish its fate from that of the surrounding sediment. Alternatively, a single model simulation with 100 sediment classes (4 grain size classes × 25 nodes) could have been used to achieve the same end result, although this was deemed computationally impractical.

7

7.3.2. DEVELOPING A NETWORK

Net fluxes of sediment determine the long-term morphological evolution, rather than the gross fluxes of sediment passing through a given cell on each tidal cycle. However, these gross fluxes are often much larger than the net fluxes. To measure the residual rather than gross fluxes (and avoid erroneously large or misleading trends), we record the mass of sediment in the bed and water column of a given cell at the end of an integer multiple of tidal cycles – twice daily (Figure 7.5b). For example, consider a case with sand transport from Node 1 to Node 9 via Node 7. If there is some deposition in Node 7, we will see connections from 1 to 7 and 1 to 9, but not necessarily 7 to 9; however, if there is no deposition or mixing with the bed, only the link from 1 to 9 will be recorded. This is unlikely in the present model because the geomorphic cells considered here are comparable in size to the tidal excursion ($\mathcal{O}(1-10km)$), and because the active layer bed schematization in Delft3D means that even minute traces of sediment will likely remain mixed in the bed if it passes through a given cell. To circumvent this, alternative approaches could be to collapse all intersecting pathways and convert this network into a planar network (*Galpern et al.*, 2011), or to use a Lagrangian transport model as input (e.g., Chapter 8). To limit the influence of numerical errors (e.g., from rounding or truncation) and focus on pathways showing a clear signal, we apply a minimum threshold of 1000 kg per 6 months to all connections (up to 7 orders of magnitude smaller than the strongest fluxes). This represents an Eulerian definition of connectivity, in comparison to Lagrangian methods which would consider the full lifetime

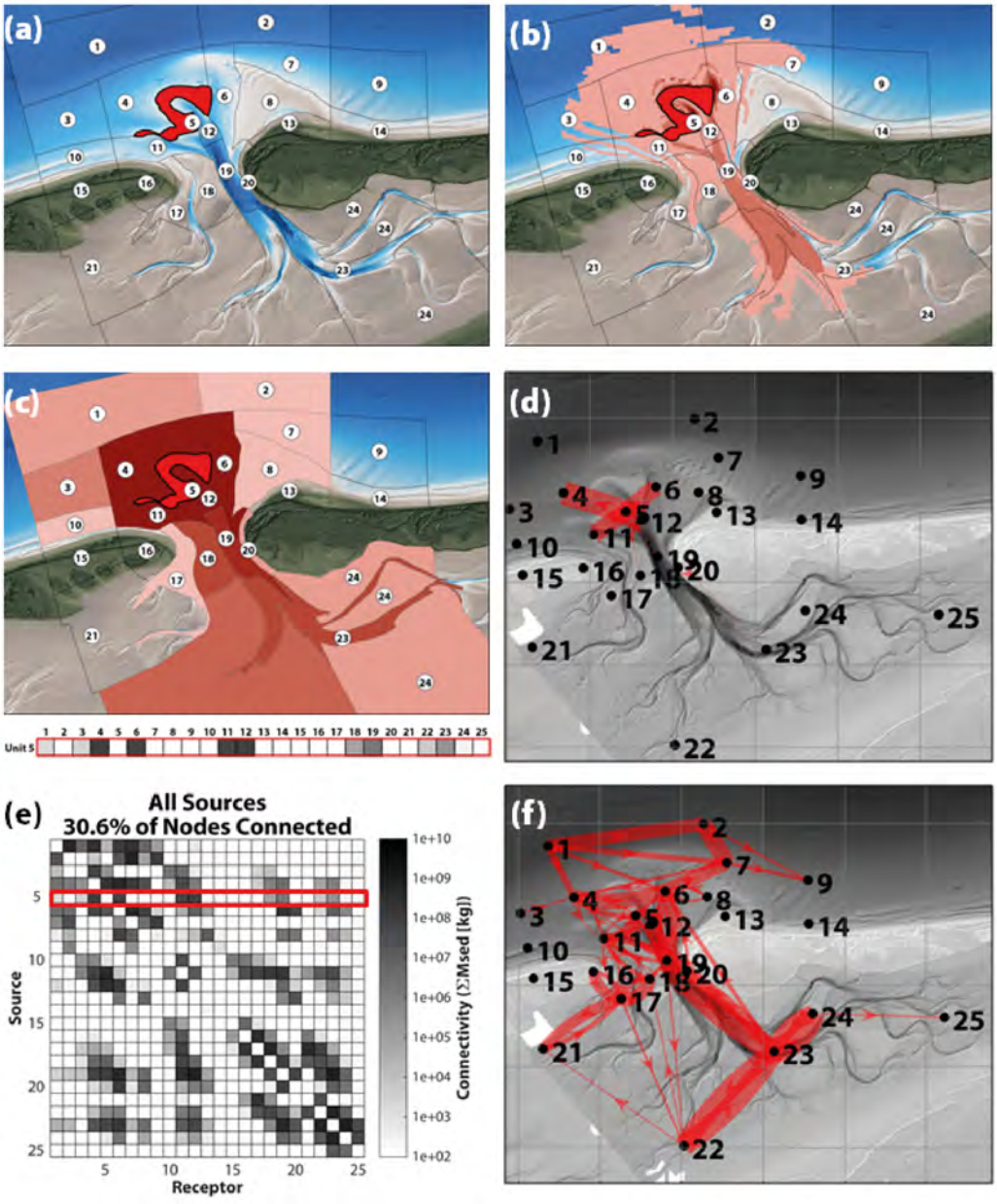

Figure 7.5: Deriving connectivity using a process-based numerical model. Example using sediment from Node 5. (a) Step 1: Definition of source/receptor nodes (numbered geomorphic cells) and labelling of tracer sediment classes. (b) Step 2: Running the model and tracking sediment, where darker shades of red indicate greater masses of tracer sediment in the seabed (all tracer sediment size classes aggregated). (c) Step 3. Tabulating the mass of tracer sediment from Node 5 to each other node (where darker shades of red indicate greater masses of tracer sediment in a given geomorphic cell), and compiling the data into one row of an adjacency matrix (where darker shades correspond to greater masses of tracer sediment from Node 5 in a given receptor cell, and hence greater connectivity). (d) Example of a network based on sediment from Node 5 alone, with thicker lines and arrows indicating larger transports between two given cells. (e) Adjacency matrix for full weighted, directed network with contribution from Unit 5 highlighted in red. (f) Network diagram for full network, where thicker links correspond to greater sediment transport. Only the top 10% of connections are shown here, in order to clarify the dominant patterns.

path of a given tracer particle.

The total mass of sediment from a given source in each receptor produces a single row of an adjacency matrix (see example in Figure 7.5c where Node 5 acts as a source to all other receptor nodes). The network diagram corresponding to this single row is shown in Figure 7.5d. Sediment from Node 5 travels to 30.6% of all nodes, principally to nearby nodes on the ebb-tidal delta and in the main channels. When this procedure is repeated for each of the source nodes, we obtain a complete weighted, directed adjacency matrix (Figure 7.5e). For context, Node 5 is highlighted in a red box. The central diagonal is empty because with the current model set up, it is not possible to differentiate between sediment from a given source that remains in the bed and sediment from that source which is mobilized but recirculates or returns. The complete adjacency matrix can also be represented as a network diagram (e.g., Figure 7.5f). Network diagrams provide a useful and intuitive means of visualizing connectivity with thicker lines and arrows representing larger transports between a given pair of nodes.

7.3.3. ANALYZING CONNECTIVITY

NETWORK ANALYSIS

As hypothesized, the network's strongest connections are in the tidal channels and ebb-tidal delta, where hydrodynamic energy is greater. It is important to note again here that waves are not included in this model, only tidal forcing. The strongest connections and hence dominant sediment transport pathways lie along the main inlet channel and across the ebb-tidal delta. This is because the main inlet channel serves as the central drainage point for the basin and is a convergence zone for flows in and out of the basin. Furthermore, the ebb-tidal delta features strong, convoluted currents and abrupt changes in bathymetry, so the sediment fluxes there are large. Conversely, the connections at the rear of the basin (e.g., Cell 25, which consists primarily of tidal flats with few major channels) are relatively weaker because of the decreased tidal energy to mobilize sediment there. There are also relatively few direct connections between the rear of the basin and the regions offshore/along the coast, since sediment must have both the time and energy to make the longer journey.

Density

The entire network (including all sediment size fractions) has a link density D of 30.6% (Figure 7.5). When we consider only $100\mu m$ sand, the network density D is 30.2% (Figure 7.6a), whereas the network density for $400\mu m$ sand is only 12.2% (Figure 7.6b and Table 7.1). The dominant pathways for $400\mu m$ sand are confined to the main channel (Figure 7.6d), whereas $100\mu m$ sand also has strong connections within the inner basin and outer delta (Figure 7.6c). These findings confirm our earlier hypotheses about expected differences in connectivity as a function of grain size.

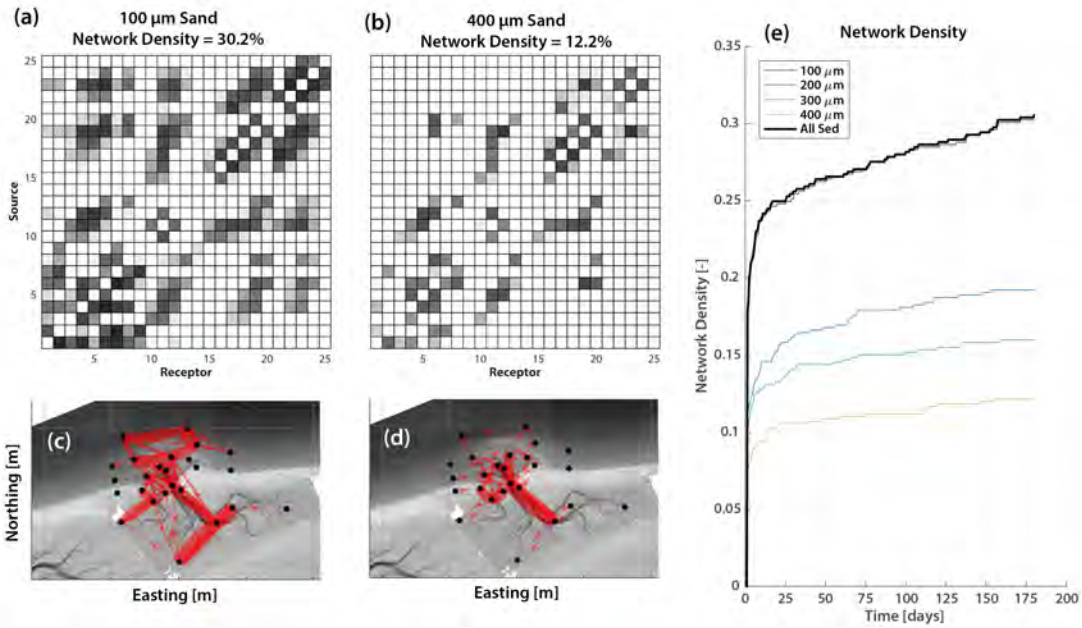

Figure 7.6: Connectivity matrices and network for $100\mu m$ (a,c) and $400\mu m$ sand (b,d). The shading of a given cell in the adjacency matrices or the thickness of the red lines in the network diagram indicate the connectivity between a given source and receptor. To illustrate the dominant patterns, only the top 10% strongest connections are displayed in (c) and (d). (e) Time series of network density D, the fraction of actual connections over potential connections.

However, the differences in connectivity for each grain size class cannot be explained solely by hydrodynamic forcing: connectivity can be supply-limited. For instance, lack of connection for 400 μm sand from the rear of the basin (e.g., Node 25) to the outer coast (e.g., Node 14) can be attributed to the relative absence of that sediment class there (Figure 7.4b).

When link density is considered as a function of time, we see that connectivity increases rapidly during the initial timesteps of the simulation, apparently due to the connection of sediment from sources to their immediate neighbours (Figure 7.6e). In subsequent timesteps, the rate of increase in link density slows considerably, suggestive of a more gradual diffusion after the main connections in the network have been made: sediment must travel greater distances to make new connections. Density is higher for all sediment fractions combined than for any one sediment class because of the spatial differences in sediment supply. For instance, between some locations there may be a connection for $400\mu m$ sand but not for $100\mu m$ sand, if there is no $100\mu m$ sand initially present in the bed there.

Table 7.1: Comparison of different connectivity metrics. Network link density, D, represents the fraction of actual connections out of all potential connections in the network. Symmetry (s) indicates the proportion of reciprocal connections between nodes, where 1 indicates perfect symmetry and 0 indicates complete asymmetry. Modularity (Q) lies between -1 and 1, where positive numbers indicate a non-random tendency to form non-overlapping groups (*Rubinov and Sporns*, 2010).

Scenario	$D[-]$	$s[-]$	$Q[-]$
All Sediment	0.306	0.292	0.455
$d_{50} = 100\mu m$	0.302	0.276	0.465
$d_{50} = 200\mu m$	0.192	0.349	0.432
$d_{50} = 300\mu m$	0.160	0.401	0.406
$d_{50} = 400\mu m$	0.122	0.337	0.408

Asymmetry

All of the networks are asymmetric ($s < 1$), which suggests that the system is characterized by non-zero net transports, and hence morphodynamic change (Table 7.1). However, the networks are not completely asymmetric ($s \approx 0$), likely due in part to the bidirectional nature of tidal transport. There is also no observable trend in asymmetry with respect to grain size.

Asymmetry in a connectivity matrix implies that sediment exchange between two nodes is unequal: a net transport in one direction. In Figure 7.7a-b, this can be examined by comparing the $634 \times 10^3 m^3$ of sediment leaving the tidal basin (export) with $902 \times 10^3 m^3$ of sediment arriving in the basin from elsewhere (import). In this case, we see a net import of $268 \times 10^3 m^3$ of sediment in 6 months, which is qualitatively consistent with historical trends for Ameland Basin (*Elias et al.*, 2012a). An exact quantitative comparison with measured sediment import volumes is not meaningful here since the present model neglects waves and wind-driven currents, which are important processes at the study site.

Modularity

Modularity is positive, which indicates the emergence of functional sediment-sharing groups at non-random levels (Table 7.1). There is relatively little variation in modularity for different size fractions, which suggests that the modularity in this case is more strongly controlled by the physical structure of the network and hydrodynamic distribution of energy than it is by grain size.

Five distinct modules or sediment-sharing groups are identified using the Louvain algorithm (*Rubinov and Sporns*, 2010): the basin (yellow), offshore/downdrift coast (teal), ebb-tidal delta and main channels (blue), updrift barrier island (light brown), and far downdrift coast (green) (Figure 7.7c-d). Although transport does occur between each of these communities, the majority occurs inside of them. For example, Cell 23 is well connected with many locations in the model domain, but modularity quantitatively shows that it is most closely linked with the basin. This grouping could also be useful for defining geomorphic cells as input for larger-scale connectivity studies (as per *Rossi et al.* (2014)), or in the development of aggregated models (e.g., ASMITA (*Stive et al.*, 1998)).

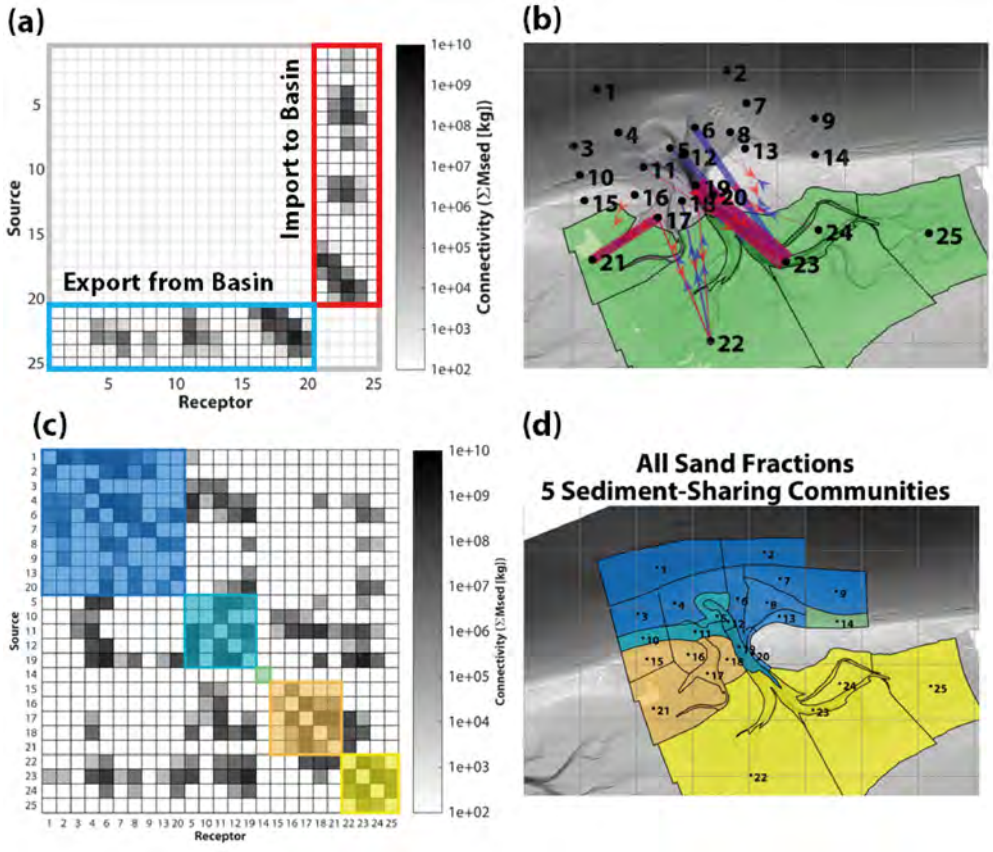

Figure 7.7: Example of different asymmetric connectivity between groups of nodes and modularity. (a) Adjacency matrix filtered to show only connections to (red, “import") or from (blue, “export") the inner basin (all grain size classes). Comparing the relative import and export reveals a net import of sediment, in line with historical trends for the site (*Elias et al.*, 2012a). (b) Network diagram illustrating the filtered adjacency matrix from (a). Cells in the basin are indicated in green. (c) Adjacency matrix sorted into functional sediment-sharing groups using the Louvain modularity algorithm, which maximizes within-group connections and minimizes inter-group connections (*Rubinov and Sporns*, 2010). Each coloured patch in (c) and (d) indicates one of the five sediment-sharing modules identified for the network (all grain size classes).

ANALYSIS OF INDIVIDUAL NODES & LINKS

In addition to statistics which characterize the entire network, it is also possible to assess the role of individual nodes.

Connectivity between Specific Nodes

Individual nodes can also be queried to answer specific questions. For instance, net sediment import into or export from a tidal basin is a vital quantity for estimating coastal sediment budgets, and can be determined by examining asymmetric connections between nodes lying inside and outside the basin. For this particular simplified model, there is a net import of sediment into the basin (Figure 7.7a-b), indicated by a larger total connectivity from cells 1-20 to cells 21-25 than from cells 21-25 to cells 1-20. When we examine connections between the updrift and downdrift islands, we find that the shortest pathway (calculated in terms of fluxes on the network, not geometric distance or Lagrangian tracking of tracer sediment in the Delft3D model) depends on the offshore distance of the source (Figure 7.8). Sediment beginning its journey in the nearshore or outer bar region will travel via the inlet (blue and yellow lines), whereas sediment originating further offshore will travel via the outer delta. This suggests that the bypassing routes of interest in Figure 7.1 depend largely on cross-shore position. Bear in mind that this model uses a schematized tidal signal and neglects key processes known to be important for bypassing, such as waves and wind-induced currents. As such, these pathways should be re-evaluated using a more comprehensive model.

Degree, Strength, & Betweenness Centrality

When nodes in our network are considered individually, we see that the nodes with highest degree and strength are generally those in the main channels and on the ebb-tidal delta (Figure 7.9a,b), which follows from the earlier observations on network density (Figure 7.6). Nodes in the main channel also have the highest betweenness centrality, which confirms and quantifies our hypothesis about the role of the channel as a transport bottleneck (Figure 7.9c).

7.3.4. SUMMARY

This case study for Ameland Inlet was intended to show a proof of concept for how sediment connectivity could be applied to a real coastal example. The most challenging part of the approach was to configure and run the model in such a way that sediment pathways could be defined. However, once the data were compiled into a network, sediment transport patterns could be easily quantified using metrics like asymmetry, modularity, and betweenness. The availability of free, open-source analysis tools makes connectivity analysis a highly accessible approach, which yields useful insights into sediment transport at both local and system levels.

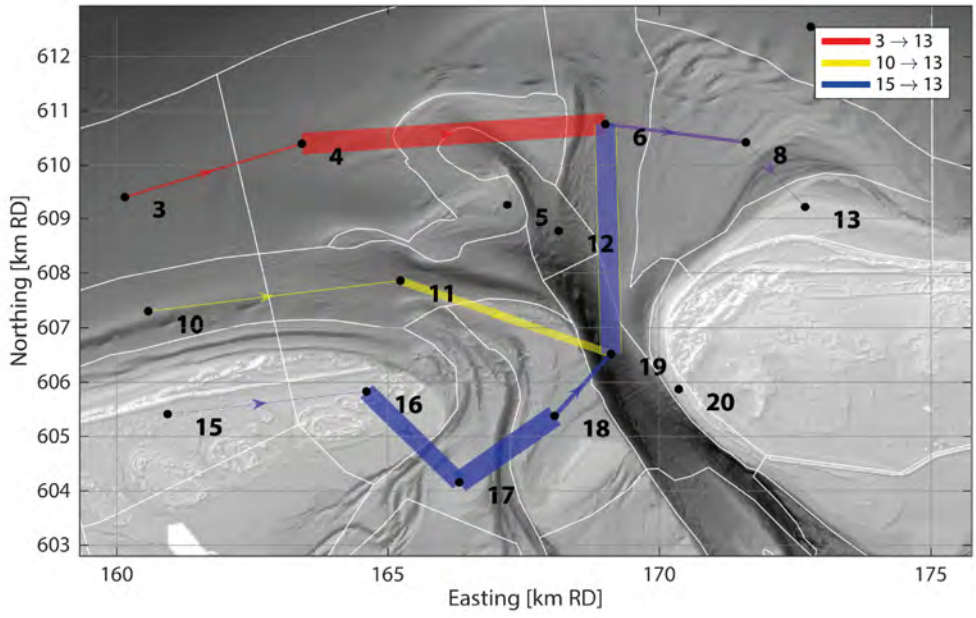

Figure 7.8: Shortest inlet bypassing pathway for different initial locations (Nodes 3, 10, & 15) on the updrift side of the inlet. Path “distance" is inversely proportional to sediment flux, such that stronger fluxes (indicated here by thicker lines) are effectively “shorter" topological distances. Sources closer to the updrift coastline (10, 15) are connected to the downdrift coast via the inlet, whereas the offshore source (3) is connected via the outer delta. Note that the underlying model presented here does not account for wave-driven bypassing

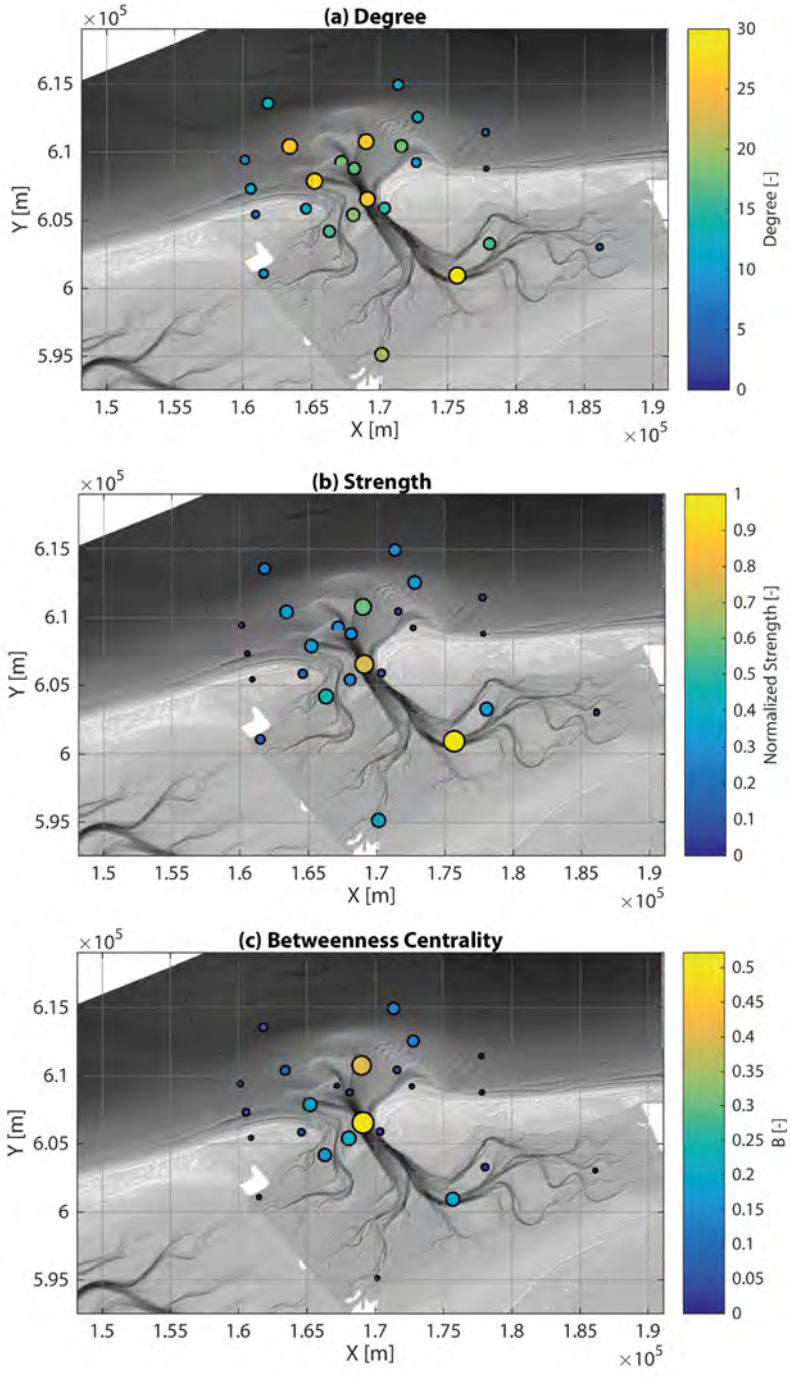

Figure 7.9: Connectivity metrics for individual nodes. (a) Total degree D (in-degree plus out-degree), which indicates the number of other nodes each node is connected to. Larger yellow dots indicate highly connected nodes and smaller blue dots indicate minimally-connected nodes. (b) Total strength S (in-strength plus out-strength) normalized by the node of maximum strength, which indicates the total sediment transported in and out of a given node. (c) Betweenness centrality, B, normalized by the total number of shortest pathways between nodes (n=625). B indicates the number of shortest pathways passing through a given node.

7.4. DISCUSSION

The sediment connectivity framework is a promising approach for analyzing coastal sediment transport pathways. Connectivity provides tools to quantify the dominant transport pathways for sediment originating from or leading to a particular location. Already well established in other disciplines, these techniques allow us to identify salient features of transport pathways that may be relevant for both fundamental understanding of a given coastal system, and for answering applied engineering questions. This methodology is generally applicable to coastal systems from beaches to estuaries to deltas, as long as detectable sediment exchange between different (sub) areas takes place. However, it would likely work best for systems where the sources and sinks are well posed. We demonstrated this by applying the approach to Ameland Inlet and addressing the example research questions posed in Figure 7.1. The analysis presented here is intended to demonstrate the novelty and usefulness of graph theory-based sediment connectivity for coastal applications, and to shine a light on the challenges which must still be addressed in order to apply the concept to its fullest potential.

Connectivity brings value to existing numerical coastal models by adding techniques in graph theory and network analysis to the “toolkit" available for interpreting sediment pathways from those models. Once sediment transport is represented in an adjacency matrix, then computing statistical metrics of connectivity using existing tools (e.g., *Csárdi and Nepusz* (2006); *Rubinov and Sporns* (2010); *Franz et al.* (2016)) is straightforward. These techniques can quantify spatial and temporal variations in sediment transport beyond just existing metrics like cumulative erosion and sedimentation patterns or mean transport fields. With connectivity, we have mathematical techniques for describing not just where sediment is going, but *which* sediment is going where. However it is more useful than Lagrangian modelling alone, because it tells us not only the history of sediment from a particular source, it tells us something about the interconnected coastal system as a whole.

There are many possible metrics for evaluating connectivity, although we believe that the ones presented in this study are the most useful for studying sediment pathways in coastal systems. In Figure 7.1, we raised six questions about sediment bypassing at tidal inlets which we can now answer using the connectivity analysis presented here.

1. Shortest-path analysis reveals that sediment bypassing routes on Ameland ebb-tidal delta vary depending on initial source, with offshore sources mainly bypassing around the outer delta, and nearshore sediment bypassing mainly via the inlet (Figure 7.8). This type of analysis could also be used to identify potential pathways for spreading of nourished or contaminated sediment.

2. Asymmetry in sediment connectivity between cells in the basin and on the adjacent coast reveals a net import of sediment (Figure 7.7). This type of information could be useful for coastal managers who wish to understand not just total sediment budgets, but also a more detailed breakdown of source and sink locations.

3. The network shows asymmetry for all sediment classes, suggesting that the system is characterized by non-zero net transports, and hence morphological change (Table 1). Examining the asymmetry like this can shed light on system-wide trends in net transport or recirculation.

4. The optimal location for a sand nourishment depends on its goal. To maximize spreading, sites like those in major channels with high degree and strength should be chosen (Figure 7.9). However, if slower dispersal is preferred, then a site with lower degree and strength should be chosen. The combination of this information with shortest-path analysis could be used to design nourishments which target a particular receptor.

5. Connectivity networks developed for finer sand ($100\mu m$) show greater connectivity throughout the model domain, whereas coarser sand ($400\mu m$) shows less connectivity, and primarily only in the main channels (Figure 7.6). These differences can be explained by spatial variations in hydrodynamic energy and local particle size distribution.

6. The Louvain modularity algorithm aggregates 25 geomorphic cells into five sediment-sharing communities (Figure 7.7). This approach could be also be used to objectively classify geomorphic cells from high-resolution input.

Future research on this topic should go beyond the application of generic connectivity metrics, and focus on the development of connectivity metrics specific to quantifying and analyzing coastal sediment transport.

It is widely acknowledged that identifying appropriate scales for analysis (both temporal and spatial) is still a huge challenge in quantifying connectivity (*Bracken et al.*, 2015; *Heckmann et al.*, 2018; *Keesstra et al.*, 2018; *Wohl et al.*, 2019). Here, we analyze connectivity using residual fluxes, since these fluxes correspond to long-term morphological evolution. However, future research on connectivity in tidal systems should investigate the influence of this choice in analysis timescale. Connectivity changes at different temporal and spatial scales, such that the choice of time or spatial scale considered will influence the connectivity observed. *Keesstra et al.* (2018) maintain that there is still “no satisfactory solution to the problem of scaling in water and sediment connectivity".

The sensitivity of connectivity to different choices of spatial units depends on the resolution of the schematization, (i.e., the size of the cells). With sufficiently fine resolution (small enough cells) the results will not be dependent on the exact manner of schematization. Two different schematizations would give different adjacency matrices, but they should give the same interpretation. However, for relatively coarse geomorphic cells, the schematization should influence the results more. Aggregation to large cells only makes sense if it is done with morphological knowledge (whether objectively via modularity and clustering algorithms (Section 7.2.3) or numerical model output, or subjectively based on expert judgment of geomorphologically meaningful units (Section 7.3.1)).

Furthermore, the issue of separating structural and functional connectivity is still unresolved in most disciplines using connectivity (*Turnbull et al.*, 2018). This problem is related to the time scaling issues described above, since eventually sediment fluxes modify morphology, and hence, structure. Although many geomorphological studies have examined structural connectivity and developed quantitative metrics for it, functional connectivity still needs to be better explored and quantified (*Najafi et al.*, 2021). *Heckmann et al.* (2018) advocate using models under varied forcing to examine the relationship between structural and functional connectivity and identify the critical timescales at which network structure is modified.

Tied to the separation of form and function is the definition of the fundamental unit of connectivity. Geomorphic cells defined based on structural criteria like bathymetry will shift from their original boundaries after sufficient fluxes of sediment modify the seabed, so how should they be defined over longer timescales? Multi-layer networks can be used to describe variations in network structure and functional connections through time, making them an ideal means for investigating these phenomena (*Thibaud et al.*, 2013; *Pilosof et al.*, 2017; *Tejedor et al.*, 2018b). Although these open questions present challenges to coastal researchers looking to apply connectivity, they also present opportunities: connectivity could be a useful approach for exploring sediment transport pathways at varying spatial and temporal scales. For instance, connectivity could be used to identify the timescales required for a coastal system to adapt to perturbations (e.g., a nourishment or coastal structure).

Recent advances in remote sensing, *in situ* measurements, and numerical modelling have created a wealth of data for coastal researchers (*Donchyts et al.*, 2016; *Ford and Dickson*, 2018; *Luijendijk et al.*, 2018; *Vos et al.*, 2019a). In this era of "big data," we need a standardized framework to integrate and compare the coastal sediment pathways derived from models and field data. Since it may be difficult to validate connectivity computed from a single model, this approach would allow multiple lines of evidence or modelled ensemble predictions to be integrated in a common framework (similarly to *Barnard et al.* (2013b)), increasing confidence in the predictions made. Future research should also assess the applicability of alternative modelling techniques (e.g., Lagrangian particle tracking (*Soulsby et al.* (2011); *MacDonald and Davies* (2007), Chapter 8) or directly computing connectivity from Eulerian transport fields) for connectivity analysis.

Connectivity is a useful approach for quantifying the transport of marine pollutants, (*Paris et al.*, 2013), including plastic particles (*van Sebille et al.*, 2019). By extension, the sediment connectivity approach presented here could be useful in applications of marine (plastic) pollution that interacts with the seabed (e.g., *Corcoran* (2015); *van Cauwenberghe et al.* (2015)).

Connectivity also distils complex systems into their basic essence in a visually effective manner (e.g., subway maps (*Derrible and Kennedy*, 2009), Figure 9.2). Furthermore, online visualization tools (e.g., Cytoscape (*Franz et al.*, 2016)) make it possible to develop interactive ways of visualizing connectivity, bringing tangible form to the often abstract concepts of sediment transport.[1] This also makes connectivity an attractive platform for communicating with stakeholders and the public (*Smetanová et al.*, 2018).

Phillips et al. (2015) note that connectivity analysis using graph theory "should certainly be included on the standard menu of relevant methods" for geoscientists. There are still major challenges associated with quantifying connectivity at varying spatiotemporal scales and making appropriate choices in schematizing and populating networks. However, further attention to these issues and the development of metrics and techniques specific to coastal systems could improve the method's usefulness and lead to new insights in coastal geoscience.

[1] For a (tragically) relevant example of the possibilities for visualization presented by connectivity, see this interactive tool for demonstrating the growth of a pandemic via international air travel: https://rocs.hu-berlin.de/project/viz-event-horizon/

7.5. CONCLUSIONS

Sediment connectivity quantifies how different locations are connected by sediment transport pathways. The concept of connectivity is well established in other disciplines, and here we use the example of Ameland Inlet to demonstrate its utility in coastal sediment transport settings. Graph theory-based sediment connectivity provides a powerful framework for identifying, analyzing, and interpreting sediment pathways in complex coastal systems.

By dividing a system into geomorphic cells and quantifying the transports between them, we can populate an adjacency matrix and network graph. In that form, existing techniques in graph theory and network analysis offer novel ways of quantifying coastal sediment transport, revealing patterns that may not be obvious with existing techniques. In the case of Ameland Inlet, density, asymmetry, and modularity are used to quantify sediment transport patterns at a system level. Other metrics like degree, strength, centrality, and shortest-path analysis are used to identify critical paths or locations within the system. These parameters give insight into natural coastal dynamics and are also useful for optimizing engineering interventions (e.g., sand nourishments).

The case study of Ameland Inlet shows the potential for connectivity to quantify sediment transport pathways in coastal systems. Quantifying connectivity across different spatial and temporal scales presents researchers with many challenges, but also many opportunities. We believe that this approach complements existing analysis techniques and that it will be valuable for addressing some of the urgent problems facing our coasts in the 21st century.

ACKNOWLEDGEMENTS

This work is part of the research programme 'Collaboration Program Water' with project number 14489 (SEAWAD), which is (partly) financed by NWO Domain Applied and Engineering Sciences. Special thanks to the Dutch Ministry of Infrastructure and Water Management (Rijkswaterstaat and Rijksrederij) for their ongoing support as part of the Kustgenese2.0 project. We also acknowledge the support of the USGS Coastal and Marine Hazards and Resources Program. We are grateful to Jaap Nienhuis, Alejandro Tejedor, an anonymous reviewer, Andrew Stevens, and Klaas Lenstra for their extensive, constructive feedback on this manuscript. Data archiving for this study is currently underway. Example model input files used in this study have been included as supplementary material here. The connectivity analysis in this study was carried out using the open-source Brain Connectivity Toolbox. Thank you to Matthew Hiatt for introducing us to the toolbox. Any use of trade, firm, or product names is for descriptive purposes only and does not imply endorsement by the U.S. Government.


SEDTRAILS
A Tool for Investigating Sediment Connectivity


Dear Reader,
Un bonjour de Bretagne!
Hello again!
Nederland
Nederland
Greetings from sunny Santa Cruz!
We are pretty excited about sediment connectivi-
ty, but want to use this method faster and in
greater detail. To do this, we developed a model
(SedTRAILS) that lets us follow sediment parti-
cles around, sort of like we did with the green
sand in Chapter 6. I was lucky to visit the USGS
in California to spend some time working on it.
SedTRAILS greatly expands the way we can
visualize and interpret sediment pathways, and we
have a lot of ideas about how we can make it
even better in the future.
Stuart
CALIFORNIA
CALIFORNIA
CALIFORNIA
Delft University of
Technology
Stevinweg 1
2628 CN Delft

8

LAGRANGIAN SEDIMENT TRANSPORT MODELLING AS A TOOL FOR INVESTIGATING COASTAL CONNECTIVITY

KEY POINTS:

- We used a Lagrangian sediment transport model and visualization tool (SedTRAILS) to estimate sediment pathways and populate a connectivity network at Ameland Inlet.
- The model enables the efficient and high-resolution computation of sediment transport pathways.
- This approach also opens the door to a variety of analysis techniques which can be used to better quantify coastal sediment pathways in future studies

This chapter has been presented as part of *Coastal Dynamics 2021: Proceedings of the 8th International Conference*:

Pearson, S.G., Elias, E.P., van Ormondt, M., Roelvink, F., Lambregts, P., Wang, Z.B., van Prooijen, B.C. (2021). Lagrangian Sediment Transport Modelling as a Tool for Investigating Coastal Connectivity. *Coastal Dynamics 2021: Proceedings of the 8th International Conference*, June 28 - July 2, 2021, Delft, the Netherlands.

THE conceptual framework of sediment connectivity developed in the previous chapter has the potential to expand our understanding of coastal systems and to address practical management problems there. Lagrangian particle tracking has been widely used to assess connectivity in the context of oceanography and marine ecology, because such models record the complete history of a particle's trajectory, not just its start and end points. This approach permits a faster and more detailed analysis of sediment connectivity than existing Eulerian approaches (e.g., Chapter 7). There is thus a need for Lagrangian sediment particle tracking tools tailored to predicting sediment transport pathways and determining connectivity of complex coastal systems. In this chapter, we present SedTRAILS, a modelling tool that aims to meet these needs.

ABSTRACT

To predict how coastal and estuarine systems evolve, we need to better understand the pathways that sediment takes from source through temporary storage areas to sink. There is thus a need for numerical models tailored to predicting sediment transport pathways and determining connectivity of complex coastal systems. To meet this need, we developed a Lagrangian sediment transport model, SedTRAILS (Sediment TRAnsport vIsualization & Lagrangian Simulator). SedTRAILS enables the efficient and high-resolution computation of sediment transport pathways, which makes it ideally suited for the development of connectivity networks. We demonstrate its application at Ameland Inlet in the Netherlands. Connectivity provides quantitative metrics for interpreting the results of the model and answering questions about sediment exchange or key transport pathways. This approach improves our understanding of complex coastal and estuarine systems and can aid in coastal management (e.g., nourishment planning). It also allows us to visualize the results of complex numerical model simulations in an intuitive way, opening the door to better communication with non-scientific audiences and more informed decision-making.

8.1. INTRODUCTION

ESTUARIES and coasts can be conceptualized as connected networks of water and sediment fluxes. These dynamic geomorphic systems are governed by waves, tides, wind, and river input, and evolve according to complex nonlinear transport processes. To predict their evolution, we need to better understand the pathways that sediment takes from source through temporary storage areas to sink. Knowledge of these pathways is essential for predicting the response of such systems to climate change impacts or human interventions (e.g., dredging and nourishment). The conceptual framework of sediment connectivity has the potential to expand our system understanding and address practical coastal management problems (Chapter 7).

Connectivity provides a structured framework for analyzing these sediment pathways, schematizing the system as a series of geomorphic cells or nodes, and the sediment fluxes between those nodes as links (*Heckmann et al.*, 2015). Once organized in this fashion, the resulting network can be expressed algebraically as an adjacency matrix: sediment moving from a given source to different receptors. There is a wealth of pre-existing statistical tools and techniques that can be used to interpret the data once it is in this form, drawing on developments in other scientific disciplines (*Newman*, 2018; *Rubinov and Sporns*, 2010). Lagrangian flow networks have been increasingly used to analyze flow and transport pathways in oceanographic and geophysical applications (*Ser-Giacomi et al.*, 2015; *Padberg-Gehle and Schneide*, 2017; *Reijnders et al.*, 2021). However, this approach has not yet been adopted to analyze coastal or estuarine sediment transport, and requires a multitude of field measurements or numerical model simulations.

Lagrangian particle tracking has been widely used to assess connectivity in the context of oceanography and marine ecology (*Hufnagl et al.*, 2016; *van Sebille et al.*, 2018), because the models record the complete history of a particle's trajectory, not only its start and end points. Particle tracking models are also relatively fast and lend themselves well to parallel computing (*Paris et al.*, 2013). This approach thus permits a faster and more detailed analysis of sediment connectivity than existing Eulerian approaches (e.g., Chapter 7). Although several Lagrangian sediment transport models have been developed (e.g., *MacDonald and Davies* (2007); *Soulsby et al.* (2011)), they have not been used to support connectivity studies. Hence, there is a need for Lagrangian sediment particle tracking tools tailored to predicting sediment transport pathways and determining connectivity of complex coastal systems.

To meet this need, we developed a Lagrangian sediment transport model, SedTRAILS (**Sed**iment **TRA**nsport v**I**sualization & **L**agrangian **S**imulator) and used it to develop a sediment connectivity network. Our approach provides new analytical techniques for distilling relevant patterns from the chaotic, spaghetti-like network of sediment pathways that often characterize estuarine and coastal systems. We demonstrate a proof of concept for our approach by applying it to a case study of Ameland Inlet in the Netherlands, and provide an outlook for future research opportunities using these tools.

8.2. METHODOLOGY

Our approach for determining sediment connectivity has four main steps (Figure 8.1): (1) Simulating hydrodynamics and (2) sediment transport with an Eulerian model; (3) Estimating Lagrangian sediment transport pathways using SedTRAILS; and (4) deriving a sediment

connectivity network from those pathways.

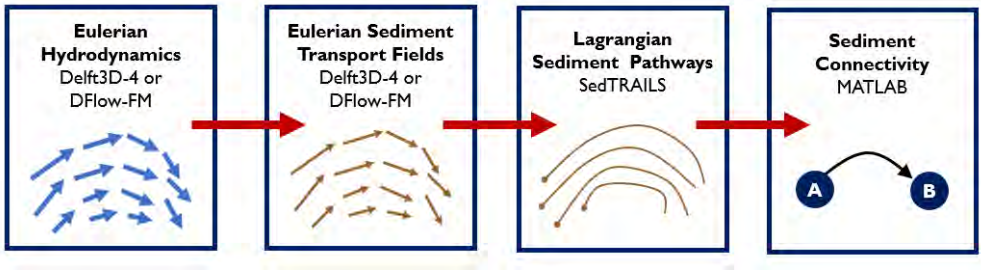

Figure 8.1: Flow chart of the modelling methodology, beginning with an Eulerian hydrodynamic and sedi-ment transport model. Lagrangian sediment pathways are then computed using SedTRAILS, which can then be used as input for connectivity analysis.

8.2.1. EULERIAN MODEL

A 2D hydrodynamic and morphostatic sediment transport Delft3D model (*Lesser et al.*, 2004) formed the basis of our analysis. The model domain was centered on Ameland Inlet and ex-tends to the adjacent Vlie and Frisian Inlets to capture inter-basin flows within the Wadden Sea. The grid resolution ranges from 50 m in Ameland Inlet to 350 m at the boundaries. The bathymetry was based on surveys from 2017, with data from 2008-2017 used to fill gaps. The model forcing was derived from tides, wind, and wave measurements spanning the entire year 2017. A more detailed description of the model set up is provided in *Nederhoff et al.* (2019).

To advect particles, we derived sediment velocity fields from suspended and bed load flux fields divided by a constant scaling factor. Diffusion was incorporated using a random displacement at each timestep. Precomputing the sediment transport velocity fields to decouple them from the sediment trajectory computation led to efficient run times.

8

8.2.2. LAGRANGIAN MODEL

We adapted the Lagrangian model described by *Storlazzi et al.* (2017) and *de Vries* (2016) to advect particles using sediment transport velocities computed in the previous step. Five hundred geomorphic cells were defined using a k-means algorithm to cluster the bathymetry, weighted by XY position and bed elevation. This ensured that cells were distributed evenly throughout the domain, in a way that prioritizes higher density for areas with larger gradients in bathymetry (Figure 8.2a). The centroids of these cells were used as the initial sources for the SedTRAILS simulations. Particles trajectories were then computed for each source using forcing corresponding to the entire year 2017.

8.2.3. DERIVATION AND ANALYSIS OF CONNECTIVITY

To estimate connectivity and compile the results into a graphical network, we started by considering the trajectory of particles from a single source (i). The position of every particle was recorded at each subsequent timestep of the model (t_{total}). A given particle may pass through several other receptor cells (j) during the simulation, and the number of timesteps it spends in each of those cells is effectively a "residence time" ($t_{r,j}$). The connectivity be-

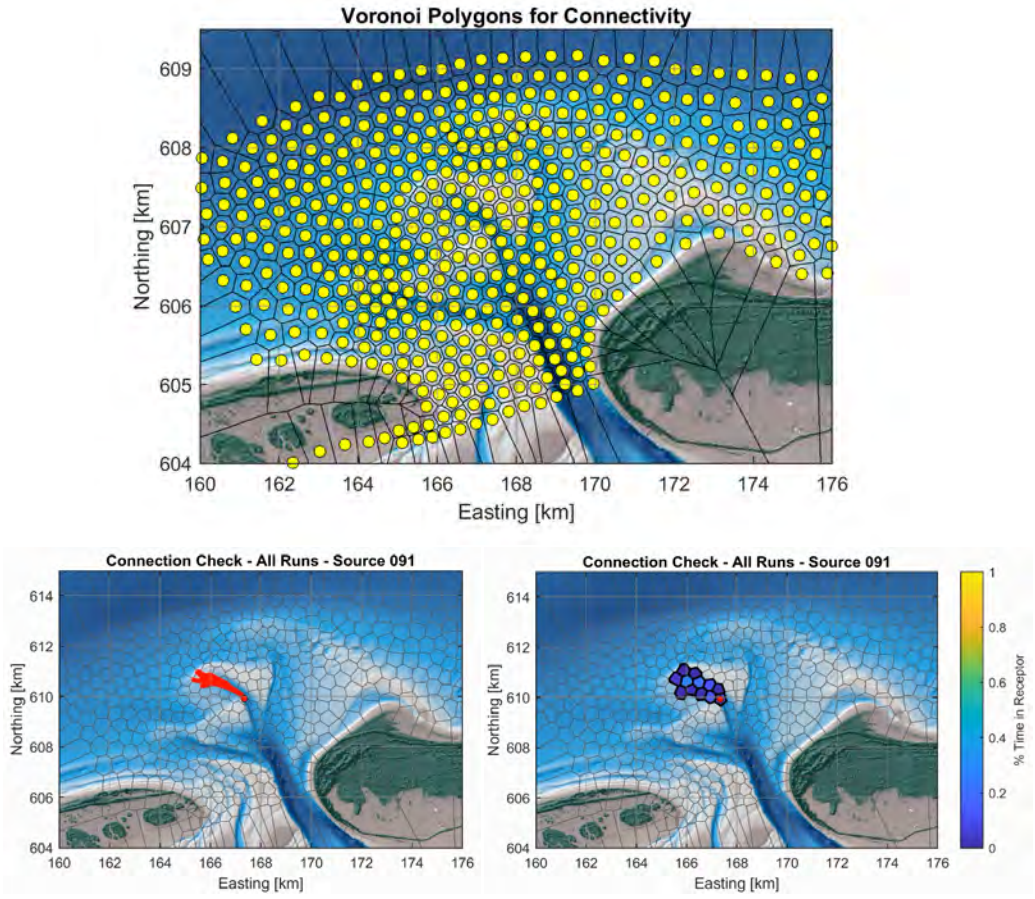

Figure 8.2: (a) Source locations for all particles, as determined via k-means cluster analysis of the bathymetry. Voronoi polygons are then drawn around each source to derive the receptor polygons. (b) Example of particle positions computed by SedTRAILS for Source 091. Particles originate at the large red and black circle, then travel in a northwesterly direction to the outer lobe of the ebb-tidal delta, passing through several geomorphic cells on its way. (c) Example of tabulated connectivity between Source 091 and its receptors. The number of particles $t_{r,j}$ in each receptor cell j is counted and divided by the total number of particles t_{total} under consideration. Since a single particle is released at the start of the simulation and its position stored at each timestep, the colour of each receptor cell thus corresponds to the percentage of a given particle's total lifespan spent in each cell. For example, if a particle spends 25 out of 500 timesteps in a cell, that receptor cell will have a connectivity C_{ij} of 0.05.

tween a given source (i) and a given receptor (j) was thus calculated as $C_{ij} = t_{r,j}/t_{total}$. For example, the sediment pathways and resulting connectivity for a single source are depicted in Figure 8.2b and c. This calculation was then repeated for each of the 500 sources.

The matrix given by C_{ij} for all i and j is known as the adjacency matrix (Figure 4a). A column j in the matrix corresponds to all the different sources i contributing to a particular receptor j. For example, sediment originating in Cell 91 ($C_{091,j}$) and travelling to all connected receptors j is indicated by the red dots in Figure 4a.

This matrix can also be represented as a network diagram, where each source or receptor be-comes a point on a map connected to one another by links. For example, we can visualize the connections from Node 91 to its receptors (given by the red dots in Figure 8.4a) as a series of red arrows in Figure 8.4b. By drawing the connections originating from all 500 nodes in the network, we arrived at the complete network diagram in Figure 8.4b. Once the network was compiled, we used connectivity metrics such as degree and strength to describe individual nodes, as well as shortest-pathway analysis to characterize transport across the entire system (Chapter 7).

8.3. RESULTS

8.3.1. SEDIMENT PATHWAYS

We first considered the transport pathways of sediment originating from each of the 500 sources across the ebb-tidal delta (Figure 8.3). Key patterns included (i) bypassing via the inlet; (ii) transport along the outer delta; (iii) pathways along the main ebb channel; (iv) recirculation at several locations. To unravel key patterns in the spaghetti-like trajectories, we then computed connectivity.

8.3.2. NETWORK ANALYSIS

In addition to the patterns visible in the SedTRAILS trajectories (Figure 8.3), the transport network (Figure 8.4b) makes several trends apparent:

(A) The network is most densely connected on the ebb shoals, Boschplaat, and tip of the main ebb channel (Akkepollegat). These are areas with strong tidal currents and/or strong wave forcing.

(B) The network shows a general eastward direction in its connections, which matches what we expect from our understanding of both the hydrodynamic forcing and historical changes to the inlet (*Elias et al.* (2019); *Van Prooijen et al.* (2020), Chapter 3).

(C) Sheltered areas on the Bornrif platform and on the Wadden Sea side of Terschelling, or deeper areas in the offshore corners of the domain are completely disconnected from the rest of the system. The low connectivity of this morphologically active region (c.f., *Elias et al.* (2019)) is likely explained by the model schematization, forcing, and timescale applied here.

(D) There appears to be little cross-channel connectivity in the main Borndiep channel, although this may be partly a limitation of the 2D model.

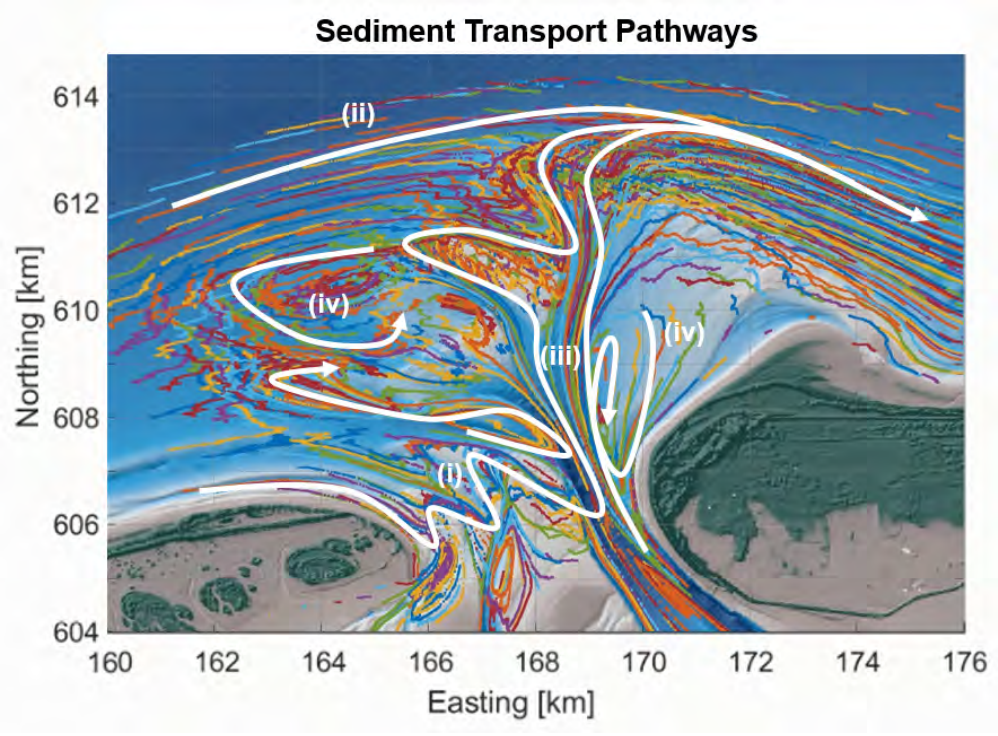

Figure 8.3: Sediment pathways derived from SedTRAILS. Each colour indicates a sediment transport pathway originating from a different source. Main pathways include (i) inlet bypassing, (ii) transport along the outer delta, (iii) transport through the main ebb channel, and (iv) recirculation.

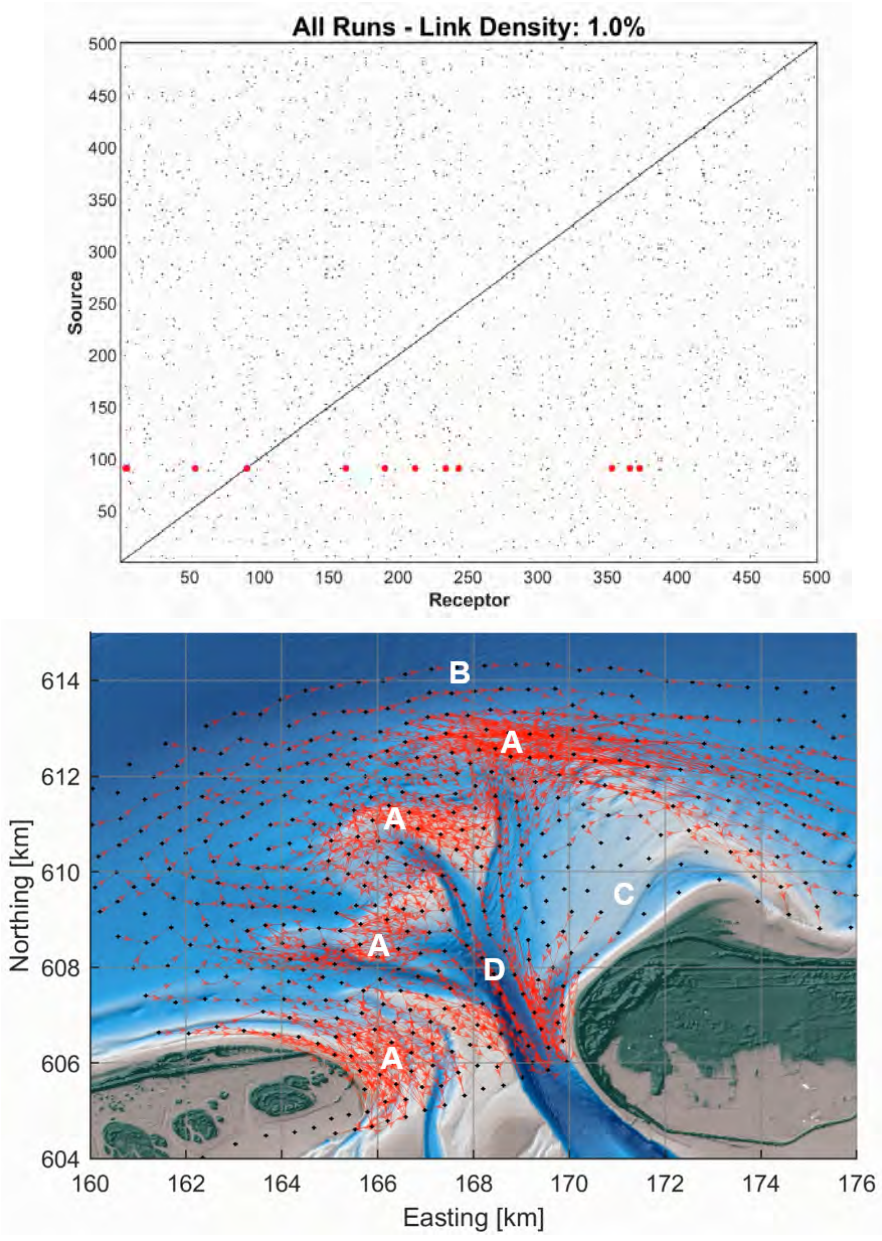

Figure 8.4: (a) Adjacency matrix for all timesteps of all 2017 scenarios. Each point on the plot is representative of a connection from source i to receptor j. The central diagonal denotes self-self interactions, which are particles that remain in or return to their source. As a demonstration, connections from Source 091 to all other receptors are highlighted in red. Link Density indicates the fraction of actual connections out of all possible connections. (b) Network diagram for all connections in the network. Red lines indicate the connection between two nodes, with their thickness implying the strength of the connection, and the arrow indicating the direction. White letters correspond to key areas described in the main text.

8.3.3. NODE ANALYSIS

The characteristics of individual nodes in the network provide useful information about local sediment transport behavior. First we considered degree, which is the number of nodes that a given node is connected to, in a binary fashion, irrespective of how many particles are passing through (Figure 8.5a). As such, degree highlights nodes that have a more diverse range of connections than the strength plot (Figure 8.5b). Degree can be considered as an indicator of mixing, comparable to the Finite-Time Lyapunov Exponent (FTLE) (*Ser-Giacomi et al.*, 2015). The main channels may be "busier", but the distal end of the ebb shoals have a higher degree be-cause particles reaching the end of the shoals come from many different origins: particles from upstream in the channel and beyond, locally resuspended material from more immediate neighbours, and also material being bypassed from updrift. It is thus a convergent zone of intense sediment mixing from many different sources.

Secondly, we considered node strength, which in our case corresponded to the number of particles passing in and out of a given receptor – highlighting the "busiest" receptors (Figure 8.5). In general, these areas corresponded to the channels and tips of shoals.

8.3.4. DOMINANT BYPASSING PATHWAYS

One of the most valuable features of network theory is that it allows us to consider connected pathways across a network as a whole. Let us consider the distance between two nodes to be the inverse of its weight (a higher weight indicates a larger flux and stronger connection, so the "distance" between those points is shorter). We can then derive a matrix of the shortest (although not necessarily fastest) path along the network between any two nodes. This matrix can then be queried to find relevant pathways, such as the main bypassing routes across or around the inlet.[1]

Here we consider the shortest bypassing routes from a transect seaward of Terschelling to a point on Ameland (Figure 8.6). This map was produced using the network and does not show actual particle trajectories (none of the particles ever travelled the entire width of the inlet during the simulation; rather, it shows the most efficient paths through the network by linking all of the particle trajectories together). The patterns here are similar to those presented in Figure 7.8, but with 500 nodes rather than 25, so the detail of the pathways is much greater.

Closer to shore, "channel bypassing" via the inlet dominates, whereas sediment originating seaward of the outer bar bypasses via the outer delta. Presumably, tidal currents are driving at least the first half of this journey, although it is likely that waves play a greater role on the shallower platform to the east. Notably, the shortest pathways avoid the morphodynamically active shoals on the western side of the delta, since the particle trajectories there are more convoluted and feature prominent recirculation zones (Figure 8.3).

[1] For a fascinating and inspiring application of this approach to identifying migratory routes of birds based on global wind fields, the reader is encouraged to investigate *Cheshire and Uberti* (2017) and *Kranstauber et al.* (2015).

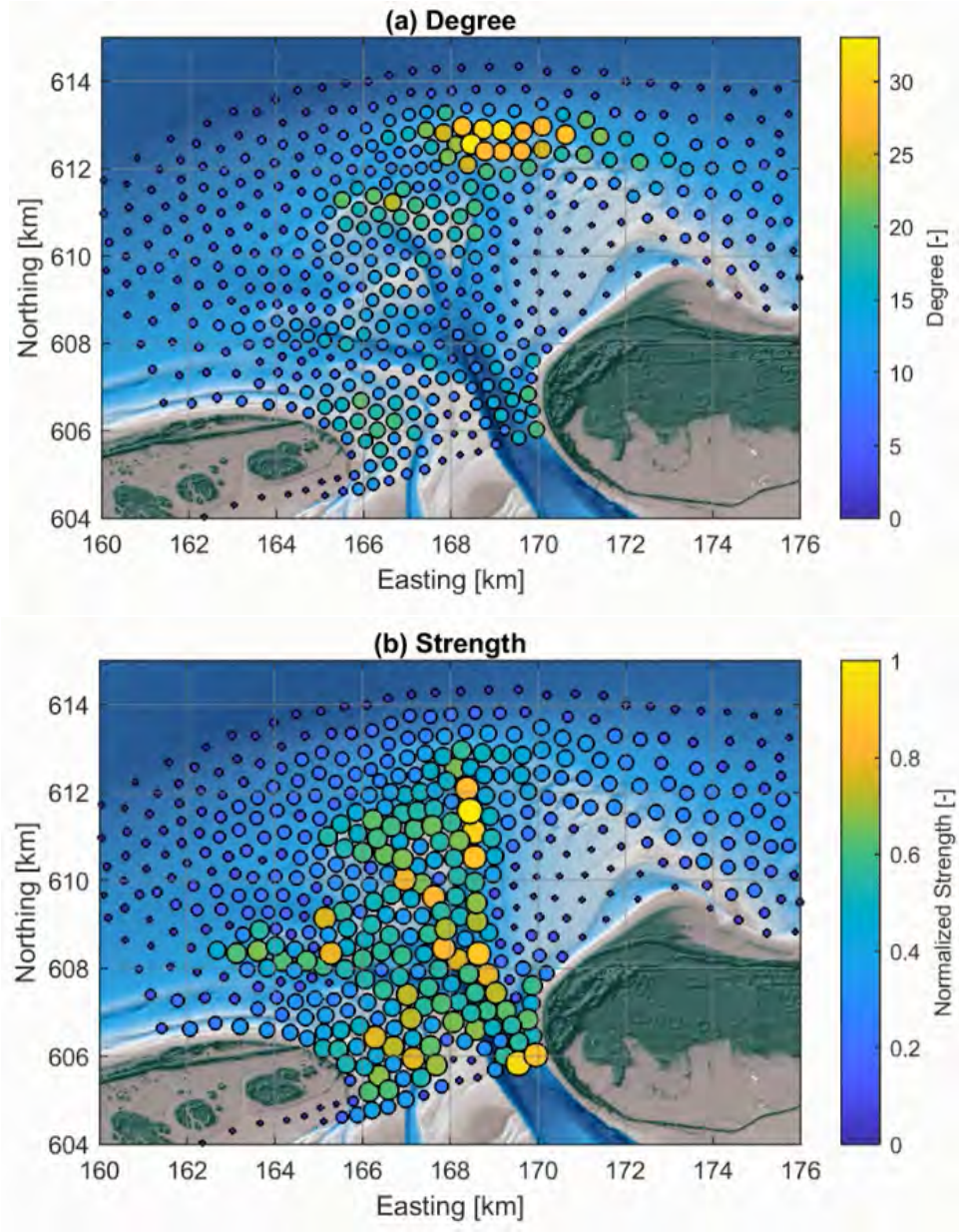

Figure 8.5: (a) Degree of each node in the network. Lighter colours and larger dots indicate that more other nodes are connected to a given node, either as sources or receptors. (b) Strength of each node in the network. Lighter colours and larger dots indicate that more particles are passing into or out of a given node.

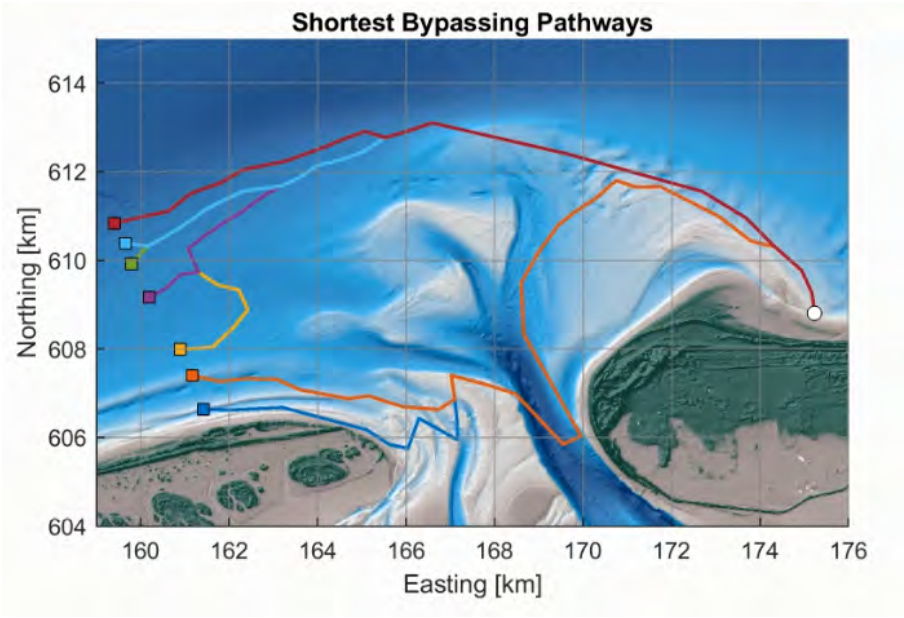

Figure 8.6: Shortest (dominant) bypassing pathways from 7 nodes offshore of Terschelling (the updrift side of the inlet) to a single point on the (downdrift) coast of Ameland.

8.4. DISCUSSION

SedTRAILS enables the fast, high-resolution mapping of sediment transport pathways and connectivity in coastal environments. This approach provides new quantitative and qualitative insights into sediment pathways in complex settings like tidal inlets. The visualizations pro-duced improve our understanding of the system dynamics and provide us with new tools for comparing models and measured data. The connectivity patterns derived here are consistent with previous studies of Ameland Inlet (*Elias et al.* (2019), Chapter 7) and with modelled and measured pathways observed at other similar sites (*Son et al.*, 2011; *Herrling and Winter*, 2018). Furthermore, these metrics can be used to address practical coastal management questions. For instance, the path-finding approach is useful for planning a nourishment or trying to determine the potential for sand to reach a specific location.

Having demonstrated a proof of concept for SedTRAILS here, the door is now open to many new possible analyses and improvements. The most essential next step is to improve the transport velocity formulations used to advect particles. SedTRAILS in its present form visualizes potential sediment trajectories but does not directly estimate volumes transported or the timescales of transport. The sediment transport velocity can be better derived from a correction based on sediment concentration (e.g., *Soulsby et al.* (2011)). Processes like burial and re-emergence are also not accounted for. After these features are implemented, validation using sediment tracers (Chapter 6) or geochronology approaches like Optically Stimulated Luminescence (*Reimann et al.*, 2015) will be used to achieve realistic sediment migration speeds.

The Lagrangian nature of SedTRAILS permits the analysis of chaotic stirring and Lagrangian coherent structures (LCS), both of which determine mixing and barriers to trans-

port in the context of coastal hydrodynamics (*Ridderinkhof and Zimmerman*, 1992; *Kuitenbrouwer et al.*, 2018). In conjunction with the development of new connectivity metrics, this sets the stage for a suite of new quantitative analysis techniques for sediment transport pathways. The speed of our approach also lends itself well to sensitivity testing and ensemble modelling to quantify predictive uncertainty, if a schematized wave climate and morphological tide are used. SedTRAILS has already been applied in this manner to sites in the Netherlands (*Bult*, 2021; *Lambregts*, 2021), Canada (*Meijers*, 2021), and USA (*Stevens et al.*, 2020), and can easily be expanded to other locations.

8.5. CONCLUSIONS

We used a Lagrangian sediment transport model and visualization tool (SedTRAILS) to estimate sediment transport pathways and populate a connectivity network at Ameland inlet in the Netherlands. This model enables the efficient and high-resolution computation of sediment transport pathways, which makes it ideally suited for the development of connectivity networks. Network-derived metrics like node degree and strength give insight into critical locations for sediment exchange. We can also determine the dominant transport pathways in the system by considering the network as a whole and not just individual particle paths. Together, these tools improve our understanding of complex coastal and estuarine systems and can be used to address practical coastal management questions. This approach also opens the door to a variety of analytical techniques (e.g., LCS analysis) which can be used to better quantify coastal sediment pathways in future studies.

ACKNOWLEDGEMENTS

This work is part of the research programme 'Collaboration Program Water' with project number 14489 (SEAWAD), which is (partly) financed by NWO Domain Applied and Engineering Sciences. Special thanks to the Dutch Ministry of Infrastructure and Water Management (Rijkswaterstaat and Rijksrederij) for their ongoing support as part of the Kustgenese2.0 project. We also thank Andrew Stevens for his support in the development and application of SedTRAILS.


SYNTHESIS


Dear Reader,
Un bonjour de Bretagne!
Hello again!
Santa Cruz!
Dear Reader,
How to summarize five years of work on the back of a postcard? We didn't have the right tools to answer our questions, so we had to develop them: new mapping techniques, an approach for "hearing" sand and "seeing" mud, techniques to follow individual grains of sand around, a new way of thinking about sediment pathways, and a computer model for predicting those paths. These helped us learn a lot about ebb-tidal deltas and how sand moves around on them, and provide useful tools and knowledge for managing our coasts.
Stuart
Nederland
Delft University of
Technology
Stevinweg 1
2628 CN Delft

9

SYNTHESIS

KEY POINTS:

- We developed new approaches for analyzing field measurements of physical processes on ebb-tidal deltas, including stratigraphic and polar morphodynamic analysis, the Sediment Composition Index (SCI), and dual-signature tracer analysis techniques.
- We then developed a conceptual framework (sediment connectivity) and process-based modelling approach (SedTRAILS) for analyzing emergent sediment transport patterns at scales relevant to coastal management.
- The improved system understanding of ebb-tidal deltas gained from these approaches and the availability of these techniques sets the stage for promising future research.

9.1. PROJECT SUMMARY

ENSURING the long-term safety and ecological health of vulnerable barrier coast systems like the Dutch Wadden Islands and Sea in the face of threats like sea level rise requires the maintenance of their sediment balance. A possible solution is the strategic nourishment of tidal inlets and ebb-tidal deltas, but the sediment dynamics in these locations are complex, and though conceptually understood, they remain poorly quantified. In order to nourish these environments, we need improved knowledge of sediment exchange between the Wadden Sea and North Sea, with a specific focus on sediment pathways on ebb-tidal deltas there. Furthermore, we need tools and techniques to analyze and predict those pathways, in order to provide practical knowledge for coastal management.

The primary goal of this dissertation was to answer, "*How can we identify and quantify the pathways that sediment takes on an ebb-tidal delta?*" There is no simple answer to this question, but it steered the direction of our inquiry. In response, we developed new tools and techniques for analyzing a combination of field measurements and numerical models.

To investigate sediment pathways, we first considered in Chapters 2 & 3 how ebb-tidal delta morphology and grain size distribution vary in space and time at the scale of Ameland Inlet ($\mathcal{O}(100m - 10km)$). Ameland ebb-tidal delta is a highly dynamic system characterized by clockwise shoal and channel migration, from the updrift island of Terschelling to the downdrift island of Ameland. The majority of shoals in the active part of the ETD are continuously reworked on timescales of less than 10 years. These actively-migrating shoals move across a more stable and well-preserved underlying platform at a rate of approximately 15^o/*decade*. Sediment in Ameland ebb-tidal delta largely consists of well-sorted, fine sand, with muddier material found in the distal regions offshore. There is a clear clockwise fining trend and reduction in grain size variation, behaviour consistent with the clockwise migration of sediment around the delta.

Next, we examined how suspended sediment transport on the ebb-tidal delta varies as a function of grain size ($\mathcal{O}(1 - 100\mu m)$) and under the influence of different hydrodynamic forcings (Chapters 4 & 5). Here we zoomed in to the scale of the physical processes acting at a point on the delta over a period of several weeks. Although the sediment within Ameland ebb-tidal delta is mainly sand, field measurements reveal the significant presence of muddy sediment travelling in suspension. At the timescale of individual tidal cycles, sand is resuspended under more energetic hydrodynamic conditions (ebb and flood tide or during storms), while mud is advected back and forth from the Wadden Sea, dominating suspension in calmer conditions or at slack water. At weekly to monthly timescales the sediment composition dynamics are largely explained by the fortnightly spring-neap cycle, with increased variation at spring. Large storms also tend to elevate fine sediment concentrations for several days afterwards.

In this dissertation, we considered a variety of field measurements, including Eulerian and Lagrangian techniques. These inform our understanding of sediment transport pathways by providing different but complementary perspectives on the same physical processes. For instance, the Eulerian measurements in Chapters 4 & 5 show that at a single point on the delta, suspended particle size varies in time as a function of the hydrodynamic forcing. Adopting a Lagrangian viewpoint in Chapter 6, the consequences of this grain size-selective transport were directly visible in the particle size distribution and spatial variation of recovered tracer particles. The Lagrangian drifter experiment (Chapter 2) confirms the spatial variations in the flow field that our numerical models show and that observed bathy-

metric changes imply. They also give a larger-scale view of the velocity field ($\mathcal{O}(10km)$) than the Eulerian measurements at a single point, albeit for a single tidal cycle (~ 12 hours) instead of for 40 days. By extending the spatial scale (Lagrangian) and timescale (Eulerian) combining these measurements paint a more complete picture of the ebb-tidal delta dynamics in space and time than either technique in isolation.

Collectively, these analyses of the physical processes shaping Ameland ebb-tidal delta give us important insights into how the system works at spatial scales ranging from grain size ($\mathcal{O}(1-100\mu m)$) up to the entire delta ($\mathcal{O}(10km)$), and timescales ranging from minutes to decades. By understanding the morphodynamics of the ebb-tidal delta in the past and present, we build a stronger basis for predict its behaviour in the future. Our findings for Ameland inlet are also relevant for other similar sites around the world.

In Chapter 7, we developed an approach to systematically manage and quantitatively interpret complex datasets of coastal sediment pathways. Sediment connectivity using graph theory provides a quantitative framework for analyzing sediment transport pathways by decomposing a complex coastal system into a network of nodes and links. This approach shows that system connectivity is a clear function of grain size, and identifies major bypassing routes across the inlet. Most importantly, connectivity provides a means of quantifying and understanding the large-scale sediment transport patterns that emerge upward from small-scale processes, rather than aggregating these processes from the top down.

To make another step towards predicting sediment transport pathways in the future, we advanced a Lagrangian sediment transport model, SedTRAILS (Chapter 8). Lagrangian sediment transport modelling provides an efficient means of predicting and visualizing sediment pathways. It is especially powerful when placed in the connectivity framework, since that opens the door to many useful analytical techniques that can examine emergent patterns at scales relevant for coastal management. A key advantage of SedTRAILS is that it presents patterns which are more intuitively analyzed than conventional process-based model output (i.e., vector fields). This enables users to squeeze more information out of the same model, while also making it easier to communicate the results with stakeholders and non-scientific audiences.

In the remainder of this chapter, we adopt elements of the Theory of Change (*NWO*, 2019) to describe the impacts of this work. The research activities carried out in the course of this project lead to output (tools, techniques, and knowledge). The immediate outcome is the application of these outputs in research and consulting contexts. We then consider potential pathways towards scientific and societal impact, as well as opportunities for new research inspired by this work, and finish by presenting a wider outlook.

9.2. OUTPUT

9.2.1. TOOLS & TECHNIQUES

Ebb-tidal deltas are highly complex environments, and in the course of this research it was found that answering even basic questions about their sediment pathways first required the development of new tools and techniques:

1. **Stratigraphic and Polar Mapping Technique**
   Developed a novel approach to analyze high-resolution bathymetry of tidal inlets and create a stratigraphic model (Chapter 3).

2. **Sediment Composition Index (SCI)**
   Derived a new technique for estimating suspended sediment composition (SCI) by combining optical and acoustic backscatter measurements (Chapter 5).
3. **Dual-Signature Tracer Analysis Techniques**
   Optimized recovery and analysis techniques for fluorescent-ferrimagnetic sediment tracers in energetic ebb-tidal delta environments and provided lessons learned for practical application (Chapter 6).
4. **Sediment Connectivity Framework**
   Established a novel graph theory-based conceptual framework for analyzing and visualizing coastal sediment transport pathways (Chapter 7).
5. **Sediment TRAnsport vIsualization and Lagrangian Simulator (SedTRAILS)**
   Advanced a new modelling approach for visualizing and simulating sediment transport pathways (SedTRAILS) (Chapter 8).

9.2.2. KNOWLEDGE

The tools and techniques described above have yielded new knowledge and insights into the morphodynamics and sediment transport pathways of Ameland ebb-tidal delta, expanding our system understanding. In addition to the findings outlined in each of the previous chapters, several key concepts emerged from our analysis, drawing on multiple lines of evidence including literature, field and laboratory measurements, and numerical model output:

Key Sediment Transport Pathways

A central finding of this research has been the delineation of key sediment pathways on Ameland ebb-tidal delta (Figure 9.1). These pathways emerge on the scale of the ebb-tidal delta at timescales ranging from months to decades:

- In general, sediment migrates in a net clockwise (eastward) direction around the ebb-tidal delta, from the updrift island of Terschelling to the downdrift island of Ameland. This coincides with both the main direction of littoral drift and the dominant tidal currents. The clockwise motion is indicated in field measurements by the migration of shoals (Chapter 3) and fining of sediment (Chapter 2), and in numerical model results (Chapter 7 & 8).
- The western half of the delta is characterized by a complex network of sediment pathways. Pathways into the inlet depend on the initial cross-shore position on the updrift coast (Figures 2.11 & 8.3). From the inlet, sediment fans out into several ebb-chutes and channels before depositing in shoals and lobes. Sediment then moves clockwise along the ebb-lobes via wave-induced transport, gradually making its way to the Ameland coast. An important observation is the apparent barrier to transport down the centre of the Westgat channel: the majority of sediment located clockwise of this point does not return to the inlet.
- Conversely, the eastern half of the delta shows much simpler transport pathways, with the majority of bypassing sediment converging at the distal lobe of the delta and passing southeast towards Ameland. This pattern is shown numerically (Chapter 7 & 8) and is corroborated in the field by the migration, accumulation, and attachment of swash bars across the Bornrif platform (Chapter 3). Recirculation of sediment back towards the inlet is also visible here.

- Transport pathways were found to be grain size dependent (Chapter 7). Finer sediment exhibits a much higher density of pathways across the entire inlet and delta, whereas coarser sediment is mainly confined to the more energetic channels.
- A point further reinforced by this study was the difference between net and gross sediment transport pathways. The net eastward transport of sediment over annual to centennial timescales is confirmed by the morphological and sedimentological measurements in Chapters 2 and 3, but we see much more chaotic gross transport patterns at daily timescales in the tracer data (Chapter 6).

These findings are also supported by modelling of *Bak* (2017) and *Lambregts* (2021).

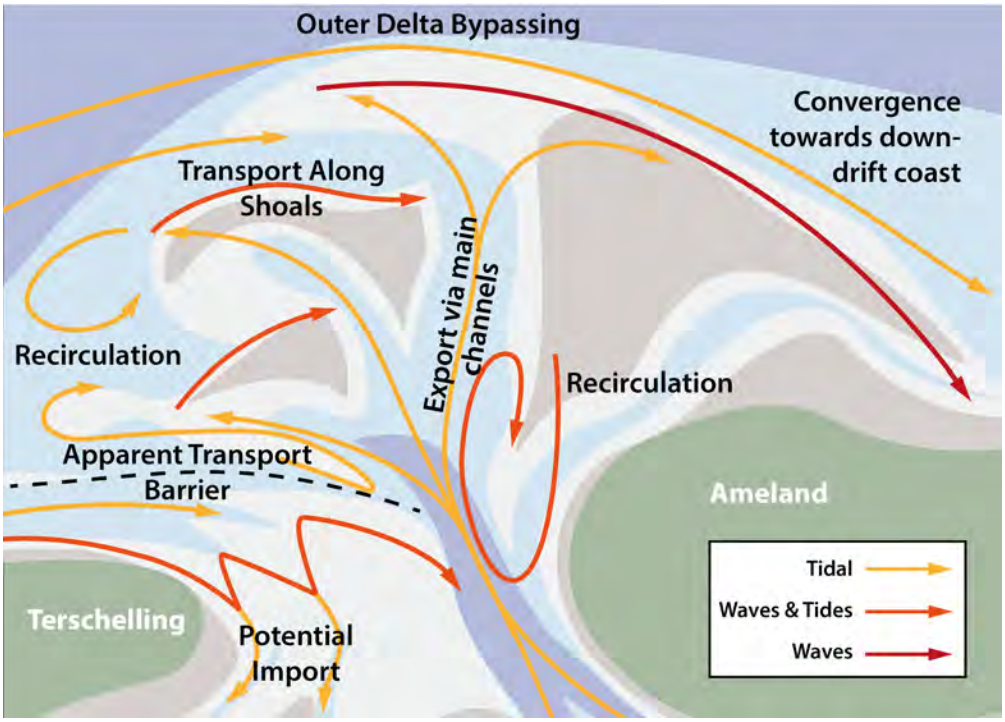

Figure 9.1: Overview of main sediment pathways on Ameland ebb-tidal delta circa 2017. Broadly speaking, sediment travels clockwise around the inlet from Terschelling to Ameland, although it may also be imported into the Wadden Sea or recirculate on the delta. Offshore and within channels, tidal transport dominates, whereas waves are most important along the eastern side of the delta. At many locations (particularly along shallow shoals), both waves and tides are important

Ebb-tidal deltas are sediment-sorting machines[1,2]

The observed sorting of tracer sediment (Chapter 6) demonstrates that grain-size selective sediment transport is important on Ameland ebb-tidal delta. This dependency of sediment transport on grain size on ebb-tidal deltas is manifest in greater connectivity for fine sand than coarse sand in Chapter 7, and is observed at other similar sites (*Son et al.*, 2011; *Herrling and Winter*, 2018). This sorting process on the scale of individual grains is manifest in large-scale patterns: Ameland ebb-tidal deltas is largely composed of well-sorted, fine sand (Figure 2.7). The sand tends to fine in a clockwise direction around the inlet, and variation in grain size is reduced. Bed shear stresses are too high for mud to linger on the active shoals, so it is only found in deeper distal areas offshore. At the outer edge of the ebb shoal, the critical bed shear stress for the local median grain size matches the current-related bed shear stress at spring flood tide (Figure 5.7). This suggests that at least in this area, sediment sorting is tidally controlled, which is consistent with (*Bruun and Gerritsen*, 1959). The observed clockwise fining appears consistent with the convergence of many separate sediment pathways (i.e., Figure 8.3), and "downdrift fining".

Ebb-tidal delta bypassing sequences

Ameland Inlet's behaviour over the past decades is conceptually well-described by the ebb-tidal-delta breaching and outer channel shifting models of (*FitzGerald et al.*, 2000). The main ebb-channel tends to deflect downdrift until a new channel is breached and the old one fills in, while the remnants of shoals migrate onshore (Figures 2.2–2.6). However, as a large and energetic system, Ameland ebb-tidal delta's dynamics are complex and do not adhere well to a strict, regular cycle (Chapters 2 & 3). Sediment tends to accumulate irregularly at certain locations until a tipping point is reached. The physical processes that push the ETD towards these tipping points are repetitive (e.g., tides or seasonal variations in wave climate). These accumulations tend to repeat in similar areas but are never exactly the same, so we never get a true cycle, even at a relatively stable inlet like Ameland.[3] Each cycle may differ in volume, pathway, and duration. A more detailed causal explanation of the physical processes is necessary to move from a purely descriptive model to quantitative predictions (*Brierley et al.*, 2021).

Regular cyclicity may be a problematic assumption for coastal engineers and managers if it is used predictively and leaves them waiting for a cycle that never comes: an island tip that doesn't grow back or a shoal that never attaches to feed a beach. Previous efforts to describe the dynamics of Ameland ebb-tidal delta argued that it followed a regular 50-60 year cycle, based on 96 years of measurements (*Israel*, 1998; *Cheung et al.*, 2007). *Israel* (1998) predicted that by 2010, the delta would revert to the same configuration it had in 1892 and 1950. As a consequence of these changes to the delta, the tip of Terschelling (the Boschplaat) would undergo massive expansion and impending shoal attachments would render nourishments unnecessary for the northwest coast of Ameland. Instead, the Boschplaat has continued to erode unabated and that section of Ameland's coast has required nearly $3 \times 10^6 m^3$ of beach nourishments in recent years. Ebb-tidal deltas may show repeating patterns, but they cannot be depended on to return to a previous state on schedule. It is thus

[1] See also *Bartoníček and Maus* (2016)'s *Jller*.

[2] Thank you to Matthieu de Schipper for this particular turn of phrase.

[3] *"Men [and women] wiser than and more learned than I have discerned in history a plot, a rhythm, a predetermined pattern. These harmonies are concealed from me. I can only see one emergency following upon another as wave follows upon wave..."* – Herbert A.L. Fisher

imperative to better quantify the uncertain nature of ebb-tidal deltas and clearly communicate that to stakeholders to inform better planning. At the very least, we should be more nuanced in how we talk about ebb-tidal delta bypassing cycles, and consider calling them "bypassing sequences" instead.

These irregularities in cyclicity may be due in part to the stochastic nature of forcing (c.f., *Morton et al.* (2007); *O'Connor et al.* (2011)). However, they could also be related to self-organized critical feedbacks in the ebb-tidal delta's behaviour. Sand piling up in an hourglass, one grain at a time, is a simple experiment widely used for assessing the concept of self-organized criticality in natural systems (*Bak and Chen*, 1991; *Puhl*, 1992; *Malamud and Turcotte*, 1999). Sand stacks up unobtrusively until part of the heap becomes critically steep and collapses in an avalanche. Small avalanches occur quite regularly, but larger ones are exponentially rarer. In this context, *Bak* (1996) noted that:

> "the sand forecaster can still make short time predictions by carefully identifying the rules and monitoring his local environment. If he sees an avalanche coming, he can predict when it will hit with some degree of accuracy. However, he cannot predict when a large [avalanching] event will occur, since this is contingent on very minor details of the configuration of the entire sandpile."

This may be a useful analogy for ebb-tidal deltas: although we can successfully propagate existing small-scale features into the near future, we have a difficult time correctly predicting the initiation of new large-scale features like ebb-lobes or channel switches on longer timescales (*Harlequin*, 2021). Part of the issue is that we do not fully understand what triggers this process or precisely what the required preconditions are.

The irregularities in Ameland's bypassing cycle could be explained in part by deterministic chaos. Formally, chaotic systems can be defined by dynamics that are bounded, deterministic, and prone to the exponential amplification of small perturbations (*Toker et al.*, 2020). Ebb channel and lobe growth is bounded by the tidal prism of the inlet and driven primarily by deterministic tidal processes. Self-enhancing positive feedback creates strong sensitivity to initial conditions, and is evident in the divergent evolution of simulated ebb-tidal deltas perturbed by different nourishments (*Harlequin*, 2021). Furthermore, chaotic stirring is a feature of hydrodynamics at tidal inlets (*Ridderinkhof and Zimmerman*, 1992), and is likely to be a property of sediment transport there, too (Chapter 6). Qualitatively observing of these symptoms of chaos demands that further quantitative investigation of the matter be carried out. Smaller inlets have shorter apparent bypassing cycles (*Ridderinkhof et al.*, 2016), so it may be easier to discern the nature of chaos versus cyclicity at such locations than at Ameland.

Chaos theory has been regarded by some as "an esoteric fad pursued only by theoreticians suffering from a severe case of physics envy" (*Hastings et al.*, 1993), but the potential explanatory power of the concept means that it merits further investigation. If not fully chaotic, then ebb-tidal deltas at least show strong tendencies of geomorphological badassery (Appendix E).

The importance of mud on a sandy ebb-tidal delta

Although ebb-tidal deltas are predominantly composed of sand, and although this dissertation is primarily concerned with the fate of sandy nourishments in the context of tidal inlet systems, the presence of mud in these environments cannot be ignored. Mud does not contribute substantially to the sediment budget of Ameland ebb-tidal delta, but it is present in suspension over the delta much of the time (Chapters 4 & 5), and not accounting for it can lead to misleading interpretations of suspended sediment measurements. Fine sediment appears to follow a path in suspension from the Wadden Sea (Chapter 5) to distal offshore regions of ETD (Chapter 2). The presence of fine sediment in the water column and on the seabed also has an important influence on the ecological functioning of the ebb-tidal delta and its surroundings (*Hendriks et al.*, 2020; *Holzhauer et al.*, 2021). Furthermore, quantifying the proportion of mud moving across the delta is essential to accurately estimating sediment budget of the neighbouring Wadden Sea and determining whether its intertidal areas can keep pace with sea level rise (*Colina Alonso et al.*, 2021).

9.3. OUTCOMES

Although this dissertation has primarily focused on Ameland Inlet in the Netherlands, the tools, techniques, and knowledge developed here can be extended to other environments. We have already made the first steps towards this through applications in various research and consulting projects, and there are clear opportunities for further immediate application:

Connectivity and SedTRAILS

SedTRAILS and connectivity have already been applied to numerous research and consulting projects to answer questions coastal sediment pathways. Applications include estimating nourishment or dredge disposal fate (*Stevens et al.*, 2020; *Elias et al.*, 2020, 2021a,b; *Lambregts*, 2021), identifying large-scale sediment transport pathways (*Stevens et al.*, 2020; *Bult*, 2021; *van Gijzen*, 2020), determining the impact of human interventions in the coastal system on centennial time scales (*Meijers*, 2021), and identifying sources of sediment to dredging hotspots (*Stevens et al.*, 2020). These projects have spanned a range of coastal environments around the world, from tidal inlets in the Wadden Sea to alongshore uniform beaches on the Holland coast, and from a muddy estuary in the United States and to a fjord on the west coast of Canada. SedTRAILS and connectivity provide added interpretive value to existing process-based models, which makes them readily applicable. Furthermore, these tools have enabled the effective communication of complex numerical model results to a non-scientific community and stakeholders in order to generate meaningful discussions.

Morphodynamic Mapping Techniques

The techniques outlined in Chapter 3 are immediately applicable to existing bathymetric datasets (e.g., *Rijkswaterstaat* (2016); *Benninghoff and Winter* (2019)), so no new field measurements are required. The statistical mapping approaches (i.e., identifying the maximum and minimum surfaces or envelope of bathymetric change) are simple, easily calculated metrics that clearly illustrate morphodynamics and characteristic zones of the ebb-tidal delta (i.e., active or passive). Furthermore, the stratigraphic modelling approach is readily applicable in siting undersea infrastructure, marine salvage operations, for planning nourishments in more stable places, as modern analogues for ancient systems, and

for interpreting geochronological data. It can also be used in an identical manner for post-processing morphodynamic models, providing new metrics for their validation.

Sediment Composition Index (SCI)

Combining commonly-paired optical and acoustic instruments opens opportunities for reanalysis of existing data in mixed sediment environments, without even needing to make new measurements. It is already possible to estimate SCI from many datasets in the literature (e.g., *Voulgaris and Meyers* (2004); *Moura et al.* (2011); *Zhu et al.* (2019b); *Lin et al.* (2020); *de Vet et al.* (2020); *Colosimo et al.* (2020); *Pomeroy et al.* (2021)). Our approach thus enhances the value of existing datasets by providing an additional, simple-to-calculate metric for interpreting sediment dynamics. To demonstrate the possibilities, we examined two well-studied datasets with paired ADVs and OBSs, in Chesapeake Bay (USA) (*Fugate and Friedrichs*, 2002) and the Sand Engine (The Netherlands) (*Horner-Devine et al.*, 2017; *Flores et al.*, 2018; *Rijnsburger et al.*, 2018)). In both cases, we found that the SCI reliably indicates high proportions of relatively finer sediment in suspension (*Pearson et al.*, 2021b).

Tracers

Our results demonstrated that tracers could be a useful technique even in energetic environments like an ebb-tidal delta (Chapter 6). The techniques explored in our tracer study (e.g., magnetic tracer retrieval and separation, microscopic analysis of tracer) provide additional ways to generate value from such studies. This gives us more chances to to tap into the unique perspective on sediment transport that tracers offer. Sediment tracing is thus a relevant approach for future nourishment monitoring and planning. Most crucially, the dataset of recovered tracer particles will serve as the basis for validation of SedTRAILS in upcoming research (Chapter 8).

9.4. IMPACT

From these initial outcomes of the project, we can define pathways toward potential future impacts and valorization. The immediate impact of the research within this dissertation is primarily scientific, but aims towards long-term societal impacts (i.e., greater coastal safety and ecosystem health due to more effective nourishments). The research conducted here directly aligns with four of the United Nations Sustainable Development goals (*United Nations*, 2017):

- Build resilient infrastructure, promote inclusive and sustainable industrialization and foster innovation.
- Make cities and human settlements inclusive, safe, resilient and sustainable.
- Take urgent action to combat climate change and its impacts.
- Conserve and sustainably use the oceans, seas and marine resources for sustainable development.

In the remainder of this section we narrow our focus, considering how this work will influence nourishment strategies, numerical modelling, field data collection and analysis, and how the knowledge and tools developed in this project will be shared. The primary indicator of success for monitoring and evaluating the impact of this dissertation will be the adoption of the tools developed here in research and practice.

How will this research improve nourishment strategies?

One of the primary motivations of this study was the need for knowledge and tools to make strategic sand nourishments on ebb-tidal deltas. Stratigraphy and polar analyses contribute to our understanding of historical morphological changes. They can be used to identify stable (passive) or dynamic (active) areas on the ebb-tidal delta depending on the desired dispersal characteristics and longevity of the nourishment. The tracer sampling and analysis techniques described here provide a new means of monitoring nourishments, and insight into potential nourishment behaviour at the scale of individual sand grains. With connectivity and SedTRAILS, we now have a framework and tool for estimating the likely fate of nourishments on the scale of the delta. Connectivity metrics can be used to identify and quantify more or less dispersive locations, as well as the main pathways connecting those locations to their surroundings. This approach can be used in the planning stages for strategic nourishments by targeting locations that should be fed (i.e., for coastal protection) or avoided (i.e., to limit ecological impact).

A necessary prerequisite to strategic nourishment is a sound description of the natural system being nourished. This is partly to understand the fate of new sand placed in that environment, but also to understand how the native sediment can be influenced by the nourishment's presence. Via field observations we improved our understanding of relevant physical processes at small and large scales. We were then able to apply this knowledge in the application of process-based numerical models to define major sediment transport pathways on Ameland ebb-tidal delta.

Knowledge of existing sediment pathways does not always ensure more effective nourishments, as pathways feeding the areas that need sediment most may not necessarily exist. Our findings suggest that there are few net transport pathways on Ameland ebb-tidal delta directly feeding the Wadden Sea, although the number of pathways does not necessarily correspond to the volume of sediment transported. If the goal is to indirectly nourish the Wadden Sea's intertidal flats, then sand placed on the updrift island coast is more likely to help than a nourishment on the ebb-tidal delta itself. Sand placed at most locations on the ebb-tidal delta will likely end up eventually feeding the downdrift island coast. Most pathways converge along the eastern edge of the Bornrif platform, connecting with Ameland. However, much of this sediment is delivered too far east to benefit the eroding coastline abutting the Oostgat channel. However, if the goal is simply to contribute to the sediment budget of the ebb-tidal delta and the Coastal Foundation, then most locations on the outer and eastward parts of the delta are suitable.

Grain size is also an important consideration in nourishment planning, and we now have a better characterization of the grain size distribution on the delta, but also about grain size selective transport. A remaining challenge is how to send the right size fraction of sand to a target location from a given source, for even more efficient nourishments. This task must be considered against unsubstantiated claims that coastal nourishments affect the sediment composition of the Wadden Sea and have been making it coarser. Competing hypotheses favour a hydrodynamic explanation. *Colina Alonso et al.* (2021) note that the Terschelling tidal divide has become sandier over the past century and suggest that this is due to changes in the tidal regime since the closure of the Zuiderzee. Given the importance of wind-driven flows over this part of the Wadden Sea (*Duran-Matute et al.*, 2016b; *Van Weerdenburg et al.*, 2021), it also seems plausible that the Zuiderzee closure could have increased wind-driven flows there, which may have contributed to coarsening. Similarly,

Dolch and Hass (2008) attribute coarsening in part of the German Wadden Sea primarily to changes in hydrodynamics. Given the degree of sediment sorting that goes on at the tidal inlets, changes in hydrodynamic forcing within the Wadden Sea seem like more plausible explanations for coarsening there than the effect of coastal nourishments. Nonetheless, this topic merits further investigation, since such sedimentological changes may disrupt local ecosystems.

Ultimately, the research carried out within this dissertation and related projects supports the viability of ebb-tidal delta nourishment as a coastal maintenance strategy at different scales (*Bak*, 2017; *van Rhijn*, 2019; *Harlequin*, 2021; *Lambregts*, 2021; *Elias*, 2021). Nourishing ebb-tidal deltas contributes to their local sediment budget ($\mathcal{O}(1km - 10km)$) and the Coastal Foundation as a whole ($\mathcal{O}(10 - 1000km)$), but can also directly or indirectly target specific sections of coastline ($\mathcal{O}(100m - 1km)$). Strategic small-scale nourishments could also be used to trigger larger-scale morphodynamic changes (*Lenstra*, 2020; *Harlequin*, 2021). For instance, filling an unstable channel could reduce its efficiency and redirect flow through another, thus hastening the breaching or channel-switching process and affecting the entire delta.

Although this study was initiated in response to Dutch coastal management needs, the findings are relevant for other regions, too. The United States Army Corps of Engineers (USACE) dredges over $100 \times 10^6 m^3$ of sediment from tidal inlets every year, and actively aims for "Beneficial Use of Dredged Materials", such as beach nourishment (*Elko et al.*, 2020). As such, the concepts and approaches developed here for strategic nourishment may also be applicable to their systems. *Elko et al.* (2020) notes that strategic reuse of dredged materials may also provide significant cost savings. In systems where use of ETD sediment is encouraged (e.g., *Beck* (2019)), our approaches could also be used for siting borrow areas on the ETD: the stratigraphic mapping approach can identify good reservoirs of sand that will be readily replenished.

By making targeted nourishments, we can be more efficient and cost-effective, making better use of limited resources. Even though the Netherlands has a relative bounty of offshore sand supplies, this is not the case for many places in the world: sand should be considered a finite resource or even rare mineral (*Roelvink*, 2015). Thus, being able to nourish strategically and more efficiently is essential for managing sediment in environments where it is scarce.

How will this research influence numerical model analysis?

This project presents several new possibilities for numerical modelling. The stratigraphic and polar mapping techniques developed in Chapter 3 give us both a new way of validating morphodynamic models and new tools for analyzing their output. The sediment composition index presented in Chapter 5 can be used to disambiguate measurements and therefore provide better input for model calibration and validation. Tracer studies (e.g., Chapter 6) can be used to validate Lagrangian sediment transport models like SedTRAILS.

The main contribution of the connectivity framework and SedTRAILS is to bridge the gap between the various scales, upscaling process-based modelling to the scales that are needed to answer bigger questions. These approaches enable more intuitive visualizations of model output, allowing non-scientists to better understand complex coastal processes and thereby enabling better management decisions in the future.

How will this research influence field data collection and analysis?

The findings of this project provide new incentives for collecting certain types of data.

For instance, Lagrangian modelling and connectivity provide motivation to invest in tracer studies or other Lagrangian field methods (e.g., Optically Stimulated Luminescence dating and tracing). The lessons learned about conducting sediment tracer studies in energetic environments (Chapter 6), can increase their effectiveness and the amount of information you can obtain from such a study. For instance, microscopy is currently underutilized for processing tracer data and recovered tracer grain size. This guidance may make sediment tracer studies a more attractive approach for monitoring nourishments. The value presented by new morphodynamic mapping techniques in Chapter 3 provides additional incentives to monitor more regularly and to keep up existing regular bathymetric surveys. The development of the SCI provides motivation for pairing optical and acoustic instruments in field settings, and puts more emphasis on interpreting instruments together rather than individually. The knowledge developed using these approaches at Ameland has been used to design seabed sediment sampling strategies for a follow-up project (*Wallinga et al.*, 2021).

Furthermore, several of the techniques presented here (morphodynamic mapping and *SCI*) can easily be used to reanalyze existing field measurements in a new light. This enables users to squeeze more value from old datasets.

How will this knowledge be shared?

To ensure that there are opportunities for the knowledge and tools developed in this project to be used and shared, we have taken several steps. Field and experimental datasets as well as model input files used here are openly accessible online. The repositories include the raw and processed data as well as relevant metadata and processing scripts. Pending further refinement and validation, the modelling software developed here will also be made available. Furthermore, all journal articles in this dissertation are freely and openly accessible.

To disseminate this research to a wider audience (scientific and general public), we have taken several initiatives to share it via educational outreach presentations (e.g., Appendix D), blogging (e.g., Appendix E, coastallycurious.com), and social media. Other media like visual art (Figure 9.2) and poetry (e.g., *Pearson and Tissier* (2018)) are also used to share the research. Where appropriate, the knowledge developed in this dissertation will be shared in university classroom settings. Illustrative examples from this project have already been presented in lectures of the introductory coastal dynamics course at TU Delft (*Bosboom and Stive*, 2021). Mentored students have also been trained in applying the techniques developed in this project (e.g., *van Gijzen* (2020); *Lambregts* (2021); *Bult* (2021); *Meijers* (2021)). Although this thesis is focused on a study site in the Netherlands, these communication efforts will also be directed abroad in places where relevant.

To ensure a productive pathway towards societal impact, we aim for better stakeholder engagement as part of the ongoing follow-up project (*Wallinga et al.*, 2021). This will include sharing tools and techniques with other researchers, implementing them in practical projects, and co-creating research plans with coastal managers, local residents, and other stakeholders to align our work with their needs. We will also work with ecologists to provide tools and a knowledge basis of relevant physical processes for their research. Local knowledge is essential in successful geoscientific investigations, so engaging with the people who live and work around ebb-tidal deltas will also be an important component of future work.

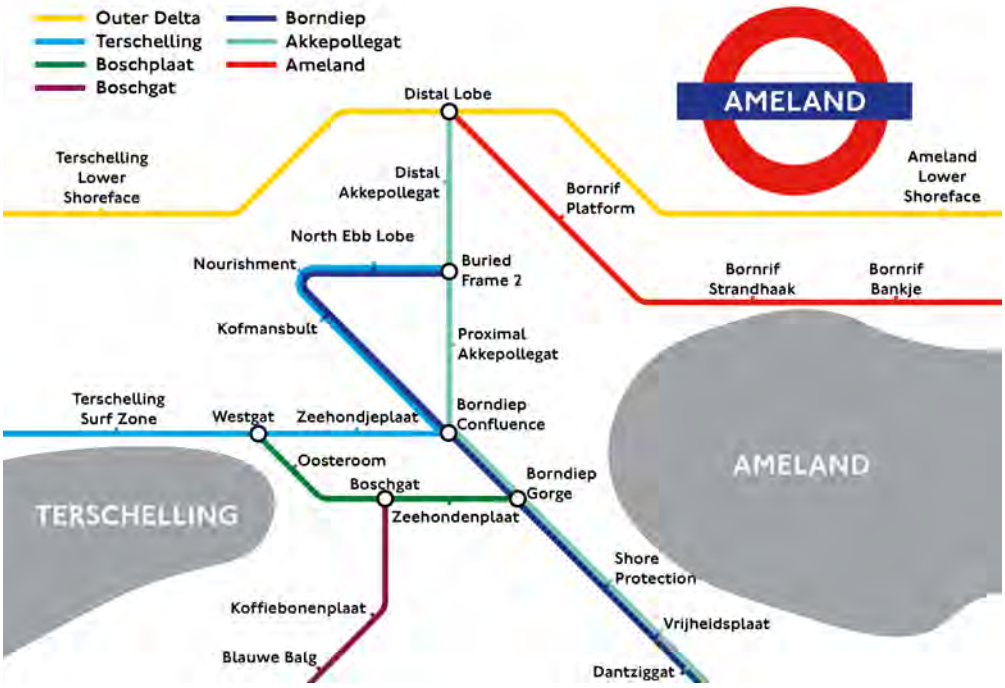

Figure 9.2: Subway map of Ameland ebb-tidal delta circa 2017. Subway lines correspond to major transport pathways as identified in this dissertation (Figure 9.1). In this way, we can depict complex information in a form more familiar to the general public.

9.5. OPPORTUNITIES

The findings of this study provide a foundation for further research. In addition to collecting more field measurements (particularly bathymetric surveys) and addressing the limitations identified in the models we used, we have identified several new opportunities for research that have arisen from this study:

Sediment connectivity across the scale cascade

In managing coastal systems, it is essential to understand how processes acting at different space and time scales affect one another. The need to balance regional sediment budgets may lead to incorrect assumptions about sediment exchange between specific features (*French et al.*, 2016). For improved management of these areas, it is essential to better delineate the actual extent of these zones of influence over different timescales, and to quantify asymmetries in transport.

The concept of connectivity (Chapter 7) provides an especially relevant and appropriate framework for approaching the issue of scale-dependent transport (*Phillips*, 2012). For instance, modularity identifies emergent sediment-sharing communities at different space and time scales (Figure 7.7c,d). We can similarly ask, what are the effective internal borders or boundaries that separate the system into cells (*Thiemann et al.*, 2010)? Rather than arbitrary coastal cells, we can make coastal management decisions based on the coastal cells that emerge naturally as a consequence of sediment fluxes.

Consider a hypothetical Wadden Sea-esque chain of barrier islands (Figure 9.3). At longer and longer timescales, more of the system becomes connected. However, even if the whole system is connected, there may be loops, asymmetries, and disconnections in the network that prevent complete sediment sharing. By understanding the system's connectivity as a function of time, we can choose where to more efficiently place nourishments to meet a particular goal.

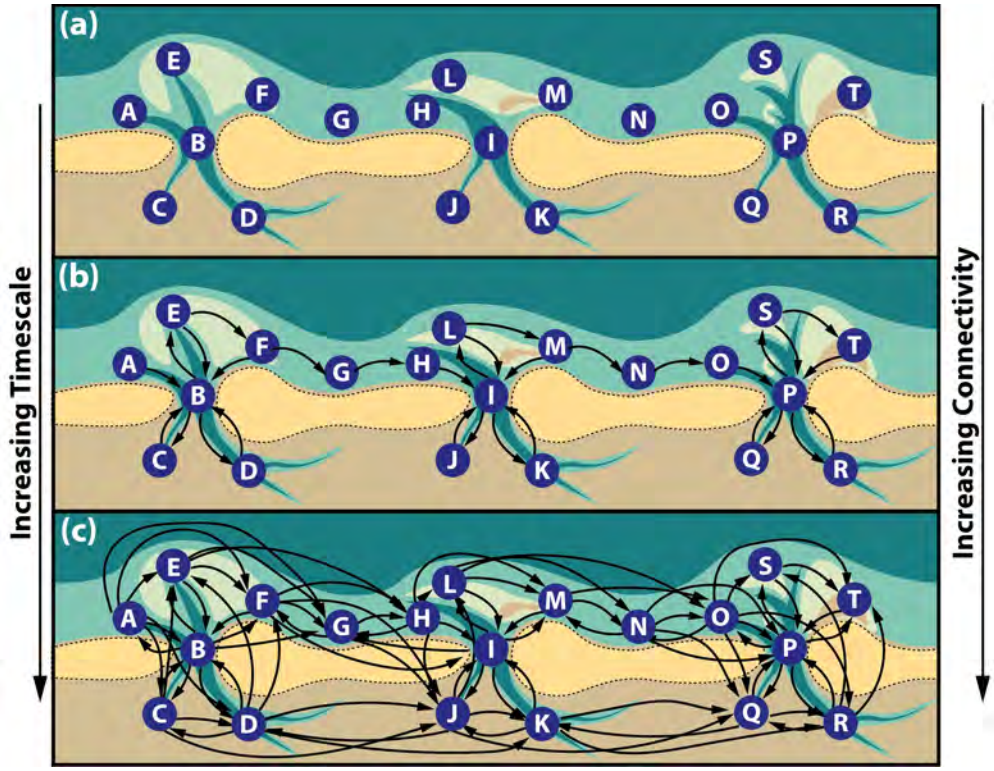

Figure 9.3: Conceptual diagram hypothesizing sediment connectivity of barrier island coasts as a function of time. (a) Over very short timescales ($\mathcal{O}$(*hours*)), nothing is connected, or at least there are only very local connections. (b) Over longer timescales ($\mathcal{O}$(*months-years*)), cells are now connected with their neighbours and there is a lot of asymmetry in those connections; (c) over much longer timescales ($\mathcal{O}$(*years-decades*)), we see many more long-distance connections. However there is likely not complete symmetry even at very long timescales, such that sharing is not completely uniform within the system as a whole. We need to analyze this connectivity in greater detail in order to make better coastal engineering and management decisions.

Connectivity and SedTRAILS as presented here do not consider morphodynamic change, but they show us the sediment transport patterns that lead to it. The equilibrium models commonly used to predict the evolution of ETDs at decadal to centennial timescales (e.g., ASMITA) usually schematize ETDs as homogeneous deposits that are directly connected to neighbouring coasts and basins (*Stive and Wang*, 2003; *Lodder et al.*, 2019; *Wang et al.*, 2020). In contrast to these assumptions, sediment transport is a very spatially heterogeneous process on the ebb-tidal delta, owing to variations in forcing, morphology, and sedimentology. Evidence from grain size (Figure 2.7), aerial imagery (Figure 4.5), stratigraphy

(Figures 3.6 & 3.7), and transport pathways (Figure 8) reveals a mosaic of sediment deposits and physical processes across the delta.

Understanding this spatial heterogeneity and the resulting implications for sediment connectivity is essential to making good long-term predictions of these systems. *Cowell et al.* (2003) note that "much of the controversy around long to mesoscale modelling stems in part from the absence of a formal rationale on aggregation". Connectivity gives us that missing rationale for aggregation, since it quantifies emergent patterns. As such, it could point the way to better decadal to centennial-scale morphodynamic models.

An additional phenomenon that should be investigated using connectivity is the synchronization of sediment transport at different scales. This matters for efficient transport across the system as a whole (e.g., large parts of the coast mobilized simultaneously during a large storm), since high levels of synchronization can amplify the effects of a smaller subsystem on its larger parent system (*Phillips*, 2012). To return to the earlier analogy of a sand pile, a well-synchronized ebb-tidal delta, poised at the edge of some critical tipping point, may be easily perturbed by a small storm to make much more dramatic, large scale changes. Conversely, low synchronization can limit the reach of such small-scale effects.

In this framework, we can also consider how ebb-tidal deltas influence larger scales. *Elias et al.* (2019) noted that the dynamics of shoals on Ameland ETD seem to cascade upward from small instabilities, transcending scales. Following through on that logic, further investigation is needed to see whether strategic nourishments could be used to perturb the larger coastal system in a more desirable direction.

Connectivity may be challenging to validate, but it could be a useful approach for generating testable hypotheses about coastal sediment exchange. These hypotheses may well become possible to validate in the future with the oncoming deluge of Big Data or advances in Lagrangian field measurements.[4]

Lagrangian field and numerical methods for analyzing sediment pathways

In this dissertation, we explored several Lagrangian techniques for measuring transport pathways, including artificial sediment tracers and surface drifters. However, other Lagrangian techniques that rely on natural tracers should also be considered, such as optically stimulated luminescence (OSL) (*Reimann et al.*, 2015; *Fruergaard et al.*, 2015), or by examining the characteristics of shells from nourishments (*Davies et al.*, 1989; *Meldahl and Flessa*, 1990). Tracking the spread of nourished sand along the seabed by monitoring its multibeam sonar backscatter signature (*Gaida et al.*, 2020) or sediment unmixing analysis of seabed samples (*Weltje and Prins*, 2007; *Zhang et al.*, 2020b) could provide complementary approaches.

Further developing these field measurement approaches will provide additional means of validating numerical Lagrangian models like SedTRAILS, increasing confidence in their output and enabling us to take full advantage of approaches like sediment connectivity. With the implementation of improved sediment velocity formulations in SedTRAILS (e.g., *Soulsby et al.* (2011)), we can better estimate the timescales associated with sediment transport. These improvements will also enable us to look into Lagrangian coherent structures (LCS) and chaotic stirring, both of which determine barriers to transport or mixing in the context of coastal hydrodynamics (*Ridderinkhof and Zimmerman*, 1992; *Kuitenbrouwer et al.*,

[4] "By all means, let the mathematical modelling of the naughty world continue apace, but let us not confuse those models with reality." – Barbara Kennedy, *The Naughty World*

2018). Combined with the metrics offered by connectivity, a veritable buffet of new quantitative analysis techniques for sediment transport pathways awaits.

Probabilistic and ensemble modelling approaches to sediment pathways and connectivity

Deterministic approaches to modelling may not be sufficient to make long-term morphodynamic predictions in light of the many uncertainties posed by the stochastic nature of wave forcing, morphodynamic feedbacks, sensitivity to initial conditions, and climate change. Hence, probabilistic approaches to modelling provide a promising way forward. Using a connectivity and/or Lagrangian flow net approach, we can define probability maps of sediment exchange (see also *Wainwright et al.* (2015); *Brommer and Bochev-Van Der Burgh* (2009)). SedTRAILS is a deterministic model, but can be run repeatedly with varying input conditions. Ensemble modelling like this could be used to obtain a range of potential outcomes (*Vitousek et al.*, 2021), which could then be aggregated in probability-weighted connectivity matrices to quantify predictive uncertainty. Once the sediment pathways have been aggregated in that form, we can use Markovian approaches - essentially treating connectivity (transition probability) matrices akin to a big game of *Snakes and Ladders* (*Althoen et al.*, 1993). Once derived, Markov chains enable more efficient calculation of transfer rates and timescales, since additional model simulations are not required (*Bacher et al.*, 2016). Alternatively, statistical mechanics approaches to sediment transport have been identified by *Furbish and Doane* (2021) as a technique with great potential.[5]

Application of statistical downscaling for prediction of ETD morphodynamics

Accurate prediction of ebb-tidal delta morphodynamics on decadal timescales remains elusive. Improved characterization of processes like nonlinear wave evolution (*de Wit et al.*, 2019; *Boechat Albernaz et al.*, 2019) and bedform dynamics (*Brakenhoff*, 2021), or the development of subgrid modelling (*Volp et al.*, 2016) hold some promise for advancing this, but a key component of successful morphodynamic modelling lies in the definition of hydrodynamic boundary conditions. Statistical downscaling of wave conditions via climate emulation has proven to be an efficient means of estimating local wave conditions and the resulting morphological change from large-scale atmospheric conditions (*Antolínez et al.*, 2016, 2018; *Rueda et al.*, 2017). Although most efforts of this sort have been limited to shoreline modelling, it may be possible to extend them to simulate the more complex morphodynamics of ebb-tidal deltas.

These downscaling approaches could be paired with the probabilistic approaches to sediment pathway and connectivity modelling proposed above. Numerous studies have linked coastal morphodynamics with climate indices like the El Niño-Southern Oscillation (ENSO) (*Ruggiero et al.*, 2010), the North Atlantic Oscillation (*O'Connor et al.*, 2011), or the Western Europe Pressure Anomaly (WEPA) (*Castelle et al.*, 2017). By using a climate emulator to identify representative wave climates for different climate index states, we could develop better long-term predictions of ebb-tidal delta evolution. The downscaling approach could also be combined with the probabilistic approach described above. Connectivity matrices associated with different wave conditions could be weighted and used to develop Markov chains to estimate the most probable sediment pathways (Figure 9.4). The resulting dataset could then be queried to answer relevant management questions regarding the

[5] Or not. As *Goodstein* (1975) warned, "Ludwig Boltzmann, who spent much of his life studying statistical mechanics, died in 1906, by his own hand. Paul Ehrenfest, carrying on the work, died similarly in 1933. Now it is our turn to study statistical mechanics. Perhaps it will be wise to approach the subject cautiously."

provenance or fate of sediment.

Comparison between sediment and ecological connectivity

Connectivity is a well-established concept in the field of ecology (*Calabrese and Fagan*, 2004; *Okin et al.*, 2009; *van der Molen et al.*, 2018), largely for assessing population dynamics. In the context of marine and coastal ecology, *Cowen and Sponaugle* (2009) define population connectivity as "the exchange of individuals among marine populations, [which] occurs mainly in the pelagic larval stage". The same hydrodynamic processes determining the transport and fate of larvae also drive sediment transport (*Tiessen et al.*, 2014).

This connection between physical and biological processes points to a link between hydrodynamic or sediment connectivity and ecological connectivity. In the context of the current project, this means that sediment and ecological connectivity could be relevant con siderations in the ecological design of nourishments. Modifications to benthic habitat (e.g., by a nourishment) may link or disrupt ecological connectivity (*Cowen and Sponaugle*, 2009), and given the influence of bioturbation (*Le Hir et al.*, 2007) or bed armoring (*Cheng et al.*, 2021) on sediment transport, it is likely that ecological factors can affect sediment connectivity (i.e., nourishment dispersal), too.

SedTRAILS was originally developed to model dispersal of coral larvae (*Storlazzi et al.*, 2017), so it could be used again for this purpose in the context of benthic organisms in the Wadden Sea and surrounding coastal region. The modelled ecological and sediment connectivity patterns could be validated using field measurements of grain size, morphological change, and benthic habitats (i.e., *Holzhauer et al.* (2021)).

Comparing ecological connectivity with hydrodynamic and sediment connectivity (similarly to the grain size comparison in Figure 7.6), would yield a more holistic view of the biogeophysical system, showing different concepts but expressed in a common framework and language.

Estuarine fronts and baroclinic processes

Although the influence of freshwater inflow has not been considered in detail in the models and analysis here, field measurements indicate the presence of a horizontal density gradient (Figure 2.10). At a similar tidal inlet, *Burchard et al.* (2008) found that such horizontal density gradients may lead to net import of sediment into the Wadden Sea. Additional measurements to determine the vertical density structure in Ameland inlet are necessary to assess stratification and mixing.

Estuarine fronts are ubiquitous in aerial images (Figure 4.5) and manifest as abrupt changes in suspended sediment, salinity, and temperature data (Figure 2.10, 4.4 & 5.6). What role do these fronts play in sediment transport pathways? Whether merely a symptom of baroclinic processes that influence sediment transport or whether they directly influence sediment paths, the fronts indicate that there is great spatial heterogeneity in water masses and suspended sediment transport on the ebb-tidal delta.

A further practical implication is that all of the modelling carried out in this thesis (and indeed for most previous studies of Ameland) has been 2DH. This has been a necessary assumption so far for reasons of computational feasibility and due to lack of sufficient field observations for calibrating a 3D model. However, pending the availability of the relevant data, future modelling efforts should explore 3D simulations to determine whether the added detail improves predictive skill.

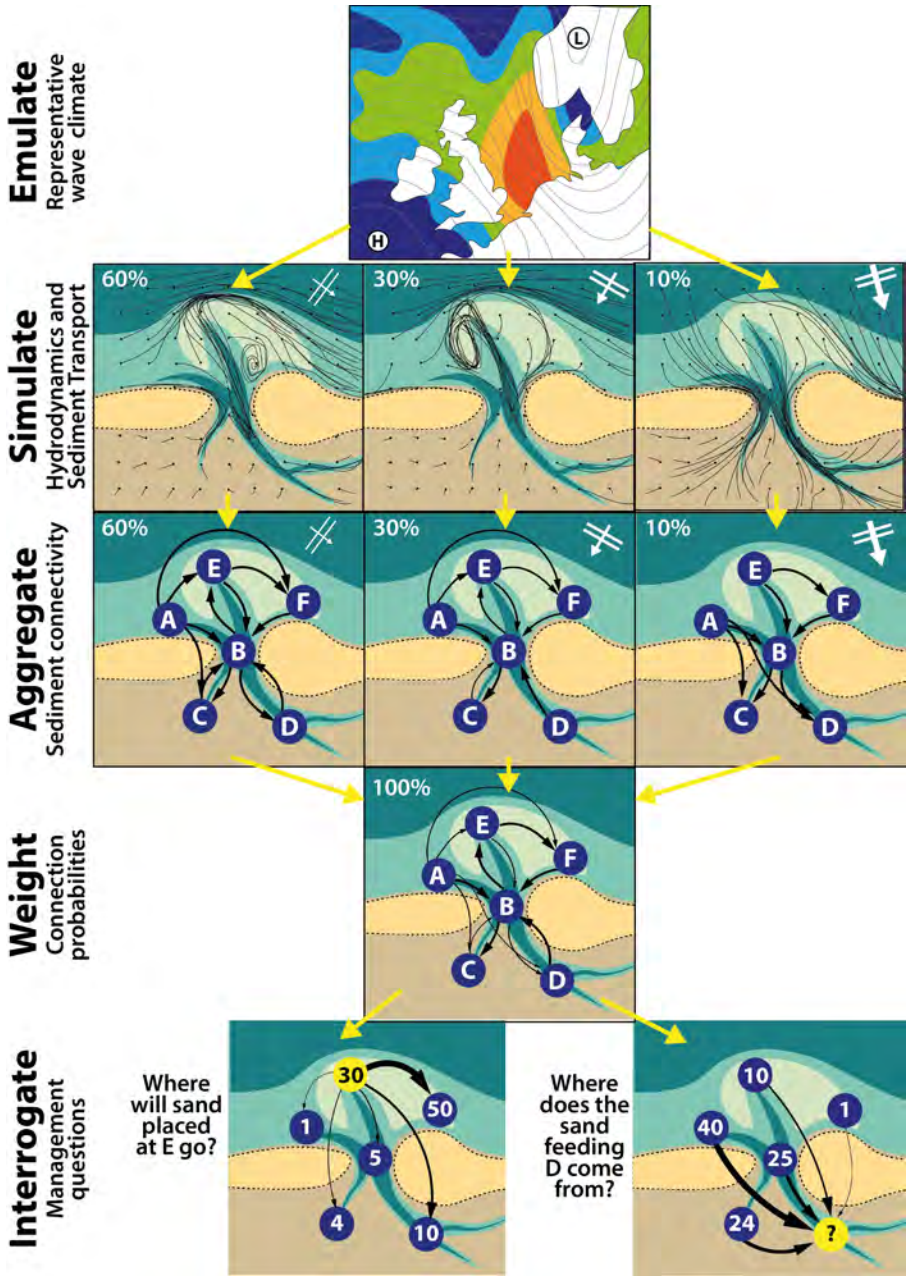

Figure 9.4: Conceptual diagram of potential model train for predicting sediment pathways. First, downscaling techniques are used to **emulate** a representative wind and wave climate. Then hydrodynamic and sediment transport models are used to **simulate** sediment pathways for a series of representative wave conditions. For example, 60% of the time there is a mild wave condition from the northwest, and 10% of the time there are more extreme conditions from the north. After that, wc could **aggregate** sediment pathways into connectivity networks. We then **weight** these networks by their probability to estimate the total likely connectivity. We can then directly **interrogate** the network or use Markovian techniques to ask management questions about sediment pathways.

Extension of the Sediment Composition Index (SCI)

The sediment composition index developed in Chapter 5 provides an additional means of characterizing suspended sediment. However, this approach of using multiple sensors can be extended to estimate not just the proportion of different grain sizes in suspension, but also concentration. The next steps towards this aim lie in the creation of larger calibration datasets in order to quantify the instrument-dependent component of SCI, which does not vary with the suspended sediment composition. Furthermore, laboratory experiments with a range of sediment mixtures and concentrations would increase the applicability of this approach to more diverse coastal environments. In particular, quantifying the influence of flocculation and organic matter on SCI would bring helpful advances. Additional lab and field experiments should integrate *in situ* particle size estimates (i.e., from LISST, Chapter 4) or multifrequency acoustic backscatter sensors (*Gray and Gartner*, 2009; *Moate and Thorne*, 2009, 2012; *Wilson and Hay*, 2015)) to further elucidate the role of particle size on combined optical-acoustic response. Ultimately, finding more ways to combine readings from multiple instruments with different operating principles will yield much-needed greater confidence in our estimates of sediment composition in uncertain mixed sand-mud environments.

Generalize ebb-tidal delta dynamics from polar analysis

To move to a more general quantitative and predictive theory of ebb-tidal deltas, we need to better elucidate the physical processes linking the steps in FitzGerald's conceptual models (*FitzGerald et al.*, 2000) and leading to state transitions. The tools and system knowledge developed in this project take a first step towards this goal.

Once a bypassing sequence is initiated, it follows a somewhat predictable path, but predicting the onset of that sequence remains a challenge. The greatest uncertainties are associated with the incipient formation and growth of new shoals. What is the exact process producing new ebb spillover lobes? Once initiated, what controls whether an ebb chute becomes the new main ebb channel or merely fades away? How do dynamics and synchronization at small scales affect the breaching process at larger scales and vice versa? Although well-studied in estuaries and river deltas (*Wang et al.*, 1995; *Kleinhans et al.*, 2013; *Moodie et al.*, 2019), only limited quantitative attention has been given to channel bifurcations and avulsions on ebb-tidal deltas (*Lenstra et al.*, 2019b).

As described earlier, Ameland ETD qualitatively shows symptoms of chaos, and we hypothesize that this could be to blame for some of its unpredictability. *Nicholl et al.* (1994) note that if one suspects that a system might be chaotic, then that demands a change in perspective for how the system should be studied, as well as new approaches to data collection and analysis. Such a perspective changes the types of questions that need to be asked, as well as the sorts of hypotheses that are formed about the behaviour of that system.

Conventional tests for chaotic behaviour require demonstrating exponential divergence in state from small changes in initial conditions. But how does one collapse such a complex multidimensional system into a phase space of the relevant parameters? We have generally favoured a reductionist (process-based, bottom-up) approach to sediment transport so far in this dissertation. However, top-down empirical modelling approaches based on simple mathematical representations of observed physical phenomena (e.g., the Hovmoeller diagram in Figure 3.5c) could also be a fruitful of way of generalizing ebb-tidal delta dynamics and quantifying chaotic behaviour. An alternative means of quantifying chaos would be to use SedTRAILS to derive Finite Time Lyapunov Exponents (FTLEs) of the sediment trans-

port field (*Rypina et al.*, 2010). This would enable us to explore the chaotic stirring tendencies of sediment in two-dimensional space.

Just because a system is chaotic, does not mean it is completely unpredictable within certain limits: chaos is bounded and follows attractors (*Toker et al.*, 2020). Perhaps ebb tidal deltas are merely orbiting a strange attractor in a phase space we have yet to identify. Chaos at smaller scales is often subject to self-organizational tendencies at larger scales (*Phillips*, 1997), so all hope is not yet lost for predictability.

The data from Ameland alone are not sufficient to prove this concept for all ebb-tidal deltas in general, so it is imperative that we collect more data from other ebb-tidal deltas around the world. *Beck* (2019) calls for the creation of a comprehensive dataset of sediment bypassing pathways to better characterize tidal inlet dynamics. This could be accomplished by compiling available modelled and measured pathways for inlets around the world in a common framework of connectivity for ease of intercomparison and analysis. Such a dataset would provide a useful starting point for unifying the concepts discussed here.

9.6. OUTLOOK

This project focused on how improved tools and system understanding can be used to better nourish a specific part of the Dutch coast. With the advent of climate change, many other coastlines around the world will need similar solutions to maintain their sediment budgets. However, this approach will not be feasible everywhere, since not every country can draw on the same sand resources, wealth, or cultural history of fighting against and living with water. How can we adapt to climate change while caring for our coasts in such a way that we don't all need to head for the hills or live in concrete fortresses? The challenges are daunting, but there is reason for hope, given recent trends in coastal science and engineering.

The long-held tendency of coastal engineers to build walls and view the sea as an adversary has seen a transition towards "building with nature" (*de Vriend et al.*, 2015) and more holistic approaches that consider how humanity can adapt to rising seas (*Hinkel et al.*, 2018). Can useful analogies for sea level rise can be drawn from sustained record high water levels on the Laurentian Great Lakes (*Gronewold and Rood*, 2019)? Once-scarce measurements of coastal systems are now pouring in thanks to advances in remote sensing (*Luijendijk et al.*, 2018; *Vos et al.*, 2019b; *Gawehn et al.*, 2021), cheaper field sensors (*Eidam et al.*, 2021), albatross-based wave observations (*Uesaka et al.*, 2022), crowd-sourcing or citizen science (*Harley et al.*, 2019), and especially open data policies (*Kinkade and Shepherd*, 2021). Some of the latest generation of coastal models improve performance by reducing complexity (*Roelvink et al.*, 2020; *Leijnse et al.*, 2021) or instead by explicitly seeking to capture complex system dynamics (*Payo et al.*, 2016; *van Maanen et al.*, 2016; *Bamunawala et al.*, 2021). Techniques like machine learning (*Pearson et al.*, 2017; *Goldstein et al.*, 2019) or data assimilation (*Vitousek et al.*, 2017b) help us extract more value from those observations and models. We must also keep our eyes open to what is going on in other fields and leverage their technology to open new possibilities for measurement, analysis, and prediction of coastal systems. For instance, how could the radical increases in speed promised by quantum computing someday open doors to improved coastal modelling? Can we derive relevant analogies for sediment transport from recent advances in stochastic modelling of particle size-dependent coronavirus dispersal (*Trivedi et al.*, 2021) or epidemiological con-

nectivity (*Schlosser et al.*, 2020)?

To navigate the Anthropocene era, we will need more than just better sediment transport models or coastline datasets. We need to work more collaboratively as a community to tackle the big problems in our field (e.g., *van Dongeren et al.* (2018); *Montaño et al.* (2020)), throw down the barriers that prevent marginalized members of our community from contributing (*Vila-Concejo et al.*, 2018; *Ali et al.*, 2021; *Tooth and Viles*, 2021), and improve the way we communicate our science and engage with the rest of the world (*Stewart and Hurth*, 2021). Ultimately, we need a more holistic and interdisciplinary view of coastal geoscience and engineering (*Koppes and King*, 2020)[6]. With a shared vision of what our coasts can look like and the tools and people to make it happen, we can ensure a sustainable and equitable future for our coasts for generations to come, in spite of the challenges that lie ahead.

[6] A manifesto of sorts for 21st century geomorphology, this article is highly recommended to the curious reader: Koppes, M., & King, L. (2020). Beyond *x,y,z(t)*; Navigating new landscapes of science in the science of landscapes. *Journal of Geophysical Research: Earth Surface*, 125(9), e2020JF005588. doi:10.1029/2020JF005588

A

SUPPORTING INFORMATION FOR "A NOVEL APPROACH TO MAPPING EBB-TIDAL DELTA MORPHODYNAMICS AND STRATIGRAPHY"

This appendix has been submitted as supporting information for the following article in *Geomorphology* (Chapter 3):

Pearson, S.G., Elias, E.P., van Prooijen, B.C., van der Vegt, H., van der Spek, A. & Wang, Z.B. A Novel Approach to Mapping Ebb-Tidal Delta Morphodynamics and Stratigraphy.

A

PEAK-FINDING

To objectively identify ridges and troughs in the volume anomaly $V_{a(t,\theta)}$ timestack of Figure 3.5c of Chapter 3, we used the MATLAB `findpeaks` algorithm. All peaks higher than $0.1 \times 10^6 m^3$ and further than 8^o apart at a given timestep were selected, discounting endpoints (Figure A.1).

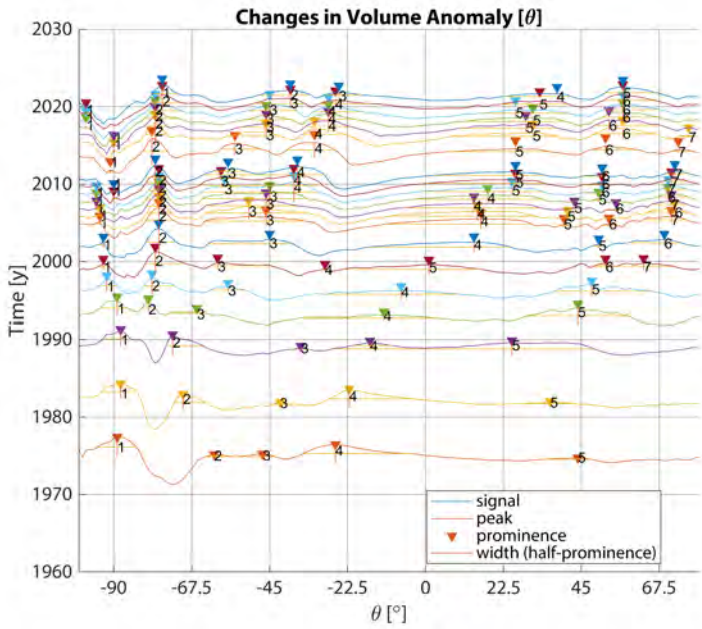

Figure A.1: Volume anomaly peaks identified in each time slice of Figure 4g, using the MATLAB `findpeaks` algorithm. Peaks are numbered sequentially from left to right.

By manually connecting these peaks and applying a linear regression (Figure A.2), we were able to estimate the rotational migration rates per shoal and channel $\omega_i = \Delta\theta/\Delta t$, which averaged 14.4^o/decade (Table A.1). We do not consider patterns counter-clockwise of -70^o, because these correspond to the shoreline dynamics of the updrift island and channel, and are independent of the delta's rotation in θ-space. This step could be further optimized and automated in future applications by use of feature-tracking algorithms (e.g., *Hodges* (1999); *Veenman et al.* (2001))

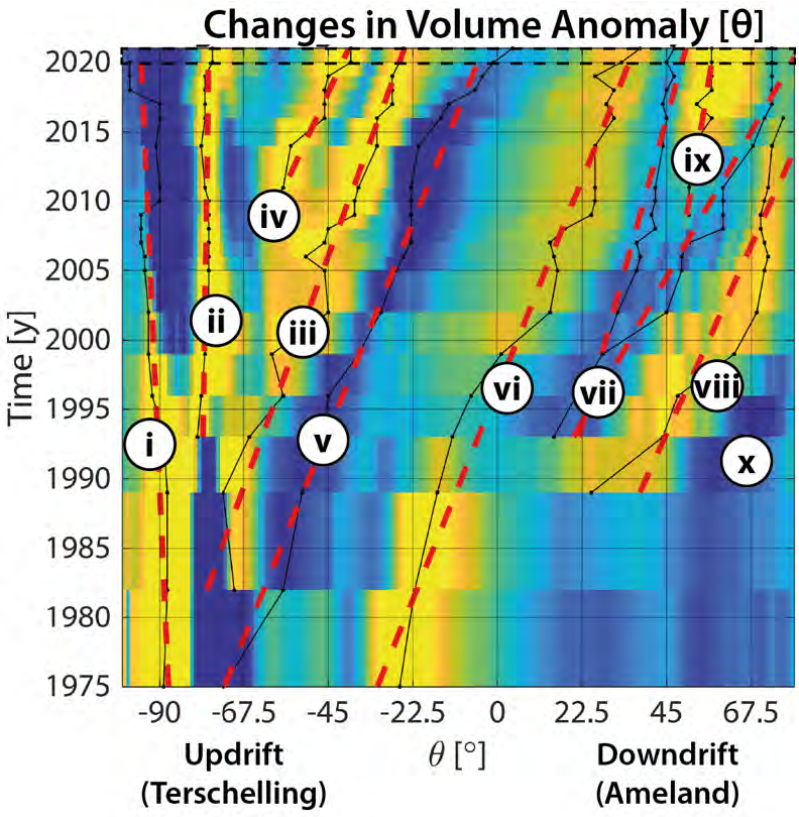

Figure A.2: Hovmöller diagrams indicating the change in volume anomaly for each year summed along the θ axis and stacked in time. Thin black lines denote the trajectory of shoals or depositional areas (yellow) and channels or eroded areas (blue) in space and time. Red dashed lines indicate linear fits through those trajectories. Trends up and to the right in $\theta - t$ space indicate clockwise motion around the inlet.

Table A.1: Migration rates of individual morphological features on Ameland ebb-tidal delta as determined by linear regression of their trajectories.

Trajectory	**Feature**	ω [^{o}/**decade**]	R^2
iii.	Ebb Lobe 1	13.5	0.95
iv.	Ebb Lobe 2	17.2	0.94
v.	Akkepollegat channel	15.0	0.97
vi.	Bornrif shoals	14.9	0.95
vii-a.	Oostgat channel (proximal)	10.1	0.88
vii-b.	Oostgat channel (distal)	21.5	0.88
viii.	Bornrif Strandhaak	16.6	0.81
ix.	Bornrif Bankje	6.0	0.80
	Mean	**14.4**	-

B

SUPPORTING INFORMATION FOR "CHARACTERIZING THE COMPOSITION OF SAND AND MUD SUSPENSIONS IN ESTUARINE ENVIRONMENTS USING COMBINED OPTICAL AND ACOUSTIC MEASUREMENTS"

This appendix has been published as supporting information for the following article in *Journal of Geophysical Research: Oceans* (Chapter 5):

Pearson, S.G., Verney, R., van Prooijen, B.C., Tran, D., Hendriks, H.C.M., Jacquet, M., Wang, Z.B. (2021). Characterizing Mixed Sand and Mud Suspensions using Combined Optical and Acoustic Measurements in Estuarine Environments. *Journal of Geophysical Research: Oceans*, 126, e2021JC017354. [Link].

DATA AVAILABILITY

Data from this study are publicly available at 4TU Centre for Research Data at https://doi.org/10.4121/collection:seawad (*Delft University of Technology et al.*, 2019). Details of this dataset can be found in *Van Prooijen et al.* (2020) and *van der Werf et al.* (2019a).

Hydrodynamic data from the Acoustic Doppler Current Profiler (ADCP-HR) can be accessed as netcdf files via this link:
https://doi.org/10.4121/uuid:e97a4b3d-a42a-426e-95b3-0ebb819317c5

The ADV SNR (signal-to-noise ratio) used in this study and laboratory results have been included here as supporting information:
https://doi.org/10.4121/14815893.v1

`ADCP-HR_azg201709_f4_processed.nc` contains additional processed hydrodynamic data from the Acoustic Doppler Current Profiler (ADCP-HR), and

`SCI_azg201709_f4_processed.nc` contains the optical and acoustic backscatter data plus derived values of the Sediment Composition Index (SCI) and fraction of sand in suspension (f_{sand}).

`SCI_LabExperiments.nc` contains the data from the laboratory experiments summarized in Figures 3 and 4 of the article.

EXPERIMENT 1 (E1) PROTOCOL

In this section, we elaborate on the experimental protocol for Experiment 1 (E1). A complete record of the sediment concentrations and sand fractions measured in E1 is provided in Table A.1.

The following measurement protocol was used in Experiment 1:

1. Tank was filled with fresh water and left overnight to reach room temperature.
2. Fine sediment, i.e., Bentonite powder (if required for the tested condition) was stabilized in suspension for 30 min in a 5 l beaker with a mixer before being introduced into DEXMES.
3. Tank was mixed for 30 mins to provide enough time for fine sediment to reach equilibrium.
4. Sand was added to the DEXMES tank 5 mins before data collection in order to reach the target total concentration.
5. At the end of the 10 min recording interval, a 1 l sample is collected using nozzle at sensor depth, i.e., 25 cm below the water surface and 12 cm away from the wall.
6. This procedure is repeated for both sand classes (d_{50} = 100 and 200μm) and the 6 total concentration levels, from 15mg/l to 200mg/l.

The water samples from mixed sand/fine experiments then were filtered with Grade GF/F Glass Microfibre filters filters and dried to estimate mass concentration. Based on preliminary experiments, we made an assumption that fine sediment is always fully suspended, and the deficiency of total concentration, if any, is the outcome of the deposition of sand. Hence, we did not separate sand/fine sediment in quantifying total concentration. For pure sand experiments, the water samples were sieved with a 40μm sieve before dried and weighted for mass concentration.

EXPERIMENT 2 (E2) PROTOCOL

In this section, we elaborate on the experimental protocol for Experiment 2 (E2). A complete record of the sediment concentrations and sand fractions measured in E1 is provided in Table A.2:

The following measurement protocol was used in Experiment 2, beginning with the $d_{50} = 100\mu m$ sand:

1. Tank was manually cleaned and instruments were mounted.
2. Tank was slowly filled with fresh water.
3. Propeller turned on to a constant rate of shear.
4. After 10 mins, mud sample added to tank to provide a consistent background composition.
5. Every 15 mins after that, sand was added to increase the sand concentration and meet the target values in Table A.2.
6. Every 10 mins after new sediment was added, we took a pumped sample (~ 30 cm beneath surface).
7. Once tests were complete, tank was flushed and manually cleaned.
8. After the $d_{50} = 100\mu m$ sand test, procedure was repeated for $d_{50} = 200\mu m$ test.

Pumped water samples were passed through a $63\mu m$ sieve to separate sand ($> 63\mu m$) from fine sediment ($< 63\mu m$). The fine sediment was additionally filtered, then the two fractions were separately dried, and weighed as per *Aminot and Kérouel* (2004) to yield baseline estimates of true suspended sediment concentrations.

The median and standard deviation of optical and acoustic backscatter for each sediment loading condition were computed for the period 3-14 mins after sediment load was added to ensure complete mixing. As samples were added every 15 minutes, this corresponded to approximately 660 samples per sediment loading condition for the OBS (1 Hz sample rate) and 5280 samples per sediment loading condition for the ADV (8 Hz sample rate).

B

Table B.1: Summary of sediment concentrations in Experiment 1 (bentonite with 100 and 200μm sand). The left column indicates the target for each test, and the centre column the actual *SSC* measured from pumped samples. The right columns indicate the sand content (f_{sand}) measured from pumped water samples.

SSC_{target}	SSC_{actual}		f_{sand}	
	$100\mu m$	$200\mu m$	$100\mu m$	$200\mu m$
15	15.0	15.0	0.0	0.0
25	25.0	25.0	0.0	0.0
50	50.0	50.0	0.0	0.0
100	100.0	100.0	0.0	0.0
150	150.0	150.0	0.0	0.0
200	200.0	200.0	0.0	0.0
15	15.4	12.1	26.9	6.9
25	24.2	19.7	22.6	4.7
50	48.1	41.0	22.1	8.5
100	93.2	75.9	19.5	1.2
150	137.0	117.7	17.9	4.4
200	NaN	149.6	NaN	NaN
15	9.4	11.0	19.8	31.9
25	24.8	13.5	49.5	7.2
50	46.5	36.8	46.2	32.1
100	75.2	73.0	33.5	31.5
150	134.7	109.9	44.3	31.8
200	182.8	128.8	45.3	22.3
15	14.5	7.7	74.2	51.6
25	18.4	14.9	66.0	58.1
50	39.8	28.4	68.6	55.9
100	81.9	45.7	69.5	45.3
150	117.2	79.0	68.0	52.5
200	160.0	96.2	68.7	48.0
15	14.0	4.8	100.0	100.0
25	20.5	15.6	100.0	100.0
50	45.5	27.8	100.0	100.0
100	85.7	52.8	100.0	100.0
150	126.2	76.9	100.0	100.0
200	175.6	115.1	100.0	100.0

Table B.2: Summary of sediment concentrations in Experiment 2 (estuarine mud with 100 and 200μm sand). The left columns indicate the target and measured sand content (f_{sand}) for each test. The right columns indicate the fine sediment ($\leq 63\mu m$), sand ($\geq 63\mu m$), and total concentration in mg/L measured from pumped water samples.

Target	f_{sand}[%] Measured		SSC_{fine}		SSC_{sand}		SSC_{total}	
	$100\mu m$	$200\mu m$	$100\mu m$	$200\mu m$	$100\mu m$	$200\mu m$	$100\mu m$	$200\mu m$
0.0	0.0	12.0	134.9	127.9	0.0	17.4	134.9	145.3
10.0	14.6	16.0	128.1	127.1	21.9	24.2	150.0	151.3
25.0	18.5	25.4	133.0	123.9	30.1	42.2	163.1	166.1
50.0	31.5	31.8	134.0	125.8	61.6	58.7	195.6	184.5
75.0	64.9	58.2	132.4	123.6	244.3	172.2	376.7	295.8
90.0	83.7	79.9	131.4	124.6	674.2	494.5	805.6	619.1
95.0	91.4	87.9	138.6	128.6	1464.4	936.0	1603.0	1064.6

C

SUPPORTING INFORMATION FOR "SEDIMENT CONNECTIVITY: A FRAMEWORK FOR ANALYZING COASTAL SEDIMENT TRANSPORT PATHWAYS"

This appendix has been published as supporting information for the following article in *Journal of Geophysical Research: Earth Surface* (Chapter 7):

Pearson, S.G., van Prooijen, B.C., Elias, E.P., Vitousek, S., Wang, Z.B. (2020). Sediment Connectivity: A Framework for Analyzing Coastal Sediment Transport Pathways. *Journal of Geophysical Research: Earth Surface*,125(10), e2020JF005595. [Link]

INTRODUCTION

Model input files used in this study have been included here as supporting information: https://doi.org/10.4121/13072820.v1. Specifically, the Delft3D model input files used to produce Figure 7.5 are provided here, including the bed sediment configuration for Node 5. Model files for the remaining 24 nodes are identical in every respect except for the initial location of the tracer sediment.

These files were then run with Delft3D Version 6.02.08.6712 to produce the results shown in this paper. Details regarding the individual file types can be found in the Delft3D User Manual (*Deltares*, 2014).

DATA SET S1

Data Set S1 contains the following Delft3D model input files:

```
Unit005_Native_100mm.dep
Unit005_Native_100mm.frc
Unit005_Native_200mm.dep
Unit005_Native_200mm.frc
Unit005_Native_300mm.dep
Unit005_Native_300mm.frc
Unit005_Native_400mm.dep
Unit005_Native_400mm.frc
Unit005_Tracer_100mm.dep
Unit005_Tracer_100mm.frc
Unit005_Tracer_200mm.dep
Unit005_Tracer_200mm.frc
Unit005_Tracer_300mm.dep
Unit005_Tracer_300mm.frc
Unit005_Tracer_400mm.dep
Unit005_Tracer_400mm.frc
ame.bcc
ame.bnd
ame.crs
ame.ddb
ame.inb
ame.mdf
ame.obs
ame.sed
ame.url
ame.wnd
ame_2016.dep
ame_2016_wave.dep
ame_low.enc
ame_low.grd
ame_nour1.obs
ameland2850_neumann0.bch
amewave.enc
```

```
config_d_hydro.xml
rif4.mor
vanrijn07.frm
vanrijn07.trt
```

D

KEEPING OUR FEET DRY AND SAFE FROM THE BIG WATER BY USING LOTS OF VERY TINY ROCKS

This chapter was originally presented at the American Geophysical Union Fall Meeting in December 2021. As part of the xkcd-inspired (*Munroe*, 2015) "Up-Goer Five" session, the subject matter had to be described using only the 1000 most-common words in the English language. Unfortunately, "sand" was not on the list.

Pearson, S.G., Gijón Mancheño, A., Ylla Arbós, C. (2020). *Keeping our feet dry and safe from the big water by using lots of very tiny rocks.* American Geophysical Union Fall Meeting 2020. December 8th, 2020.

There is a very low land next to the big water. It has a lot of wind and rains there most of the time.

The Very-Low-Land is so low that it would be under water now if people didn't build big walls around it and suck all the water out.

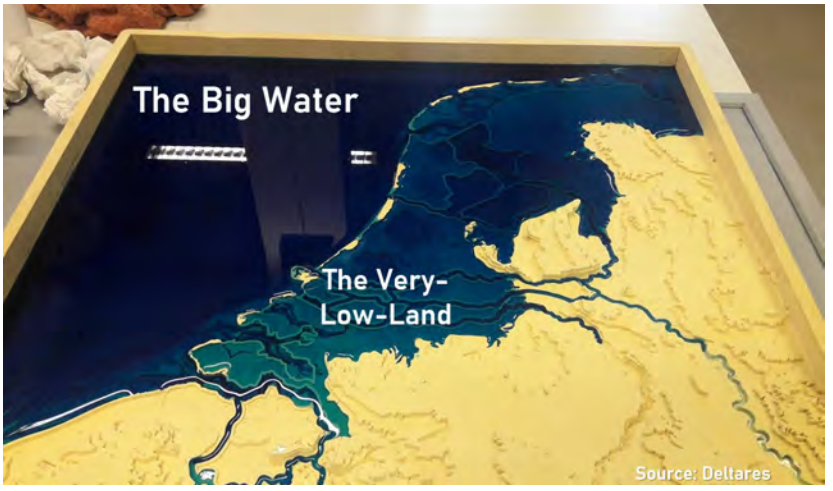

The big water is going up and up and up, and we want to keep everyone's feet dry so that they stay safe for a long time to come. [1]

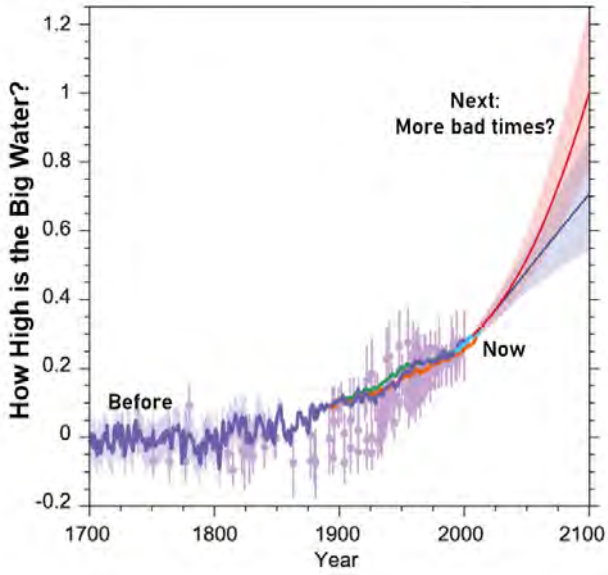

The plan to guard the Very-Low-Land is to put lots and lots of very tiny rocks along the edge between the big water and the land.

[1] This picture is from a book made by people who are very good at thinking about the big water and how it is changing, now that the world is getting warmer. They teamed up from all over the world and checked each other's work a lot to make sure we could trust their guesses.

When there is too much wind, the big water will make huge waves. These will hurt the wall of very tiny rocks, but if we have enough very tiny rocks, the big water won't get inside the Very-Low-Land and the people there will be safe.

It is hard to guess where these very tiny rocks will go when we put them on the edge of the big water, because the waves move them around.

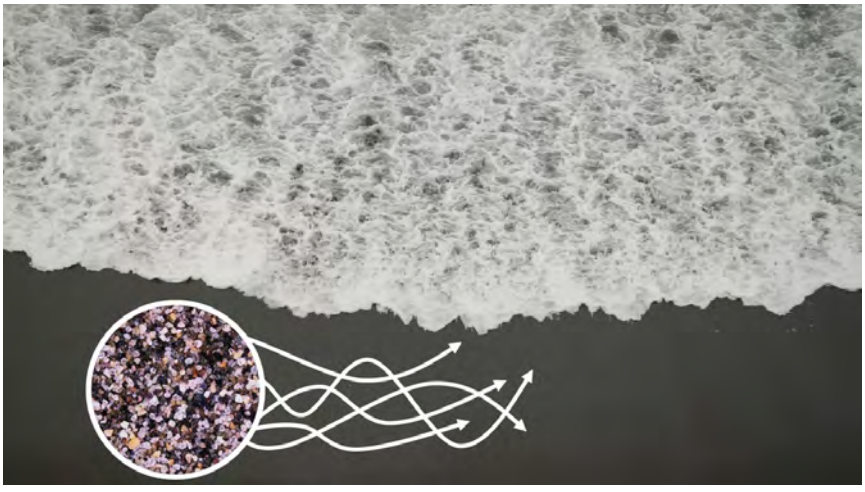

At the top of the Very-Low-Land, there are some small lands that have big water on all sides.

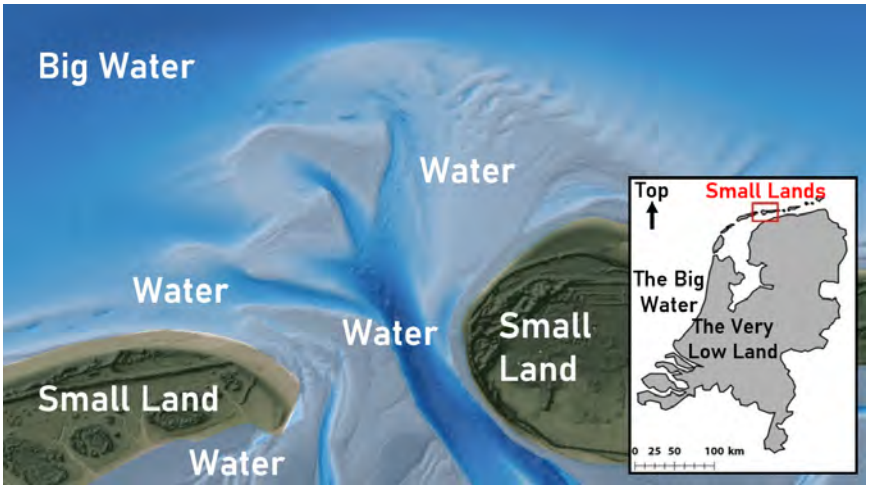

Two times a day, the big water goes up and down. This up-and-downing pushes and pulls water through the space between these small lands, and it goes very fast. If there are also waves, the water becomes quite confusing. Guessing how this confusing water moves very tiny rocks through the Space-between-the-lands is really hard.

This is my problem, and it is a big one.

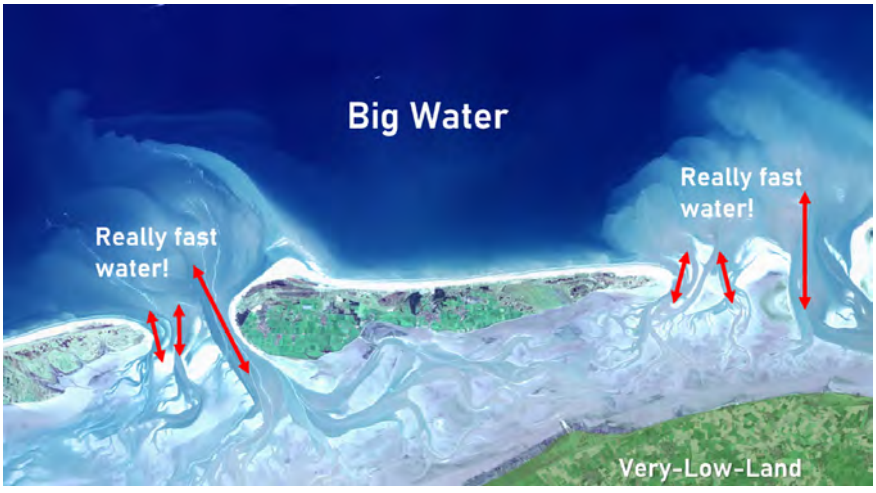

The most important question is: where do the tiny rocks go after we put them on the edge of the big water? When I tried to answer this question, even more questions appeared. This seems to happen a lot. They tell me it's just how these things work.

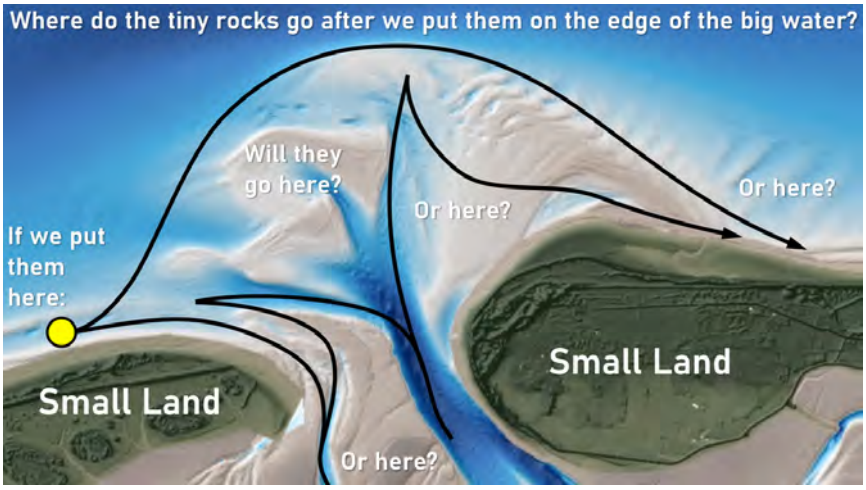

First, we can look at old pictures of the Space-between-the-lands to see how it has changed. If we know what it did before, we hope we can guess what it will do next.

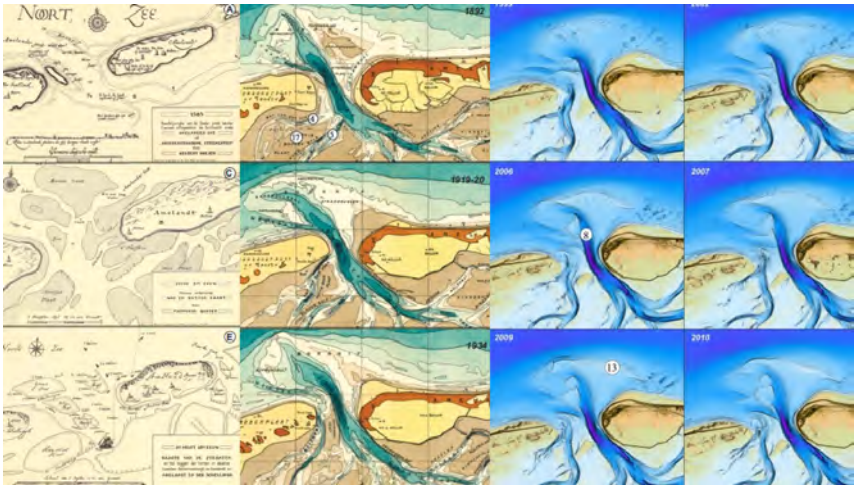

To know how fast the water is going and how many tiny rocks are moving through the water, we put water-counters and tiny-rock-counters on the bottom of the big water and left them there for a few weeks. One of our water-counters died after big waves pushed a lot of tiny rocks on top of it. It is still at the bottom of the big water, three years later (Picture **??** F-F').

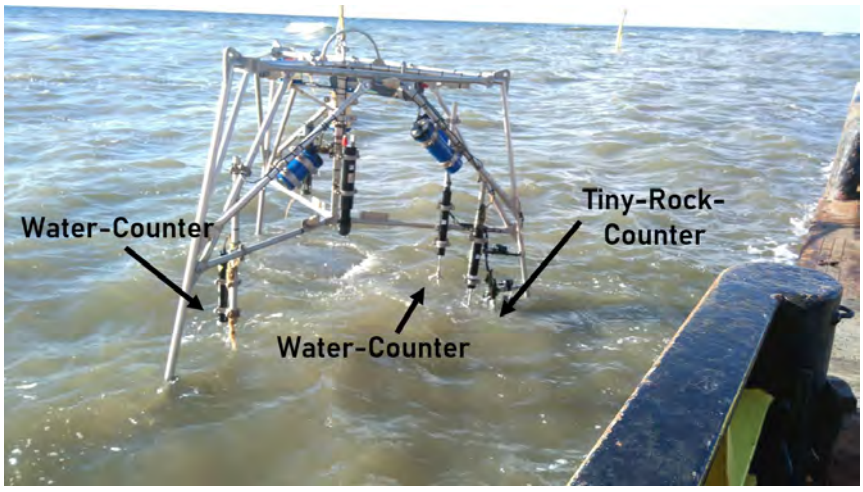

If we plan to put some tiny rocks on the bottom of the big water to guard the Very-Low-Land, we need to know where they will go. We tried to guess this by putting a few tiny green rocks in the water and following the trail they left behind.

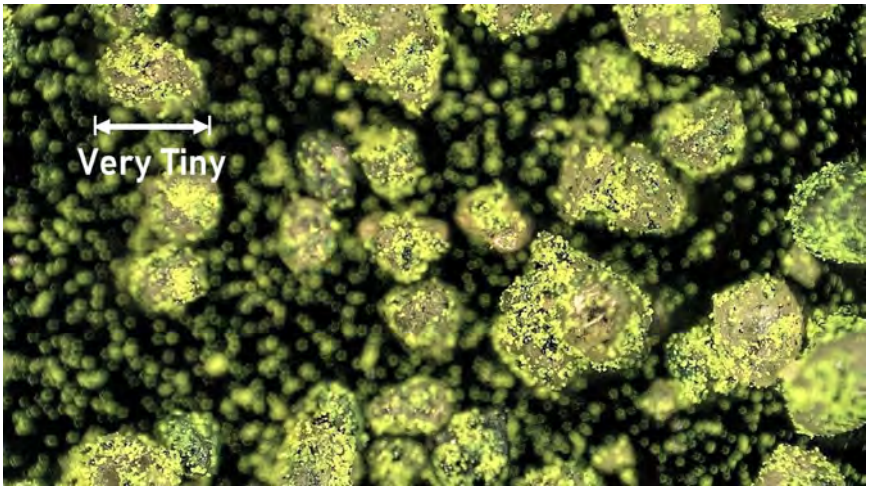

We then went around for weeks in a water-car trying to grab tiny rocks from the bottom of the big water, hoping that some of them would be green. We actually found some back, and I was the happiest eventually-doctor-student in the world.

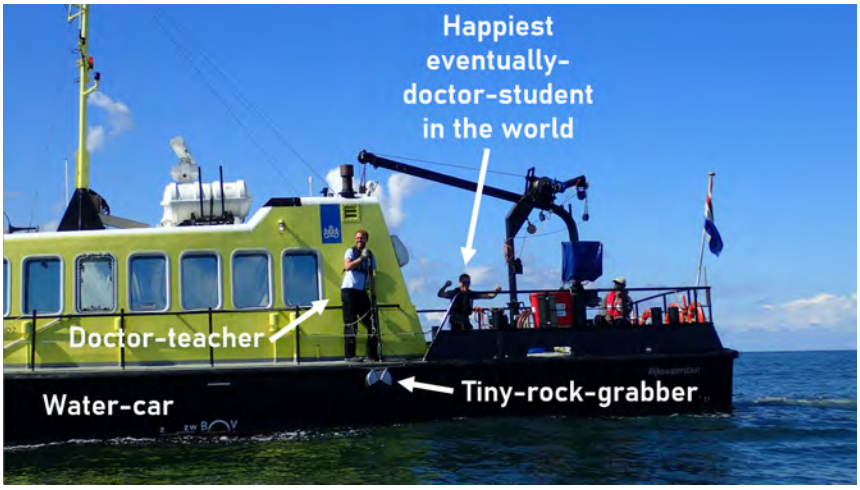

After this, I spent many weeks as a tiny-green-rock-counter in a dark room with no windows. This was not as fun as being in the water-car, but again, they tell me that's just how these things work.

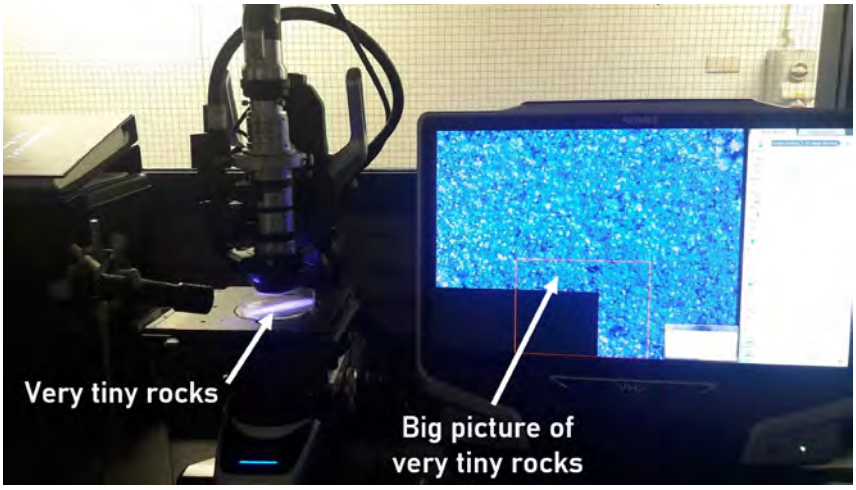

If we learn enough about tiny-rock-trails, we can even use computers to guess where the tiny rocks will go next. This part is sort of like playing computer games and is almost as fun as being in a water-car.

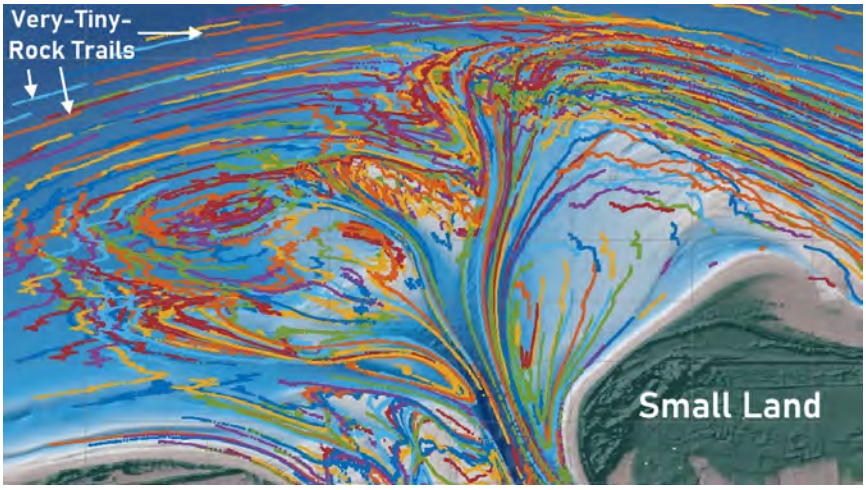

There are a lot of tiny rocks in this story. How do we keep track of them all or explain them to people? We made a new way to sort all the tiny-rock trails into a picture which looks like the ones that tell us where trains go.

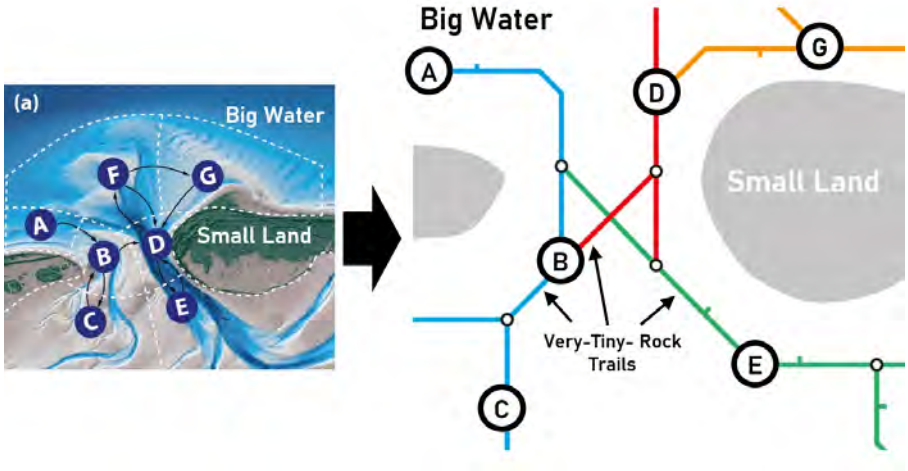

Together, all these things should help us figure out where the tiny rocks will go after we put them on the edge of the big water. I hope this keeps my Very-Low-Land friends safe for a long time. People in many other lands are also worried about huge waves and the big water going up, so we hope that the things we learn in the Very-Low-Land can help them too.

E

Ebb-tidal deltas: Badass Morphological Features (BAMFs)

Parts of this chapter were originally published as a blog post at CoastallyCurious.com.

WHAT I LEARNED FROM COUNTING SAND FOR 5 YEARS

AFTER nearly five years of scrutinizing sand and contemplating connectivity, my research has led me to an inescapable conclusion:

Ebb-tidal deltas are badass morphological features (BAMFs)
(c.f. Phillips (2015)).

What, pray tell, is an ebb-tidal delta, and why is it so badass? Ebb-tidal deltas are large underwater piles of sand at the mouth of estuaries and tidal inlets, deposited by outflowing tides and reshaped by waves. I spend my days studying how waves and tides move sand around on the Ameland ebb-tidal delta in the northern part of the Netherlands (Figure E.1). We need to know this in order to plan ecologically-sustainable flood protection measures for the Dutch coast. A morphological feature is just a technical name for some physical part of a landscape, like a hill or a beach.

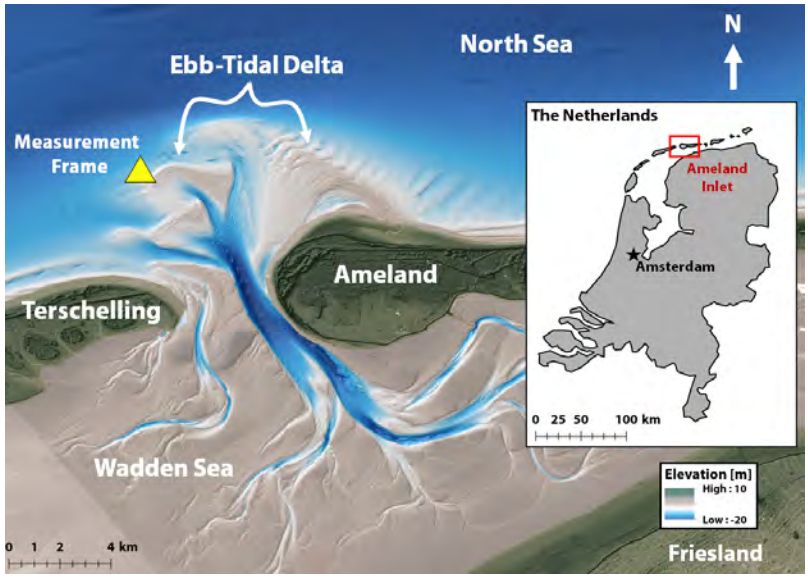

Figure E.1: An ebb-tidal delta is the giant pile of sand located at the mouth of a tidal inlet like this one. This may not sound glamorous, but understanding the way it moves around is extremely important for ensuring safe navigation and for predicting erosion and flooding of adjacent coasts.

WHAT MAKES A BADASS "BADASS"?

Phillips (2015) defines the archetypal badass as "**individualistic**, **non-conformist**, and **able to produce disproportionate results**", and applies this concept to geomorphology (the study of how landscapes evolve, at the crossroads of geology and physical geography). Ebb-tidal deltas meet these three criteria, which makes them badass morphological features (BAMFs):

1. Ebb-tidal deltas are each unique (in shape, location, composition, and in terms of the environmental forces shaping them (like waves and tides) (*Sha*, 1989a; *Hayes*, 1994;

Gaudiano and Kana, 2001; *Ridderinkhof et al.*, 2016)), and hence **individualistic**. Intrinsic noise, chaos, and sensitivity to initial conditions in many of these processes mean that events rarely duplicate and that the probability of the same feature appearing twice is virtually zero (*Kleinhans et al.*, 2005).

2. Ebb-tidal deltas and tidal inlets are systems characterized by chaotic internal transport processes (*Ridderinkhof and Zimmerman*, 1992). This is further complicated by the stochastic nature of non-tidal forcing (e.g., wind and waves) which they are subject to. The consequence is that ebb-tidal deltas tend to defy accurate prediction using physics-based numerical models, at least for annual to decadal timescales (*Elias et al.*, 2015b). ETDs are hence **non-conformist** or "naughty" (*Kennedy*, 1979). This numerical naughtiness is a serious problem for coastal engineers and scientists, since a failure to accurately forecast ebb-tidal delta evolution can threaten public safety and lead to costly property or infrastructure damage. They do not "play by the rules" of our existing physics-based deterministic models, which points to a need for other approaches such as probabilistic or ensemble modelling that can better account for uncertainties (e.g., *Davidson et al.* (2017); *Ranasinghe* (2020); *Vitousek et al.* (2021)).
3. Ebb-tidal deltas are highly nonlinear large-scale systems shaped by highly nonlinear small-scale processes (e.g., sediment transport scales with at least the third power of velocity) and feedback mechanisms. These can greatly amplify small instabilities(*Elias et al.*, 2019, 2022) or disturbances (*Harlequin*, 2021) and hence **produce disproportionate results**.

In addition to the strict definitions of *Phillips* (2015), ebb-tidal deltas are also "belligerent or intimidating, ruthless, and tough", other traits reflective of badassery. The Columbia River ebb-tidal delta alone is responsible for dozens of shipwrecks in the past century, and Ameland ebb-tidal delta has also caused over 20 wrecks throughout its history (*Wrecksite*, 2017). The most famous victim of this coastal violence was none other than the pirate Blackbeard, whose ship *Queen Anne's Revenge* ran aground on the ebb-tidal shoals of Beaufort Inlet, North Carolina (*McNinch et al.*, 2006).

Quoting *Pynchon* (1984), Phillips also notes that badasses are "able to work mischief on a large scale". Ameland ebb-tidal delta covers an area of approximately $100 km^2$, roughly the size of Den Haag. Many other ebb-tidal deltas are even larger (e.g., Noorderhaaks at the Marsdiep Inlet (*Elias*, 2006)). Furthermore, they are found on coastlines around the world, making mischief at a global scale.

SERIOUSLY?

Now admittedly, ebb-tidal deltas are just big piles of sand. A big pile of sand is probably not the first thing that comes to mind when you hear the word "badass". This could probably also be considered gratuitous personification or anthropomorphization.

I'm sure that many of my friends and family have been scratching their heads as to why I would sacrifice the latter half of my 20s to understand them better. A critical reader might ask, "is it possible that you have only convinced yourself that ebb-tidal deltas are cool out of self-preservation?" And the answer is yes. Yes, I have. Nonetheless, I remain steadfast in my assertion that ebb-tidal deltas exhibit major symptoms of geomorphological badassery.

Although the notion of geomorphological badassery may seem silly at first, it illuminates several important truths about our (mis)understanding of these complex bathymetric

features. Ebb-tidal deltas are important to study for reasons of coastal flood protection, navigational safety, and ecological value, but predicting how they will evolve is still immensely challenging. Each ebb-tidal delta is unique, making it challenging to generalize their behavior. Furthermore, their seemingly chaotic, non-conformist behavior renders many of our usual prediction techniques ineffective, especially at decadal timescales. Lastly, the amplifying effect of highly nonlinear physical processes means that small physical changes (e.g., the development of a tiny shoal) can have disproportionately large consequences (e.g., relocation of a channel several kilometers wide). As such, badassery provides a useful conceptual framework for describing the challenges presented by ebb-tidal deltas to coastal engineers and scientists.

Badass.

REFERENCES

Aagaard, T., K. P. Black, and B. Greenwood (2002), Cross-shore suspended sediment transport in the surf zone: A field-based parameterization, *Marine Geology*, *185*(3-4), 283–302, doi:10.1016/S0025-3227(02)00193-7.

Agrawal, Y. C., and H. C. Pottsmith (2000), Instruments for particle size and settling velocity observations in sediment transport, *Marine Geology*, *168*(1-4), 89–114, doi:10.1016/S0025-3227(00)00044-X.

Ali, H. N., S. L. Sheffield, J. E. Bauer, R. P. Caballero-Gill, N. M. Gasparini, J. Libarkin, K. K. Gonzales, J. Willenbring, E. Amir-Lin, J. Cisneros, D. Desai, M. Erwin, E. Gallant, K. J. Gomez, B. A. Keisling, R. Mahon, E. Marín-Spiotta, L. Welcome, and B. Schneider (2021), An actionable anti-racism plan for geoscience organizations, *Nature Communications*, *12*(1), 1–6, doi:10.1038/s41467-021-23936-w.

Allison, M. A., B. T. Yuill, E. A. Meselhe, J. K. Marsh, A. S. Kolker, and A. D. Ameen (2017), Observational and numerical particle tracking to examine sediment dynamics in a Mississippi River delta diversion, *Estuarine, Coastal and Shelf Science*, *194*, 97–108, doi:10.1016/j.ecss.2017.06.004.

Althoen, S., L. King, and K. Schilling (1993), How Long Is a Game of Snakes and Ladders?, *The Mathematical Gazette*, *77*(478), 71–76.

Ambrosio, B. G., P. H. Sousa, M. H. Gagliardi, and E. Siegle (2020), Wave energy distribution at inlet channel margins as a function of ebb tidal delta morphology: Cananéia Inlet, São Paulo, Brazil, *Anais da Academia Brasileira de Ciencias*, *92*(1), doi:10.1590/0001-3765202020180677.

Aminot, A., and R. Kérouel (2004), *Hydrologie des écosystèmes marins: paramètres et analyses*, 1 ed., 336 pp., IFREMER.

Amoudry, L. O., and A. J. Souza (2011), Deterministic coastal morphological and sediment transport modeling: A review and discussion, *Reviews of Geophysics*, *49*(2), 1–21, doi:10.1029/2010RG000341.

Anthony, E. J., and T. Aagaard (2020), The lower shoreface: Morphodynamics and sediment connectivity with the upper shoreface and beach, doi:10.1016/j.earscirev.2020.103334.

Antolínez, J. A. Á., F. J. Méndez, P. Camus, S. Vitousek, E. M. González, P. Ruggiero, and P. Barnard (2016), A multiscale climate emulator for long-term morphodynamics (MUSCLE-morpho), *Journal of Geophysical Research: Oceans*, *121*(1), 775–791, doi:10.1002/2015JC011107.

Antolínez, J. A. Á., A. B. Murray, F. J. Méndez, L. J. Moore, G. Farley, and J. Wood (2018), Downscaling Changing Coastlines in a Changing Climate: The Hybrid Approach, *Journal of Geophysical Research: Earth Surface*, *123*(2), 229–251, doi:10.1002/2017JF004367.

Bacher, C., R. Filgueira, and T. Guyondet (2016), Probabilistic approach of water residence time and connectivity using Markov chains with application to tidal embayments, *Journal of Marine Systems*, *153*(January), 25–41, doi:10.1016/j.jmarsys.2015.09.002.

Bak, J. (2017), Nourishment strategies for Ameland Inlet, Master's thesis, Delft University of Technology.

Bak, P. (1996), *How Nature Works: The Science of Self-Organized Criticality*, 212 pp., Springer-Verlag New York, Inc., New York.

Bak, P., and K. Chen (1991), Self-Organized Criticality, *Scientific American*, *264*(1), 46–53.

Balouin, Y., H. Howa, and D. Michel (2001), Swash platform morphology in the ebb-tidal delta of the Barra Nova inlet, South Portugal, *Journal of Coastal Research*, *784*(174), 784–791.

Bamunawala, J., R. Ranasinghe, A. Dastgheib, R. J. Nicholls, A. B. Murray, P. L. Barnard, T. A. J. G. Sirisena, T. M. Duong, S. J. M. H. Hulscher, and A. van der Spek (2021), Twenty-first-century projec-

tions of shoreline change along inlet-interrupted coastlines, *Scientific Reports*, *11*(1), 14,038, doi:10.1038/s41598-021-93221-9.

Baptist, M. J., E. Van Eekelen, P. J. Dankers, B. Grasmeijer, T. Van Kessel, and D. S. Van Maren (2017), Working with nature in Wadden Sea ports, in *Australasian Coasts and Ports 2017 Conference*, June, pp. 40–46.

Baptist, M. J., T. Gerkema, B. C. van Prooijen, D. S. van Maren, M. van Regteren, K. Schulz, I. Colosimo, J. Vroom, T. van Kessel, B. Grasmeijer, P. Willemsen, K. Elschot, A. V. de Groot, J. Cleveringa, E. M. van Eekelen, F. Schuurman, H. J. de Lange, and M. E. van Puijenbroek (2019), Beneficial use of dredged sediment to enhance salt marsh development by applying a 'Mud Motor', *Ecological Engineering*, *127*(November 2018), 312–323, doi:10.1016/j.ecoleng.2018.11.019.

Barnard, P. L., L. H. Erikson, E. P. Elias, and P. Dartnell (2013a), Sediment transport patterns in the San Francisco Bay Coastal System from cross-validation of bedform asymmetry and modeled residual flux, *Marine Geology*, *345*(November), 72–95, doi:10.1016/j.margeo.2012.10.011.

Barnard, P. L., A. C. Foxgrover, E. P. Elias, L. H. Erikson, J. R. Hein, M. McGann, K. Mizell, R. J. Rosenbauer, P. W. Swarzenski, R. K. Takesue, F. L. Wong, and D. L. Woodrow (2013b), Integration of bed characteristics, geochemical tracers, current measurements, and numerical modeling for assessing the provenance of beach sand in the San Francisco Bay Coastal System, *Marine Geology*, *345*, 181–206, doi:10.1016/j.margeo.2013.08.007.

R

Barry, S. J., P. J. Cowell, and C. D. Woodroffe (2007), A morphodynamic model of reef-island development on atolls, *Sedimentary Geology*, *197*(1-2), 47–63, doi:10.1016/j.sedgeo.2006.08.006.

Bartholdy, J., A. Bartholomä, and B. W. Flemming (2002), Grain Size Control Of Large Compound Flow Transverse Bedforms In A Tidal Inlet Of The Danish Wadden Sea, *Marine Geology*, *188*, 391–413.

Bartoníček, P., and B. Maus (2016), Jller.

Bass, S. J., J. N. Aldridge, I. N. McCave, and C. E. Vincent (2002), Phase relationships between fine sediment suspensions and tidal currents in coastal seas, *Journal of Geophysical Research: Oceans*, *107*(10), 1–14, doi:10.1029/2001jc001269.

Bass, S. J., I. N. McCave, J. M. Rees, and C. E. Vincent (2007), Sand and mud flux estimates using acoustic and optical backscatter sensors: Measurements seaward of the Wash, southern North Sea, *Geological Society Special Publication*, *274*, 25–35, doi:10.1144/GSL.SP.2007.274.01.04.

Bassett, D. S., D. L. Greenfield, A. Meyer-Lindenberg, D. R. Weinberger, S. W. Moore, and E. T. Bullmore (2010), Efficient physical embedding of topologically complex information processing networks in brains and computer circuits, *PLoS Computational Biology*, *6*(4), doi:10.1371/journal.pcbi.1000748.

Batagelj, V., and A. Mrvar (1998), Pajek – Program for Large Network Analysis, *Connections*, *21*(2), 47–57.

Beamsley, B. J., K. P. Black, and T. Healy (2001), Micro-scale Pumped Measurements of Suspended Sediment Over a Mixed Sand/Mud Bed: Profiles, Grain Sizes and Sediment Diffusivity, *Journal of Coastal Research*, (34), 342–356.

Becherer, J., H. Burchard, G. Flöser, V. Mohrholz, and L. Umlauf (2011), Evidence of tidal straining in well-mixed channel flow from micro-structure observations, *Geophysical Research Letters*, *38*(17), doi:10.1029/2011GL049005.

Becherer, J., M. T. Stacey, L. Umlauf, and H. Burchard (2015), Lateral Circulation Generates Flood Tide Stratification and Estuarine Exchange Flow in a Curved Tidal Inlet, *Journal of Physical Oceanography*, *45*(3), 638–656, doi:10.1175/JPO-D-14-0001.1.

Becherer, J., G. Flöser, L. Umlauf, and H. Burchard (2016), Estuarine circulation versus tidal pumping: Sediment transport in a well-mixed tidal inlet, *Journal of Geophysical Research: Oceans*, *121*(8), 6251–6270, doi:10.1002/2016JC011640.

Becherer, J., J. Hofstede, U. Gräwe, K. Purkiani, E. Schulz, and H. Burchard (2018), The Wadden Sea in transition - consequences of sea level rise, *Ocean Dynamics*, *68*(1), 131–151, doi:10.1007/s10236-017-1117-5.

Beck, T. M. (2019), Review of Coastal Tidal Inlet Morphodynamics in the Context of Barrier-Inlet Sustainability Coastal and Hydraulics Laboratory, *Tech. Rep. August*, U.S. Army Engineer Research and Development Center, Vicksburg, MS.

Beck, T. M., and D. Arnold (2019), U.S. Tidal Inlets Atlas: An Update to the CIRP Inlets Database, *Tech. Rep. May*, USACE.

Beck, T. M., and P. Wang (2019), Morphodynamics of barrier-inlet systems in the context of regional sediment management, with case studies from west-central Florida, USA, *Ocean and Coastal Management*, *177*(April), 31–51, doi:10.1016/j.ocecoaman.2019.04.022.

Beckering Vinckers, J. (1943), Amelander Gat, 1943. Report D98. (In Dutch)., *Tech. rep.*, Rijkswaterstaat Studiedienst Hoorn, Hoorn, The Netherlands.

Benninghoff, M., and C. Winter (2019), Recent morphologic evolution of the German Wadden Sea, *Scientific Reports*, *9*(1), 1–9, doi:10.1038/s41598-019-45683-1.

Bertin, X., B. Mengual, A. De Bakker, T. Guérin, K. Martins, M. Pezert, and L. Lavaud (2020), Recent Advances in Tidal Inlet Morphodynamic Modelling, *Journal of Coastal Research*, *95*(sp1), 1016–1020, doi:10.2112/SI95-198.1.

Bishop, M. J., C. H. Peterson, H. C. Summerson, H. S. Lenihan, and J. H. Grabowski (2006), Deposition and long-shore transport of dredge spoils to nourish beaches: Impacts on benthic infauna of an ebb-tidal delta, *Journal of Coastal Research*, *223*, 530–546, doi:10.2112/03-0136.1.

Black, K. S., S. Athey, P. Wilson, and D. Evans (2007), The use of particle tracking in sediment transport studies: a review, *Geological Society, London, Special Publications*, *274*(1), 73–91, doi:10.1144/GSL.SP.2007.274.01.09.

Black, K. S., J. Poleykett, R. J. Uncles, and M. R. Wright (2017), Sediment Transport: Instrumentation and Methodologies, in *Estuarine and Coastal Hydrography and Sediment Transport*, edited by R. J. Uncles and S. Mitchell, pp. 261–289, Cambridge University Press, Cambridge, UK.

Blackley, M. W., and A. D. Heathershaw (1982), Wave and tidal-current sorting of sand on a wide surf-zone beach, *Marine Geology*, *49*(3-4), 345–355, doi:10.1016/0025-3227(82)90048-2.

Blott, S. J., and K. Pye (2001), Gradistat: A grain size distribution and statistics package for the analysis of unconsolidated sediments, *Earth Surface Processes and Landforms*, *26*(11), 1237–1248, doi:10.1002/esp.261.

Boechat Albernaz, M., G. Ruessink, H. R. Jagers, and M. G. Kleinhans (2019), Effects of wave orbital velocity parameterization on nearshore sediment transport and decadal morphodynamics, *Journal of Marine Science and Engineering*, *7*(6), doi:10.3390/jmse7060188.

Bosboom, J., and M. J. Stive (2021), *Coastal Dynamics*, 1269 ed., TU Delft Open, Delft University of Technology, Delft, The Netherlands, doi:10.5074/T.2021.001.

Bosnic, I., J. Cascalho, R. Taborda, T. Drago, J. Hermínio, M. Rosa, J. Dias, and E. Garel (2017), Nearshore sediment transport: Coupling sand tracer dynamics with oceanographic forcing, *Marine Geology*, *385*, 293–303, doi:10.1016/j.margeo.2017.02.004.

Boss, E., W. H. Slade, M. Behrenfeld, and G. Dall'Olmo (2009a), Acceptance angle effects on the beam attenuation in the ocean, *Optics Express*, *17*(3), 1535, doi:10.1364/oe.17.001535.

Boss, E., W. Slade, and P. Hill (2009b), Effect of particulate aggregation in aquatic environments on the beam attenuation and its utility as a proxy for particulate mass, *Optics Express*, *17*(11), 9408, doi:10.1364/oe.17.009408.

Boss, E., C. R. Sherwood, P. Hill, and T. Milligan (2018), Advantages and limitations to the use of optical measurements to study sediment properties, *Applied Sciences*, *8*(12), doi:10.3390/app8122692.

Bracken, L. J., L. Turnbull, J. Wainwright, and P. Bogaart (2015), Sediment connectivity: A framework for understanding sediment transfer at multiple scales, *Earth Surface Processes and Landforms*, *40*(2), 177–188, doi:10.1002/esp.3635.

Brakenhoff, L., M. Van der Vegt, and G. Ruessink (2019a), Local spatio-temporal bedform patterns on an ebb-tidal delta, in *Marine and River Dune Dynamics – MARID VI*, 1-3 April, pp. 17–22.

Brakenhoff, L., G. Ruessink, and M. van der Vegt (2019b), Characteristics of saw-tooth bars on the ebb-tidal deltas of the Wadden Islands, *Ocean Dynamics*, doi:10.1007/s10236-019-01315-w.

Brakenhoff, L., R. Schrijvershof, J. van der Werf, B. Grasmeijer, G. Ruessink, and M. van der Vegt (2020a), From ripples to large-scale sand transport: The effects of bedform-related roughness on hydrodynamics and sediment transport patterns in delft3d, *Journal of Marine Science and Engineering*, *8*(11), 1–25, doi:10.3390/jmse8110892.

Brakenhoff, L., M. Kleinhans, G. Ruessink, and M. van der Vegt (2020b), Spatio-temporal characteristics of small-scale wave–current ripples on the Ameland ebb-tidal delta, *Earth Surface Processes and Landforms*, *45*(5), 1248–1261, doi:10.1002/esp.4802.

Brakenhoff, L. B. (2021), Bedforms and their effect on sediment transport on ebb-tidal deltas, Phd, Universiteit Utrecht.

Bridge, J. S. (1993), The interaction between channel geometry, water flow, sediment transport and deposition in braided rivers, in *Braided Rivers*, edited by J. L. Best and C. S. Bristow, 75, pp. 13–71.

Brière, C., S. K. Janssen, A. P. Oost, M. Taal, and P. K. Tonnon (2018), Usability of the climate-resilient nature-based Sand Motor pilot, The Netherlands, *Journal of Coastal Conservation*, *22*(3), 491–502, doi:10.1007/s11852-017-0527-3.

Brierley, G., K. Fryirs, H. Reid, and R. Williams (2021), The dark art of interpretation in geomorphology, *Geomorphology*, *390*, 107,870, doi:10.1016/j.geomorph.2021.107870.

Brommer, M. B., and L. M. Bochev-Van Der Burgh (2009), Sustainable coastal zone management: A concept for forecasting long-term and large-scale coastal evolution, *Journal of Coastal Research*, *25*(1), 181–188, doi:10.2112/07-0909.1.

Bruun, P., and F. Gerritsen (1959), Natural By-Passing of Sand at Coastal Inlets, *Journal of the Waterways and Harbors Division: Proceedings of the American Society of Civil Engineers*, *85*(4), 75–107, doi:10.1061/taceat.0008322.

Bult, S. V. (2021), The influence of the tide, wind and waves on the large-scale sediment transport patterns in the Dutch Wadden Sea, Master's thesis, Delft University of Technology.

Burchard, H., G. Flöser, J. V. Staneva, T. H. Badewien, and R. Riethmüller (2008), Impact of Density Gradients on Net Sediment Transport into the Wadden Sea, *Journal of Physical Oceanography*, *38*(3), 566–587, doi:10.1175/2007JPO3796.1.

Burgess, S. C., K. J. Nickols, C. D. Griesemer, L. A. K. Barnett, A. G. Dedrick, E. V. Satterthwaite, L. Yamane, S. G. Morgan, J. W. White, and L. W. Botsford (2013), Beyond connectivity: how empirical methods can quantify population persistence to improve marine protected area design, *Ecological Applications*, p. 130819190545008, doi:10.1890/13-0710.1.

Burt, T. P., and R. J. Allison (2009), Sediment Cascades in the Environment: An Integrated Approach, *Sediment Cascades: An Integrated Approach*, pp. 1–15, doi:10.1002/9780470682876.ch1.

Calabrese, J. M., and W. F. Fagan (2004), A comparison-shopper's guide to connectivity metrics, *Frontiers in Ecology and the Environment*, *2*(10), 529–536, doi:10.1890/1540-9295(2004)002[0529:ACGTCM]2.0.CO;2.

Callaway, D. S., M. E. Newman, S. H. Strogatz, and D. J. Watts (2000), Network robustness and fragility: percolation on random graphs, *Physical Review Letters*, *85*(25), 5468–5471, doi:10.1103/PhysRevLett.85.5468.

Campbell Scientific Inc. (2014), OBS-3+ and OBS300 Suspended Solids and Turbidity Monitors, *Tech. rep.*, Campbell Scientific Inc., Logan, utah.

Cantwell, M. D., and R. T. T. Forman (1993), Landscape graphs: Ecological modeling with graph theory to detect configurations common to diverse landscapes, *Landscape Ecology*, *8*(4), 239–255.

Carrasco, A. R., Ó. Ferreira, A. Matias, P. Freire, X. Bertin, and J. A. Dias (2013), Sediment transport measurements with tracers in very low-energy beaches, *Earth Surface Processes and Landforms*, *38*(6), 561–569, doi:10.1002/esp.3300.

Castelle, B., G. Dodet, G. Masselink, and T. Scott (2017), A new climate index controlling winter wave

activity along the Atlantic coast of Europe: The West Europe Pressure Anomaly, *Geophysical Research Letters*, *44*(3), 1384–1392, doi:10.1002/2016GL072379.

Chanson, H., M. Trevethan, and S. ichi Aoki (2008), Acoustic Doppler velocimetry (ADV) in small estuary: Field experience and signal post-processing, *Flow Measurement and Instrumentation*, *19*(5), 307–313, doi:10.1016/j.flowmeasinst.2008.03.003.

Chapalain, M., R. Verney, M. Fettweis, M. Jacquet, D. Le Berre, and P. Le Hir (2019), Investigating suspended particulate matter in coastal waters using the fractal theory, *Ocean Dynamics*, *69*(1), 59–81, doi:10.1007/s10236-018-1229-6.

Cheng, C., J. de Smit, G. Fivash, S. Hulscher, B. Borsje, and K. Soetaert (2021), Sediment shell-content diminishes current-driven sand ripple development and migration, *Earth Surface Dynamics Discussions*, pp. 1–26, doi:10.5194/esurf-2021-13.

Cheshire, J., and O. Uberti (2017), *Where the Animals Go: Tracking Wildlife with Technology in 50 Maps and Graphics*, 174 pp., W.W. Norton and Company, Inc., New York.

Cheung, K. F., F. Gerritsen, and J. Cleveringa (2007), Morphodynamics and Sand Bypassing at Ameland Inlet, The Netherlands, *Journal of Coastal Research*, *231*, 106–118, doi:10.2112/04-0403.1.

Chmiel, O., I. Baselt, and A. Malcherek (2018), Applicability of Acoustic Concentration Measurements in Suspensions of Artificial and Natural Sediments Using an Acoustic Doppler Velocimeter, *Acoustics*, *1*(1), 59–77, doi:10.3390/acoustics1010006.

Ciavola, P., and E. Grottoli (2017), Tracers and Coarse Sediment, in *Encyclopedia of Coastal Science-Coastal Science*, edited by C. Finkl and C. Makowski, pp. 1796–1803, Springer International Publishing AG 2017, doi:10.1007/978-3-319-93806-6_330.

Ciavola, P., N. Dias, Ó. Ferreira, R. Taborda, and J. M. Dias (1998), Fluorescent sands for measurements of longshore transport rates: A case study from Praia de Faro in southern Portugal, *Geo-Marine Letters*, *18*(1), 49–57, doi:10.1007/s003670050051.

Cleary, W. J. (2002), Variations in Inlet Behavior and Shoreface Sand Resources: Factors Controlling Management Decisions, Figure Eight Island, NC, USA, *Journal of Coastal Research*, *36*, 148–163, doi:10.2112/1551-5036-36.sp1.148.

Clemens, K. E., and P. D. Komar (1988), Tracers of sand movement on the Oregon coast, in *Coastal Engineering 1988*, pp. 1338–1351.

Colina Alonso, A., D. van Maren, E. Elias, S. Holthuijsen, and Z. Wang (2021), The contribution of sand and mud to infilling of tidal basins in response to a closure dam, *Marine Geology*, *439*(February), 106,544, doi:10.1016/j.margeo.2021.106544.

Colosimo, I., P. L. de Vet, D. S. van Maren, A. Reniers, J. C. Winterwerp, and B. C. van Prooijen (2020), The impact of wind on flow and sediment transport over intertidal flats, *Journal of Marine Science and Engineering*, *8*(11), 1–26, doi:10.3390/jmse8110910.

Compton, T. J., J. Van der Meer, S. Holthuijsen, A. Dekinga, J. Horn, and L. Klunder (2013), Synoptic Intertidal Benthic Surveys Across the Dutch Wadden Sea 2008 to 2011, *Tech. rep.*, NIOZ.

Condie, S. A., M. Herzfeld, K. Hock, J. R. Andrewartha, R. Gorton, R. Brinkman, and M. Schultz (2018), System level indicators of changing marine connectivity, *Ecological Indicators*, *91*(November 2017), 531–541, doi:10.1016/j.ecolind.2018.04.036.

Conner, C. S., and A. M. De Visser (1992), A laboratory investigation of particle size effects on an optical backscatterance sensor, *Marine Geology*, *108*(2), 151–159, doi:10.1016/0025-3227(92)90169-I.

Cooke, B. C., A. R. Jones, I. D. Goodwin, and M. J. Bishop (2012), Nourishment practices on Australian sandy beaches: A review, *Journal of Environmental Management*, *113*, 319–327, doi:10.1016/j.jenvman.2012.09.025.

Corcoran, P. L. (2015), Benthic plastic debris in marine and fresh water environments, *Environmental Sciences: Processes and Impacts*, *17*(8), 1363–1369, doi:10.1039/c5em00188a.

Cossart, E., V. Viel, C. Lissak, R. Reulier, M. Fressard, and D. Delahaye (2018), How might sediment connectivity change in space and time?, *Land Degradation and Development*, *29*(8), 2595–2613, doi:10.1002/ldr.3022.

Courtois, G., and A. Monaco (1969), Radioactive methods for the quantitative determination of coastal drift rate, *Marine Geology*, *7*(3), 183–206, doi:10.1016/0025-3227(69)90008-5.

Cowell, P. J., M. J. Stive, A. W. Niedoroda, H. J. De Vriend, D. J. P. Swift, G. M. Kaminsky, and M. Capobianco (2003), The Coastal-Tract (Part 1): A Conceptual Approach to Aggregated Modeling of Low-Order Coastal Change, *Journal of Coastal Research*, *19*(4), 812–827.

Cowen, R. K., and S. Sponaugle (2009), Larval Dispersal and Marine Population Connectivity, *Annu. Rev. Mar. Sci*, *1*, 443–466, doi:10.1146/annurev.marine.010908.163757.

Csárdi, G., and T. Nepusz (2006), The igraph software package for complex network research, *InterJournal Complex Systems*, *1695*, 1–9, doi:10.3724/SP.J.1087.2009.02191.

Dankers, P. J., and J. C. Winterwerp (2007), Hindered settling of mud flocs: Theory and validation, *Continental Shelf Research*, *27*(14), 1893–1907, doi:10.1016/j.csr.2007.03.005.

Davidson, M. A., I. L. Turner, K. D. Splinter, and M. D. Harley (2017), Annual prediction of shoreline erosion and subsequent recovery, *Coastal Engineering*, *130*(July), 14–25, doi:10.1016/j.coastaleng.2017.09.008.

Davies, D. J., E. N. Powell, and R. J. Stanton (1989), Taphonomic signature as a function of environmental process: Shells and shell beds in a hurricane-influenced inlet on the Texas coast, *Palaeogeography, Palaeoclimatology, Palaeoecology*, *72*(C), 317–356, doi:10.1016/0031-0182(89)90150-8.

Davis, R. A. J., and P. L. Barnard (2000), How anthropogenic factors in the back-barrier area influence tidal inlet stability: examples from the Gulf Coast of Florida, USA, *Geological Society London Special Publications*, *175*(1), 293, doi:10.1144/GSL.SP.2000.175.01.21.

de Fockert, A. (2008), Impact of Relative Sea Level Rise on the Amelander Inlet Morphology, *MSc thesis*, p. 189.

de Jonge, V. N., K. Essink, and R. Boddeke (1993), The Dutch Wadden Sea: a changed ecosystem, *Hydrobiologia*, *265*(1-3), 45–71, doi:10.1007/BF00007262.

de Schipper, M. A., S. de Vries, G. Ruessink, R. C. de Zeeuw, J. Rutten, C. van Gelder-Maas, and M. J. Stive (2016), Initial spreading of a mega feeder nourishment: Observations of the Sand Engine pilot project, *Coastal Engineering*, *111*, 23–38, doi:10.1016/j.coastaleng.2015.10.011.

de Schipper, M. A., B. C. Ludka, B. Raubenheimer, A. P. Luijendijk, and T. A. Schlacher (2021), Beach nourishment has complex implications for the future of sandy shores, *Nature Reviews Earth & Environment*, doi:10.1038/s43017-020-00109-9.

de Vet, P. L., B. C. van Prooijen, I. Colosimo, N. Steiner, T. Ysebaert, P. M. Herman, and Z. B. Wang (2020), Variations in storm-induced bed level dynamics across intertidal flats, *Scientific Reports*, *10*(1), 1–15, doi:10.1038/s41598-020-69444-7.

De Vriend, H. J. (1991), Mathematical modelling and large- scale coastal behaviour Part 1: Physical processes, *Journal of Hydraulic Research*, *29*(6), 727–740, doi:10.1080/00221689109498955.

de Vriend, H. J., M. van Koningsveld, S. G. Aarninkhof, M. B. de Vries, and M. J. Baptist (2015), Sustainable hydraulic engineering through building with nature, *Journal of Hydro-Environment Research*, *9*(2), 159–171, doi:10.1016/j.jher.2014.06.004.

de Vries, S. (2016), Modeling sediment transport pathways in the mouth of the Scheldt estuary, Msc, University of Twente.

de Wit, F. P., M. F. S. Tissier, S. G. Pearson, M. Radermacher, M. J. P. V. D. Ven, and A. P. V. Langevelde (2018), Measuring the Spatial and Temporal Variability of Currents on Ameland Ebb-Tidal Delta, in *NCK Days 2018*, Haarlem.

de Wit, F. P., M. Tissier, and A. Reniers (2019), Characterizing wave shape evolution on an ebb-tidal shoal, *Journal of Marine Science and Engineering*, *7*(10), 1–20, doi:10.3390/jmse7100367.

de Wit, F. P., M. Tissier, and A. Reniers (2020), The relationship between sea-swell bound wave height and wave shape, *Journal of Marine Science and Engineering*, *8*(9), doi:10.3390/JMSE8090643.

Dean, R. G. (2002), *Beach Nourishment: Theory and Practice*, 396 pp., World Scientific, Singapore.

Defeo, O., A. McLachlan, D. S. Schoeman, T. A. Schlacher, J. Dugan, A. Jones, M. Lastra, and F. Scapini (2009), Threats to sandy beach ecosystems: A review, *Estuarine, Coastal and Shelf Science*, *81*(1), 1–12, doi:10.1016/j.ecss.2008.09.022.

Defne, Z., N. K. Ganju, and A. Aretxabaleta (2016), Estimating time-dependent connectivity in marine systems, *Geophysical Research Letters*, *43*(3), 1193–1201, doi:10.1002/2015GL066888.

Delft University of Technology, Utrecht University, and University of Twente (2019), *SEAWAD: SEdiment supply At the WAdden Sea ebb-tidal Delta*, 4TU.Centre for Research Data, doi:10.4121/collection:seawad.

Deltares (2014), *Delft3D-FLOW, User Manual*, 1–684 pp., Deltares, Delft, the Netherlands.

Derrible, S., and C. Kennedy (2009), Network Analysis of World Subway Systems Using Updated Graph Theory, *Transportation Research Record: Journal of the Transportation Research Board*, *2112*, 17–25, doi:10.3141/2112-03.

Dodet, G., X. Bertin, N. Bruneau, A. B. Fortunato, A. Nahon, and A. Roland (2013), Wave-current interactions in a wave-dominated tidal inlet, *Journal of Geophysical Research: Oceans*, *118*(3), 1587–1605, doi:10.1002/jgrc.20146.

Dolch, T., and H. C. Hass (2008), Long-term changes of intertidal and subtidal sediment compositions in a tidal basin in the northern Wadden Sea (SE North Sea), *Helgoland Marine Research*, *62*(1), 3–11, doi:10.1007/s10152-007-0090-7.

Donchyts, G., F. Baart, H. Winsemius, N. Gorelick, J. Kwadijk, and N. Van De Giesen (2016), Earth's surface water change over the past 30 years, *Nature Climate Change*, *6*(9), 810–813, doi:10.1038/nclimate3111.

Downing, J. (2006), Twenty-five years with OBS sensors: The good, the bad, and the ugly, *Continental Shelf Research*, *26*(17-18), 2299–2318, doi:10.1016/j.csr.2006.07.018.

Downing, J. P., R. W. Sternberg, and C. R. Lister (1981), New instrumentation for the investigation of sediment suspension processes in the shallow marine environment, *Developments in Sedimentology*, *32*(C), 19–34, doi:10.1016/S0070-4571(08)70292-9.

Duane, D., and W. James (1980), Littoral transport in the surf zone elucidated by an Eulerian sediment tracer experiment, doi:10.1306/212F7B26-2B24-11D7-8648000102C1865D.

Duc, D. M., D. X. Thanh, D. T. Quynh, and P. McLaren (2016), Analysis of sediment distribution and transport for mitigation of sand deposition hazard in Tam Quan estuary, Vietnam, *Environmental Earth Sciences*, *75*(9), 741, doi:10.1007/s12665-016-5560-2.

Duong, T. M., R. Ranasinghe, D. J. R. Walstra, and D. Roelvink (2016), Assessing climate change impacts on the stability of small tidal inlet systems: Why and how?, *Earth-Science Reviews*, *154*, 369–380, doi:10.1016/j.earscirev.2015.12.001.

Duran-Matute, M., T. Gerkema, G. J. De Boer, J. J. Nauw, and U. Grawe (2014), Residual circulation and freshwater transport in the Dutch Wadden Sea: A numerical modelling study, *Ocean Science*, *10*(4), 611–632, doi:10.5194/os-10-611-2014.

Duran-Matute, M., T. Gerkema, and M. G. Sassi (2016a), Quantifying the residual volume transport through a multiple-inlet system in response to wind forcing: The case of the western Dutch Wadden Sea, *Journal of Geophysical Research: Oceans*, *121*(12), 8888–8903, doi:10.1002/2016JC011807.

Duran-Matute, M., T. Gerkema, and M. G. Sassi (2016b), Anisotropic response to wind forcing of the residual circulation in a multiple-inlet system: the case of the western Dutch Wadden Sea, *Journal of Geophysical Research: Oceans*, pp. 1–36.

Eelkema, M., Z. B. Wang, and M. J. Stive (2012), Impact of back-barrier dams on the development of the ebb-tidal delta of the Eastern Scheldt, *Journal of Coastal Research*, *28*(6), 1591–1605, doi:10.2112/JCOASTRES-D-11-00003.1.

Eelkema, M., Z. B. Wang, A. Hibma, and M. J. Stive (2013), Morphological Effects of the Eastern Scheldt Storm Surge Barrier on the Ebb-Tidal Delta, *Coastal Engineering Journal*, *55*(03), 1350,010, doi:10.1142/S0578563413500101.

Eidam, E. F., T. Langhorst, and E. B. Goldstein (2021), OpenOBS: Open-source , low-cost optical backscatter sensors for water quality and sediment-transport research, *EarthArXiv Preprint*, pp. 1–31, doi:10.31223/X5KC9W.

Eide, A., B. Malherbe, M. Mercanti, and B. Lahousse (1992), Assessment of Coastal Processes for the Design and the Construction of the Zeepipe Landfall in Zeebrugge, in *Coastal Engineering 1992*, pp. 1565–1569, American Society of Civil Engineers, Venice, Italy.

Eisma, D. (1993), *Suspended matter in the aquatic environment*, Springer, New York.

Elias, E. (2018), *Bench-mark morphodynamic model Ameland Inlet - Kustgenese 2.0 (ZG-C2)*, 70 pp., Deltares, Delft, The Netherlands.

Elias, E., S. G. Pearson, A. van der Spek, and S. Pluis (2022), Understanding meso-scale processes at a mixed-energy tide-dominated tidal inlet: Ameland Inlet, *Submitted to Ocean and Coastal Management*.

Elias, E. P. (2006), Morphodynamics of Texel Inlet, Phd, TU Delft.

Elias, E. P. (2017), Stroming en sedimenttransport langs de Boschplaat op Terschelling, *Deltares report*.

Elias, E. P. (2021), Morfologische analyse buitendelta suppletie Ameland, *Tech. rep.*, Deltares, Delft, The Netherlands.

Elias, E. P., and J. E. Hansen (2013), Understanding processes controlling sediment transports at the mouth of a highly energetic inlet system (San Francisco Bay, CA), *Marine Geology*, *345*(November 2013), 207–220, doi:10.1016/j.margeo.2012.07.003.

Elias, E. P., and A. J. van der Spek (2017), Dynamic preservation of Texel Inlet, the Netherlands: understanding the interaction of an ebb-tidal delta with its adjacent coast, *Netherlands Journal of Geosciences*, *96*(04), 293–317, doi:10.1017/njg.2017.34.

Elias, E. P., M. J. Stive, H. Bonekamp, and J. Cleveringa (2003), Tidal Inlet Dynamics in Response To Human Intervention, *Coastal Engineering Journal*, *45*(04), 629–658, doi:10.1142/S0578563403000932.

Elias, E. P., J. Cleveringa, M. C. Buijsman, J. A. Roelvink, M. J. Stive, D. Roelvink, A. J. F. Van Der Spek, J. Cleveringa, M. C. Buijsman, J. A. Roelvink, and M. J. Stive (2006), Field and model data analysis of sand transport patterns in Texel Tidal inlet (the Netherlands), *Coastal Engineering*, *53*(5-6), 505–529, doi:10.1016/j.coastaleng.2005.11.006.

Elias, E. P., G. Gelfenbaum, M. van Ormondt, and H. R. Moritz (2011), Predicting sediment transport patterns at the mouth of the Columbia River, in *Coastal Sediments 2011*, pp. 588–601, doi:10.1142/9789814355537_0045.

Elias, E. P., A. J. F. van der Spek, Z. B. Wang, and J. De Ronde (2012a), Morphodynamic development and sediment budget of the Dutch Wadden Sea over the last century, *Geologie en Mijnbouw/Netherlands Journal of Geosciences*, *91*(3), 293–310, doi:10.1017/S0016774600000457.

Elias, E. P., G. Gelfenbaum, and A. J. Van Der Westhuysen (2012b), Validation of a coupled wave-flow model in a high-energy setting: The mouth of the Columbia River, *Journal of Geophysical Research: Oceans*, *117*(9), 1–21, doi:10.1029/2012JC008105.

Elias, E. P., A. J. F. van der Spek, and M. Lazar (2015a), The 'Voordelta', the contiguous ebb-tidal deltas in the SW Netherlands; Large-scale morphological changes and sediment budget 1965-2013; Impacts of large-scale engineering., *Netherlands Journal of Geosciences*, (November), doi:10.1017/njg.2016.37.

Elias, E. P., R. Teske, A. J. F. van der Spek, and M. Lazar (2015b), Modelling Tidal-Inlet Morphodynamics on Medium Time Scales, in *Coastal Sediments 2015*, pp. 1–14, San Diego, CA.

Elias, E. P., A. J. F. Van Der Spek, S. G. Pearson, and J. Cleveringa (2019), Understanding sediment bypassing processes through analysis of high- frequency observations of Ameland Inlet , the Netherlands, *Marine Geology*, *415*(May), 105,956, doi:10.1016/j.margeo.2019.06.001.

Elias, E. P., F. E. Roelvink, S. G. Pearson, and B. Huisman (2020), Investigation of sediment pathways in the Put Van Hansweert: Morphological effects of dumping in a deep pit of the Western Scheldt, *Tech. rep.*, Deltares, Delft, The Netherlands.

Elias, E. P., E. Quataert, and S. G. Pearson (2021a), Morfologische analyse systeemsuppletie Callantsoog, *Tech. rep.*, Deltares, Delft, The Netherlands.

Elias, E. P., F. E. Roelvink, and S. G. Pearson (2021b), Systeemsuppleties op Eilandkoppen Modellering suppletievarianten: Texel en Ameland, *Tech. rep.*, Deltares, Delft, The Netherlands.

Elko, N., K. Mckenna, T. R. Briggs, N. Brown, M. Walther, and D. York (2020), Best management practices for coastal inlets, *88*(3).

Erikson, L. H., S. a. Wright, E. P. Elias, D. M. Hanes, D. H. Schoellhamer, and J. L. Largier (2013), The use of modeling and suspended sediment concentration measurements for quantifying net suspended sediment transport through a large tidally dominated inlet, *Marine Geology*, *345*, 96–112, doi:10.1016/j.margeo.2013.06.001.

Esposito, U., M. Giugliano, M. Van Rossum, and E. Vasilaki (2014), Measuring symmetry, asymmetry and randomness in neural network connectivity, *PLoS ONE*, *9*(7), doi:10.1371/journal.pone.0100805.

Fettweis, M., M. Sas, and J. Monbaliu (1998), Seasonal, neap-spring and tidal variation of cohesive sediment concentration in the Scheldt Estuary, Belgium, *Estuarine, Coastal and Shelf Science*, *47*(1), 21–36, doi:10.1006/ecss.1998.0338.

Fettweis, M., R. Riethmüller, R. Verney, M. Becker, J. Backers, M. Baeye, M. Chapalain, S. Claeys, J. Claus, T. Cox, J. Deloffre, D. Depreiter, F. Druine, G. Flöser, S. Grünler, F. Jourdin, R. Lafite, J. Nauw, B. Nechad, R. Röttgers, A. Sottolichio, T. V. Engeland, W. Vanhaverbeke, H. Vereecken, T. Van Engeland, W. Vanhaverbeke, and H. Vereecken (2019), Uncertainties associated with in situ high-frequency long-term observations of suspended particulate matter concentration using optical and acoustic sensors, *Progress in Oceanography*, *178*(July 2018), 102,162, doi:10.1016/j.pocean.2019.102162.

FitzGerald, D. M. (1983), Sediment Bypassing At Mixed Energy Tidal Inlets., *Proceedings of the Coastal Engineering Conference*, *2*, 1094–1118, doi:10.9753/icce.v18.68.

FitzGerald, D. M. (1984), Interactions between the ebb-tidal delta and landward shoreline; Price Inlet, South Carolina, *Journal of Sedimentary Research*, *54*(4), 1303–1318, doi:10.1306/212F85C6-2B24-11D7-8648000102C1865D.

FitzGerald, D. M. (1988), Shoreline Erosional-Depositional Processes Associated with Tidal Inlets, in *Hydrodynamics and Sediment Dynamics of Tidal Inlets*, pp. 186–225, Springer, New York.

FitzGerald, D. M., S. Penland, and D. Nummedal (1984), Control of Barrier Island Shape by Inlet Sediment Bypassing: East Frisian Islands, West Germany, *Developments in Sedimentology*, *39*(C), 355–376, doi:10.1016/S0070-4571(08)70154-7.

FitzGerald, D. M., I. V. Buynevich, M. S. Fenster, and P. A. McKinlay (2000), Sandy dynamics at the mouth of a rock-bound, tide-dominated estuary, *Sedimentary Geology*, *131*(1-2), 25–49, doi:10.1016/S0037-0738(99)00124-4.

FitzGerald, D. M., I. Buynevich, and C. Hein (2012), Morphodynamics and Facies Architecture of Tidal Inlets and Tidal Deltas, in *Principles of Tidal Sedimentology*, edited by R. A. Davis and R. W. Dalrymple, chap. 12, pp. 301–333, Springer Netherlands, Dordrecht, doi:10.1007/978-94-007-0123-6.

Flemming, B. W., and K. Ziegler (1995), High-Resolution Grain Size Distribution Patterns and Textural Trends in the Backbarrier Environment of Spiekeroog Island (Southern North Sea), *Senckengbergiana Maritima*, *26*, 1–24.

Floor, J. R., C. S. van Koppen, and J. P. van Tatenhove (2016), Uncertainties in the assessment of "significant effect" on the Dutch Natura 2000 Wadden Sea site - The mussel seed fishery and powerboat race controversies, *Environmental Science and Policy*, *55*, 380–392, doi:10.1016/j.envsci.2015.03.008.

Flores, R. P., S. Rijnsburger, A. R. Horner-Devine, A. J. Souza, and J. D. Pietrzak (2017), The impact of storms and stratification on sediment transport in the Rhine region of freshwater influence, *Journal of Geophysical Research: Oceans*, *122*(5), 4456–4477, doi:10.1002/2016JC012362.

Flores, R. P., S. Rijnsburger, S. Meirelles, A. R. Horner-Devine, A. J. Souza, J. D. Pietrzak, M. Henriquez, and A. Reniers (2018), Wave generation of gravity-driven sediment flows on a predominantly sandy seabed, *Geophysical Research Letters*, *45*(15), 7634–7645, doi:10.1029/2018GL077936.

Fokker, P., F. van Leijen, B. Orlic, H. van der Marel, and R. Hanssen (2018), Subsidence in the Dutch Wadden Sea, *Netherlands Journal of Geosciences*, *97*(03), 129–181, doi:10.1017/njg.2018.9.

Fontolan, G., S. Pillon, F. Delli Quadri, and A. Bezzi (2007), Sediment storage at tidal inlets in northern Adriatic lagoons: Ebb-tidal delta morphodynamics, conservation and sand use strategies, *Estuarine, Coastal and Shelf Science*, *75*(1-2), 261–277, doi:10.1016/j.ecss.2007.02.029.

Ford, M. R., and M. E. Dickson (2018), Detecting ebb-tidal delta migration using Landsat imagery, *Marine Geology*, *405*(December 2017), 38–46, doi:10.1016/j.margeo.2018.08.002.

Fortunato, A., P. Freire, B. Mengual, X. Bertin, C. Pinto, K. Martins, T. Guérin, and A. Azevedo (2021), Sediment dynamics and morphological evolution in the Tagus Estuary inlet, *Marine Geology*, p. 106590, doi:10.1016/j.margeo.2021.106590.

Foster, G., T. R. Healy, and W. P. De Lange (1994), Sediment budget and equilibrium beach profiles applied to renourishment of an ebb tidal delta adjacent beach, Mt. Maunganui, New Zealand, *Journal of Coastal Research*, *10*(3), 564–575.

Foster, I. D. L. (2000), *Tracers in Geomorphology*, 1–560 pp., John Wiley & Sons Ltd, Chichester, UK.

Franz, M., C. T. Lopes, G. Huck, Y. Dong, O. Sumer, and G. D. Bader (2016), Cytoscape.js: A graph theory library for visualisation and analysis, *Bioinformatics*, *32*(2), 309–311, doi:10.1093/bioinformatics/btv557.

French, J., H. Burningham, G. Thornhill, R. Whitehouse, and R. J. Nicholls (2016), Conceptualising and mapping coupled estuary, coast and inner shelf sediment systems, *Geomorphology*, *256*, 17–35, doi:10.1016/j.geomorph.2015.10.006.

Friedrichs, C. T. (2012), Tidal Flat Morphodynamics: A Synthesis, in *Treatise on Estuarine and Coastal Science*, vol. 3, pp. 137–170, Elsevier Inc., doi:10.1016/B978-0-12-374711-2.00307-7.

Fruergaard, M., M. Pejrup, A. S. Murray, and T. J. Andersen (2015), On luminescence bleaching of tidal channel sediments, *Geografisk Tidsskrift - Danish Journal of Geography*, *115*(1), 57–65, doi:10.1080/00167223.2015.1011418.

Fryirs, K. (2013), (Dis)Connectivity in catchment sediment cascades: A fresh look at the sediment delivery problem, *Earth Surface Processes and Landforms*, *38*(1), 30–46, doi:10.1002/esp.3242.

Fugate, D. C., and C. T. Friedrichs (2002), Determining concentration and fall velocity of estuarine particle populations using ADV, OBS and LISST, *Continental Shelf Research*, *22*(11-13), 1867–1886, doi:10.1016/S0278-4343(02)00043-2.

Furbish, D. J., and T. H. Doane (2021), Rarefied particle motions on hillslopes – Part 4: Philosophy, *Earth Surface Dynamics*, *9*(3), 629–664, doi:10.5194/esurf-9-629-2021.

Gaida, T. C., T. A. van Dijk, M. Snellen, T. Vermaas, C. Mesdag, and D. G. Simons (2020), Monitoring underwater nourishments using multibeam bathymetric and backscatter time series, *Coastal Engineering*, *158*, 103,666, doi:10.1016/j.coastaleng.2020.103666.

Gallaway, E., A. S. Trenhaile, M. T. Cioppa, and R. G. Hatfield (2012), Magnetic mineral transport and sorting in the swash-zone: northern Lake Erie, Canada, *Sedimentology*, *59*(6), 1718–1734, doi:10.1111/j.1365-3091.2012.01323.x.

Galpern, P., M. Manseau, and A. Fall (2011), Patch-based graphs of landscape connectivity: A guide to construction, analysis and application for conservation, *Biological Conservation*, *144*(1), 44–55, doi:10.1016/j.biocon.2010.09.002.

Gao, S., and M. Collins (1991), Discussion: A Critique of the "McLaren Method" for Defining Sediment Transport Paths, *Journal of Sedimentary Petrology*, *61*(1), 143–146.

Garel, E., C. Sousa, Ó. Ferreira, and J. A. Morales (2014a), Decadal morphological response of an ebb-tidal delta and down-drift beach to artificial breaching and inlet stabilisation, *Geomorphology*, *216*, 13–25, doi:10.1016/j.geomorph.2014.03.031.

Garel, E., C. Sousa, Ó. Ferreira, and J. A. Morales (2014b), Decadal morphological response of an ebb-tidal delta and down-drift beach to artificial breaching and inlet stabilisation, *Geomorphology*, *216*, 13–25, doi:10.1016/j.geomorph.2014.03.031.

Gartner, J. W., R. T. Cheng, P. F. Wang, and K. Richter (2001), Laboratory and field evaluations of the LISST-100 instrument for suspended particle size determinations, *Marine Geology*, *175*(1-4), 199–219, doi:10.1016/S0025-3227(01)00137-2.

Gatto, V. M., B. C. van Prooijen, and Z. B. Wang (2017), Net sediment transport in tidal basins: quantifying the tidal barotropic mechanisms in a unified framework, *Ocean Dynamics*, *67*(11), 1385–1406, doi:10.1007/s10236-017-1099-3.

Gaudiano, D. J., and T. W. Kana (2001), Shoal Bypassing in Mixed Energy Inlets: Geomorphic Variables and Empirical Predictions for Nine South Carolina Inlets, *Journal of Coastal Research*, *17*(2), 280–291.

Gawehn, M., A. van Dongeren, S. de Vries, C. Swinkels, R. Hoekstra, S. G. Aarninkhof, and J. Friedman (2020), The application of a radar-based depth inversion method to monitor near-shore nourishments on an open sandy coast and an ebb-tidal delta, *Coastal Engineering*, *159*, 103,716, doi:10.1016/j.coastaleng.2020.103716.

Gawehn, M., S. D. Vries, and S. G. Aarninkhof (2021), A Self-Adaptive Method for Mapping Coastal Bathymetry On-The-Fly from Wave Field Video, *Remote Sensing*, *13*(4742), 1–33, doi:10.3390/rs13234742.

Gelfenbaum, G., and G. M. Kaminsky (2010), Large-scale coastal change in the Columbia River littoral cell: An overview, *Marine Geology*, *273*(1-4), 1–10, doi:10.1016/j.margeo.2010.02.007.

Gelfenbaum, G., E. P. Elias, and A. W. Stevens (2017), Investigation of Input Reduction Techniques for Morphodynamic Modelling of Complex Inlets with Baroclinic Forcing, in *Coastal Dynamics 2017*, 260, pp. 1142–1154, Helsingor, Denmark.

Giebels, D., A. van Buuren, and J. Edelenbos (2013), Ecosystem-based management in the Wadden Sea: Principles for the governance of knowledge, *Journal of Sea Research*, *82*, 176–187, doi:10.1016/j.seares.2012.11.002.

Gillanders, B. M., T. S. Elsdon, and M. Roughan (2012), Connectivity of Estuaries, in *Treatise on Estuarine and Coastal Science*, vol. 7, pp. 119–142, Elsevier Inc., doi:10.1016/B978-0-12-374711-2.00709-9.

Goldstein, E. B., G. Coco, and N. G. Plant (2019), A review of machine learning applications to coastal sediment transport and morphodynamics, doi:10.1016/j.earscirev.2019.04.022.

Goodstein, D. L. (1975), *States of Matter*, 500 pp., Prentice-Hall, Englewood Cliffs, NJ.

Gray, H. J., M. Jain, and A. O. Sawakuchi (2019), Luminescence as a Sediment Tracer and Provenance Tool, pp. 1–31, doi:10.1029/2019RG000646.

Gray, J., and M. Elliott (2009), *Ecology of Marine Sediments*, 2nd ed., 241 pp., Oxford University Press, Oxford.

Gray, J. R., and J. W. Gartner (2009), Technological advances in suspended-sediment surrogate monitoring, *Water Resources Research*, *46*(4), doi:10.1029/2008WR007063.

Green, M. O., and J. D. Boon (1993), The measurement of constituent concentrations in nonhomogeneous sediment suspensions using optical backscatter sensors, *Marine Geology*, *110*(1-2), 73–81, doi:10.1016/0025-3227(93)90106-6.

Green, M. O., R. G. Bell, T. J. Dolphin, and A. Swales (2000), Silt and sand transport in a deep tidal channel of a large estuary (Manukau Harbour, New Zealand), *Marine Geology*, *163*(1-4), 217–240, doi:10.1016/S0025-3227(99)00102-4.

Grober-Dunsmore, S. J. Pittman, C. Caldow, M. S. Kendall, and T. K. Frazer (2009), *Ecological Connectivity among Tropical Coastal Ecosystems*, 1–615 pp., Springer Netherlands, Dordrecht, doi:10.1007/978-90-481-2406-0.

Gronewold, A. D., and R. B. Rood (2019), Recent water level changes across Earth's largest lake system

and implications for future variability, *Journal of Great Lakes Research*, *45*(1), 1–3, doi:10.1016/j.jglr.2018.10.012.

Guo, C., Q. He, B. C. van Prooijen, L. Guo, A. J. Manning, and S. Bass (2018), Investigation of flocculation dynamics under changing hydrodynamic forcing on an intertidal mudflat, *Marine Geology*, *395*(October 2017), 120–132, doi:10.1016/j.margeo.2017.10.001.

Guymer, I., V. Stovin, P. Gaskell, P. L. Maltby, and J. Pearson (2010), Predicting the Deposition of Highway-Derived Sediments in a Receiving River Reach, in *Proc. 17th IAHR-APD Congress*, Auckland, New Zealand.

Ha, H. K., W. Y. Hsu, J. P. Maa, Y. Y. Shao, and C. W. Holland (2009), Using ADV backscatter strength for measuring suspended cohesive sediment concentration, *Continental Shelf Research*, *29*(10), 1310–1316, doi:10.1016/j.csr.2009.03.001.

Haasnoot, M., J. Kwadijk, J. Van Alphen, D. Le Bars, B. Van Den Hurk, F. Diermanse, A. Van Der Spek, G. Oude Essink, J. Delsman, and M. Mens (2020), Adaptation to uncertain sea-level rise; how uncertainty in Antarctic mass-loss impacts the coastal adaptation strategy of the Netherlands, *Environmental Research Letters*, *15*(3), doi:10.1088/1748-9326/ab666c.

Hanes, D. M. (1988), Intermittent sediment suspension and its implications to sand tracer dispersal in wave-dominated environments, *Marine Geology*, *81*(1-4), 175–183, doi:10.1016/0025-3227(88)90024-2.

Hanley, M. E., S. P. Hoggart, D. J. Simmonds, A. Bichot, M. A. Colangelo, F. Bozzeda, H. Heurtefeux, B. Ondiviela, R. Ostrowski, M. Recio, R. Trude, E. Zawadzka-Kahlau, and R. C. Thompson (2014), Shifting sands? Coastal protection by sand banks, beaches and dunes, *Coastal Engineering*, *87*, 136–146, doi:10.1016/j.coastaleng.2013.10.020.

Hansen, J. E., E. P. Elias, and P. L. Barnard (2013), Changes in surfzone morphodynamics driven by multi-decadal contraction of a large ebb-tidal delta, *Marine Geology*, *345*, 221–234, doi:10.1016/j.margeo.2013.07.005.

Hanson, H., A. Brampton, M. Capobianco, H. H. Dette, L. Hamm, C. Laustrup, A. Lachuga, and R. Spanhoff (2002), Beach nourishment projects, practices and objectives – a European overview, *Coastal Engineering*, *47*(0378), 81–111.

Harlequin, D. (2021), Decadal Morphodynamic Modelling of Ameland Inlet, Msc thesis, Delft University of Technology.

Harley, M. D., I. L. Turner, A. D. Short, and R. Ranasinghe (2011), A reevaluation of coastal embayment rotation: The dominance of cross-shore versus alongshore sediment transport processes, Collaroy-Narrabeen Beach, southeast Australia, *Journal of Geophysical Research: Earth Surface*, *116*(4), 1–16, doi:10.1029/2011JF001989.

Harley, M. D., M. A. Kinsela, E. Sánchez-García, and K. Vos (2019), Shoreline change mapping using crowd-sourced smartphone images, *Coastal Engineering*, *150*(April), 175–189, doi:10.1016/j.coastaleng.2019.04.003.

Harrison, S. R., K. R. Bryan, and J. C. Mullarney (2017), Observations of morphological change at an ebb-tidal delta, *Marine Geology*, *385*, 131–145, doi:10.1016/j.margeo.2016.12.010.

Harvey, A. (2001), Coupling between hillslopes and channels in upland fluvial systems: implications for landscape sensitivity, illustrated from the Howgill Fells, northwest England, *CATENA*, *42*(2-4), 225–250, doi:10.1016/S0341-8162(00)00139-9.

Hastings, A., C. L. Hom, S. Ellner, P. Turchin, and H. C. Godfray (1993), Chaos in ecology: Is mother nature a strange attractor?, *Annual Review of Ecology and Systematics*, *24*, 1–33, doi:10.1146/annurev.es.24.110193.000245.

Hawley, N. (2004), A comparison of suspended sediment concentrations measured by acoustic and optical sensors, *Journal of Great Lakes Research*, *30*(2), 301–309, doi:10.1016/S0380-1330(04)70348-2.

Hayes, M. O. (1980), General morphology and sediment patterns in tidal inlets, *Sedimentary Geology*, *26*(1-3), 139–156, doi:10.1016/0037-0738(80)90009-3.

Hayes, M. O. (1994), The Georgia Bight Barrier System, in *Geology of Holocene Barrier Island Systems*, pp. 233–304, doi:10.1007/978-3-642-78360-9_7.

Heckmann, T., and W. Schwanghart (2013), Geomorphic coupling and sediment connectivity in an alpine catchment - Exploring sediment cascades using graph theory, *Geomorphology*, *182*, 89–103, doi:10.1016/j.geomorph.2012.10.033.

Heckmann, T., W. Schwanghart, and J. D. Phillips (2015), Graph theory—Recent developments of its application in geomorphology, *Geomorphology*, *243*, 130–146, doi:10.1016/j.geomorph.2014.12.024.

Heckmann, T., M. Cavalli, O. Cerdan, S. Foerster, M. Javaux, E. Lode, A. Smetanova, D. Vericat, and F. Brardinoni (2018), Indices of sediment connectivity: opportunities, challenges and limitations, *Earth-Science Reviews*, *187*(December 2017), 77–108, doi:10.1016/J.EARSCIREV.2018.08.004.

Heimhuber, V., K. Vos, W. Fu, and W. Glamore (2021), InletTracker: An open-source Python toolkit for historic and near real-time monitoring of coastal inlets from Landsat and Sentinel-2, *Geomorphology*, *389*, 107,830, doi:10.1016/j.geomorph.2021.107830.

Hein, J. R., K. Mizell, and P. L. Barnard (2013), Sand sources and transport pathways for the San Francisco Bay coastal system, based on X-ray diffraction mineralogy, *Marine Geology*, *345*, 154–169, doi:10.1016/j.margeo.2013.04.003.

Hendriks, H., B. C. van Prooijen, S. G. Aarninkhof, and J. Winterwerp (2020), How human activities affect the fine sediment distribution in the Dutch Coastal Zone seabed, *Geomorphology*, p. 107314, doi:10.1016/j.geomorph.2020.107314.

Herman, P. M. J., J. J. S. Moons, J. W. M. Wijsman, A. P. Luijendijk, and T. Ysebaert (2021), A Mega-Nourishment (Sand Motor) Affects Landscape Diversity of Subtidal Benthic Fauna, *Frontiers in Marine Science*, *8*(May), 1–21, doi:10.3389/fmars.2021.643674.

Herrling, G., and C. Winter (2014), Morphological and sedimentological response of a mixed-energy barrier island tidal inlet to storm and fair-weather conditions, *Earth Surface Dynamics*, *2*(1), 363–382, doi:10.5194/esurf-2-363-2014.

Herrling, G., and C. Winter (2018), Tidal inlet sediment bypassing at mixed-energy barrier islands, *Coastal Engineering*, *140*(October 2017), 342–354, doi:10.1016/j.coastaleng.2018.08.008.

Hiatt, M., W. Sonke, E. A. Addink, W. M. van Dijk, M. van Kreveld, T. Ophelders, K. Verbeek, J. Vlaming, B. Speckmann, and M. G. Kleinhans (2020), Geometry and Topology of Estuary and Braided River Channel Networks Automatically Extracted From Topographic Data, *Journal of Geophysical Research: Earth Surface*, *125*(1), 1–19, doi:10.1029/2019JF005206.

Hicks, D. M., and T. M. Hume (1996), Morphology and size of ebb tidal deltas at natural inlets on open-sea and pocket-bay coasts, North Island, New Zealand, *Journal of Coastal Research*, *12*(1), 47–63.

Hicks, D. M., and T. M. Hume (1997), Determining Sand Volumes and Bathymetric Change on an Ebb-Tidal Delta, *Journal of Coastal Research*, *13*(2), 407–416.

Hicks, M. D., T. M. Hume, A. Swales, and M. O. Green (1999), Magnitudes, spacial extent, time scales and causes of shoreline change adjacent to an ebb tidal delta, Katikati Inlet, New Zealand, *Journal of Coastal Research*, *15*(1), 220–240, doi:10.1590/S0100-67622003000600004.

Hill, D. C., S. E. Jones, and D. Prandle (2003), Derivation of sediment resuspension rates from acoustic backscatter time-series in tidal waters, *Continental Shelf Research*, *23*(1), 19–40, doi:10.1016/S0278-4343(02)00170-X.

Hill, P. S., T. G. Milligan, and W. R. Geyer (2000), Controls on effective settling velocity of suspended sediment in the Eel River flood plume, *Continental Shelf Research*, *20*(16), 2095–2111, doi:10.1016/S0278-4343(00)00064-9.

Hill, P. S., E. Boss, J. P. Newgard, B. A. Law, and T. G. Milligan (2011), Observations of the sensitivity of beam attenuation to particle size in a coastal bottom boundary layer, *Journal of Geophysical Research: Oceans*, *116*(2), 1–14, doi:10.1029/2010JC006539.

Hillen, R., and P. Roelse (1995), Dynamic Preservation of the Coastline in the Netherlands, *Journal of Coastal Conservation*, *1*(1), 17–28.

Hine, A. C. (1975), Bedform distribution and migration patterns on tidal deltas in the Chatham Harbor Estuary, Cape Cod, Massachusetts, in *Estuarine Research, Volume II: Geology and Engineering*, vol. 2, pp. 235–253, Myrtle Beach, South Carolina.

Hinkel, J., J. C. Aerts, S. Brown, J. A. Jiménez, D. Lincke, R. J. Nicholls, P. Scussolini, A. Sanchez-Arcilla, A. Vafeidis, and K. A. Addo (2018), The ability of societies to adapt to twenty-first-century sea-level rise, *Nature Climate Change*, *8*(7), 570–578, doi:10.1038/s41558-018-0176-z.

Hock, K., N. H. Wolff, J. C. Ortiz, S. A. Condie, K. R. Anthony, P. G. Blackwell, and P. J. Mumby (2017), Connectivity and systemic resilience of the Great Barrier Reef, *PLoS Biology*, *15*(11), 1–23, doi:10.1371/journal.pbio.2003355.

Hodges, K. I. (1999), Adaptive constraints for feature tracking, *Monthly Weather Review*, *127*(6 II), 1362–1373, doi:10.1175/1520-0493(1999)127<1362:acfft>2.0.co;2.

Hoitink, A. J., and P. Hoekstra (2005), Observations of suspended sediment from ADCP and OBS measurements in a mud-dominated environment, *Coastal Engineering*, *52*(2), 103–118, doi:10.1016/j.coastaleng.2004.09.005.

Holland, K. T., and P. A. Elmore (2008), A review of heterogeneous sediments in coastal environments, *Earth-Science Reviews*, *89*(3-4), 116–134, doi:10.1016/j.earscirev.2008.03.003.

Holzhauer, H., B. W. Borsje, J. A. van Dalfsen, K. M. Wijnberg, S. J. Hulscher, and P. M. Herman (2020), Benthic species distribution linked to morphological features of a barred coast, *Journal of Marine Science and Engineering*, *8*(1), doi:10.3390/JMSE8010016.

Holzhauer, H., B. W. Borsje, P. M. J. Herman, C. A. Schipper, and K. M. Wijnberg (2021), The geomorphology of an ebb-tidal-delta linked to benthic species distribution and functionality.

Honey, C. J., R. Kötter, M. Breakspear, and O. Sporns (2007), Network structure of cerebral cortex shapes functional connectivity on multiple time scales., *Proceedings of the National Academy of Sciences*, *104*(24), 10,240–10,245, doi:10.1073/pnas.0701519104.

Horner-Devine, A. R., J. D. Pietrzak, A. J. Souza, M. A. McKeon, S. Meirelles, M. Henriquez, R. P. Flores, and S. Rijnsburger (2017), Cross-shore transport of nearshore sediment by river plume frontal pumping, *Geophysical Research Letters*, *44*(12), 6343–6351, doi:10.1002/2017GL073378.

Hovmoller, E. (1949), The Trough-and-Ridge diagram, *Tellus*, *1*(2), 62–66.

Hubbard, D., G. Oertel, and D. Nummedal (1979), The role of waves and tidal currents in the development of tidal-inlet sedimentary structures and sand body geometry: examples from North Carolina, South Carolina, and Georgia, *Journal of Sedimentary Petrology*, *49*(4), 1073–1092.

Hufnagl, M., M. Payne, G. Lacroix, L. J. Bolle, U. Daewel, M. Dickey-Collas, T. Gerkema, M. Huret, F. Janssen, M. Kreus, J. Pätsch, T. Pohlmann, P. Ruardij, C. Schrum, M. D. Skogen, M. C. Tiessen, P. Petitgas, J. K. van Beek, H. W. van der Veer, and U. Callies (2016), Variation that can be expected when using particle tracking models in connectivity studies, *Journal of Sea Research*, *127*(May), 133–149, doi:10.1016/j.seares.2017.04.009.

Huisman, B. J., D. J. R. Walstra, M. Radermacher, M. A. de Schipper, and B. G. Ruessink (2019), Observations and modelling of shoreface nourishment behaviour, *Journal of Marine Science and Engineering*, *7*(3), doi:10.3390/jmse7030059.

Huisman, B. J. A., M. A. de Schipper, and B. G. Ruessink (2016), Sediment sorting at the Sand Motor at storm and annual time scales, *Marine Geology*, *381*, 209–226, doi:10.1016/j.margeo.2016.09.005.

Huisman, B. J. A., B. G. Ruessink, M. A. de Schipper, A. P. Luijendijk, and M. J. Stive (2018), Modelling of bed sediment composition changes at the lower shoreface of the Sand Motor, *Coastal Engineering*, *132*(November 2017), 33–49, doi:10.1016/j.coastaleng.2017.11.007.

Humberston, J., T. Lippmann, and J. McNinch (2019), Observations of wave influence on alongshore ebb-tidal delta morphodynamics at Oregon Inlet, NC, *Marine Geology*, *418*(December), 106,040, doi:10.1016/j.margeo.2019.106040.

Imeson, R. J., and J. C. Van Den Bergh (2006), Policy failure and stakeholder dissatisfaction in complex ecosystem management: The case of the Dutch Wadden Sea shellfishery, *Ecological Economics*, *56*(4), 488–507, doi:10.1016/j.ecolecon.2005.02.007.

Imperato, D. P., W. J. Sexton, and M. O. Hayes (1988), Stratigraphy and Sediment Characteristics of a Mesotidal Ebb-Tidal Delta, North Edisto Inlet, South Carolina, *SEPM Journal of Sedimentary Research*, *Vol. 58*(6), 950–958, doi:10.1306/212f8ec7-2b24-11d7-8648000102c1865d.

Israel, C. G. (1998), Morfologische Ontwikkeling Amelander Zeegat - RIKZ-OS-98.147X, *Tech. rep.*, Ministerie van Verkeer en Waterstaat; Director-Generaal Rijkswaterstaat; Rijksinstituut voor Kust en Zee, Den Haag, Netherlands.

Israel, C. G., and D. W. Dunsbergen (1999), Cyclic morphological development of the Ameland Inlet, the Netherlands, in *Proceedings of Symposium on River, Coastal and Estuarine Morphodynamics*, pp. 705–714, Genova, Italy.

Jaffe, B. E., J. H. List, and A. H. Sallenger (1997), Massive sediment bypassing on the lower shoreface offshore of a wide tidal inlet - Cat Island Pass, Louisiana, *Marine Geology*, *136*(3-4), 131–149, doi:10.1016/S0025-3227(96)00050-3.

Jalón-Rojas, I., S. Schmidt, and A. Sottolichio (2015), Turbidity in the fluvial Gironde Estuary (southwest France) based on 10-year continuous monitoring: Sensitivity to hydrological conditions, *Hydrology and Earth System Sciences*, *19*(6), 2805–2819, doi:10.5194/hess-19-2805-2015.

Jerolmack, D. J., and C. Paola (2010), Shredding of environmental signals by sediment transport, *Geophysical Research Letters*, *37*(19), 1–5, doi:10.1029/2010GL044638.

Jeuken, M. C. J. L., and Z. B. Wang (2010), Impact of dredging and dumping on the stability of ebb-flood channel systems, *Coastal Engineering*, *57*(6), 553–566, doi:10.1016/j.coastaleng.2009.12.004.

Kabat, P., J. Bazelmans, J. van Dijk, P. M. Herman, T. van Oijen, M. Pejrup, K. Reise, H. Speelman, and W. J. Wolff (2012), The Wadden Sea Region: Towards a science for sustainable development, *Ocean and Coastal Management*, *68*, 4–17, doi:10.1016/j.ocecoaman.2012.05.022.

Kaminsky, G. M., P. Ruggiero, M. C. Buijsman, D. McCandless, and G. Gelfenbaum (2010), Historical evolution of the Columbia River littoral cell, *Marine Geology*, *273*(1-4), 96–126, doi:10.1016/j.margeo.2010.02.006.

Kana, T. W., E. J. Hayter, and P. A. Work (1999a), Mesoscale sediment transport at southeastern U.S. tidal inlets: Conceptual model applicable to mixed energy settings, *Journal of Coastal Research*, *15*(2), 303–313.

Kana, T. W., E. J. Hayter, and P. a. Work (1999b), Mesoscale Sediment Transport at Southeastern U.S. Tidal Inlets: Conceptual Model Applicable to Mixed Energy Settings, *Journal of Coastal Research*, *15*(2), pp. 303—-313.

Kana, T. W., S. B. Traynum, and H. L. Kaczkowski (2014), Scales & Signatures of Episodic Sand Bypassing At a Tide-Dominated Inlet — Fripp Inlet, South Carolina, *Coastal Engineering Proceedings*, *1*(34), 52, doi:10.9753/icce.v34.sediment.52.

Kato, S., T. Okabe, Y. Aoki, and S. Kamohara (2014), Field measurement of sand movement on river-mouth tidal flat using color sand tracing, *Proceedings of the Coastal Engineering Conference*, *2014-Janua*, 1–9.

Katsman, C. a., a. Sterl, J. J. Beersma, H. W. van den Brink, J. a. Church, W. Hazeleger, R. E. Kopp, D. Kroon, J. Kwadijk, R. Lammersen, J. Lowe, M. Oppenheimer, H. P. Plag, J. Ridley, H. von Storch, D. G. Vaughan, P. Vellinga, L. L. a. Vermeersen, R. S. W. van de Wal, and R. Weisse (2011), Exploring high-end scenarios for local sea level rise to develop flood protection strategies for a low-lying delta-the Netherlands as an example, *Climatic Change*, *109*(3-4), 617–645, doi:10.1007/s10584-011-0037-5.

Keesstra, S., J. Pedro, P. Saco, T. Parsons, R. Poeppl, R. Masselink, and A. Cerdà (2018), The way forward: Can connectivity be useful to design better measuring and modelling schemes for water and sediment dynamics?, *Science of The Total Environment*, *644*, 1557–1572, doi:10.1016/J.SCITOTENV.2018.06.342.

Kennedy, B. A. (1979), A Naughty World, *The Royal Geographical Society (with the Institute of British Geographers)*, *4*(4), 550–558.

Keyence Corporation (2014), *VHX-5000 Digital Microscope User's Manual*, 320 pp., Keyence Corporation, Osaka, Japan.

Khalfani, D., and M. Boutiba (2019), Longshore Sediment Transport Rate Estimation near Harbor under Low and High Wave-Energy Conditions: Fluorescent Tracers Experiment, *Journal of Waterway, Port, Coastal, and Ocean Engineering*, *145*(4), 04019,015, doi:10.1061/(ASCE)WW.1943-5460.0000517.

Khelifa, A., and P. S. Hill (2006), Models for effective density and settling velocity of flocs, *Journal of Hydraulic Research*, *44*(3), 390–401, doi:10.1080/00221686.2006.9521690.

Kindlmann, P., and F. Burel (2008), Connectivity measures: A review, *Landscape Ecology*, *23*(8), 879–890, doi:10.1007/s10980-008-9245-4.

Kineke, G., and R. Sternberg (1992), Using the Optical Backscatterance Sensor, *Marine Geology*, *108*, 253–258.

Kinkade, D., and A. Shepherd (2021), Geoscience data publication: Practices and perspectives on enabling the FAIR guiding principles, *Geoscience Data Journal*, (December 2020), 1–10, doi:10.1002/gdj3.120.

Kivela, M., A. Arenas, M. Barthelemy, J. P. Gleeson, Y. Moreno, and M. A. Porter (2014), Multilayer networks, *Journal of Complex Networks*, *2*(3), 203–271, doi:10.1093/comnet/cnu016.

Kleinhans, M. G. (2010), Sorting out river channel patterns, *Progress in Physical Geography*, *34*(3), 287–326, doi:10.1177/0309133310365300.

Kleinhans, M. G., C. J. Buskes, and H. W. De Regt (2005), Terra incognita: Explanation and reduction in earth science, *International Studies in the Philosophy of Science*, *19*(3), 289–317, doi:10.1080/02698590500462356.

Kleinhans, M. G., R. I. Ferguson, S. N. Lane, and R. J. Hardy (2013), Splitting rivers at their seams: Bifurcations and avulsion, *Earth Surface Processes and Landforms*, *38*(1), 47–61, doi:10.1002/esp.3268.

KNMI (2019), Klimatologie: Daggegevens van het weer in Nederland.

Koch, M., and H. Niemeyer (1978), Sturmtiden-Strommessungen im Bereich des Norderneyer Seegats., *Forschungsstelle Norderney Jahresbericht*, *29*, 91–108.

Komar, P. D. (1978), Relative Quantities of Suspension Versus Bed-Load Transport on Beaches, *SEPM Journal of Sedimentary Research*, *Vol. 48*(3), 921–932, doi:10.1306/212f75a9-2b24-11d7-8648000102c1865d.

Koohafkan, M. C., and S. Gibson (2018), Geomorphic trajectory and landform analysis using graph theory, *Progress in Physical Geography: Earth and Environment*, p. 030913331878314, doi:10.1177/0309133318783143.

Kool, J. T., A. Moilanen, and E. A. Treml (2013), Population connectivity: Recent advances and new perspectives, *Landscape Ecology*, *28*(2), 165–185, doi:10.1007/s10980-012-9819-z.

Koppes, M., and L. King (2020), Beyond x,y,z(t); Navigating New Landscapes of Science in the Science of Landscapes, *Journal of Geophysical Research: Earth Surface*, *125*(9), doi:10.1029/2020JF005588.

Koster, M. J., and R. Hillen (1995), Combat erosion by law: coastal defence policy for the Netherlands, *Journal of Coastal Research*, *11*(4), 1221–1228.

Kranstauber, B., R. Weinzierl, M. Wikelski, and K. Safi (2015), Global aerial flyways allow efficient travelling, *Ecology Letters*, *18*(12), 1338–1345, doi:10.1111/ele.12528.

Kraus, N. C. (1985), Field Experiments on Vertical Mixing of Sand in the Surf Zone, *Journal of Sedimentary Petrology*, *55*(1), 3–14, doi:10.1306/212F85E9-2B24-11D7-8648000102C1865D.

Kraus, N. C. (2000), Reservoir Model of Ebb-Tidal Shoal Evolution and Sand Bypassing, *Journal of Waterway, Port, Coastal, and Ocean Engineering*, *126*(December), 305–313, doi:10.1061/(ASCE)0733-950X(2000)126:6(305).

Kraus, N. C., M. Isobe, H. Igarashi, T. Sasaki, and K. Horikawa (1982), Field experiments on longshore sand transport in the surf zone, *Coastal Engineering 1982*, pp. 969–988.

Krause, J., D. P. Croft, and R. James (2007), Social network theory in the behavioural sciences : potential applications, pp. 15–27, doi:10.1007/s00265-007-0445-8.

Krogel, F. (1995), Sedimentverteilung und Morphodynamik des Otzumer Ebbdeltas (sudliche Nordsee), *Senckenbergiana Maritima*, *25*(4), 127–136.

Kroon, A., M. De Schipper, K. Den Heijer, S. G. Aarninkhof, and P. Van Gelder (2017), Uncertainty Assessment in Coastal Morphology Prediction with a Bayesian Network, *Coastal Dynamics*, (254), 1909–1920.

Kuitenbrouwer, D., A. Reniers, J. MacMahan, and M. K. Roth (2018), Coastal protection by a small scale river plume against oil spills in the Northern Gulf of Mexico, *Continental Shelf Research*, *163*(April), 1–11, doi:10.1016/j.csr.2018.05.002.

Kundu, P. K., and I. M. Cohen (2008), *Fluid Mechanics*, 4th ed., 872 pp., Elsevier, Burlington, MA.

Lambregts, P. (2021), Understanding sediment bypassing at Ameland inlet, Msc thesis, Delft University of Technology.

Latteux, B. (1995), Techniques for long-term morphological simulation under tidal action, *Marine Geology*, *126*(1-4), 129–141, doi:10.1016/0025-3227(95)00069-B.

Lavelle, J. W., H. O. Mofjeld, and E. T. Baker (1984), An in situ erosion rate for a fine-grained marine sediment., doi:10.1029/JC089iC04p06543.

Lazarus, E. D., M. D. Harley, C. E. Blenkinsopp, and I. L. Turner (2019), Environmental signal shredding on sandy coastlines, *Earth Surface Dynamics*, *7*(1), 77–86, doi:10.5194/esurf-7-77-2019.

Le Hir, P., Y. Monbet, and F. Orvain (2007), Sediment erodability in sediment transport modelling: Can we account for biota effects?, *Continental Shelf Research*, *27*(8), 1116–1142, doi:10.1016/j.csr.2005.11.016.

Le Roux, J. P., and E. M. Rojas (2007), Sediment transport patterns determined from grain size parameters: Overview and state of the art, *Sedimentary Geology*, *202*(3), 473–488, doi:10.1016/j.sedgeo.2007.03.014.

Lee, B. J., M. Fettweis, E. Toorman, and F. J. Molz (2012), Multimodality of a particle size distribution of cohesive suspended particulate matters in a coastal zone, *Journal of Geophysical Research: Oceans*, *117*(3), doi:10.1029/2011JC007552.

Leicht, E. A., and M. E. Newman (2008), Community structure in directed networks, *Physical Review Letters*, *100*(11), 1–4, doi:10.1103/PhysRevLett.100.118703.

Leijnse, T., M. van Ormondt, K. Nederhoff, and A. van Dongeren (2021), Modeling compound flooding in coastal systems using a computationally efficient reduced-physics solver: Including fluvial, pluvial, tidal, wind- and wave-driven processes, *Coastal Engineering*, *163*(October 2020), 103,796, doi:10.1016/j.coastaleng.2020.103796.

Lenstra, K. J. (2020), Cyclic channel-shoal dynamics of ebb-tidal deltas, Phd, Utrecht University.

Lenstra, K. J., S. R. Pluis, W. Ridderinkhof, G. Ruessink, and M. van der Vegt (2019a), Cyclic channel-shoal dynamics at the Ameland inlet: the impact on waves, tides, and sediment transport, *Ocean Dynamics*, *69*(4), 409–425, doi:10.1007/s10236-019-01249-3.

Lenstra, K. J., W. Ridderinkhof, and M. van der Vegt (2019b), Unraveling the Mechanisms That Cause Cyclic Channel-Shoal Dynamics of Ebb-Tidal Deltas: A Numerical Modeling Study, *Journal of Geophysical Research: Earth Surface*, *124*(12), 2778–2797, doi:10.1029/2019JF005090.

Leopold, M. F., and M. J. Baptist (2016), De buitengewone biologie van de buitendelta' s van de Nederlandse Waddenzee, *Tech. rep.*, IMARES, Den Helder, Netherlands.

Lesser, G. (2009), An Approach to Medium-term Coastal Morphological Modelling, Phd, IHE Delft Institute for Water Education.

Lesser, G. R., D. Roelvink, J. a. T. M. van Kester, and G. S. Stelling (2004), Development and validation of a three-dimensional morphological model, *Coastal Engineering*, *51*(8-9), 883–915, doi:10.1016/j.coastaleng.2004.07.014.

Li, C., P. Wang, and D. Fan (2006), Tidal Flats, Open Ocean Coasts, in *Encyclopedia of Coastal Science*, edited by M. Schwartz, pp. 975–978, Springer Science & Business Media.

Li, H., T. M. Beck, H. R. Moritz, K. Groth, T. Puckette, and J. Marsh (2019), Sediment Tracer Tracking and Numerical Modeling at Coos Bay Inlet, Oregon, *Journal of Coastal Research*, *35*(1), 4, doi:10.2112/jcoastres-d-17-00218.1.

Li, Y., J. Jia, Q. Zhu, P. Cheng, S. Gao, and Y. P. Wang (2018), Differentiating the effects of advection and resuspension on suspended sediment concentrations in a turbid estuary, *Marine Geology*, *403*(November 2017), 179–190, doi:10.1016/j.margeo.2018.06.001.

Lin, J., Q. He, L. Guo, B. C. van Prooijen, and Z. B. Wang (2020), An integrated optic and acoustic (IOA) approach for measuring suspended sediment concentration in highly turbid environments, *Marine Geology*, *421*(October 2019), 106,062, doi:10.1016/j.margeo.2019.106062.

Liu, G., F. Cai, H. Qi, J. Zhu, G. Lei, H. Cao, and J. Zheng (2019), A method to nourished beach stability assessment: The case of China, *Ocean and Coastal Management*, *177*(178), 166–178, doi:10.1016/j.ocecoaman.2019.05.015.

Lodder, Q., and J. H. Slinger (2021), The 'Research for Policy' cycle in Dutch coastal flood risk management : the Coastal Genesis 2 research programme, *Ocean and Coastal Management*.

Lodder, Q. J., Z. B. Wang, E. P. Elias, A. J. van der Spek, H. de Looff, and I. H. Townend (2019), Future response of the Wadden Sea tidal basins to relative sea-level rise-an aggregated modelling approach, *Water*, *11*(10), doi:10.3390/w11102198.

Ludka, B. C., R. T. Guza, and W. C. O'Reilly (2018), Nourishment evolution and impacts at four southern California beaches: A sand volume analysis, *Coastal Engineering*, *136*(December 2017), 96–105, doi:10.1016/j.coastaleng.2018.02.003.

Luijendijk, A., G. Hagenaars, R. Ranasinghe, F. Baart, G. Donchyts, and S. G. Aarninkhof (2018), The State of the World's Beaches, *Scientific Reports*, *8*(1), 6641, doi:10.1038/s41598-018-24630-6.

Luijendijk, A. P., R. Ranasinghe, M. A. de Schipper, B. J. A. Huisman, C. M. Swinkels, D. J. R. Walstra, and M. J. Stive (2017), The initial morphological response of the Sand Engine: A process-based modelling study, *Coastal Engineering*, *119*(August 2015), 1–14, doi:10.1016/j.coastaleng.2016.09.005.

Lunven, M., and P. Gentien (2000), Suspended sediments in a macrotidal estuary: Comparison and use of different sensors, *Oceanologica Acta*, *23*(3), 245–260, doi:10.1016/S0399-1784(00)00126-2.

MacDonald, N. J., and M. H. Davies (2007), Particle-Based Sediment Transport Modelling, in *Coastal Engineering 2006*, vol. 3, pp. 3117–3128, World Scientific Publishing Company.

MacLeod, A. (1999), *No Great Mischief*, 283 pp., McClelland and Stewart, Toronto.

Malamud, B. D., and D. L. Turcotte (1999), Self-organized criticality applied to natural hazards, *Natural Hazards*, *20*(2-3), 93–116, doi:10.1023/a:1008014000515.

Malvern Instruments Limited (2017), *Mastersizer 3000 User Manual*, Malvern Instruments Limited, Worcestershire, UK.

Manning, A. J., S. J. Bass, and K. R. Dyer (2006), Floc properties in the turbidity maximum of a mesotidal estuary during neap and spring tidal conditions, *Marine Geology*, *235*(1-4 SPEC. ISS.), 193–211, doi:10.1016/j.margeo.2006.10.014.

Many, G., X. Durrieu de Madron, R. Verney, F. Bourrin, P. R. Renosh, F. Jourdin, and A. Gangloff (2019), Geometry, fractal dimension and settling velocity of flocs during flooding conditions in the Rhône ROFI, *Estuarine, Coastal and Shelf Science*, *219*(January), 1–13, doi:10.1016/j.ecss.2019.01.017.

Martin, R. L., D. J. Jerolmack, and R. Schumer (2012), The physical basis for anomalous diffusion in bed load transport, *Journal of Geophysical Research: Earth Surface*, *117*(1), 1–18, doi:10.1029/2011JF002075.

Maslov, S., and K. Sneppen (2002), Specificity and Stability in Topology of Protein Networks, *Science*, *296*(5569), 910–913, doi:10.1126/science.1065103.

Masselink, G., A. Kroon, and R. G. D. Davidson-Arnott (2006), Morphodynamics of intertidal bars in wave-dominated coastal settings - A review, *Geomorphology*, *73*(1-2), 33–49, doi:10.1016/j.geomorph.2005.06.007.

McCave, I. N. (1984), Erosion, transport and deposition of fine-grained marine sediments, *Fine-grained sediments; deep-water processes and facies*, *15*(1), 35–69, doi:10.1144/GSL.SP.1984.015.01.03.

McComb, P., and K. P. Black (2005), Detailed Observations of Littoral Transport Using Artificial Sediment Tracer, in a High-Energy, Rocky Reef and Iron Sand Environment, *Journal of Coastal Research*, *212*(212), 358–373, doi:10.2112/03-574.1.

McDougall, J., and P. M. Barker (2017), Getting started with TEOS-10 and the Gibbs Seawater (GSW) Oceanographic Toolbox, *Tech. Rep. July*, SCOR/IAPSO WG127.

McGann, M., L. Erikson, E. Wan, C. Powell, and R. F. Maddocks (2013), Distribution of biologic, anthropogenic, and volcanic constituents as a proxy for sediment transport in the San Francisco Bay Coastal System, *Marine Geology*, *345*, 113–142, doi:10.1016/j.margeo.2013.05.006.

McLachlan, A. (1996), Physical factors in benthic ecology: Effects of changing sand particle size on beach fauna, *Marine Ecology Progress Series*, *131*(1-3), 205–217, doi:10.3354/meps131205.

McLaren, P. (2013), Sediment Trend Analysis (STA ®): Kinematic vs. Dynamic Modeling, *Journal of Coastal Research*, *30*(3), 429–437, doi:10.2112/JCOASTRES-D-13-00121.1.

McLaren, P., and D. Bowles (1985), The Effects of Sediment Transport on Grain Size Distributions, *Journal of Sedimentary Petrology*, *55*(4), 0457–0470.

McLaren, P., F. Steyaert, and R. Powys (1998), Sediment Transport Studies in the Tidal Basins of the Dutch Waddenzee, *Senckenbergiana Maritima*, *29*(1), 53–61.

McNinch, J. E., J. T. Wells, and T. G. Drake (2001), The fate of artifacts in an energetic, shallow-water environment: Scour and burial at the wreck site of Queen Anne's Revenge, *Southeastern Geology*, *40*(1), 19–27.

McNinch, J. E., J. T. Wells, and A. C. Trembanis (2006), Predicting the fate of artefacts in energetic, shallow marine environments: An approach to site management, *International Journal of Nautical Archaeology*, *35*(2), 290–309, doi:10.1111/j.1095-9270.2006.00105.x.

Meijers, C. (2021), Sediment Transport Pathways in Burrard Inlet, Msc thesis, Delft University of Technology.

Meldahl, K. H., and K. W. Flessa (1990), Taphonomic pathways and comparative biofacies and taphofacies in a Recent intertidal/shallow shelf environment, *Lethaia*, *23*(1), 43–60, doi:10.1111/j.1502-3931.1990.tb01780.x.

Mikkelsen, O. A., and M. Pejrup (2001), The use of a LISST-100 laser particle sizer for in-situ estimates of floc size, density and settling velocity, *Geo-Marine Letters*, *20*(4), 187–195, doi:10.1007/s003670100064.

Miller, I. M., and J. A. Warrick (2012), Measuring sediment transport and bed disturbance with tracers on a mixed beach, *Marine Geology*, *299-302*, 1–17, doi:10.1016/j.margeo.2012.01.002.

Milligan, T. G., and P. S. Hill (1998), A laboratory assessment of the relative importance of turbulence, particle composition, and concentration in limiting maximal floc size and settling behaviour, *Journal of Sea Research*, *39*(3-4), 227–241, doi:10.1016/S1385-1101(97)00062-2.

Moate, B. D., and P. D. Thorne (2009), Measurements and inversion of acoustic scattering from suspensions having broad size distributions, *The Journal of the Acoustical Society of America*, *126*(6), 2905–2917, doi:10.1121/1.3242374.

Moate, B. D., and P. D. Thorne (2012), Interpreting acoustic backscatter from suspended sediments of different and mixed mineralogical composition, *Continental Shelf Research*, *46*, 67–82, doi:10.1016/j.csr.2011.10.007.

Moilanen, A. (2011), On the limitations of graph-theoretic connectivity in spatial ecology and conservation, *Journal of Applied Ecology*, *48*(6), 1543–1547, doi:10.1111/j.1365-2664.2011.02062.x.

Montaño, J., G. Coco, J. A. Á. Antolínez, T. Beuzen, K. R. Bryan, L. Cagigal, B. Castelle, M. A. Davidson, E. B. Goldstein, R. Ibaceta, D. Idier, B. C. Ludka, S. Masoud-Ansari, F. J. Méndez, A. B. Murray, N. G. Plant, K. M. Ratliff, A. Robinet, A. Rueda, N. Sénéchal, J. A. Simmons, K. D. Splinter, S. Stephens,

I. Townend, S. Vitousek, and K. Vos (2020), Blind testing of shoreline evolution models, *Scientific Reports*, *10*(1), 1–10, doi:10.1038/s41598-020-59018-y.

Moodie, A. J., J. A. Nittrouer, H. Ma, B. N. Carlson, A. J. Chadwick, M. P. Lamb, and G. Parker (2019), Modeling Deltaic Lobe-Building Cycles and Channel Avulsions for the Yellow River Delta, China, *Journal of Geophysical Research: Earth Surface*, *124*(11), 2438–2462, doi:10.1029/2019JF005220.

Morales, J. A., J. Borrego, I. Jiménez, J. Monterde, and N. Gil (2001), Morphostratigraphy of an ebb-tidal delta system associated with a large spit in the Piedras Estuary mouth (Huelva Coast, Southwestern Spain), *Marine Geology*, *172*(3-4), 225–241, doi:10.1016/S0025-3227(00)00135-3.

Moritz, H., T. Puckette, J. Marsh, R. Boudreau, M. Siipola, and M. Ott (2011), Utilizing Sediment Tracer Studies to Evaluate Transport Pathways at the Mouth of the Columbia River, USA, in *The Proceedings of the Coastal Sediments 2011*, pp. 1565–1579, World Scientific Publishing Company, Miami, FL.

Morton, R. A., H. E. Clifton, N. A. Buster, R. L. Peterson, and G. Gelfenbaum (2007), Forcing of large-scale cycles of coastal change at the entrance to Willapa Bay, Washington, *Marine Geology*, *246*(1), 24–41, doi:10.1016/j.margeo.2007.07.008.

Moslow, T. F., and R. S. Tye (1985), Recognition and characterization of Holocene tidal inlet sequences, *Marine Geology*, *63*(1-4), 129–151, doi:10.1016/0025-3227(85)90081-7.

Moura, M. G., V. S. Quaresma, A. C. Bastos, and P. Veronez (2011), Field observations of SPM using ADV, ADP, and OBS in a shallow estuarine system with low SPM concentration-Vitória Bay, SE Brazil, *Ocean Dynamics*, *61*(2-3), 273–283, doi:10.1007/s10236-010-0364-5.

Mulder, J. P., S. Hommes, and E. M. Horstman (2011), Implementation of coastal erosion management in the Netherlands, *Ocean and Coastal Management*, *54*(12), 888–897, doi:10.1016/j.ocecoaman.2011.06.009.

Mulhern, J. S., C. L. Johnson, and A. N. Green (2021), When Is a Barrier Island Not an Island? When It Is Preserved in the Rock Record, *Frontiers in Earth Science*, *8*(February), doi:10.3389/feart.2020.560437.

Munroe, R. (2015), *Thing explainer: complicated stuff in simple words.*, 64 pp., Houghton Mifflin Harcourt.

Najafi, S., D. Dragovich, T. Heckmann, and S. H. Sadeghi (2021), Sediment connectivity concepts and approaches, *Catena*, *196*(March 2020), 104,880, doi:10.1016/j.catena.2020.104880.

Nederhoff, C., R. Schrijvershof, P. Tonnon, J. van der Werf, and E. P. Elias (2019), Modelling Hydrodynamics in the Ameland Inlet As a Basis for Studying Sand Transport, in *Coastal Sediments 2019*, pp. 1971–1983, St. Petersburg, Florida, doi:10.1142/9789811204487_0170.

Newman, M. (2018), *Networks*, 2nd ed., 780 pp., Oxford University Press, Oxford, UK.

Newman, M. E. J. (2003), The Structure and Function of Complex Networks, *SIAM*, *45*(2), 167–256.

Nicholas, A. P., G. H. Sambrook Smith, M. L. Amsler, P. J. Ashworth, J. L. Best, R. J. Hardy, S. N. Lane, O. Orfeo, D. R. Parsonsm, A. J. Reesink, S. D. Sandbach, C. J. Simpson, and R. N. Szupiany (2016), The role of discharge variability in determining alluvial stratigraphy, *Geology*, *44*(1), 3–6, doi:10.1130/G37215.1.

Nicholl, M. J., S. W. Wheatcraft, S. W. Tyler, and B. Berkowitz (1994), Is Old Faithful a strange attractor?, *Journal of Geophysical Research*, *99*(B3), 4495–4503, doi:10.1029/93JB02575.

Nienhuis, J. H., and A. D. Ashton (2016), Mechanics and rates of tidal inlet migration: Modeling and application to natural examples, *Journal of Geophysical Research: Earth Surface*, *121*(11), 2118–2139, doi:10.1002/2016JF004035.

Nienhuis, J. H., and J. Lorenzo-Trueba (2019), Simulating barrier island response to sea level rise with the barrier island and inlet environment (BRIE) model v1.0, *Geoscientific Model Development*, *12*(9), 4013–4030, doi:10.5194/gmd-12-4013-2019.

Nortek (2008), AQD HR Manual, (May).

Nortek AS (2005), Vector Current Meter - User Manual, *Tech. Rep. N 300-100 Rev. H*, Nortek Group, Vangkroken, Norway.

Nortek AS (2008), Aquadopp High Resolution - User Manual, *Tech. Rep. AHR00-0101-0508*, Nortek AS, Vangkroken, Norway.

NWO (2019), Societal impact through knowledge utilisation, *Tech. rep.*, Nederlandse Organisatie voor Wetenschappelijk Onderzoek.

O'Brien, M. P. (1966), Equilibrium Flow Areas of Tidal Inlets on Sandy Coasts, in *Coastal Engineering 1966*, chap. 39, pp. 676–686, Tokyo, Japan.

O'Connor, M. C., J. A. G. Cooper, and D. W. Jackson (2011), Decadal behavior of tidal inlet-associated beach systems, northwest ireland, in relation to climate forcing, *Journal of Sedimentary Research*, *81*(1), 38–51, doi:10.2110/jsr.2011.3.

Oertel, G. (1972), Sediment transport of estuary entrance shoals and the formation of swash platforms, *Journal of Sedimentary Research*, *42*(4), 858–863, doi:10.1306/74D72658-2B21-11D7-8648000102C1865D.

Oertel, G. F. (1977), Geomorphic cycles in ebb deltas and related patterns of shore erosion and accretion, *Journal of Sedimentary Research*, *47*(3), 1121–1131.

Okabe, T., and S. Kato (2018), Temporal changes in the ebb-tidal delta bathymetry of Imagire-guchi inlet in Japan, *Coastal Engineering Journal*, *60*(4), 437–448, doi:10.1080/21664250.2018.1503403.

Okin, G. S., A. J. Parsons, J. Wainwright, J. E. Herrick, B. T. Bestelmeyer, D. C. Peters, and E. L. Fredrickson (2009), Do Changes in Connectivity Explain Desertification?, *BioScience*, *59*(3), 237–244, doi:10.1525/bio.2009.59.3.8.

Oliveira, S., D. Moura, J. Horta, A. Nascimento, A. Gomes, and C. Veiga-Pires (2017), The morphosedimentary behaviour of a headland–beach system: Quantifying sediment transport using fluorescent tracers, *Marine Geology*, doi:10.1016/j.margeo.2017.02.010.

Oost, A. P., P. Hoekstra, A. Wiersma, B. W. Flemming, E. J. Lammerts, M. Pejrup, J. Hofstede, B. van der Valk, P. Kiden, J. Bartholdy, M. W. van der Berg, P. C. Vos, S. de Vries, and Z. B. Wang (2012), Barrier island management: Lessons from the past and directions for the future, *Ocean and Coastal Management*, *68*, 18–38, doi:10.1016/j.ocecoaman.2012.07.010.

Öztürk, M. (2017), Sediment size effects in acoustic doppler velocimeter-derived estimates of suspended sediment concentration, *Water (Switzerland)*, *9*(7), doi:10.3390/w9070529.

Padberg-Gehle, K., and C. Schneide (2017), Network-based study of Lagrangian transport and mixing, *Nonlinear Processes in Geophysics*, *24*(4), 661–671, doi:10.5194/npg-24-661-2017.

Paphitis, D., and M. B. Collins (2005), Sand grain threshold, in relation to bed 'stress history': An experimental study, *Sedimentology*, *52*(4), 827–838, doi:10.1111/j.1365-3091.2005.00710.x.

Paris, C. B., J. Helgers, E. van Sebille, and A. Srinivasan (2013), Connectivity Modeling System: A probabilistic modeling tool for the multi-scale tracking of biotic and abiotic variability in the ocean, *Environmental Modelling and Software*, *42*, 47–54, doi:10.1016/j.envsoft.2012.12.006.

Parker, G., and O. Sequeiros (2006), Large scale river morphodynamics: Application to the Mississippi Delta, in *Proceedings of the International Conference on Fluvial Hydraulics - River Flow 2006*, vol. 1, pp. 3–11.

Passalacqua, P. (2017), The Delta Connectome: A network-based framework for studying connectivity in river deltas, *Geomorphology*, *277*, 50–62, doi:10.1016/j.geomorph.2016.04.001.

Payo, A., J. W. Hall, J. French, J. Sutherland, B. van Maanen, R. J. Nicholls, and D. E. Reeve (2016), Causal Loop Analysis of coastal geomorphological systems, *Geomorphology*, *256*, 36–48, doi:10.1016/j.geomorph.2015.07.048.

Pearson, S. G., and M. Tissier (2018), The Curious Undular Bore, in *AGU Fall Meeting 2018*, December, p. 1, Washington, DC, doi:10.1002/essoar.10500093.1.

Pearson, S. G., R. Lubbad, T. M. Le, and R. B. Nairn (2016), Thermomechanical erosion modelling of Baydaratskaya Bay, Russia with COSMOS, *Scour and Erosion - Proceedings of the 8th International Conference on Scour and Erosion, ICSE 2016*, pp. 281–291, doi:10.1201/9781315375045-34.

Pearson, S. G., C. D. Storlazzi, A. R. van Dongeren, M. F. Tissier, and A. Reniers (2017), A Bayesian-Based System to Assess Wave-Driven Flooding Hazards on Coral Reef-Lined Coasts, *Journal of Geophysical Research: Oceans*, pp. 99–117, doi:10.1002/2017JC013204.

Pearson, S. G., B. C. van Prooijen, F. P. de Wit, H. Meijer-Holzhauer, A. de Looff, and Z. B. Wang (2019), Observations of Suspended Particle Size Distribution on an Energetic Ebb-Tidal Delta, *Coastal Sediments 2019*, pp. 1991–2003, doi:10.1142/9789811204487_0172.

Pearson, S. G., B. C. Prooijen, E. P. L. Elias, S. Vitousek, and Z. B. Wang (2020), Sediment Connectivity: A Framework for Analyzing Coastal Sediment Transport Pathways, *Journal of Geophysical Research: Earth Surface*, *125*(10), doi:10.1029/2020JF005595.

Pearson, S. G., R. Verney, B. C. van Prooijen, D. Tran, E. Hendriks, M. Jacquet, and Z. B. Wang (2021a), Characterizing Mixed Sand and Mud Suspensions using Combined Optical and Acoustic Measurements in Estuarine Environments, *Earth and Space Science Open Archive*, p. 36, doi:10.1002/essoar.10506576.1.

Pearson, S. G., R. Verney, H. Hendricks, D. Tran, M. Jacquet, Z. Wang, and B. C. van Prooijen (2021b), Characterizing the Composition of Suspended Sand and Mud Suspensions in Coastal Environments using Combined Optical and Acoustic Measurements: Ameland Ebb-Tidal Delta, in *INTERCOH 2021*, Delft, The Netherlands.

Peterson, C. H., M. J. Bishop, L. M. D'Anna, and G. A. Johnson (2014), Multi-year persistence of beach habitat degradation from nourishment using coarse shelly sediments, *Science of the Total Environment*, *487*(1), 481–492, doi:10.1016/j.scitotenv.2014.04.046.

Phillips, J. (1997), Simplexity and the reinvention of equifinality, *Geographical Analysis*, *29*(1), 1–15, doi:10.1111/j.1538-4632.1997.tb00942.x.

Phillips, J. D. (2012), Synchronization and scale in geomorphic systems, *Geomorphology*, *137*(1), 150–158, doi:10.1016/j.geomorph.2010.09.028.

Phillips, J. D. (2015), Badass geomorphology, *Earth Surface Processes and Landforms*, *40*(1), 22–33, doi:10.1002/esp.3682.

Phillips, J. D., W. Schwanghart, and T. Heckmann (2015), Graph theory in the geosciences, *Earth-Science Reviews*, *143*, 147–160, doi:10.1016/j.earscirev.2015.02.002.

Pianca, C., R. Holman, and E. Siegle (2014), Mobility of meso-scale morphology on a microtidal ebb delta measured using remote sensing, *Marine Geology*, *357*, 334–343, doi:10.1016/j.margeo.2014.09.045.

Pilosof, S., M. A. Porter, M. Pascual, and S. Kéfi (2017), The multilayer nature of ecological networks, *Nature Ecology & Evolution*, *1*(4), 0101, doi:10.1038/s41559-017-0101.

Poeppl, R. E., and A. J. Parsons (2018), The geomorphic cell: a basis for studying connectivity, *Earth Surface Processes and Landforms*, *43*(5), 1155–1159, doi:10.1002/esp.4300.

Poizot, E., Y. Mear, M. Thomas, and S. Garnaud (2006), The application of geostatistics in defining the characteristic distance for grain size trend analysis, *Computers and Geosciences*, *32*(3), 360–370, doi:10.1016/j.cageo.2005.06.023.

Poizot, E., Y. Mear, and L. Biscara (2008), Sediment Trend Analysis through the variation of granulometric parameters: A review of theories and applications, *Earth-Science Reviews*, *86*(1-4), 15–41, doi:10.1016/j.earscirev.2007.07.004.

Pomázi, F., and S. Baranya (2020), Comparative assessment of fluvial suspended sediment concentration analysis methods, *Water*, *12*(3), doi:10.3390/w12030873.

Pomeroy, A. W., C. D. Storlazzi, K. J. Rosenberger, R. J. Lowe, J. E. Hansen, and M. L. Buckley (2021), The contribution of currents, sea-swell waves, and infragravity waves to suspended-sediment transport across a coral reef-lagoon system., *Journal of Geophysical Research: Oceans*, pp. 1–26, doi:10.1029/2020jc017010.

Postma, H. (1961), Suspended Matter and Secchi Disc Visibility in Coastal Waters, *Netherlands Journal of Sea Research*, *1*(3), 359–390.

Poulter, B., J. L. Goodall, and P. N. Halpin (2008), Applications of network analysis for adaptive management of artificial drainage systems in landscapes vulnerable to sea level rise, *Journal of Hydrology*, *357*(3-4), 207–217, doi:10.1016/j.jhydrol.2008.05.022.

Powell, M. A., R. J. Thieke, and A. J. Mehta (2006), Morphodynamic relationships for ebb and flood delta volumes at Florida's tidal entrances, *Ocean Dynamics*, *56*(3-4), 295–307, doi:10.1007/s10236-006-0064-3.

Power, H. E., A. W. M. Pomeroy, M. A. Kinsela, and T. P. Murray (2021), Research Priorities for Coastal Geoscience and Engineering: A Collaborative Exercise in Priority Setting From Australia, *Frontiers in Marine Science*, *8*(April), doi:10.3389/fmars.2021.645797.

Puhl, H. (1992), On the modelling of real sand piles, *Physica A: Statistical Mechanics and its Applications*, *182*(3), 295–319, doi:10.1016/0378-4371(92)90344-P.

Purdy, A. (1996), Gondwanaland, in *rooms for rent in the outer planets: selected poems 1962-1996*, p. 148, Harbour Publishing, Madeira Park, BC.

Purkiani, K., J. Becherer, K. Klingbeil, and H. Burchard (2016), Wind-induced variability of estuarine circulation in a tidally energetic inlet with curvature, *Journal of Geophysical Research: Oceans*, *121*(5), 3261–3277, doi:10.1002/2015JC010945.

Pynchon, T. (1984), Is it O.K. to be a Luddite?, doi:10.4324/9781315804927-3.

Ranasinghe, R. (2020), On the need for a new generation of coastal change models for the 21st century, *Scientific Reports*, *10*(1), 1–6, doi:10.1038/s41598-020-58376-x.

Ranasinghe, R., T. M. Duong, S. Uhlenbrook, D. Roelvink, and M. J. Stive (2013), Climate-change impact assessment for inlet-interrupted coastlines, *Nature Climate Change*, *3*(1), 83–87, doi:10.1038/nclimate1664.

Read, J. M., K. T. Eames, and W. J. Edmunds (2008), Dynamic social networks and the implications for the spread of infectious disease, *Journal of the Royal Society Interface*, *5*(26), 1001–1007, doi:10.1098/rsif.2008.0013.

Reijnders, D., E. J. van Leeuwen, and E. van Sebille (2021), Ocean Surface Connectivity in the Arctic: Capabilities and Caveats of Community Detection in Lagrangian Flow Networks, *Journal of Geophysical Research: Oceans*, *126*(1), doi:10.1029/2020JC016416.

Reimann, T., P. D. Notenboom, M. A. de Schipper, and J. Wallinga (2015), Testing for sufficient signal resetting during sediment transport using a polymineral multiple-signal luminescence approach, *Quaternary Geochronology*, *25*, 26–36, doi:10.1016/j.quageo.2014.09.002.

Reise, K., M. Baptist, P. Burbridge, N. Dankers, L. Fischer, B. W. Flemming, A. Oost, and C. Smit (2010), The Wadden Sea – A universally outstanding tidal wetland, *Tech. rep.*, Common Wadden Sea Secretariat, Wilhelmshaven, Germany.

Reniers, A., F. P. de Wit, M. F. S. Tissier, S. G. Pearson, L. B. Brakenhoff, M. van der Vegt, J. Mol, and B. C. van Prooijen (2019), Wave-Skewness and Current-Related Ebb-Tidal Sediment Transport: Observations and Modeling, in *Coastal Sediments 2019*, pp. 2018–2028, St. Petersburg, Florida, doi:10.1142/9789811204487_0174.

Ribeiro, M. S. A. (2017), Headland sediment bypassing processes, Phd, University of Lisbon.

Ridderinkhof, H., and J. T. Zimmerman (1992), Chaotic stirring in a tidal system, *Science*, *258*(5085), 1107–1111, doi:10.1126/science.258.5085.1107.

Ridderinkhof, W., P. Hoekstra, M. Van Der Vegt, and H. E. de Swart (2016), Cyclic behavior of sandy shoals on the ebb-tidal deltas of the Wadden Sea, *Continental Shelf Research*, *115*, 14–26, doi:10.1016/j.csr.2015.12.014.

Rijkswaterstaat (1999), *Sedimentatlas Waddenzee*, 36–38 pp., Rijkswaterstaat, Haren, Netherlands.

Rijkswaterstaat (2016), Vaklodingen Dataset.

Rijkswaterstaat (2020), Kustgenese 2.0: kennis voor een veilige kust, *Tech. rep.*, Rijkswaterstaat.

Rijnsburger, S., R. P. Flores, J. D. Pietrzak, A. R. Horner-Devine, and A. J. Souza (2018), The influence of tide and wind on the propagation of fronts in a shallow river plume, *Journal of Geophysical Research: Oceans*, doi:10.1029/2017JC013422.

Robin, N., F. Levoy, and O. Monfort (2009), Short term morphodynamics of an intertidal bar on megatidal ebb delta, *Marine Geology*, *260*(1-4), 102–120, doi:10.1016/j.margeo.2009.02.006.

Roelvink, D., and A. Reniers (2012), *A guide to modeling coastal morphology*, doi:10.1142/9789814304269.

Roelvink, D., B. Huisman, A. Elghandour, M. Ghonim, and J. Reyns (2020), Efficient Modeling of Complex Sandy Coastal Evolution at Monthly to Century Time Scales, *Frontiers in Marine Science*, *7*(July), 1–20, doi:10.3389/fmars.2020.00535.

Roelvink, J. (2015), Addressing Local And Global Sediment Imbalances: Coastal Sediments As Rare Minerals, in *Coastal Sediments 2015*, pp. 1–13, San Diego, CA.

Rogers, J. S., S. G. Monismith, O. B. Fringer, D. A. Koweek, and R. B. Dunbar (2016), A coupled wave-hydrodynamic model of an atoll with high friction: mechanisms for flow, connectivity, and ecological implications, *Ocean Modelling*, *0*, 1–17, doi:10.1016/j.ocemod.2016.12.012.

Ronchi, L., A. Fontana, A. Correggiari, and A. Remia (2019), Anatomy of a transgressive tidal inlet reconstructed through high-resolution seismic profiling, *Geomorphology*, *343*, 65–80, doi:10.1016/j.geomorph.2019.06.026.

Rosati, J. D. (2005), Concepts in sediment budgets, *Journal of Coastal Research*, *21*(2), 307–322, doi:10.2112/02-475A.1.

Rosenbauer, R. J., A. C. Foxgrover, J. R. Hein, and P. W. Swarzenski (2013), A Sr-Nd isotopic study of sand-sized sediment provenance and transport for the San Francisco Bay coastal system, *Marine Geology*, *345*, 143–153, doi:10.1016/j.margeo.2013.01.002.

Rossi, V., E. Ser-Giacomi, C. Lõpez, and E. Hernández-García (2014), Hydrodynamic provinces and oceanic connectivity from a transport network help designing marine reserves, *Geophysical Research Letters*, *41*(8), 2883–2891, doi:10.1002/2014GL059540.

Rowling, J. K. (1997), *Harry Potter and the Philosopher's Stone*, 223 pp., Bloomsbury Publishing, London.

Rubinov, M., and O. Sporns (2010), Complex network measures of brain connectivity: Uses and interpretations, *NeuroImage*, *52*(3), 1059–1069, doi:10.1016/j.neuroimage.2009.10.003.

Rueda, A., C. A. Hegermiller, J. A. Á. Antolínez, P. Camus, S. Vitousek, P. Ruggiero, P. L. Barnard, L. H. Erikson, A. Tomás, and F. J. Mendez (2017), Multiscale climate emulator of multimodal wave spectra: MUSCLE-spectra, *Journal of Geophysical Research: Oceans*, *122*(2), 1400–1415, doi:10.1002/2016JC011957.

Ruggiero, P., M. Buijsman, G. M. Kaminsky, and G. Gelfenbaum (2010), Modeling the effects of wave climate and sediment supply variability on large-scale shoreline change, *Marine Geology*, *273*(1-4), 127–140, doi:10.1016/j.margeo.2010.02.008.

Ruggiero, P., G. M. Kaminsky, G. Gelfenbaum, and N. Cohn (2016), Morphodynamics of prograding beaches: A synthesis of seasonal- to century-scale observations of the Columbia River littoral cell, *Marine Geology*, *376*, 51–68, doi:10.1016/j.margeo.2016.03.012.

Rypina, I. I., L. J. Pratt, J. Pullen, J. Levin, and A. L. Gordon (2010), Chaotic advection in an archipelago, *Journal of Physical Oceanography*, *40*(9), 1988–2006, doi:10.1175/2010JPO4336.1.

Salehi, M., and K. Strom (2011), Using velocimeter signal to noise ratio as a surrogate measure of suspended mud concentration, *Continental Shelf Research*, *31*(9), 1020–1032, doi:10.1016/j.csr.2011.03.008.

Salles, P., A. Valle-Levinson, A. Sottolichio, and N. Senechal (2015), Wind-driven modifications to the residual circulation in an ebb-tidal delta: Arcachon Lagoon, Southwestern France, *Journal of Geophysical Research: Oceans*, *120*(2), 728–740, doi:10.1002/2014JC010311.

Schinzinger, R., and P. A. A. Laura (2003), *Conformal Mapping: Methods and Applications*, 608 pp., Dover Publications, Mineola, New York.

Schlosser, F., B. F. Maier, O. Jack, D. Hinrichs, A. Zachariae, and D. Brockmann (2020), COVID-19 lockdown induces disease-mitigating structural changes in mobility networks, *Proceedings of*

the National Academy of Sciences of the United States of America, *117*(52), 32,883–32,890, doi:10.1073/PNAS.2012326117.

Schwartz, M. A. (2008), The importance of stupidity in scientific research, *Journal of Cell Science*, *121*(11), 1771, doi:10.1242/jcs.033340.

Scott, J. (2011), Social network analysis: developments, advances, and prospects, *Social Network Analysis and Mining*, *1*(1), 21–26, doi:10.1007/s13278-010-0012-6.

Seapoint Sensors Incorporated (2013), Seapoint turbidity meter user manual, *Tech. rep.*, Seapoint Sensors, Inc, Exeter, NH.

Sengupta, S. (1979), Grain-size distribution of suspended load in relation to bed materials and flow velocity, *Sedimentology*, *26*, 63–82.

Sequoia Scientific (2015), *LISST-100X Particle Size Analyzer User's Manual*, version 5. ed., 144 pp., Sequoia Scientific, Inc., Bellevue, WA.

Ser-Giacomi, E., V. Rossi, C. López, and E. Hernández-García (2015), Flow networks: A characterization of geophysical fluid transport, *Chaos*, *25*(3), doi:10.1063/1.4908231.

Sexton, W. J., and M. O. Hayes (1983), Natural Bar-Bypassing of Sand at a Tidal Inlet, in *Proceedings of the Coastal Engineering Conference*, vol. 2, pp. 1479–1495, doi:10.9753/icce.v18.90.

Sha, L. P. (1989a), Variation in ebb-delta morphologies along the West and East Frisian Islands, The Netherlands and Germany, *Marine Geology*, *89*(1-2), 11–28, doi:10.1016/0025-3227(89)90025-X.

Sha, L. P. (1989b), Holocene-Pleistocene interface and three-dimensional geometry of the ebb-delta complex, Texel Inlet, The Netherlands, *Marine Geology*, *89*(3-4), 207–228, doi:10.1016/0025-3227(89)90076-5.

Sha, L. P. (1989c), Sand transport patterns in the ebb-tidal delta off Texel Inlet, Wadden Sea, The Netherlands, *Marine Geology*, *86*, 137–154, doi:10.1016/0025-3227(89)90046-7.

Sha, L. P., and P. L. De Boer (1991), Ebb-tidal delta deposits along the west Frisian Islands (the Netherlands): processes, facies architecture and preservation, *Clastic tidal sedimentology*, *16*(1991), 199–218.

Shen, X., B. J. Lee, M. Fettweis, and E. A. Toorman (2018), A tri-modal flocculation model coupled with TELEMAC for estuarine muds both in the laboratory and in the field, *Water Research*, *145*, 473–486, doi:10.1016/j.watres.2018.08.062.

Sijtsma, F. J., M. N. Daams, H. Farjon, and A. E. Buijs (2012), Deep feelings around a shallow coast. A spatial analysis of tourism jobs and the attractivity of nature in the Dutch Wadden area, *Ocean and Coastal Management*, *68*, 138–148, doi:10.1016/j.ocecoaman.2012.05.018.

Silva, A., R. Taborda, A. Rodrigues, J. Duarte, and J. Cascalho (2007), Longshore drift estimation using fluorescent tracers: New insights from an experiment at Comporta Beach, Portugal, *Marine Geology*, *240*(1-4), 137–150, doi:10.1016/j.margeo.2007.02.009.

Smetanová, A., E. N. Paton, C. Maynard, S. Tindale, A. P. Fernández-Getino, M. J. Marqéus Pérez, L. Bracken, Y. Le Bissonnais, and S. D. Keesstra (2018), Stakeholders' perception of the relevance of water and sediment connectivity in water and land management, *Land Degradation and Development*, *29*(6), 1833–1844, doi:10.1002/ldr.2934.

Smith, J. B., and D. M. FitzGerald (1994), Sediment transport patterns at the Essex River Inlet ebb-tidal delta, Massachusetts, U.S.A. , *Journal of Coastal Research*, *10*(3), 752–774.

Smith, S. J., J. Marsh, and T. Puckette (2007), Analysis of fluorescent sediment tracer for evaluating nearshore placement of dredged material, *Proceedings of 18th World Dredging Congress, World Organisation of Dredging Association*, *44*(0), 1345–1358.

Son, C. S., B. W. Flemming, and A. Bartholomä (2011), Evidence for sediment recirculation on an ebb-tidal delta of the East Frisian barrier-island system, southern North Sea, *Geo-Marine Letters*, *31*(2), 87–100, doi:10.1007/s00367-010-0217-8.

Soulsby, R. L. (1997), *Dynamics of marine sands: a manual for practical applications*, Thomas Telford.

Soulsby, R. L., C. T. Mead, B. R. Wild, and M. J. Wood (2011), Lagrangian model for simulating the dispersal of sand-sized particles in coastal waters, *Journal of Waterway, Port, Coastal and Ocean Engineering*, *137*(3), 123–131, doi:10.1061/(ASCE)WW.1943-5460.0000074.

Spencer, T., and D. J. Reed (2010), Estuaries, in *Sediment Cascades: An Integrated Approach*, edited by T. Burt and R. J. Allison, 1 ed., chap. 14, pp. 403–432, John Wiley & Sons, Chichester, UK.

Sperry, M. M., Q. K. Telesford, F. Klimm, and D. S. Bassett (2017), Rentian scaling for the measurement of optimal embedding of complex networks into physical space, *Journal of Complex Networks*, *5*(2), 199–218, doi:10.1093/comnet/cnw010.

Speybroeck, J., D. Bonte, W. Courtens, T. Gheskiere, P. Grootaert, J. P. Maelfait, M. Mathys, S. Provoost, K. Sabbe, E. W. Stienen, V. Van Lancker, M. Vincx, and S. Degraer (2006), Beach nourishment: An ecologically sound coastal defence alternative? A review, *Aquatic Conservation: Marine and Freshwater Ecosystems*, *16*(4), 419–435, doi:10.1002/aqc.733.

Stevens, A. W., E. P. Elias, S. G. Pearson, G. M. Kaminsky, P. R. Ruggiero, H. M. Weiner, and G. R. Gelfenbaum (2020), Observations of coastal change and numerical modeling of sediment-transport pathways at the mouth of the Columbia River and its adjacent littoral cell, *Open-File Report*, doi:10.3133/ofr20201045.

Stewart, I. S., and V. Hurth (2021), Selling planet Earth: re-purposing geoscience communications, *Geological Society, London, Special Publications*, *508*(1), 265–283, doi:10.1144/SP508-2020-101.

Stive, M. J., and Z. B. Wang (2003), Morphodynamic modeling of tidal basins and coastal inlets, *Elsevier Oceanography Series*, *67*(C), 367–392, doi:10.1016/S0422-9894(03)80130-7.

Stive, M. J., M. Capobianco, Z. B. Wang, P. Ruol, and M. Buijsman (1998), Morphodynamics of a tidal lagoon and the adjacent coast, in *Eighth International Biennial Conference on Physics of Estuaries and Coastal Seas, September 1996*, pp. 397–407, The Hague, The Netherlands.

Stive, M. J., M. A. de Schipper, A. P. Luijendijk, R. Ranasinghe, J. van Thiel de Vries, S. G. Aarninkhof, C. van Gelder-Maas, S. de Vries, M. Henriquez, and S. Marx (2013), The Sand Engine: A solution for vulnerable deltas in the 21st century?, in *Coastal Dynamics 2013*, pp. 1537–1546.

Storlazzi, C. D., M. van Ormondt, Y.-L. Chen, and E. P. Elias (2017), Modeling Fine-Scale Coral Larval Dispersal and Interisland Connectivity to Help Designate Mutually-Supporting Coral Reef Marine Protected Areas: Insights from Maui Nui, Hawaii, *Frontiers in Marine Science*, *4*(December), 1–14, doi:10.3389/fmars.2017.00381.

Straub, K. M., R. A. Duller, B. Z. Foreman, and E. A. Hajek (2020), Buffered, Incomplete, and Shredded: The Challenges of Reading an Imperfect Stratigraphic Record, *Journal of Geophysical Research: Earth Surface*, *125*(3), 1–44, doi:10.1029/2019JF005079.

Su, M., P. Yao, Z. B. Wang, C. Zhang, Y. Chen, and M. J. Stive (2016), Conversion of electro-optical signals to sediment concentration in a silt–sand suspension environment, *Coastal Engineering*, *114*, 284–294, doi:10.1016/j.coastaleng.2016.04.014.

Sunamura, T., and N. C. Kraus (1984), Prediction of average mixing depth of sediment in the surf zone, *Marine Geology*, *62*(1-2), 1–12, doi:10.1016/0025-3227(84)90051-3.

Sutherland, T. F., P. M. Lane, C. L. Amos, and J. Downing (2000), The calibration of optical backscatter sensors for suspended sediment of varying darkness levels, *Marine Geology*, *162*(2-4), 587–597, doi:10.1016/S0025-3227(99)00080-8.

Sylvester, Z., C. Pirmez, and A. Cantelli (2011), A model of submarine channel-levee evolution based on channel trajectories: Implications for stratigraphic architecture, *Marine and Petroleum Geology*, *28*(3), 716–727, doi:10.1016/j.marpetgeo.2010.05.012.

Tejedor, A., A. Longjas, I. Zaliapin, and E. Foufoula-Georgiou (2015a), Delta channel networks: 1. A graph-theoretic approach for studying connectivity and steady state transport on deltaic surfaces, *Water Resources Research*, *51*(6), 3998–4018, doi:10.1002/2014WR016577.

Tejedor, A., A. Longjas, I. Zaliapin, and E. Foufoula-Georgiou (2015b), Delta channel networks: 2. Metrics of topologic and dynamic complexity for delta comparison, physical inference, and vulnerability assessment, *Water Resources Research*, *51*(6), 4019–4045, doi:10.1002/2014WR016604.

R

Tejedor, A., A. Longjas, R. Caldwell, D. A. Edmonds, I. Zaliapin, and E. Foufoula-Georgiou (2016), Quantifying the signature of sediment composition on the topologic and dynamic complexity of river delta channel networks and inferences toward delta classification, *Geophysical Research Letters*, *43*(7), 3280–3287, doi:10.1002/2016GL068210.

Tejedor, A., A. Longjas, D. A. Edmonds, I. Zaliapin, T. T. Georgiou, A. Rinaldo, and E. Foufoula-Georgiou (2017), Entropy and optimality in river deltas, *Proceedings of the National Academy of Sciences*, *114*(44), 11,651–11,656, doi:10.1073/pnas.1708404114.

Tejedor, A., A. Longjas, E. Foufoula-georgiou, T. T. Georgiou, and Y. Moreno (2018a), Diffusion Dynamics and Optimal Coupling in Multiplex Networks with Directed Layers, *Physical Review X*, *8*(3), 31,071, doi:10.1103/PhysRevX.8.031071.

Tejedor, A., A. Longjas, P. Passalacqua, Y. Moreno, and E. Foufoula-Georgiou (2018b), Multiplex Networks: A Framework for Studying Multiprocess Multiscale Connectivity Via Coupled-Network Theory With an Application to River Deltas, *Geophysical Research Letters*, *45*(18), 9681–9689, doi:10.1029/2018GL078355.

Temmerman, S., P. Meire, T. J. Bouma, P. M. Herman, T. Ysebaert, and H. J. De Vriend (2013), Ecosystem-based coastal defence in the face of global change, *Nature*, *504*(7478), 79–83, doi:10.1038/nature12859.

Thibaud, R., G. Del Mondo, T. Garlan, A. Mascret, and C. Carpentier (2013), A Spatio-Temporal Graph Model for Marine Dune Dynamics Analysis and Representation, *Transactions in GIS*, pp. n/a–n/a, doi:10.1111/tgis.12006.

Thiemann, C., F. Theis, D. Grady, R. Brune, and D. Brockmann (2010), The structure of borders in a small world, *PLoS ONE*, *5*(11), 1–7, doi:10.1371/journal.pone.0015422.

Thorne, P. D., and D. M. Hanes (2002), A review of acoustic measurement of small-scale sediment processes, *Continental Shelf Research*, *22*(4), 603–632, doi:10.1016/S0278-4343(01)00101-7.

Thorne, P. D., and D. Hurther (2014), An overview on the use of backscattered sound for measuring suspended particle size and concentration profiles in non-cohesive inorganic sediment transport studies, *Continental Shelf Research*, *73*, 97–118, doi:10.1016/j.csr.2013.10.017.

Thorne, P. D., and R. Meral (2008), Formulations for the scattering properties of suspended sandy sediments for use in the application of acoustics to sediment transport processes, *Continental Shelf Research*, *28*(2), 309–317, doi:10.1016/j.csr.2007.08.002.

Thorne, P. D., P. J. Hardcastle, and R. L. Soulsby (1993), Analysis of Acoustic Measurements of Suspended Sediments, *Journal of Geophysical Research*, *98*(92), 899–910.

Thorne, P. D., I. D. Lichtman, and D. Hurther (2021), Acoustic scattering characteristics and inversions for suspended concentration and particle size above mixed sand and mud beds, *Continental Shelf Research*, *214*(November 2020), 104,320, doi:10.1016/j.csr.2020.104320.

Tiessen, M. C., L. Fernard, T. Gerkema, J. Van Der Molen, P. Ruardij, and H. W. Van Der Veer (2014), Numerical modelling of physical processes governing larval transport in the southern North Sea, *Ocean Science*, *10*(3), 357–376, doi:10.5194/os-10-357-2014.

TNO (2017), DINOloket: Ondergrondgegevens bekijken en aanvragen.

Toker, D., F. T. Sommer, and M. D'Esposito (2020), A simple method for detecting chaos in nature, *Communications Biology*, *3*(1), 1–13, doi:10.1038/s42003-019-0715-9.

Tooth, S., and H. A. Viles (2021), Equality, diversity, inclusion: ensuring a resilient future for geomorphology, doi:10.1002/esp.5026.

Torres, R. D. O. (2015), The Archaeology of Shore Stranded Shipwrecks of Southern Brazil, Ph.D. thesis, Texas A&M University.

Treml, E. A., P. N. Halpin, D. L. Urban, and L. F. Pratson (2008), Modeling population connectivity by ocean currents, a graph-theoretic approach for marine conservation, *Landscape Ecology*, *23*(S1), 19–36, doi:10.1007/s10980-007-9138-y.

Trivedi, S., S. Gkantonas, L. C. C. Mesquita, S. Iavarone, P. M. D. Oliveira, and E. Mastorakos (2021),

Estimates of the stochasticity of droplet dispersion by a cough, *Physics of Fluids*, *33*(11), 115,130, doi:10.1063/5.0070528.

Turnbull, L., K. Tockner, R. Poeppl, M.-t. Hütt, S. Keesstra, L. J. Bracken, A. J. Parsons, S. Kininmonth, R. Masselink, L. Liu, and A. A. Ioannides (2018), Connectivity and complex systems: learning from a multi-disciplinary perspective, *Applied Network Science*, *3*(1), doi:10.1007/s41109-018-0067-2.

Tye, R. S., and T. F. Moslow (1993), Tidal Inlet Reservoirs: Insights from Modern Examples, (May 2015), 77–99, doi:10.1007/978-1-4757-0160-9_4.

Uesaka, L., Y. Goto, Y. Yonehara, K. Komatsu, M. Naruoka, H. Weimerskirch, K. Sato, and K. Q. Sakamoto (2022), Ocean wave observation utilizing motion records of seabirds, *Progress in Oceanography*, *200*(July 2021), 102,713, doi:10.1016/j.pocean.2021.102713.

United Nations (2017), Work of the Statistical Commission pertaining to the 2030 Agenda for Sustainable Development.

Urban, D. L., E. S. Minor, E. A. Treml, and R. S. Schick (2009), Graph models of habitat mosaics, *Ecology Letters*, *12*(3), 260–273, doi:10.1111/j.1461-0248.2008.01271.x.

van Aken, H. M. (2008a), Variability of the salinity in the western Wadden Sea on tidal to centennial time scales, *Journal of Sea Research*, *59*(3), 121–132, doi:10.1016/j.seares.2007.11.001.

van Aken, H. M. (2008b), Variability of the water temperature in the western Wadden Sea on tidal to centennial time scales, *Journal of Sea Research*, *60*(4), 227–234, doi:10.1016/j.seares.2008.09.001.

van Cauwenberghe, L., L. Devriese, F. Galgani, J. Robbens, and C. R. Janssen (2015), Microplastics in sediments: A review of techniques, occurrence and effects, *Marine Environmental Research*, *111*, 5–17, doi:10.1016/j.marenvres.2015.06.007.

van de Kreeke, J., and A. Hibma (2005), Observations on silt and sand transport in the throat section of the Frisian Inlet, *Coastal Engineering*, *52*(2), 159–175, doi:10.1016/j.coastaleng.2004.10.002.

van der Hout, C. M., R. Witbaard, M. J. N. Bergman, G. C. A. Duineveld, M. J. C. Rozemeijer, and T. Gerkema (2017), The dynamics of suspended particulate matter (SPM) and chlorophyll- a from intratidal to annual time scales in a coastal turbidity maximum, *Journal of Sea Research*, *127*(March), 105–118, doi:10.1016/j.seares.2017.04.011.

Van Der Molen, J., and B. Van Dijck (2000), The evolution of the Dutch and Belgian coasts and the role of sand supply from the North Sea, *Global and Planetary Change*, *27*(1-4), 223–244, doi:10.1016/S0921-8181(01)00068-6.

van der Molen, J., L. M. García-García, P. Whomersley, A. Callaway, P. E. Posen, and K. Hyder (2018), Connectivity of larval stages of sedentary marine communities between hard substrates and offshore structures in the North Sea, *Scientific Reports*, *8*(1), 1–14, doi:10.1038/s41598-018-32912-2.

van der Spek, A. (1995), Reconstruction of tidal inlet and channel dimensions in the Frisian Middelzee, a former tidal basin in the Dutch Wadden Sea, *Spec. Publs int. Ass. Sediment.*, *24*, 239–258.

van der Spek, A. J., and Q. J. Lodder (2015), A New Sediment Budget for the Netherlands; the Effects of 15 Years of Nourishing (1991-2005), in *Coastal Sediments 2015*, July, doi:10.1142/9789814689977_0074.

van der Spek, A. J., A. Forzoni, and T. Vermaas (2021), Geology of the Dutch Lower Shoreface, *Submitted to Ocean & Coastal Management*, pp. 1–26.

van der Spek, A. J. F. (1994), Large-scale Evolution of Holocene Tidal Basins in the Netherlands, Phd, Utrecht University.

van der Spek, A. J. F. (1996), Holocene depositional sequences in the Dutch Wadden Sea south of the island of Ameland, *Mededelingen Rijks Geologische Dienst*, *57*, 41–78.

van der Vegt, H. (2018), From fluvial supply to delta deposits: Simulating sediment delivery, transport and deposition, Phd, Delft University of Technology, doi:10.4233/uuid:c049ea67-23a1-4e7eaf52-1275802839f1.

van der Vegt, H., J. E. Storms, D. R. Walstra, K. Nordahl, N. C. Howes, and A. W. Martinius (2020), Grain size fractionation by process-driven sorting in sandy to muddy deltas, *The Depositional Record*, *6*(1), 217–235, doi:10.1002/dep2.85.

van der Wegen, M., A. Dastgheib, B. E. Jaffe, and D. Roelvink (2011), Bed composition generation for morphodynamic modeling: Case study of San Pablo Bay in California, USA, *Ocean Dynamics*, *61*(2-3), 173–186, doi:10.1007/s10236-010-0314-2.

van der Werf, J., J. A. Á. Antolínez, L. Brakenhoff, M. Gawehn, K. den Heijer, H. de Looff, R. Wilmink, M. van Maarsseveen, H. Meijer-Holzhauer, J.-W. Mol, S. G. Pearson, B. C. van Prooijen, G. Santinelli, C. Schipper, M. Tissier, P. K. Tonnon, L. de Vet, T. Vermaas, R. J. Wilmink, and F. P. de Wit (2019a), Datareport Kustgenese 2.0., *Tech. Rep. 1220339-015-ZKS-0004*, Rijkswaterstaat, Delft, The Netherlands.

van der Werf, J. J., P. L. de Vet, M. P. Boersema, T. J. Bouma, A. J. Nolte, R. A. Schrijvershof, L. M. Soissons, J. Stronkhorst, E. van Zanten, and T. Ysebaert (2019b), An integral approach to design the Roggenplaat intertidal shoal nourishment, *Ocean and Coastal Management*, *172*(February), 30–40, doi:10.1016/j.ocecoaman.2019.01.023.

van Dongeren, A., P. Ciavola, G. Martinez, C. Viavattene, T. Bogaard, O. Ferreira, R. Higgins, and R. McCall (2018), Introduction to RISC-KIT: Resilience-increasing strategies for coasts, *Coastal Engineering*, *134*(February 2017), 2–9, doi:10.1016/j.coastaleng.2017.10.007.

van Dongeren, A. R., A. J. van der Westhuysen, J. Groeneweg, G. Van Vledder, J. Lansen, A. Smale, C. Gautier, H. Peters, and I. Wenneker (2011), Spectral Wave Modelling in Tidal Inlet Seas: Results From the SBW Wadden Sea Project, *Coastal Engineering Proceedings*, *1*, 1–15, doi:10.9753/icce.v32.waves.44.

van Gijzen, L. (2020), Sediment Pathways and Connectivity in San Francisco South Bay, Msc thesis, Delft University of Technology.

van Maanen, B., R. J. Nicholls, J. R. French, A. Barkwith, D. Bonaldo, H. Burningham, A. Brad Murray, A. Payo, J. Sutherland, G. Thornhill, I. H. Townend, M. van der Wegen, and M. J. Walkden (2016), Simulating mesoscale coastal evolution for decadal coastal management: A new framework integrating multiple, complementary modelling approaches, *Geomorphology*, *256*, 68–80, doi:10.1016/j.geomorph.2015.10.026.

Van Prooijen, B. C., M. F. Tissier, F. P. de Wit, S. G. Pearson, L. B. Brakenhoff, M. C. Van Maarseveen, M. Van Der Vegt, J. W. Mol, F. Kok, H. Holzhauer, J. J. Van Der Werf, T. Vermaas, M. Gawehn, B. Grasmeijer, E. P. Elias, P. K. Tonnon, G. Santinelli, J. A. Á. Antolínez, P. L. M. De Vet, A. Reniers, Z. B. Wang, C. Den Heijer, C. Van Gelder-Maas, R. J. Wilmink, C. A. Schipper, and H. De Looff (2020), Measurements of hydrodynamics, sediment, morphology and benthos on Ameland ebb-tidal delta and lower shoreface, *Earth System Science Data*, *12*(4), 2775–2786, doi:10.5194/essd-12-2775-2020.

van Rhijn, M. (2019), Sediment transport during the execution of the pilot nourishment Ameland Inlet, Msc thesis, Delft University of Technology.

van Sebille, E., S. M. Griffies, R. Abernathey, T. P. Adams, P. Berloff, A. Biastoch, B. Blanke, E. P. Chassignet, Y. Cheng, C. J. Cotter, E. Deleersnijder, K. Döös, H. F. Drake, S. Drijfhout, S. F. Gary, A. W. Heemink, J. Kjellsson, I. M. Koszalka, M. Lange, C. Lique, G. A. MacGilchrist, R. Marsh, C. G. Mayorga Adame, R. McAdam, F. Nencioli, C. B. Paris, M. D. Piggott, J. A. Polton, S. Rühs, S. H. Shah, M. D. Thomas, J. Wang, P. J. Wolfram, L. Zanna, and J. D. Zika (2018), Lagrangian ocean analysis: Fundamentals and practices, *Ocean Modelling*, *121*(October 2017), 49–75, doi:10.1016/j.ocemod.2017.11.008.

van Sebille, E., P. Delandmeter, J. Schofield, D. Hardesty, J. Jones, and A. Donnelly (2019), Basin-scale sources and pathways of microplastic that ends up in the Galápagos Archipelago, *Ocean Science Discussions*, pp. 1–15, doi:10.5194/os-2019-37.

van Slobbe, E., H. J. de Vriend, S. G. Aarninkhof, K. Lulofs, M. de Vries, and P. Dircke (2013), Building with Nature: In search of resilient storm surge protection strategies, *Natural Hazards*, *66*(3), 1461–1480, doi:10.1007/s11069-013-0612-3.

Van Weerdenburg, R. J. (2019), Exploring the relative importance of wind for exchange processes around a tidal inlet system: the case of Ameland Inlet, Master's thesis, Delft University of Technology.

Van Weerdenburg, R. J., S. G. Pearson, B. C. van Prooijen, S. Laan, and E. Elias (2021), Field measurements and numerical modelling of wind-driven exchange flows in a tidal inlet system in the Dutch Wadden Sea, *Ocean & Coastal Management*, *215*(October), 105,941, doi:10.1016/j.ocecoaman.2021.105941.

Van Wesenbeeck, B. K., J. P. Mulder, M. Marchand, D. J. Reed, M. B. De Vries, H. J. De Vriend, and P. M. Herman (2014), Damming deltas: A practice of the past? Towards nature-based flood defenses, *Estuarine, Coastal and Shelf Science*, *140*, 1–6, doi:10.1016/j.ecss.2013.12.031.

Veenman, C. J., M. J. Reinders, and E. Backer (2001), Resolving motion correspondence for densely moving points, *IEEE Transactions on Pattern Analysis and Machine Intelligence*, *23*(1), 54–72, doi:10.1109/34.899946.

Veenstra, H. J., and A. M. Winkelmolen (1976), Size, shape and density sorting around two barrier islands along the north coast of Holland, *Geologie en Mijnbouw*, *55*(1-2), 87–104.

Velegrakis, A. F., M. B. Collins, A. C. Bastos, D. Paphitis, and A. Brampton (2007), Seabed sediment transport pathway investigations: review of scientific approach and methodologies, *Geological Society, London, Special Publications*, *274*(1), 127–146, doi:10.1144/GSL.SP.2007.274.01.13.

Verhoeff, S. (2018), Het zeegat van Ameland. Het digitaliseren van historische zeekaarten. (In Dutch)., Master's, Maritiem Institute Willem Barentsz, Terschelling.

Vermeersen, B. L. A., A. B. A. Slangen, T. Gerkema, F. Baart, K. M. Cohen, S. Dangendorf, M. Duranmatute, T. Frederikse, A. Grinsted, M. P. Hijma, S. Jevrejeva, P. Kiden, M. Kleinherenbrink, E. W. Meijles, M. D. Palmer, R. Rietbroek, R. E. M. Riva, E. Schulz, D. C. Slobbe, M. J. R. Simpson, P. Sterlini, P. Stocchi, R. S. W. Van, D. Wal, and M. V. D. Wegen (2018), Sea-level change in the Dutch Wadden Sea, *2018*, 79–127, doi:10.1017/njg.2018.7.

Vila-Concejo, A., Ó. Ferreira, A. Matias, and J. M. Dias (2003), The first two years of an inlet: Sedimentary dynamics, *Continental Shelf Research*, *23*(14-15), 1425–1445, doi:10.1016/S0278-4343(03)00142-0.

Vila-Concejo, A., Ó. Ferreira, P. Ciavola, A. Matias, and J. M. Dias (2004), Tracer studies on the updrift margin of a complex inlet system, *Marine Geology*, *208*(1), 43–72, doi:10.1016/j.margeo.2004.04.020.

Vila-Concejo, A., S. L. Gallop, S. M. Hamylton, L. S. Esteves, K. R. Bryan, I. Delgado-Fernandez, E. Guisado-Pintado, S. Joshi, G. M. Da Silva, A. R. De Alegria-Arzaburu, H. E. Power, N. Senechal, and K. Splinter (2018), Steps to improve gender diversity in coastal geoscience and engineering, *Palgrave Communications*, *4*(1), doi:10.1057/s41599-018-0154-0.

Vitousek, S., P. L. Barnard, and P. Limber (2017a), Can beaches survive climate change?, *Journal of Geophysical Research: Earth Surface*, *122*(4), 1060–1067, doi:10.1002/2017JF004308.

Vitousek, S., P. L. Barnard, P. Limber, L. Erikson, and B. Cole (2017b), A model integrating longshore and cross-shore processes for predicting long-term shoreline response to climate change, *Journal of Geophysical Research: Earth Surface*, *122*(4), 782–806, doi:10.1002/2016JF004065.

Vitousek, S., L. Cagigal, J. Montaño, A. Rueda, F. Mendez, G. Coco, and P. L. Barnard (2021), The Application of Ensemble Wave Forcing to Quantify Uncertainty of Shoreline Change Predictions, *Journal of Geophysical Research: Earth Surface*, *126*(7), 1–43, doi:10.1029/2019jf005506.

Volp, N. D., B. C. V. Prooijen, J. D. Pietrzak, and G. S. Stelling (2016), A subgrid based approach for morphodynamic modelling, *Advances in Water Resources*, *93*, 105–117.

Vonhögen-Peeters, L. M., S. van Heteren, A. P. Wiersma, M. P. de Kleine, and V. C. Marges (2013), Quantifying sediment dynamics within the Dutch Wadden Sea using bathymetric monitoring series, *Journal of Coastal Research*, *165*(65), 1611–1616, doi:10.2112/si65-272.1.

Vos, K., M. D. Harley, K. D. Splinter, J. A. Simmons, and I. L. Turner (2019a), Sub-annual to multi-decadal shoreline variability from publicly available satellite imagery, *Coastal Engineering*, *150*(November 2018), 160–174, doi:10.1016/j.coastaleng.2019.04.004.

Vos, K., K. D. Splinter, M. D. Harley, J. A. Simmons, and I. L. Turner (2019b), CoastSat: A Google Earth

Engine-enabled Python toolkit to extract shorelines from publicly available satellite imagery, *Environmental Modelling and Software*, *122*, 104,528, doi:10.1016/j.envsoft.2019.104528.

Voulgaris, G., and S. T. Meyers (2004), Temporal variability of hydrodynamics, sediment concentration and sediment settling velocity in a tidal creek, *Continental Shelf Research*, *24*(15), 1659–1683, doi:10.1016/j.csr.2004.05.006.

Wainwright, D. J., R. Ranasinghe, D. P. Callaghan, C. D. Woodroffe, R. Jongejan, A. J. Dougherty, K. Rogers, and P. J. Cowell (2015), Moving from deterministic towards probabilistic coastal hazard and risk assessment: Development of a modelling framework and application to Narrabeen Beach, New South Wales, Australia, *Coastal Engineering*, *96*, 92–99, doi:10.1016/j.coastaleng.2014.11.009.

Wallinga, J., D. Goldsborough, R. Witbaard, B. C. van Prooijen, A. van der Spek, E. Elias, Q. Lodder, A. de Boer, T. Kooistra, and S. G. Pearson (2021), Introducing the TRAILS project: Tracking Ameland inlet living lab sediment, in *NCK Days 2021*, p. 51, Online.

Walton, T. L., and W. D. Adams (1976), Capacity of Inlet Outer Bars to Store Sand, *15th Coastal Engineering Conference*, pp. 1919–1937, doi:10.9753/icce.v15.

Wang, Y., Q. Yu, J. Jiao, P. K. Tonnon, Z. B. Wang, and S. Gao (2016), Coupling bedform roughness and sediment grain-size sorting in modelling of tidal inlet incision, *Marine Geology*, *381*(September), 128–141, doi:10.1016/j.margeo.2016.09.004.

Wang, Z. B., M. De Vries, R. J. Fokkink, and A. Langerak (1995), Stability of river bifurcations in ID morphodynamic models, *Journal of Hydraulic Research*, *33*(6), 739–750, doi:10.1080/00221689509498549.

Wang, Z. B., D. S. Van Maren, P. X. Ding, S. L. Yang, B. C. van Prooijen, P. de Vet, J. C. Winterwerp, H. J. De Vriend, M. J. Stive, and Q. He (2015), Human impacts on morphodynamic thresholds in estuarine systems, *Continental Shelf Research*, *111*, 174–183, doi:10.1016/j.csr.2015.08.009.

Wang, Z. B., E. P. Elias, A. J. van der Spek, and Q. J. Lodder (2018), Sediment budget and morphological development of the Dutch Wadden Sea: impact of accelerated sea-level rise and subsidence until 2100, *Netherlands Journal of Geosciences*, *97*(03), 183–214, doi:10.1017/njg.2018.8.

Wang, Z. B., I. Townend, and M. J. Stive (2020), Aggregated morphodynamic modelling of tidal inlets and estuaries, *Water Science and Engineering*, *13*(1), 1–13, doi:10.1016/j.wse.2020.03.004.

Warrick, J. A., A. W. Stevens, I. M. Miller, S. R. Harrison, A. C. Ritchie, and G. Gelfenbaum (2019), World's largest dam removal reverses coastal erosion, *Scientific Reports*, *9*(1), 13,968, doi:10.1038/s41598-019-50387-7.

Weeks, A. R., J. H. Simpson, and D. Bowers (1993), The relationship between concentrations of suspended particulate material and tidal processes in the Irish Sea, *Continental Shelf Research*, *13*(12), 1325–1334, doi:10.1016/0278-4343(93)90086-D.

Wells, J. T., and J. E. McNinch (2003), Role of inlet dynamics in scour and burial of marine artifacts in energetic coastal settings, *WIT Transactions on the Built Environment*, *65*, 87–96.

Weltje, G. J., and M. A. Prins (2007), Genetically meaningful decomposition of grain-size distributions, *Sedimentary Geology*, *202*(3), 409–424, doi:10.1016/j.sedgeo.2007.03.007.

WET Labs Inc (2019), User manual: ECO Fluorometers and Scattering Sensors, *Tech. rep.*, Philomath, OR.

WETLabs (2010), ECO 3-Measurement Sensor User's Guide, *Tech. rep.*, WET Labs, Inc., Philomath, OR.

White, T. E. (1998), Status of measurement techniques for coastal sediment transport, *Coastal Engineering*, *35*(1-2), 17–45, doi:10.1016/S0378-3839(98)00033-7.

Wilson, G. W. (2018), Anomalous Diffusion of Sand Tracer Particles Under Waves, *Journal of Geophysical Research: Earth Surface*, *123*(11), 3055–3068, doi:10.1029/2018JF004780.

Wilson, G. W., and A. E. Hay (2015), Measuring multi-phase particle flux with a multi-frequency acoustic profiler, in *Proceedings of the Institute of Acoustics*, vol. 37, pp. 343–348, doi:10.1121/1.4938219.

Winkelmolen, A. M., and H. J. Veenstra (1974), Size and shape sorting in a Dutch tidal inlet, *Sedimentology*, *21*(1), 107–126, doi:10.1111/j.1365-3091.1974.tb01784.x.

Wittebrood, M., S. De Vries, P. Goessen, and S. G. Aarninkhof (2018), Aeolian Sediment Transport At a Man-Made Dune System; Building With Nature At the Hondsbossche Dunes, *Coastal Engineering Proceedings*, (36), 83, doi:10.9753/icce.v36.papers.83.

Wohl, E., G. Brierley, D. Cadol, T. J. Coulthard, T. Covino, K. A. Fryirs, G. Grant, R. G. Hilton, S. N. Lane, F. J. Magilligan, K. M. Meitzen, P. Passalacqua, R. E. Poeppl, S. L. Rathburn, and L. S. Sklar (2019), Connectivity as an emergent property of geomorphic systems, *Earth Surface Processes and Landforms*, *44*(1), 4–26, doi:10.1002/esp.4434.

Wong, F. L., D. L. Woodrow, and M. McGann (2013), Heavy mineral analysis for assessing the provenance of sandy sediment in the San Francisco Bay Coastal System, *Marine Geology*, *345*, 170–180, doi:10.1016/j.margeo.2013.05.012.

Wrecksite (2017), Wrecksite: Zeegat van Ameland tot Terschelling.

YSI Incorporated (2012), *6-Series Multiparameter Water Quality Sondes User Manual*, revision j ed., 374 pp., YSI Incorporated, Yellow Springs, Ohio.

Zhang, H., D. Li, J. Wang, H. Zhou, W. Guan, X. Lou, W. Cao, A. Shi, P. Chen, K. Fan, L. Ren, G. Zheng, and Y. Li (2020a), Long time-series remote sensing analysis of the periodic cycle evolution of the inlets and ebb-tidal delta of Xincun Lagoon, Hainan Island, China, *ISPRS Journal of Photogrammetry and Remote Sensing*, *165*(April), 67–85, doi:10.1016/j.isprsjprs.2020.05.006.

Zhang, X., H. Wang, S. Xu, and Z. Yang (2020b), A basic end-member model algorithm for grain-size data of marine sediments, *Estuarine, Coastal and Shelf Science*, *236*(February), 106,656, doi:10.1016/j.ecss.2020.106656.

Zhu, H., L. Zuo, and Y. Lu (2019a), Process-Based Modeling on Morphology Evolution of Laolonggou Tidal Inlet in Bohai Bay of China, in *Coastal Sediments 2019*, pp. 2057–2079, World Scientific, St. Petersburg, Florida, doi:10.1142/9789811204487_0177.

Zhu, Q., B. C. van Prooijen, D. C. Maan, Z. B. Wang, P. Yao, T. Daggers, and S. L. Yang (2019b), The heterogeneity of mudflat erodibility, *Geomorphology*, *345*, doi:10.1016/j.geomorph.2019.106834.

Zijderveld, A., and H. Peters (2009), Measurement programme Dutch Wadden Sea, in *Coastal Engineering 2008*, pp. 404–410, World Scientific, Hamburg, Germany.

Zimmerman, J. T. (1976), Mixing and flushing of tidal embayments in the western Dutch Wadden Sea part I: Distribution of salinity and calculation of mixing time scales, *Netherlands Journal of Sea Research*, *10*(2), 149–191, doi:10.1016/0077-7579(76)90013-2.

ACKNOWLEDGEMENTS

I feel profoundly, absurdly grateful. This has been an incredibly humbling experience and I have so many people to thank. However, unleashing a tsunami of thankfulness[1] on the world as ***Stuart's Gratitude: The Unabridged 250-Page Director's Cut*** may have been a bit much, so with great restraint I have kept it to around 3% of that. It may take a village to produce a PhD, but I feel like I had a whole city behind me. Furthermore, many systemic barriers related to our background, our gender, and our race still persist in engineering and academia. I recognize that I have been enormously privileged in these and many other respects throughout my life and PhD journey, and that this has made my road smoother. Let's work together to dismantle these barriers and build a more equitable research and education community.

To me, the acknowledgements are the one of the most important parts of a thesis and they were the last part that I wrote before going to press (if this were a movie, the printing staff would have had to dramatically rip the manuscript from my hands). I must admit to writing this section with some trepidation, since this is likely the only part of my thesis that most people will actually read (if that's you: Hi! No offence taken – I am usually the one in your shoes). To those whom I have wrongfully omitted, I offer you my sincerest apologies and my favourite YouTube video in consolation.

This work is part of the research programme 'Collaboration Program Water' with project number 14489 (SEAWAD), which is (partly) financed by NWO Domain Applied and Engineering Sciences. Thank you to NWO for funding the coolest job I have ever had.

* * *

To my PhD committee:

First and foremost, thank you to my daily supervisor and promotor *Bram van Prooijen.* In April 2016 I was wrapping up my MSc thesis and saw an ad for a cool PhD position in Delft. I was hesitant about doing a PhD, as the idea of spending 4+ years on a single topic held little appeal for me, but I had recently developed a taste for research and thought it was at least worth meeting this Bram fellow to learn more. My apprehensions dissolved almost the instant I met you, and my instincts told me that I should give this a shot. From the very first day we got along like a house on fire, and it didn't let up once in five years. Taking on this PhD was one of the best decisions I ever made. I want everyone reading this to know how important you were to this outcome: your ideas on science, communication, cheerful collaboration in good faith, and making our lab a better place were essential to everything that I have done in the past five years. Thank you for giving me a sense of security and confidence in myself: you encouraged me to make mistakes, **BE BOLD** (not just *kind of bold*), follow tangents, and get lost in the wilderness, but were always there to shepherd me back towards the sacred path of thesis completion if I strayed too far. Thank you for trusting me and taking chances on my stranger ideas and ambitions, but also for teaching

[1] Although perhaps sea level rise is a more apt metaphor, since it keeps on growing...

me to be judicious in pruning the overgrowth of my side projects and lit reviews[2]. Beyond just your scientific contributions, thank you for the profound impact that you have had on me personally. In spite of the challenges, I just had so much darn fun with my PhD, and I pin a lot of the credit for that squarely on your shoulders. I hope to bring your energy and collaborative spirit with me wherever my career takes me, and that we can keep doing science and having fun together for many years to come.

To my promotor *Zheng Bing Wang*, thank you for your constructively critical view, good humour, and for keeping a steady hand on the wheel. I always knew that I could count on your keen eye to point out and work together to resolve any fundamental issues with my research. You have been a source of great reassurance at many points in my PhD. Thank you for encouraging me to take risks and try new things in my research. I hope that we can continue collaborating for a long time to come!

Thank you *Edwin Elias*, for being one of my biggest supporters and collaborators. I am so glad that we started working together; this thesis would likely have taken a completely different trajectory if you were not involved. Thank you for believing in me, for seeing potential in my weird ideas, and bringing me along for collaborations in your work. Although I have fallen in deep with science during these past years, I still consider myself an engineer first and foremost; to this end, I am grateful for your support in giving me many opportunities to apply my research in practice. I am confident that this PhD is just the start of a long and fruitful collaboration and am excited to see what comes next. Lastly, thank you for hosting me in California and welcoming me into your family there – I will always be grateful for your hospitality and kindness.

I would also like to thank the independent members of my committee for their time and energy: *Dano Roelvink*, *Kathelijne Wijnberg*, *Christian Winter*, *Duncan FitzGerald*, and reserve member *Ad Reniers*. I really hope that this moment will spark future collaborations between us!

To the SEAWAD Team:

I think that one of the most important factors in finishing a PhD is to have a well-defined and well-supported project, and I was immeasurably lucky to be a part of the SEAWAD and KUSTGENESE2.0 teams. Not only did we have the opportunity to do some incredibly cool fieldwork and analyze the amazing dataset that resulted from it, but I was also surrounded by great colleagues. *Floris de Wit*: TU Delft partner-in-crime, King of the Drifters, and captain of the ship! Thank you for taking me along for the final day of your drifter campaign, that was probably the most memorable (work)day of my whole PhD. *Laura Brakenhoff*: Queen of the Dunes and Ripples – thank you! *Harriette Holzhauer*: tireless benthos sampler, collaborative thinker, and source of good energy – thank you for all of the good conversations and the good memories of fieldwork! Thank you also to *Klaas Lenstra* for prompting me to think more deeply about how ebb-tidal deltas really work. Thank you to *Marcel van Maarseveen* and *Henk Markies* for your technical wizardry, which was essential to making our field campaign a reality. Thank you to *Jack Poleykett*, *Matthew Wright*, and *Kevin Black* from Partrac for their support with the sediment tracing project in Chapter 6. I had a great time working with you and am grateful for your role in bringing such a cool field experiment to fruition!

[2] I didn't give you the chance to prune these acknowledgements, but I make no apologies for my wordiness here. *La cabra siempre tira al monte.*

Thank you to *Marion Tissier* – you have been an important mentor and role model to me in perseverence, thinking critically about how to do good science, and in leading and supporting students with empathy. Your contributions to my PhD, both direct and indirect, have been essential. Thank you also for many fun memories in the world of SEAWAD, coral reefs, and well beyond. Thank you, *Ad Reniers*, for always being supportive and encouraging of my curiosity. You have an uncanny knack for asking precisely the right questions. Also, thank you for taking me to the hospital after the incident at the axe-throwing competition[3]. Lastly, thanks to *Peter Herman* for all of the curiosity-triggering discussions at the coffee machine. A three-minute conversation with you inevitably sparks an entire afternoon of writing frantically and losing myself down a Google Scholar rabbit hole. I hope we can have more of these soon.

To my Deltares colleagues:

During my PhD, I had the great privilege of working one day per week in the Applied Morphodynamics department at Deltares. In this group, I always felt like the dumbest person in room, but in the best possible way.[4] I learn so much from all of you every time I walk through the door, and am continually delighted by your kindness and camaraderie.

First, I would like to thank *Ap van Dongeren* for being my perpetual supporter from the first day I set foot in Deltares for my MSc thesis. Your encouragement to pursue a PhD was an important factor in my decision to follow this path. Your support with our first paper gave me an extremely valuable experience, and the advice you gave to me then made navigating the peer review process during my PhD much less daunting. Thank you for helping me to keep one toe in the coral reef/infragravity wave world while I was busy wrestling with ebb-tidal deltas. You continued to be a trusted mentor even as the foci of our research diverged, and I always looked forward to our weekly pandemic coffee quests. I would also like to commend the positive atmosphere and attitude that you cultivate in students and young researchers – thank you for bringing out the best in so many of us.

Thank you to *Dirk-Jan Walstra* for hiring me in the first place and pushing me to find ways of aligning my work at Deltares with my PhD research. Thank you to *Bob Hoogendoorn* for always challenging me to make an impact with my research and for your support of my postdoc. Thank you to *Robert McCall* for being a great role model – you are always resourceful, encouraging, curious, and lead with a positive and practical attitude. Thank you *Helena van der Vegt* for your sense of humour and relentless enthusiasm in all matters deltaic – you also gave an essential geological perspective to Chapter 3. Thank you *Ad van der Spek* for the useful papers you always seem to have up your sleeve, and for your patience and willingness to explain geological and geomorphobilinguistic matters. Thanks to *Kees Nederhoff* for your good company in California. I would also especially like to acknowledge *Maarten van Ormondt* for his creative wizardry as the source of the original SedTRAILS code and many other useful computational creations. Thank you also to *Stefan de Vries* for his improvements and documentation of an early version of SedTRAILS and to *Floortje Roelvink* for her considerable feedback and thoughtful discussions on both SedTRAILS and BEWARE. Thank you to *Saskia Huisman* for helping me in the laboratory with the Malvern – Chapter 6 wouldn't have happened without you.

Thank you to the rest of my colleagues in the Applied Morphodynamics department and

[3] The real story is much less exciting than it sounds, so I will leave the rest to your imagination, dear reader.
[4] Thanks to *Ap* for illuminating the importance of stupidity in science (*Schwartz*, 2008).

beyond at Deltares – *Alessio*, *Ana*, *Anouk*, *Bart*, *Bas*, *Bert*, *Bert*, *Björn*, *Dano*, *Denzel*, *Ellen*, *Giorgio*, *Jebbe*, *Johan*, *João*, *Kees*, *Lodewijk*, *Marlies*, *Matthijs*, *Mick*, *Pieter Koen*, *Reinier*, *Roel*, *Tim*, and *Ymkje*. I hope to work more closely with you all in the coming years!

To Rijkswaterstaat:

My PhD project was only possible due to the unwavering support of Rijkswaterstaat, the Dutch Ministry of Water and Infrastructure. Thank you to *Harry de Looff* for your leadership in the Kustgenese 2.0 project. Thank you also to *Rinse Wilmink* and *Judith Litchens* for your support. Thank you to *Stefan Pluis* for your interest in SedTRAILS and cheerful collaboration. The field measurements that underpin the bulk of this thesis were only possible because of the dedication of *Jan-Willem Mol* and *Arjen Ponger* in coordinating everything from ships to 40 buckets of green sand. In that breath, thanks also to the crews of the *MS Schuitengat*, *MS Siege*, and *MS Terschelling*. Thank you to *Carola van Gelder* for providing opportunities to share my work with a wider audience. You helped me to see how my research could have an impact beyond the confines of the university. Lastly, thank you to *Quirijn Lodder* for your firm support and interest in my work. Our discussions about the management implications of this research were enormously helpful in shaping Chapters 1 & 9 of this thesis and in changing the way I thought about my work in a wider context. Thank you for sharing your confidence in my ideas.

To my colleagues at USGS:

In 2019, I had the great privilege of visiting the US Geological Survey in California. Thank you to *Andrew Stevens* for your hospitality and for making me feel so welcome in Santa Cruz. Thank you also for inviting me along for the beach surveys at the mouth of the Columbia – that was one of the highlights of my PhD. I am excited to continue working together on SedTRAILS development. Thank you to *Sean Vitousek* for your thoughtfulness and interest in my work – you gave me a huge boost of inspiration and confidence when I was struggling with Chapter 7. Thank you also to *Guy Gelfenbaum* for inviting me to Santa Cruz and making my stay possible, and to the rest of the USGS team who gave me such a warm welcome.

Lastly, thank you to *Curt Storlazzi* for keeping me involved in the world of coral reefs, for your warm hospitality in Santa Cruz, and for helping me learn to navigate the world of paper revisions. When we wrote our BEWARE paper, your feedback and mentorship on academic writing and managing the peer-review process was so valuable, not just for that article but for everything else that came afterwards in my PhD. Thank you for your constant reminders of the bigger picture of what we were trying to achieve, and for advocating for the use of my work in research and in practice. You are a great source of motivation.

À mes collègues de l'Ifremer:

Merci beaucoup à *Romaric Verney* pour notre merveilleuse collaboration! Meeting you in Bordeaux in 2018 marked a turning point in my PhD in two respects: the unknotting of a tricky technical problem when we couldn't tell our sand from mud, and the beginning of a most enjoyable collaboration. Thank you for entrusting me with your visions for mixed sediment monitoring; I hope I have done them justice. Chapter 5 would not have happened without you. I have learned a lot from you about mud and measurements, but also from your quiet and capable form of leadership. Of all the people I know, you may be the one who is most modest in proportion to their considerable ability and I really look up to you

as both a scientist and a human being. I hope we can continue to work together for a long time to come.

Duc Tran! You saved me! The inclusion of your additional lab experiments in Chapter 5 marked a turning point for my morale during a dark period of the pandemic. *Matthias Jacquet*, thank you for your technical expertise and efforts with the DEXMES experiments. Thank you also to *France Floc'h*, *Florent Grasso*, *Marion Chapalain*, *Marylin Uchasara*, and *Melanie Diaz* for making my time in Brest a pleasant one! I hope we continue to cross paths and have opportunities to work together.

To my colleagues in Canada:

My coastal engineering journey – my whole journey, really – began on the surprisingly Dutch-looking delta of the Fraser River, and I feel so lucky that I could return to Vancouver to work on coastal challenges there. Thank you to *Patrick Lilley* at Kerr Wood Leidal, *Spencer Taft* at Tsleil-Waututh First Nation, and *Kees Lokman* at UBC for the opportunity to contribute to your projects, and for taking good care of our students. Thank you to all of my former colleagues at Baird & Associates for your continued interest in my research and your efforts to build collaborations. Thank you to *Ryan Mulligan* for your enthusiasm in sharing my work and connecting me to your research group at Queen's. Most of all, I would like to thank *Amir Taleghani*, not only for building the bridge between Delft and Vancouver, but for introducing me to coastal engineering in the first place. You encouraged me to ditch the Steel Design class for Hydraulics all those years ago, and I never looked back. You have continued to be a true friend and an important part of my career – I hope that we keep finding ways to work together far into the future. Who knows what I'd be doing today without your influence?

To the students along my journey:

Thank you to the MSc students who welcomed me to collaborate in their thesis projects: *Hithaishi*, *Jochem*, *Albert*, *Michelle*, *Rens*, *Timo*, *Rieneke*, *Floortje*, *Fred*, *Matteo*, *Hilary*, *Camila*, *Laurie*, *Tije*, *Paul*, *Mayra*, *Math*, *Vesna*, *Jan*, *Charlotte*, *Carlijn*, and *Lars*. Working with such clever, motivated young researchers on a huge range of topics was one of the best parts about my PhD, and I learned so much from you all. You will go far! I would especially like to thank *Jasper Bak*, *Roy van Weerdenburg*, *Paula Lambregts*, and *Denzel Harlequin* for their efforts within the SEAWAD project. Your work has made important direct and indirect contributions to this dissertation. Thank you also to the students of Coastal Dynamics 1 for keeping me on my toes with nasty questions about radiation stresses, and for giving me something to pour myself into and connect with during those first scary weeks of lockdown in Spring 2020 – it helped a lot.

To my new TRAILS family:

I would like to extend a thank you, partly in advance, to *Anna-Maartje de Boer*, *Tjitske Kooistra*, *Jakob Wallinga*, *Rob Witbaard*, *David Goldsborough*, and the rest of the TRAILS team. I have really enjoyed working with you so far and am so excited to see what we can accomplish together in the coming years!

To my early teachers:

Although this thesis was mainly a product of the last five years, I would be remiss to neglect the important groundwork laid for it by teachers in my earlier years. To *Lou Masi*, for giving a shy bookworm confidence and for helping me to find my voice as a writer. To *Jean (Faught) McCalmont*, for organizing School Reach and for transforming a love of reading into a love of writing. To *Sally Barros* for encouraging me to sign up for the high school science fair. To *Martin Lawlor*, for teaching us not to be afraid of the reference library and for preparing me so well for a career in research, even though I didn't realize it at the time. And to *Dave Nixon*, who played a huge role in shaping me into the adult I am today and showed me the importance of building a good community.

To my friends outside the lab:

An important part of staying sane in grad school is to have a life outside of the lab, and for their part in this, I am profoundly thankful to my curling team. To *Scott*, *Andrew*, *Alex*, and the rest of the regulars at the club in Zoetermeer, thank you for keeping a little piece of Canada alive here for me. Thanks for letting me be the Ringo to your John, Paul, and George (I leave you to fight over who is who). Thank you to *Camila* for the many musical memories and solidarity in the twists and turns of grad student life. Thanks to *Johanna* for bringing your good Canadian vibes and butter tarts to Delft, and to *Mads* for welcoming me into your quantum gang back at the start of my PhD. *Daan*! Thank you for all the fun dinners and stimulating conversations – you give me a lot of good energy! Thank you to *Ana* in New Zealand for all of the joyful escapes from research that you instigated and for a lifetime supply of laughter rooted in those good memories. Thank you to *Matt Coles* for sharing your teaching wisdom, your scotch, and for being my scientific partner-in-crime and fellow "rock detective" since we were five years old. Thank you to my Waterloo crew and all of my other friends back in Canada for continuing to make the effort to keep me in your lives in spite of the distance. I am so lucky.

To my colleagues and friends at TU Delft:

Matthieu de Schipper, thank you for always welcoming me to join your fieldwork on the beach – I get so much good energy from you and your students. I consider you an important role model, and especially admire your inclusive outlook and calm, empathetic attitude in times of crisis. *Sierd de Vries*, I am always happy to see you emerge from around a corner. You ask the right critical questions, are perpetually supportive, and are barrels of fun – thank you! To *Nina Piccoli*, for saving my sanity during those first crazy weeks of the pandemic and for your camaraderie as we navigated the treacherous seas of remote learning for the first time. Thank you to *Stefan Aarninkhof* for your trust and for giving me opportunities to challenge myself. And especially thank you to *Judith Bosboom* – from the first day that I set foot in your classroom as an MSc student, you made me feel like I was in the right place and that this was something I urgently needed to be a part of. Working with you on

CD1 has been one of the most rewarding experiences of my PhD. I am so grateful for your mentorship, for pushing me to become a better teacher, and for reminding me to always think critically about the fundamentals before I get too carried away. Thank you for your trust and of course for the many laughs we had along the way.

Thank you also to *Karin van Nispen* for your insightful feedback on the first draft of my dissertation introduction and structure, and for helping me see the light at the end of the tunnel.

I am so grateful for my colleagues and friends on the second and third floors who have been a part of my PhD journey in one way or another. Thank you to *Alissa*, *Anne*, *Anna*, *Arjen*, *Bas*, *Carine*, *Chris*, *Christa*, *Chunyan*, *Ermano*, *Grace*, *Hassan*, *Irene*, *Jeremy*, *Jianliang*, *José*, *Julia*, *Lennart*, *Marlies*, *Matthijs*, *Nils*, *Sabine*, *Sander*, *Sien*, *Silke*, *Sotiria*, *Tung*, *Xuexue*, and *Yu*. Thank you to *Said Alhaddad* for the many years of friendship and countless dinners we shared. *Robert* and *Jessica* – thank you for all the fun memories and for brightening up some of the darkest parts of the pandemic. Thank you to *Otti* and *Inge* for your administrative help and for keeping the wheels running smoothly around here.

One of the best parts of the last five years has been working in the Waterlab. I count among them some of the best friends I've ever had and some of the finest people I know. Thank you to *Maria* for the adventures in India and always having my back whenever peanuts threatened. To *Merel*, thank you for being so welcoming and kind since Day One. You radiate goodness wherever you go. To *Yorick*: thank you for your CD1 camaraderie and being a dependable beer buddy. Your wedding will always stand out to me as a golden moment, especially as the last awesome party we had before the pandemic showed up. *Erik*, thank you for your friendship and support through many different parts of our PhD and Deltares journeys. I especially appreciate the boost of momentum that you gave to Chapter 5 of this thesis. Thank you to *Wim* for reliably rallying to the weekly call to PSOR and for lending a touch of scientific respectability to our Bavarian Fluid Mechanics Workshop. Thank you *Claire* for your floc wisdom and for introducing me to the microscope and Malvern – they made a big difference to my tracer study. Thank you also to *Andres*, *Astrid*, *Bas*, *Chantal*, *Cynthia*, *Gonzalo*, *Han*, *Jianwei*, *Khifayath*, *Laura*, *Meles*, *Nici*, *Pieter*, *Shelby*, *Sienna*, *Üwe*, *Xin*, *Zeinab* and the rest of the Waterlab crew for all the nice chats and for making the office such a nice place to be (even when none of us could be in it!). To all the newcomers since the pandemic began – I am sorry we haven't got to know each other very well yet, but I look forward to changing that in the years to come!

To *Jill Hanssen*: in the Sediment Dynamics class back in 2015 you became my first Dutch friend here, and you have stood out as a beacon of kindness and thoughtfulness in our community ever since. *Lodewijk de Vet*, King of the Mudflats! I have learned much from your meticulous and thoughtful approach to research, and am grateful for many good memories from our times at both TU and Deltares. Bedankt ook voor het nalezen van mijn Nederlands in de samenvatting en stellingen, en voor het doordachte commentaar op de nuances van uw taal. *Clàudia Ylla Arbós*: from the day you walked into the lab I knew we would become good friends, and you did not disappoint – a fountain of artistic and culinary inspiration, I know can count on you for quality conversation about books, art, and everything in between. I always look forward to your next creation – keep 'em coming!

To my officemates in S3.00.120, past and present: *Jakob Maljaars*: for many enlightening discussions and for helping me to appreciate the beautiful Dutch mornings, regardless of how fair or foul the weather. *Irene Colosimo*: thank you for the warm energy that you bring

to any room you walk into. I will never forget our fieldwork in the mud with the Italian filmmakers. *Ana Colina Alonso*: you are quick to help and slow to judge, and I really admire that you always seem to give the people around you your best. Thank you also for the many fruitful discussions on mixed sediments in the Wadden Sea. *Marco Gatto*: Thank you for your friendship and for keeping the joy of live music alive here, for our caterwauling karaoke sessions, for risotto so good I still get teary-eyed thinking about it, and of course also for your many insights into sediment transport.

Liselot Arkesteijn: thank you for board games and bike rides, for late night beers and early morning runs (seldom sequential), and above all for your steadfast friendship. You and Tom fill up my tank whenever we hang out (metaphorically and literally), and I know that we will remain good friends for a long time.

On the first day of my PhD, *Victor Chavarrias* rallied the troops and we all went out for pizza and beer. From day one, you welcomed me not just to the lab but also into your family. You, Elisa, Silke, and Ilse have treated me as one of your own and brought out my hitherto-undiscovered Spanish side, introducing me to the wonders of tortilla and the delights of your language. We will find our ridiculous Ignobel idea someday.

Alejandra Gijón Mancheño! It feels like an eternity since we started our masters' in Trondheim 8 years ago. Thank you for being my closest friend when I needed it most in a land far away from home, and for more hilarious and joyful tales than can be retold here without doubling my word count. Sanity-checker and does-this-make-senser for a thousand paragraphs and figures, you have also been an essential scientific sparring partner and motivator to do my best research. Through trials, tribulations, tragedies, and triumphs, I knew that I could always count on you for commiseration or celebration with pizza and a glass of wine. Muchas gracias por todo! I look forward to new adventures and misadventures in our postdocs!

In March 2020, our lives all turned upside down with the arrival of the pandemic, and as of this writing I think most of us still feel flipped. In the first wave, we lost my grandma, *Betty Pearson*, a truly incredible woman. The last two years have been alternatingly scary, boring, stressful, and frustrating. We are perpetually in flux but also frozen in time; destabilized by the need to constantly reassess risks to ourselves and others, surprised with our newfound and completely unwanted fluency in the language of epidemiology. Needless to say, these are hardly good conditions for finishing one's PhD. In spite of these things, I consider myself a very lucky person, and I had just the right people to help me get through it all[5].

Matt Czapiga: river-wrangler, culinary wizard, hard-hurrying curler, and pandemic housemate extraordinaire – you are truly Michigan's finest. Moving in with you in December 2020 marked a pivotal upswing in my morale and energy, and it would have taken much longer to finish this thesis without your influence. You were a stalwart source of friendship and food during a period when I really needed both. We all miss you in Delft, and you are always welcome at my table.

Thank you, *Patricia Buffon*, for being the best surprise of my PhD and the biggest silver lining of the pandemic. You shine brightly in dark times. A highly dependable source of love and lasagna, you have become so important to me. Thank you for your patience as I wrestled with my thesis, especially in the final months when I spent far too many late nights ensnared in mortal combat with this book. Thank you for turning our apartment into

[5] Escaping seriousness for a moment, I would also like to thank Dan Mangan, Jeff Tweedy, Kristian Matsson, Ed Yong, Richard Powers, and Adriene of *Yoga with Adriene* for being my pandemic muses from afar.

a cozy island of peace in the stormy seas of the pandemic. Your love and companionship were essential to the completion of this book, and I hope that you feel shared sense of accomplishment from it. I feel like a new person (or rather, like the old Stuart again) since finishing it, and I look forward to sunnier days together!

* * *

I began this book with a quote from *Alistair MacLeod* (1999), and would like to end with one too: "*All of us are better when we are loved.*" So thank you most of all to my family for their love that spans oceans. *Mom*, *Dad*, *Cameron*, and *Elizabeth* – you got me here and you keep me going, and that is everything.

Stuart Grant Pearson
Delft, February 11th, 2022

About the Author

Stuart Pearson was born on September 24, 1989 in Richmond, British Columbia, on the low-lying delta of Canada's Fraser River. After growing up on the shores of the Great Lakes in Ontario, he followed a meandering path through civil engineering at the University of Waterloo, which eventually led him to discover the joys of river hydraulics. After spending a few years as a river and coastal modelling consultant near Toronto, he leapt at the chance for a new adventure and moved to Europe to study his Master's in coastal and maritime engineering. Studying at NTNU in Norway, the University of Southampton in the UK, and TU Delft in the Netherlands, he completed his MSc thesis in coral reef hydrodynamics. At this point he realized that he loved research and life in Delft so much that he stuck around for a PhD, also working part-time at Deltares. During this time he lived out his childhood dreams of reading and writing all the time while playing with sand, riding around in boats, making maps, and meeting good people from all corners of the world. Stuart is overjoyed to continue developing his PhD research as a postdoc at TU Delft and Deltares. When not concerning himself with wayward sand grains, he can be found sweeping hard at the curling rink, geeking out about music and the relative merits of different David Bowie albums, cooking with friends, or curled up with a good book.

List of Publications

Peer-Reviewed Journal Articles

First Author

5. **Pearson, S.G.**, Elias, E.P., van der vegt, H., van Prooijen, B.C., van der Spek, A., & Wang, Z.B. (In Review). *A Novel Approach to Mapping Ebb-Tidal Delta Morphodynamics and Stratigraphy.* Accepted by Geomorphology pending minor revisions. [Preprint, Chapter 3].

4. **Pearson, S.G.**, van Prooijen, B.C., Poleykett, J., Wright, M., K. Black, K., & Wang, Z.B. (2021). *Tracking fluorescent and ferrimagnetic sediment tracers on an energetic ebb-tidal delta to monitor grain size-selective dispersal.* Ocean & Coastal Management. [Link, Chapter 6].

3. **Pearson, S.G.**, Verney, R., van Prooijen, B.C., Tran, D., Hendriks, H.C.M., Jacquet, M., Wang, Z.B. (2021). *Characterizing Mixed Sand and Mud Suspensions using Combined Optical and Acoustic Measurements in Estuarine Environments.* Journal of Geophysical Research: Oceans. [Link, Chapter 5].
   - ***AGU Editor's Highlight*** [Link].

2. **Pearson, S.G.**, van Prooijen, B.C., Elias, E.P., Vitousek, S., Wang, Z.B. (2020). *Sediment Connectivity: A Framework for Analyzing Coastal Sediment Transport Pathways.* Journal of Geophysical Research: Earth Surface. [Link, Chapter 7]

1. **Pearson, S.G.**, Storlazzi, C.D., van Dongeren, A.R., Tissier, M.F.S., Reniers, A.J.H.M. (2017). *A Bayesian-based system to assess wave-driven flooding hazards on coral reef-lined coasts.* Journal of Geophysical Research: Oceans, 122. [Link]

Co-Author

11. Uphues, C.F.K., van IJzendoorn, C., Hallin, C., **Pearson, S.G.**, van Prooijen, B.C., Miot da Silva, G. & de Vries, S. (In Review). *Coastal aeolian sediment transport in an Active Bed Surface Layer: tracer study and conceptual model.* Submitted to Earth Surface Processes and Landforms.
10. Bakker, T., Antolinez, J.A.A., Leijse, T., **Pearson, S.G.** & Giardino, A. (In Review). *Estimating tropical cyclone-induced wind, waves, and surge: a general methodology based on representative tracks.* Submitted to Coastal Engineering.
9. Elias, E.P.L, **Pearson, S.G.**., van der Spek, A., & Pluis, S. (In Press). *Understanding meso-scale processes at mixed-energy tide-dominated tidal inlet; Ameland Inlet, the Netherlands.*. In Press with Ocean & Coastal Management.
8. van Weerdenburg, R., **Pearson, S.G.**, van Prooijen, B.C., Laan, S., Elias, E.P., Wang, Z.B. (2021). *Field measurements and numerical modelling of wind-driven exchange flows in a tidal inlet system in the Dutch Wadden Sea.* Ocean & Coastal Management. [Link].
7. Roelvink, F.E., Storlazzi, C.D., van Dongeren, A.R., & **Pearson, S.G.** (2021). *Coral reef restorations can be optimized to reduce coastal flooding hazards.* Frontiers of Marine Science [Link].
6. van Prooijen, B.C., Tissier, M.F.S., de Wit, F.P., **Pearson, S.G**., Brakenhoff, L.B., van Maarseveen, M.C.G., van der Vegt, M., Mol, J.W., Kok, F., Holzhauer, H., Borsje, B.W., van der Werf, J., Vermaas, T., Gawehn, M., Grasmeijer, B., Elias, E.P., Tonnon, P.K., Reniers, A.J.H.M., Wang, Z.B., den Heijer, K., van Gelder-Maas, C., Wilmink, R.J.A., Schipper, C., & de Looff, H. (2020). *Measurements of Hydrodynamics, Sediment, Morphology and Benthos on Ameland Ebb-Tidal Delta and Lower Shoreface.* Earth System Science Data. [Link]

5. Parodi, M.U., Giardino, A., van Dongeren, A.R., **Pearson, S.G.**, Bricker, J., Reniers, A.J.H.M. (2020). *Investigating Uncertainty in Coastal Flood Risk Assessment in Small Island Developing States.* Natural Hazards and Earth System Sciences. [Link]
4. Scott, F., Antolinez, J.A.A., McCall, R.C., Storlazzi, C.D., Reniers, A.J.H.M., & **Pearson, S.G.** (2020). *Hydro-morphological characterization of coral reefs for wave-runup prediction.* Frontiers in Marine Science. [Link]
3. Elias, E.P.L., van der Spek, A.J.F., **Pearson, S.G.**, & Cleveringa, J. (2019). *Understanding sediment bypassing processes through analysis of high-frequency observations of Ameland Inlet, the Netherlands.* Marine Geology. [Link]
2. Rueda, A., Cagigal, L., **Pearson, S.G.**, Antolinez, J.A.A., Storlazzi, C.D., van Dongeren, A.R., Camus, P., Mendez, F.J. (2019). *HyCReWW: A Hybrid Coral Reef Wave and Water Level Metamodel.* Computers and Geosciences. [Link]
1. Giardino, A., Diamantidou, E., **Pearson, S.G.**, Santinelli, G., & den Heijer, C.K. (2019). *A regional application of Bayesian modelling for coastal erosion management.* Water, 11(1), 61. [Link]

PEER-REVIEWED CONFERENCE PAPERS

FIRST AUTHOR

3. **Pearson, S.G.**, Elias, E.P., Roelvink, F., Lambregts, P., Wang, Z.B., van Prooijen, B.C. (2021). *Lagrangian Sediment Transport Modelling as a Tool for Investigating Coastal Connectivity* [Oral Presentation]. Coastal Dynamics 2021, June 2021. [Chapter 8].
2. **Pearson, S.G.**, van Prooijen, B.C., de Wit, F.P., Holzhauer-Meijer, H., de Loof, A.P., & Wang, Z.B. (2019). *Observations of suspended particle size distribution on an energetic ebb-tidal delta* [Poster]. Coastal Sediments '19, May 27-31, 2019, St. Petersburg, Florida. [Link, Chapter 4].
1. **Pearson, S.G.**, Lubbad, R., Le, T.M.H., Nairn, R.B. (2016). *Thermo-mechanical Erosion Modelling using COSMOS: A case study at Baydaratskaya Bay, Russia* [Paper & Oral Presentation]. 8th International Conference on Scour and Erosion (ICSE 2016), Oxford, UK. https://doi.org/10.1201/9781315375045-34 [Link]

CO-AUTHOR

4. Reniers, A.J.H.M., de Wit, F.P., Tissier, M.F.S., **Pearson, S.G.**, Brakenhoff, L., van der Vegt, M., & van Prooijen, B.C. (2019). *Wave-and current-related ebb-tidal sediment transport: observations and modeling* [Oral Presentation]. Coastal Sediments '19, May 27-31, 2019, St. Petersburg, Florida. [Link].
3. Rueda, A., Cagigal, L., Anderson, D. Storlazzi, C.S., van Dongeren, A.R., **Pearson, S.G.**, Marra, J., Ruggiero, P., Mendez, F. (2019). *Towards A Flood Risk Assessment On A Reef-lined Coastline* [Poster]. Coastal Sediments '19, May 27-31, 2019, St. Petersburg, Florida. [Link].
2. Tissier, M.F.S., Dekkers, J., van Dongeren, A.R., **Pearson, S.G.**, Reniers, A.J.H.M. (2018). *Etude experimentale de la formation de ressauts ondules sur un recif frangeant* [Oral Presentation]. Journees Nationales Genie Cotier - Genie Civil, May 29, 2018, La Rochelle, France. [Link].
1. van Dongeren, A.R., Storlazzi, C.S., Quataert, E., **Pearson, S.G.** (2017). *Wave dynamics and flooding on low-lying tropical reef-lined coasts* [Oral Presentation]. Coastal Dynamics 2017, June 12-16, 2019, Helsingor, Denmark. [Link].

OTHER CONFERENCE ABSTRACTS, PRESENTATIONS, & POSTERS

FIRST AUTHOR

23. **Pearson, S.G.** (2022). Invited Talk: *Sandy solutions for saving our shores from sea level rise: a Dutch perspective* [Oral Presentation]. BWRC and LEADERS Seminar Series at Queen's University, Canada, January 26, 2022. [Link].
22. **Pearson, S.G.** (2021). Invited Talk: *Sediment Connectivity – A Framework for Analyzing Coastal Sediment Transport Pathways* [Oral Presentation]. Eurocoast Zoominar, December 17, 2021.
21. **Pearson, S.G.**, van Prooijen, B.C., & Wang, Z.B. (2021). Invited Talk: *Speaking Simply About Complex Coastal Morphodynamics* [e-Lightning Presentation]. American Geophysical Union (AGU) Fall Meeting 2021. [Link].
20. **Pearson, S.G.**., Elias, E.P.L, van der Vegt, H., van der Spek, A., van Prooijen, B.C. & Wang, Z.B. (2021). *A Novel Methodology for Mapping Decadal-Scale Ebb-Tidal Delta Morphodynamics and Stratigraphy* [Virtual Presentation]. AGU Fall Meeting 2021. [Link].
19. **Pearson, S.G.**. (2021). *Weird waves cause big trouble on small lands in the middle of the big blue wet thing* [Virtual Presentation]. AGU Fall Meeting 2021. [Link].
18. **Pearson, S.G.** (2021). *Where Does All The Sand Go? Simulating Sand Pathways* [Virtual Presentation]. European Maritime Day 2021, September 2021.
17. **Pearson, S.G.**, Verney, R., Hendricks, H.C.M., Tran, D., Jacquet, M., Wang, Z.B., van Prooijen, B.C. (2021). *Characterizing the Composition of Suspended Sand and Mud Suspensions in Coastal Environments using Combined Optical and Acoustic Measurements: Ameland Ebb-Tidal Delta* [Oral Presentation]. INTERCOH 2021, September 2021.
    - ***Awarded*** 2^{nd} ***Place – Intercoh Ray Krone Award***.
16. **Pearson, S.G.**, Verney, R., Hendricks, H.C.M., Tran, D., Jacquet, M., Wang, Z.B., van Prooijen, B.C. (2021). *Characterizing the Suspended Sand and Mud Composition on Ameland Ebb-Tidal Delta using Combined Optical and Acoustic Measurements* [Virtual Presentation]. NCK Days 2021, March 2021. [Link].
15. **Pearson, S.G.**. (2021). *Sediment connectivity in estuaries and coastal systems* [Virtual Presentation]. IAG Working Group on Connectivity in Geomorphology, Connectivity Conversations III. January 21, 2021. [Link].
14. **Pearson, S.G.**, Elias, E.P., Vitousek, S., Roelvink, F., Stevens, A., van Weerdenburg, R., van Gijzen, L., van der Wegen, M., Wang, Z.B., van Prooijen, B.C. (2020). *Sediment Connectivity of Estuaries around the World* [e-Lightning Presentation]. American Geophysical Union Fall Meeting 2020, Online Conference due to COVID-19, December 16th, 2020. [Link].
13. **Pearson, S.G.**, Gijón Mancheño, A., Ylla Arbós, C. (2020). *Keeping our feet dry and safe from the big water by using lots of very tiny rocks* [Virtual Presentation]. American Geophysical Union Fall Meeting 2020, Online Conference due to COVID-19, December 8th, 2020. [Link]. [Video].
    - ***Awarded Outstanding Student Presentation Award (OSPA)***. [Link].
12. **Pearson, S.G.**, Elias, E.P.L., Roelvink, F.E. (2020). *Following Coastal Sediment Transport Pathways with SedTRAILS* [Virtual Presentation]. Delft3D User Days - Australian Time zone: Coast, Lagoon and Estuary, Online Conference due to COVID-19, November 10th, 2020. [Link].
11. **Pearson, S.G.**, van Prooijen, B.C., & Wang, Z.B. (2020). *Connectivity: A Framework for Interdisciplinary Collaboration on Transport Pathways in Coastal Environments* [Oral Presentation]. IHE PhD Symposium 2020, Online Conference due to COVID-19, October 8th, 2020. [Link].
    - ***Awarded Best Presentation (Hydraulic Engineering Session)***
10. **Pearson, S.G.**, van Prooijen, B.C., & Wang, Z.B. (2020). *Sediment Connectivity: A Framework for Analyzing Coastal Sediment Transport Pathways* ['Hotplot' Presentation]. Eurocoast Webinar (Hosted by the University of Plymouth), October 7th, 2020.
9. **Pearson, S.G.**, van Prooijen, B.C., Elias, E.P., Wang, Z.B. (2020). *Sediment Connectivity: a Framework for Analyzing Coastal Sediment Transport Pathways* [Cancelled due to COVID-19]. NCK Days 2020, Texel, Netherlands, March 19-20, 2020.

8. **Pearson, S.G.**, van Prooijen, B.C., Poleykett, J., Wright, M., K. Black, K., Wang, Z.B. (2018). *Monitoring sediment transport patterns on an energetic ebb-tidal delta using dual-signature tracers* [Poster]. American Geophysical Union Fall Meeting 2018, Washington, D.C. [Link]
7. **Pearson, S.G.**, Tissier, M.F.S. (2018). *The Curious Undular Bore* [Poster]. American Geophysical Union Fall Meeting 2018, Washington, D.C.[Link]
6. **Pearson, S.G.**, van der Lugt, M., van Dongeren, A.R., Hagenaars, G., Burzel, A., van Zanten, B.T. (2018). *Assessment of runup reduction potential due to coral reef restoration* [Oral Presentation]. XBeach User Day 2018, Delft, the Netherlands, November 15, 2018. [Link].
5. **Pearson, S.G.**, van Prooijen, B.C., Poleykett, J., Wright, M., K. Black, K., Wang, Z.B. (2018). *Sediment Transport Patterns on Ameland Ebb-Tidal Delta Determined by Dual-Signature Sediment Tracers* [Oral Presentation]. NCK Days Conference, March 23 2018, Haarlem, the Netherlands. [Link]
4. **Pearson, S.G.**, van Prooijen, B.C., Wang, Z.B., Bak, J.P. (2018). *Sediment Connectivity and Exchange in Ameland Inlet* [Oral Presentation]. NCK Symposium on Sediment Sorting, January 11 2018, Delft, the Netherlands. https://doi.org/10.13140/RG.2.2.15706.03527 [Link]
3. **Pearson, S.G.**, van Prooijen, B.C., Wang, Z.B. Bak, J.P. (2017). *Sediment Connectivity and Transport Pathways in Tidal Inlets: a Conceptual Framework with Application to Ameland Inlet* [Oral Presentation]. American Geophysical Union Fall Meeting 2017, New Orleans, Louisiana. [Link]
2. **Pearson, S.G.**, van Dongeren, A.R., Storlazzi, C.D., Tissier, M.F.S, Reniers, A.J.H.M, Lapidez, J.P, Tajima, Y., Shimozono, T. (2017). *BEWARE: Bayesian estimation of wave attack in reef environments* [Oral Presentation]. XBeachX Conference 2017, Delft, The Netherlands. [Link]
1. **Pearson, S.G.**, van Prooijen, B.C., Wang, Z.B. *The Influence of Grain Size on Sediment Transport Pathways at Ameland Inlet* [Poster]. NCK Days Conference 2017, Den Helder, Netherlands https://doi.org/10.13140/RG.2.2.14690.12481 [Link]

CO-AUTHOR

20. Uphues, C.F.K., van IJzendoorn, C.O., Miot da Silva, G., **Pearson, S.G.**, de Vries, S. 2021). *Observations of Coastal Aeolian Sediment Transport in an Active Surface Layer using Tracers* [Oral Presentation]. American Geophysical Union Fall Meeting 2021. [Link].
19. Tran, D., **Pearson, S.G.**, Jacquet, M., van Prooijen, B.C., Verney, R. (2021). *Characterizing the Composition of Suspended Sand and Mud Suspensions in Coastal Environments using Combined Optical and Acoustic Measurements: Laboratory Experiments* [Oral Presentation]. INTERCOH 2021, September 2021.
18. Tran, D., Bocher, A., Jacquet, M., **Pearson, S.G.**, Floc'h, F., Le Dantec, N., Dorval, F., Fromant, G., Vergne, A., Jourdin, F., Crave, A., Lintanf, H., & Verney, R., (2021). *DEXMES: A novel cylindrical device for SPM experiments* [Poster]. INTERCOH 2021, September 2021.
17. McCall, R., **Pearson, S.G.**, Roelvink, F., Antolinez, J.A.A., Storlazzi, C.D., de Goede, R., Scott, F. (2021). *Rapid Prediction of Wave Runup and Flooding on Reef-Lined Coasts* [Oral Presentation]. Coastal Dynamics 2021, June 2021.
16. van Gorsel, J., Patil, A., Bricker, J., **Pearson, S.G.**, Raby, A., Dassanayake, D., Antonini., A. (2021). *Numerical Investigation Of Breaking And Broken Regular Wave Forces On A Shoal Mounted Cylinder* [-]. 16th OpenFOAM Workshop, June 2021.
15. Tran, D., Jacquet, M., **Pearson, S.G.**, Verney, R. (2021). *Investigating suspended particulate matters from multi-wavelength optical and multi-frequency acoustic measurements* [Virtual Presentation]. EGU General Assembly 2021, Online Conference due to COVID-19, May 19-30, 2021. [Link].
14. Bertoncelj, V., Leijnse, T., Roelvink, F.E., **Pearson, S.G.**, Bricker, J., Tissier, M.F., van Dongeren., A.R. (2021). *Efficient and accurate modeling of wave-driven flooding on coral reef-lined coasts: Case Study of Majuro Atoll, Republic of the Marshall Islands* [Virtual Presentation]. EGU General Assembly 2021, Online Conference due to COVID-19, May 19-30, 2021. [Link].
13. Wallinga, J., Goldsborough, D., Witbaard, R., van Prooijen, B.C., van der Spek, A.F.J., Elias, E.P.,

Lodder, Q., de Boer, A.M., Kooistra, T., **Pearson, S.G.** (2021). *Introducing the TRAILS project: Tracking Ameland Inlet Living lab Sediment.* NCK Days 2021, March 2021. [Link].

12. Gaido, C., Tissier, M.F.S., Reniers, A.J.H.M., **Pearson, S.G.**, Bricker, J. (2020). *Numerical Experiments on Resonant Wave Amplification Over a Fringing Reef* [Oral Presentation]. 37th International Conference on Coastal Engineering 2020, 5-9 October 2020, Online Conference due to COVID-19.
11. van Gijzen, L., Herman, P.M.J., van der Wegen, M., van Prooijen, B.C., **Pearson, S.G.** (2020). *Fine sediment transport pathways and connectivity in San Francisco Bay* [Cancelled due to COVID-19]. NCK Days 2020, Texel, Netherlands, March 19-20, 2020.
10. Lowe, R.J., Quataert, E., McCall, R., van Dongeren, A.R., Antolinez, J.A.A., Buckley, M., Hansen, J., & **Pearson, S.G.** (2019). *Global contributions to extreme sea levels at reef coastlines* [Oral Presentation]. 16th International Workshop on Waves, Storm Surges and Coastal Hazards, November 10-15, 2019, Melbourne, Australia. [Link].
9. Tissier, M.F.S., Dekkers, J., Reniers, A.J.H.M., **Pearson, S.G.**, van Dongeren, A.R. (2019). *Undular bore formation and extreme runup on reef-lined coasts* [Invited Talk]. EGU General Assembly 2019, Vienna, Austria, April 7-12, 2019.
8. van Weerdenburg, R.J.A., van Prooijen, B.C., **Pearson, S.G.**, Tonnon, P.K., Tissier, M.F.S., Wang, Z.B. (2019) *Exploring the relative importance of wind for exchange processes around Ameland Inlet* [Oral Presentation]. NCK Days 2019, Enkhuizen, Netherlands, March 20-22, 2019. [Link]
7. van Prooijen, B.C., de Looff, H., **Pearson, S.G.**, Mol, J.W., de Wit, F.P., Kok, F., Tonnon, P.K., van de Vegt, M., Tissier, M.F.S., Brakenhoff, L., Wilmink, R., van Weerdenburg, R., Wang, Z.B. (2018). *Large-scale field campaign for improving nourishment strategies in the Netherlands - Exploring the effects of wind* [Oral Presentation]. American Geophysical Union Fall Meeting 2018, Washington, D.C. [Link]
6. McCall, R., Nederhoff, K., Quataert, E., Hagenaars, G., Storlazzi, C., **Pearson, S.G.**, van Dongeren, A.R. (2018). *Towards an global forecast for wave-induced flooding on coral reef-lined coastlines* [Poster]. American Geophysical Union Fall Meeting 2018, Washington, D.C. [Link].
5. Tissier, M.F.S., Dekkers, J., Reniers, A.J.H.M., **Pearson, S.G.**, van Dongeren, A.R. (2018). *Undular Bore Development Over a Laboratory Fringing Reef* [Oral Presentation]. 36th International Conference on Coastal Engineering 2018, Baltimore, MD, July 30-August 3, 2018. [Link].
4. de Wit, F.P., Tissier, M.F.S., **Pearson, S.G.**, Radermacher, M., van de Ven, M.J.P., van Langevelde, A.P., Vos, T.A., Reniers, A.J.H.M. (2018). *Measuring the spatial and temporal variability of currents on Ameland Ebb-Tidal Delta* [Poster]. NCK Days Conference, March 23 2018, Haarlem, the Netherlands. [Link]
3. van Prooijen, B.C., de Looff, H., Holzhauer, H., Mol, J.W., van Maarseveen, M., de Wit, F.P., Kok, F., van de Vegt, M., Tissier, M.F.S., **Pearson, S.G.**, Brakenhoff, L., Wilmink, R., Wang, Z.B. *Kustgenese2/SEAWAD - Ameland Inlet Field Campaign* [Oral Presentation]. NCK Days Conference, March 23 2018, Haarlem, the Netherlands. [Link]
2. Rueda, A., Cagigal, L., Antolinez, J.A.A., **Pearson, S.G.**, Mendez, F.J., Storlazzi, C.D., van Dongeren, A.R. (2017). *A Metamodel to Estimate Runup Along Coral Reef-Lined Shorelines* [Oral Presentation]. XBeachX Conference 2017, Delft, The Netherlands. [Link]
1. Dekkers, J., Tissier, M.F.S., Reniers, A.J.H.M., **Pearson, S.G.**, van Dongeren, A.R. (2017). *Experimental Study on Undular Bore Development Over a Fringing Reef* [Poster]. XBeachX Conference 2017, Delft, The Netherlands.

Dear Reader,

Un bonjour de Bretagne!

So, the sand lasec

How does sediment move around on ebb-tidal deltas? This is a question that we need to answer in order to sustainably manage barrier coastlines in the face of sea level rise and climate change. To do so, we use a combination of field measurements and numerical models at Ameland Inlet in the Netherlands. Here several new methods are developed, including morphodynamic mapping techniques, a sediment composition index (SCI) derived from optical and acoustic measurements, techniques for sediment tracing, the sediment connectivity framework, and a Lagrangian sediment transport model (SedTRAILS). Together, these approaches reveal new knowledge about ebb-tidal deltas which can be used for managing complex coastal systems.

Stuart Pearson

Delft University of
Technology
Stevinweg 1
2628 CN Delft